UNIVERSITY OF BIRMINGHAM

DEFINING MECHANISMS AND NEW TREATMENTS FOR HEADACHE IN RAISED INTRACRANIAL PRESSURE

By OLIVIA GRECH

A thesis submitted to the University of Birmingham for the degree of

DOCTOR OF PHILOSOPHY

Institute of Biomedical Research

College of Medical and Dental Sciences

University of Birmingham

2023

UNIVERSITY OF
BIRMINGHAM

University of Birmingham Research Archive

e-theses repository

This unpublished thesis/dissertation is copyright of the author and/or third parties. The intellectual property rights of the author or third parties in respect of this work are as defined by The Copyright Designs and Patents Act 1988 or as modified by any successor legislation.

Any use made of information contained in this thesis/dissertation must be in accordance with that legislation and must be properly acknowledged. Further distribution or reproduction in any format is prohibited without the permission of the copyright holder.

ABSTRACT

Headache disorders are common and debilitating neurological conditions. While treatments can alleviate pain, our understanding of the mechanisms triggering attacks is incomplete. Evidence suggests that metabolic dysfunction may play a role in headache development and susceptibility, with fasting being a suspected migraine trigger, highlighting the importance of glucose metabolism. Identifying these energy-related mechanisms could lead to targeted interventions. Elevated intracranial pressure (ICP) can also cause headaches that are migraine-like, as seen in idiopathic intracranial hypertension (IIH), which additionally features metabolic disturbances. Although migraine treatments have exhibited some efficacy for raised ICP headaches, there is a lack of targeted therapies for IIH-related headaches, and the underlying mechanisms are poorly understood.

Cortical spreading depression (CSD) is a pivotal mechanism involved in migraine and has been established as energetically demanding. This thesis explored the metabolic consequences of CSD by analysing calcium signalling, mitochondrial activity, and metabolite profiles in an *ex vivo* acute brain slice model. This thesis also investigated the influence of ICP on headache mechanisms including CSD using a rodent model of raised ICP. Additionally, it examined the impact of reducing ICP with glucagon-like peptide-1 (GLP-1) receptor agonism and blocking calcitonin gene-related peptide (CGRP), a key factor in migraine.

Brain slices showed astrocytic calcium movement and markers of increased aerobic and anaerobic glycolysis in response to CSD. When challenged with glucose deprivation, mitochondrial activity was downregulated, potentially indicating

exhaustion. Interestingly, there was evidence of metabolic adaptability in glucose absence, suggesting the utilization alternative energetic pathways and substrates under metabolically stressful conditions. These findings enhance the understanding of the role of metabolism in CSD but also unveil altered energetic pathways, thereby identifying potential targets for therapeutic interventions.

The rodent model of raised ICP identified altered pain behaviour (indicative of changes in trigeminal sensitivity), disrupted cortical blood flow (CBF) and CSD responses. GLP-1 receptor agonism reduced ICP which was associated with prevention of pain behaviours and demonstrated restored cortical and CBF CSD responses. CGRP receptor antagonism ameliorated cranial pain behaviour, indicating a role for CGRP in driving pain responses in elevated ICP. Reduction of ICP through GLP-1R agonism and nociception attenuation via CGRP antagonism could represent potential therapeutic approaches. This pre-clinical evidence highlights the efficacy of therapeutics in managing headache behaviours and pathways, essential for guiding future clinical trials given the lack of targeted therapies for elevated ICP.

ACKNOWLEDGEMENTS

‘You steer the ship the best way you know. Sometimes it’s smooth. Sometimes you hit the rocks. In the meantime, you find your pleasures where you can.’ Junior Soprano

Throughout the turbulent journey that has been my PhD, there are a number of people who have helped me steer the ship and ensured the smooth sailing of my PhD. To my supervisor, Professor Alex Sinclair, who has been an excellent mentor, provided me with unbelievable opportunities, and continues to inspire me. I cannot thank her enough for taking a chance on me four years ago and nurturing me into the scientist I am today. Thank you for your support, leadership and friendship. My journey had its share of rough waters, and I am grateful for the support and knowledge of my supervisors, Dr Daniel Fulton and Professor Gareth Lavery and to Dr Lisa Hill for making sure I steered the academic challenges successfully.

I would also like to acknowledge the Translational Brain Science group in Birmingham, Susie, Andreas, James, Hannah, Jess and Mark, I have enjoyed working with you, celebrating the wins, and helping each other navigate the losses. Thank you for making this a truly translational project and providing me your vast clinical knowledge and insight. Members of the Lavery group played a crucial role in settling me into my PhD and sharing their technical expertise. Thank you Sam, who sacrificed countless hours and late nights preparing samples with me, and Silke for always having the answers to all of my many questions. I would like to express my gratitude to the Brain Research UK for funding this project and supporting my progression into science.

To the Headache Group at King’s College London, who kindly adopted me for almost two years, thank you for making me feel welcome in unfamiliar waters and keeping me sane during late nights in the lab. Eloisa, Emily, and Alejandro, your knowledge, teaching, and insight were invaluable. Hannah, Hui, and Ishita, you kept my spirits high and offered your assistance tirelessly. I'd like to express my appreciation to Dr Phil Holland in particular for continuing to ignite my passion for science. His curiosity, expertise, and vast knowledge have driven me to produce the data presented in this thesis and encouraged me to think outside the box.

Finally, I want to thank my family. To my parents, who have been the steadfast lighthouses guiding me through my doctoral journey by providing me endless support, encouragement, and love. My sister, Eve, who consistently brought a smile to my face, no matter how tough things got. And last but not least, my partner and my compass Ben. This journey had its fair share of rough seas, and if it wasn’t for his guidance, endless support and patience, I surely would not have completed this PhD.

PUBLICATIONS

PUBLICATIONS

GRECH, O., SASSANI, M., TERWINDT, G., LAVERY, G. G., MOLLAN, S. P. & SINCLAIR, A. J. 2022. Alterations in metabolic flux in migraine and the translational relevance. The Journal of Headache and Pain, 23, 127.

GRECH, O., MOLLAN, S. P., WAKERLEY, B. R., FULTON, D., LAVERY, G. G. & SINCLAIR, A. J. 2021b. The Role of Metabolism in Migraine Pathophysiology and Susceptibility. Life, 11.

GRECH, O., MOLLAN, S. P., WAKERLEY, B. R., ALIMAJSTOROVIC, Z., LAVERY, G. G. & SINCLAIR, A. J. 2020. Emerging themes in idiopathic intracranial hypertension. Journal of Neurology, 267, 3776-3784.

ASSOCIATED PUBLICATIONS

ALIMAJSTOROVIC, Z., MITCHELL, J. L., YIANGOU, A., HANCOX, T., SOUTHAM, A. D., **GRECH, O**., OTTRIDGE, R., WINDER, C. L., TAHRANI, A. A., TAN, T. M., MOLLAN, S. P., DUNN, W. B., & SINCLAIR, A. J. 2023. Determining the role of novel metabolic pathways in driving intracranial pressure reduction after weight loss. Brain communications, 5(5), fcad272.

ALIMAJSTOROVIC, Z., MOLLAN, S. P., **GRECH, O**., MITCHELL, J. L., YIANGOU, A., THALLER, M., LYONS, H., SASSANI, M., SENEVIRATNE, S., HANCOX, T., JANKEVICS, A., NAJDEKR, L., DUNN, W., & SINCLAIR, A. J. 2023. Dysregulation of Amino Acid, Lipid, and Acylpyruvate Metabolism in Idiopathic Intracranial Hypertension: A Non-targeted Case Control and Longitudinal Metabolomic Study. Journal of proteome research, 22(4), 1127–1137.

ELLIOT, L., FREW, E., MOLLAN, S. P., MITCHELL, J. L., YIANGOU, A., ALIMAJSTOROVIC, Z., OTTRIDGE, R. S., WAKERLEY, B. R., THALLER, M., **GRECH, O**., SINGHAL, R., TAHRANI, A. A., HARRISON, M., SINCLAIR, A. J. & AGUIAR, M. 2021. Cost-effectiveness of bariatric surgery versus community weight management to treat obesity-related idiopathic intracranial hypertension: evidence from a single-payer healthcare system. Surg Obes Relat Dis, 17, 1310-1316.

GRECH, O., MITCHELL, J. L., LYONS, H. S., YIANGOU, A., THALLER, M., TSERMOULAS, G., BROCK, K., MOLLAN, S. P., & SINCLAIR, A. J. 2024. Effect of glucagon like peptide-1 receptor agonist exenatide, used as an intracranial pressure lowering agent, on cognition in Idiopathic Intracranial Hypertension. Eye (London, England), 10.1038/s41433-023-02908-y.

GRECH, O., CLOUTER, A., MITCHELL, J. L., ALIMAJSTOROVIC, Z., OTTRIDGE, R. S., YIANGOU, A., ROQUE, M., TAHRANI, A. A., NICHOLLS, M., TAYLOR, A. E., SHAHEEN, F., ARLT, W., LAVERY, G. G., SHAPIRO, K., MOLLAN, S. P. & SINCLAIR, A. J. 2021a. Cognitive performance in idiopathic intracranial hypertension and relevance of intracranial pressure. Brain Commun, 3, fcab202.

GRECH, O., SENEVIRATNE, S. Y., ALIMAJSTOROVIC, Z., YIANGOU, A., MITCHELL, J. L., SMITH, T. B., MOLLAN, S. P., LAVERY, G. G., LUDWIG, C. & SINCLAIR, A. J. 2022b. Nuclear Magnetic Resonance Spectroscopy Metabolomics in Idiopathic Intracranial Hypertension to Identify Markers of Disease and Headache. Neurology, 99, e1702-e1714.

MITCHELL, J. L., LYONS, H. S., WALKER, J. K., YIANGOU, A., **GRECH, O**., ALIMAJSTOROVIC, Z., GREIG, N. H., LI, Y., TSERMOULAS, G., BROCK, K., MOLLAN, S. P. & SINCLAIR, A. J. 2023. The effect of GLP-1RA exenatide on idiopathic intracranial hypertension: a randomized clinical trial. Brain, awad003.

MOLLAN, S. P., MOMIN, S. N. A., KHATKAR, P. S., **GRECH, O**., SINCLAIR, A. J., & TSERMOULAS, G. 2023. A Neuro-Ophthalmologist's Guide to Advances in Intracranial Pressure Measurements. Eye and brain, 15, 113–124.

MOLLAN, S. P., CHONG, Y. J., **GRECH, O**., SINCLAIR, A. J. & WAKERLEY, B. R. 2021a. Current Perspectives on Idiopathic Intracranial Hypertension without Papilloedema. Life, 11, 472.

MOLLAN, S. P., **GRECH, O**., ALIMAJSTOROVIC, Z., WAKERLEY, B. R. & SINCLAIR, A. J. 2020. New horizons for idiopathic intracranial hypertension: advances and challenges. British Medical Bulletin, 136, 118-126.

MOLLAN, S. P., **GRECH, O**., O'SULLIVAN, E. & MACKIE, S. L. 2021b. Practice points for ophthalmologists from the 2020 British Society for Rheumatology Giant Cell Arteritis guidelines. Eye, 35, 699-701.

MOLLAN, S. P., **GRECH, O**. & SINCLAIR, A. J. 2021c. Headache attributed to idiopathic intracranial hypertension and persistent post-idiopathic intracranial hypertension headache: A narrative review. Headache: The Journal of Head and Face Pain, 61, 808-816.

MOLLAN, S. P., MITCHELL, J. L., OTTRIDGE, R. S., AGUIAR, M., YIANGOU, A., ALIMAJSTOROVIC, Z., CARTWRIGHT, D. M., **GRECH, O**., LAVERY, G. G., WESTGATE, C. S. J., VIJAY, V., SCOTTON, W., WAKERLEY, B. R., MATTHEWS, T. D., ANSONS, A., HICKMAN, S. J., BENZIMRA, J., RICK, C., SINGHAL, R., TAHRANI, A. A., BROCK, K., FREW, E. & SINCLAIR, A. J. 2021d. Effectiveness of Bariatric Surgery vs Community Weight Management Intervention for the Treatment of Idiopathic Intracranial Hypertension: A Randomized Clinical Trial. JAMA Neurology.

MOLLAN, S. P., WAKERLEY, B. R., ALIMAJSTOROVIC, Z., MITCHELL, J., OTTRIDGE, R., YIANGOU, A., THALLER, M., GUPTA, A., **GRECH, O**., LAVERY, G., BROCK, K. & SINCLAIR, A. J. 2021e. Intracranial pressure directly predicts headache morbidity in idiopathic intracranial hypertension. The Journal of Headache and Pain, 22, 118.

WESTGATE, C. S., BOTFIELD, H. F., ALIMAJSTOROVIC, Z., YIANGOU, A., WALSH, M., SMITH, G., SINGHAL, R., MITCHELL, J. L., **GRECH, O**., MARKEY, K. A., HEBENSTREIT, D., TENNANT, D. A., TOMLINSON, J. W., MOLLAN, S. P., LUDWIG, C., AKERMAN, I., LAVERY, G. G. & SINCLAIR, A. J. 2021. Systemic and adipocyte transcriptional and metabolic dysregulation in idiopathic intracranial hypertension. JCI Insight, 6.

YIANGOU, A., MITCHELL, J. L., FISHER, C., EDWARDS, J., VIJAY, V., ALIMAJSTOROVIC, Z., **GRECH, O**., LAVERY, G. G., MOLLAN, S. P. & SINCLAIR, A. J. 2021. Erenumab for headaches in idiopathic intracranial hypertension: A prospective open-label evaluation. Headache: The Journal of Head and Face Pain, 61, 157-169.

YIANGOU, A., MITCHELL, J. L., VIJAY, V., **GRECH, O**., BILTON, E., LAVERY, G. G., FISHER, C., EDWARDS, J., MOLLAN, S. P. & SINCLAIR, A. J. 2020. Calcitonin gene related peptide monoclonal antibody treats headache in patients with active idiopathic intracranial hypertension. The Journal of Headache and Pain, 21, 116.

CONTENTS

LIST OF FIGURES

LIST OF TABLES

LIST OF ABBREVIATIONS

18F-FDG PET: 18F-Fluorodeoxyglucose Positron Emission Tomography

α-KG: Alpha-ketoglutarate

ADP: Adenosine di-phosphate

AMY1: Amylin type 1 receptor

ATP: Adenosine triphosphate

ATPase: Adenosine Triphosphatase

cAMP: Cyclic Adenosine Monophosphate

Ca2+: Calcium

CBF: Cortical Blood Flow

CBP: Cyclic adenosine monophosphate-binding protein

CGRP: Calcitonin Gene-Related Peptide

CGRP-RA: Calcitonin Gene-Related Peptide Receptor Agonist

ChR2: Channelrhodopsin-2

Cl-: Chloride

CoQ: Coenzyme Q10

CSD: Cortical Spreading Depression

CSF: Cerebrospinal Fluid

CYT C: Cytochrome C

DC: Direct Current

dH_2O: Deionized Water

EcoRI: Restriction Enzyme EcoRI

F0: Baseline Fluorescence

F/F0: Fluorescence Ratio

FAD: Flavin Adenine Dinucleotide

FCCP: Carbonyl Cyanide-P-Trifluoromethoxyphenylhydrazone

FHM: Familial Hemiplegic Migraine

GCMS: Gas Chromatography Mass Spectrometry

GLUT: Glucose Transporter

GLP-1: Glucagon-Like Peptide 1

GLP-1RA: Glucagon-Like Peptide 1 Receptor Agonist

GPCR: G-Protein Coupled Receptors

H_2O_2: Hydrogen Peroxide

HindIII: Restriction Enzyme HindIII

ICP: Intracranial Pressure

IIH: Idiopathic Intracranial Hypertension

KCl: Potassium Chloride

Mg: Magnesium

mAbs: Monoclonal Antibodies

Na+: Sodium

NaCl: Sodium Chloride

NAD: Nicotinamide Adenine Dinucleotide

NADH: Nicotinamide Adenine Dinucleotide (Reduced Form)

NMR: Nuclear Magnetic Resonance

PFA: Paraformaldehyde

PBS: Phosphate-Buffered Saline

PCOS: Polycystic Ovary Syndrome

PER: Proton Efflux Rate

PI3K/Akt: Phosphoinositide 3-Kinase/Protein Kinase B

Pka: Protein Kinase A

Pvul: Restriction Enzyme Pvul

ROI: Region of Interest

RT: Room Temperature

SaCSF: Artificial Cerebrospinal Fluid

SEM: Standard Error of the Mean

SUIT: Substrate-Uncoupler-Inhibition Titrate

TBI: Traumatic Brain Injury

TCA: Tricarboxylic Acid Cycle

THY1: Thymus 1

TNC: Trigeminal Nucleus Caudalis

WT: Wild Type

XF: Extracellular Flux

YFP: Yellow Fluorescent Protein

^{1}H-MRS: Proton Magnetic Resonance Spectroscopy

^{31}P-MRS: Phosphorus-31 Magnetic Resonance Spectroscopy

CHAPTER 1 INTRODUCTION

1.1 Headache

Headache disorders are classified as primary if idiopathic or secondary if resulting from another cause or condition.[1] Despite having a significant morbidity internationally,[2] headache disorders do not receive sufficient social or clinical attention.[3] Moreover, the mechanisms underlying pathology and risk factors of headache are not fully understood, leading to limited targeted therapeutics.

1.1.1 Epidemiology of headache disorders

Headache disorders are ranked the second most prevalent disease worldwide,[4] with migraine in particular affecting 1 billion people.[5] The estimated global prevalence of headache disorders is 52.0% and it is approximated that on any given day, 15.8% of the world's population experience headache.[2] Migraine in particular is more common in females (3:1) with a prevalence of 18.9% in women versus 9.8% in men,[6] and is the most disabling condition in young women worldwide.[7]

Not only is migraine highly prevalent, but the costs associated are high as the burden of migraine peaks at 35-39 years of age;[5] typically, the most productive career years. This is estimated to cost €93 billion in Europe[8] and $13 billion in the United States per annum,[9] due to healthcare fees and lost productivity. For instance, an individual suffering from migraines in the UK will miss an average of 11.4 workdays each year, contributing to an annual loss of approximately 86 million workdays.[8]

In addition to economical loss, migraine significantly reduces quality of life,[10] and is often comorbid with stress, anxiety and depression.[11] Migraine is the leading cause of disability amongst neurological disorders,[12] but does not receive equivalent funding to other neurological disorders such as Parkinson's disease.[13] Despite the recent advances in migraine therapeutics, disability measures have not improved between 1990 and 2016,[14] inferring that improvements in therapeutics have not enabled a decrease in disability. Therefore, headache disorders remain an important target of therapeutic development and research.

1.1.2 Migraine pathophysiology

Although migraine likely stem from the interplay of various neuronal structures and pathways, two mechanisms are commonly proposed as underpinning migraine development and pain. These pathways involve heightened sensitivity of the trigeminal system, and modified brain excitability and neurovascular dynamics.[15]

1.1.2.1 Trigeminal sensitization

Sensitization of the trigeminovascular system is a pivotal mechanism in headache nociception. This system consists of 1st order trigeminal nerves originating from the trigeminal ganglion and upper cervical dorsal roots, which innervate cerebral blood vessels and dura mater. Signals are then transmitted to 2nd order trigeminal nerves in the trigeminal nucleus caudalis (TNC) and project to 3rd order neurons in the thalamus. Neurons in the sensory cortex then transmit nociceptive information

(Figure 1).[16] The thalamus has bidirectional connections with several regions including the somatosensory cortex and amygdala. These networks integrate nociceptive inputs with cognition, emotion, and autonomic responses forming the complex “pain matrix”.[17]

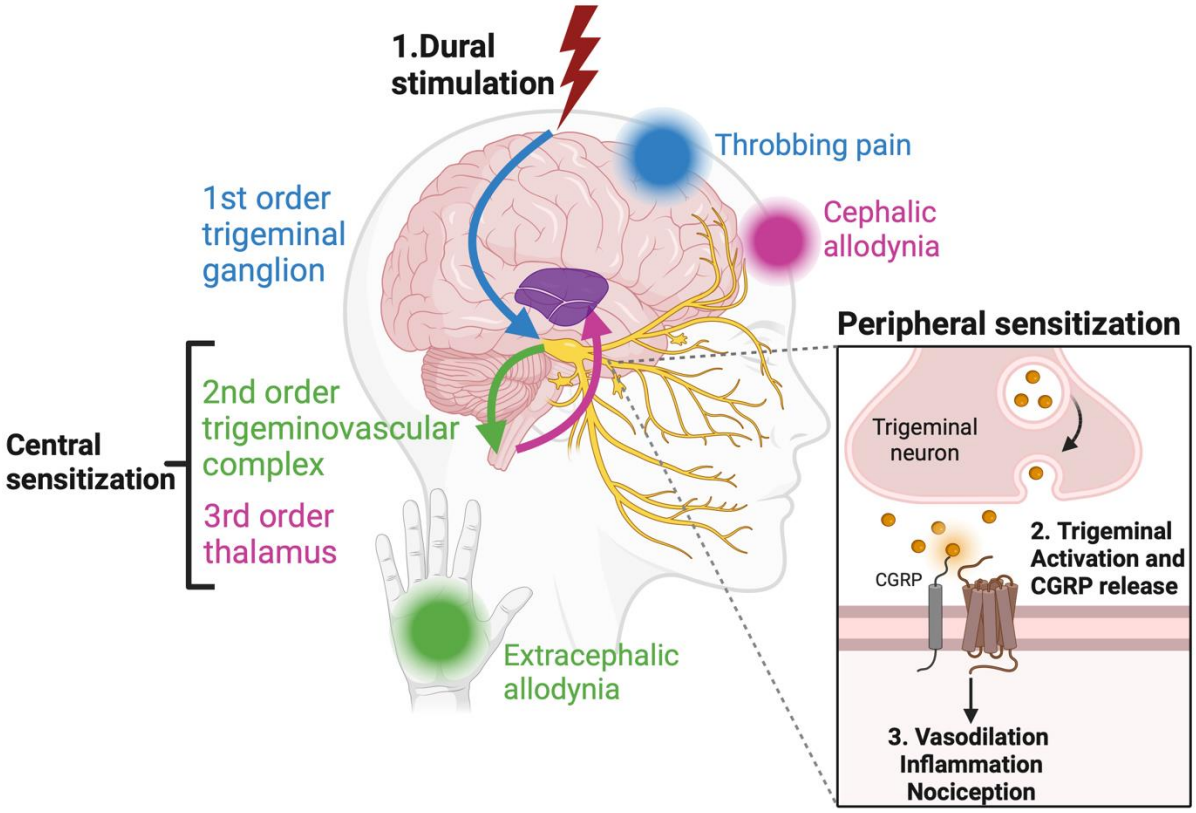

Figure 1. Organisation of the trigeminal nerves involved in headache perception including central and peripheral sensitization.

Dural stimulation (lightning bolt) activates 1st order trigeminal nerves leading to peripheral sensitisation, which is responsible for throbbing pain. This is facilitated by nociceptive peptide release including CGRP. Peripheral input is received by 2nd order trigeminal nerves in the TNC and project to 3rd order neurons in the thalamus. This process underlies central sensitization and results in allodynia. CGRP; calcitonin gene-related peptide, TNC; trigeminal nucleus caudalis. Figure created with BioRender.

Heightened sensitivity and increased responsiveness to stimuli in peripheral nerve trigeminals underlies peripheral sensitisation.[18] In experimental animal models, dural stimulation causes release of nociceptive peptides such as calcitonin gene-related peptide (CGRP) and substance P (Figure 1) from trigeminal nerves.[19] This results in lowered activation thresholds increasing sensitivity to mechanical stimuli,[20] and is hypothesised to underlie the throbbing pain of headache. Second order neurons in the TNC receive repetitive peripheral input, and sensitisation is thought to underlie cephalic allodynia.[19 21] In response to stimulation, central trigeminovascular neurons develop hypersensitivity in the periorbital skin.[22] Prolonged activation of 2nd and 3rd order neurons is hypothesised to drive the transition from episodic to chronic migraine.[23] Understanding the factors which initiate sensitization are important to prevent headache attacks and chronification of migraine.

1.1.2.2 Calcitonin gene-related peptide

Trigeminal afferents express a variety of receptors targeted by nociceptive and vasoactive agents, whose activation promotes allodynia, hyperalgesia, and induces headache attacks.[24] A significant molecule released by trigeminal afferents is CGRP, a 37-amino acid peptide, which has recently become a target for effective migraine therapeutics.[25 26]

CGRP receptors are within the B subclass of G protein-coupled receptors (GPCR) composed of a receptor activity-modifying protein 1, calcitonin receptor-like receptor and receptor component protein.[27] The binding of agonists to the CGRP receptor induces a conformational change and interaction with various G proteins to facilitate diverse signalling pathways. This includes activating adenylate cyclase driven by Gαs

proteins, increasing cAMP levels and activating protein kinase A.[28] Gαq/11 signalling additionally activates phospholipase C,[29] mitogen-activated protein kinase activation, nitric oxide (NO) production,[30] and a range of transcriptional events.[31]

CGRP exists in two forms: an α-isoform found in primary spinal afferents from sensory ganglia and a β-isoform predominantly located in the enteric nervous system.[32] α-CGRP pathways underlie cAMP-mediated vasodilation in cerebral and meningeal arteries, contributing to migraine pathophysiology. Additionally, α-CGRP acts within the TNC to facilitate nociceptive signal transmission.[33] Abundant evidence underscores the role of CGRP in migraine nociceptive signalling, including increased plasma CGRP during migraine attacks,[34] the capacity of CGRP administration to trigger attacks in individuals with migraine without aura,[35] and trials showcasing the efficacy of CGRP-attenuating agents in alleviating migraine pain.[26]

1.1.2.3 Cortical spreading depression

Evidence also suggests that changes in cerebral cortex hyperexcitability and cortical blood flow (CBF) play a role in headache generation and migraine pathophysiology.[36] [37] Hyperresponsiveness of the cortex may underlie associated symptoms of migraine, with changes in excitability of the visual cortex associated with photophobia and of the auditory cortex corresponding to phonophobia.[38] Moreover, some hereditary forms of migraine (familial hemiplegic migraine (FHM)), are characterised by mutations in the Na^+/K^+ pump,[39] or voltage gated Ca^{2+},[40] or Na^+ channels,[41] resulting in a lowered threshold for neuronal activation.[42]

A predominant mechanism of aura in migraine is cortical spreading depression (CSD): a wave of depolarization propagating slowly (2 to 5mm/min) across the

cortical surface, leading to release in neuropeptides and alterations in CBF.[43-45] Significant changes in ion levels occur during spreading depolarization, involving elevated extracellular K^+ concentrations, intracellular influxes of Na^+ and Cl^-, and the release of glutamate (Figure 2), all of which contribute to the propagation of depolarization.[46] [47] Following these extensive shifts in ion distributions, and tissue excitability, a phase of inhibited electrical and synaptic activity follows, referred to as neuronal silencing. This phenomenon has been recorded in humans[43] and can similarly be experimentally induced in animals.

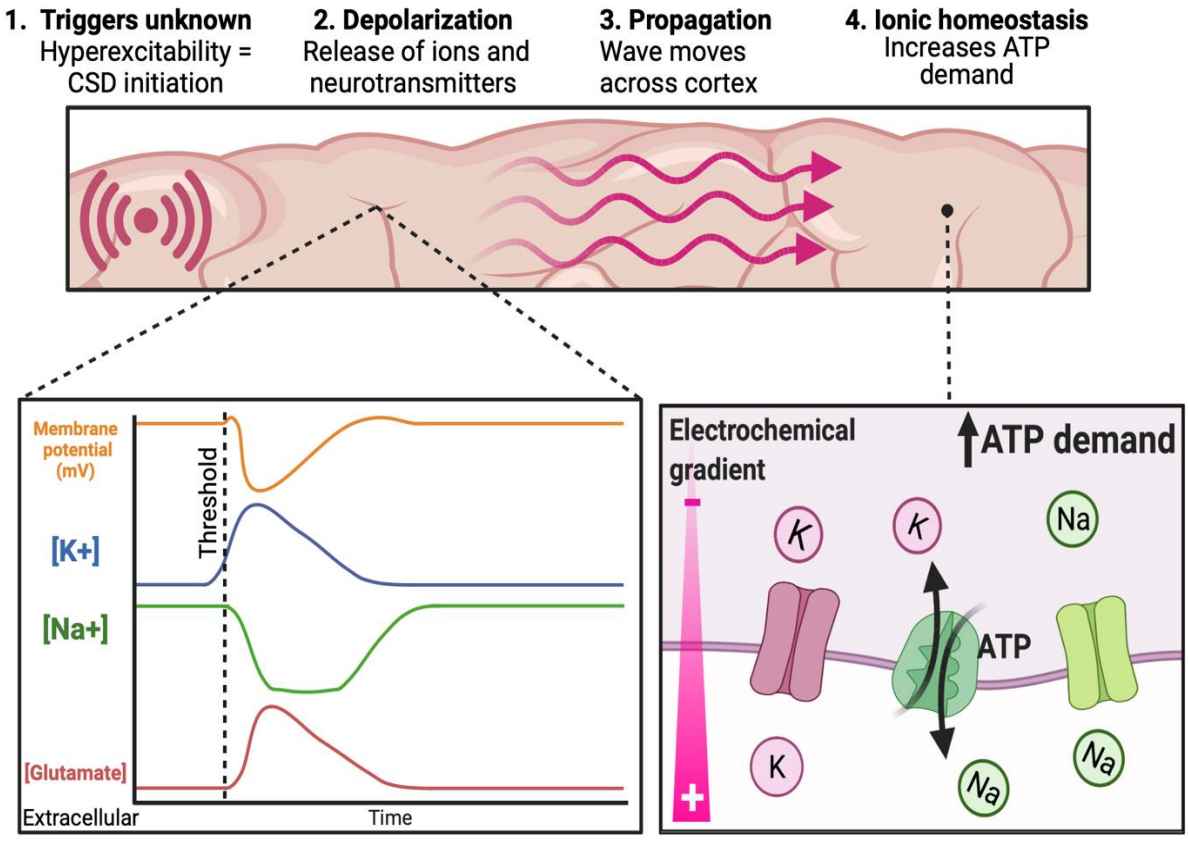

Figure 2. Changes in membrane potential, ion and neurotransmitter concentrations which occur during CSD, leading to an increase in ATP demand.

Triggers of CSD are poorly understood but initiate depolarisation driven by changes in membrane potential, K^+ Na^+ concentrations and glutamate release. This propagates the spread of depolarization across the cortex and causes an increase in ATP demand to restore ionic gradients. (Adapted from [48]) ATP; adenosine triphosphate, CSD; cortical spreading depression, K^+; potassium, mv; millivolts, Na^+; sodium. Figure created with BioRender.

Functional imaging studies have associated this neurophysiological event with migraine with aura, a subtype which features visual, sensory, or central nervous system symptoms preceding headache attack.[1] [49] CSD has also been recorded in traumatic brain injury (TBI), stroke and subarachnoid haemorrhage.[49-51] Although the exact implications of CSD in headache pain are yet to be revealed, mechanistic insights from animal studies suggest that CSD can activate meningeal nociceptors, stimulate CGRP release,[52] and induce pain and anxiety behaviour in rats.[53] Hence suggesting that CSD may also contribute towards headache generation and pain.[54] CSD serves as an important translational model as evidenced by the impact of CGRP-blocking drugs on reducing the intensity of CSD or increasing thresholds in some experimental animal models.[52] [53]

1.1.3 Secondary headache disorders

Several secondary headache conditions exhibit headache symptoms resembling those of migraines. These conditions include post-traumatic headache[55] and headache associated with idiopathic intracranial hypertension (IIH).[56] IIH headaches are driven by elevated intracranial pressure (ICP)[1], and some studies have indicated that reducing this pressure can alleviate headache.[57] Despite the normalization of

ICP, many individuals continue to experience persistent post-IIH headache that closely mimic migraines.[58]

The importance of CGRP has also began to emerge in secondary headache disorders, wherein infusion in post-traumatic headache patients induced headache attacks.[59] Moreover, CGRP therapeutics have also exhibited efficacy in both post-traumatic headache[60] and IIH patients,[58 61] indicating that this molecule may also play a role in secondary headache pathophysiology. The exploration of the biological underpinnings for shared characteristics between migraine and post traumatic headache suggest shared biological foundations.[62]

1.1.4 Animal models of headache

Progress in the knowledge and treatment of headache hinges upon translational animal models. Nevertheless, replicating the complex nature of human headache disorders in their entirety has proven to be challenging. The subjective nature of headache pain and reliance on verbal scoring of pain makes it difficult to assess in animals. Moreover, since little is known about the genetic component of migraine it is challenging to create transgenic animals, and a lack of well-established biomarkers further complicates these models.

1.1.4.1 Headache symptoms and pain models

The modelling of headache pain is frequently accomplished by sensitizing elements of the trigeminovascular system. This is achieved via techniques such as electrically stimulating trigeminal ganglia, applying inflammatory substances to the meninges, administering nociceptive peptides such as CGRP, or allogenic substances such as

nitric oxide donor nitroglycerin (NTG) (Figure 3).[22] [63-65] Although this allows investigation of nociceptive structure activation, these models are often invasive and separating headache-specific pain from pain associated with experimental procedures may be difficult to achieve.[66]

While such models explore nociception in the context of headache, a significant constraint lies in the challenge of assessing pain sensation in animals (Figure 3). Electrophysiological techniques can be employed to evaluate changes in trigeminal activity and involve recording from the dorsal horn of the spinal cord where the trigeminal nucleus is located. Immunohistochemistry is also frequently utilised to quantify activation of nociceptive structures in response to stimulation. For instance, c-fos is a proto-oncogene used as an indirect marker of neuronal activity. Hence immunoreactivity for c-fos can map neuronal activity in trigeminovascular structures and thereby elucidate activation of headache pathways. [67] [68]

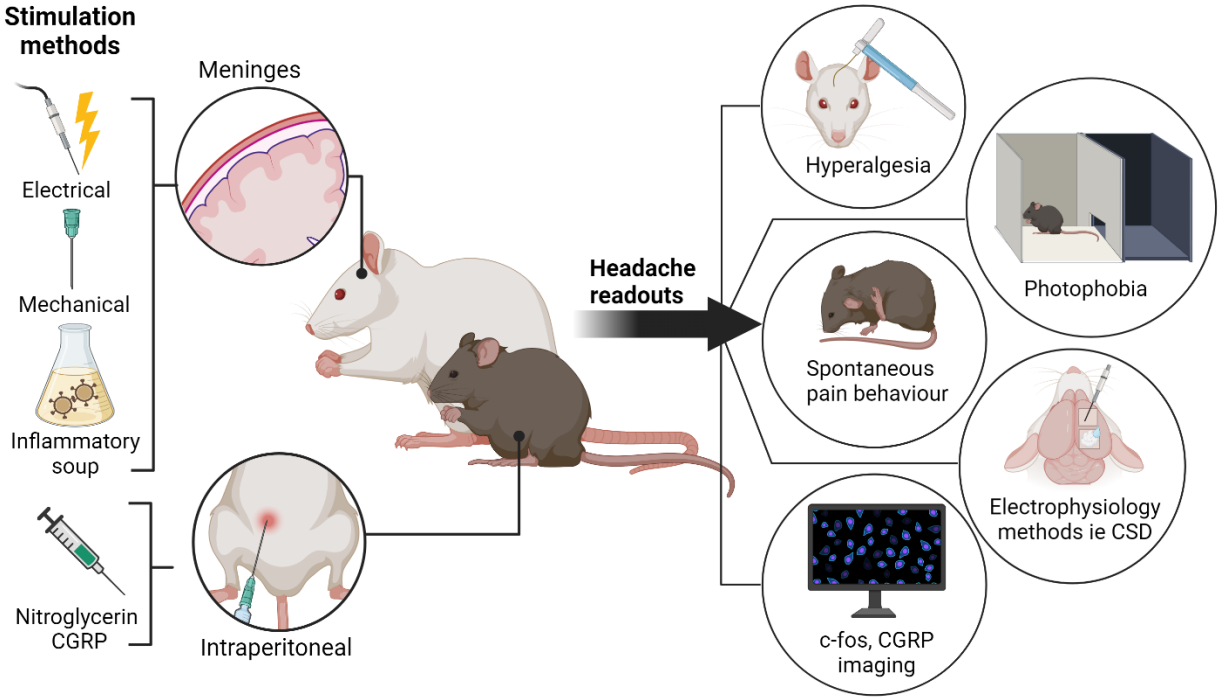

Figure 3. Animal models and headache measurements.

Typical stimulation methods and routes of administration in addition to commonly used readouts of headache pathophysiology. CGRP; calcitonin gene related peptide, CSD; cortical spreading depression. Figure created with BioRender.

Behavioural cues can also be employed in animal models to evaluate the efficacy of potential pharmacological agents (Figure 3). Approaches include measuring spontaneous pain behaviour such as freezing, grooming, decreased locomotion, head shaking, and rearing as indicators of headache pain.[69] Testing withdrawal thresholds from heat stimulation elucidates to changes in thermal sensitivity.[70] Moreover, monitoring the behaviour of animals in light/dark boxes can be used to investigate photophobia.[70] Finally, measuring changes in mechanical thresholds of hind paw and periorbital areas can reveal shifts in sensitivity in extracephalic and cephalic cutaneous domains.[71] These changes mirror allodynia, perception of pain in response to normally innocuous stimuli, encountered by individuals with migraine.[57 72]

Animal models of headache can provide a readouts of multiple facets of headache disorders including changes in electrophysiological, biochemical and behavioural signals.

1.1.4.2 Cortical spreading depression models

Both *in vivo* and *in vitro* models of CSD are used to investigate changes in neuronal excitability. CSD can be induced in both awake and anesthetised animals using electrical, mechanical, or thermal stimulation, topical administration of inflammatory substances or concentrated solutions of KCl to the cortex.[54] [73] These stimuli induce action potential firing in cortical neurons and initiate depolarization across the brain. The ability to modulate CSD threshold in these paradigms provides a valuable experimental readout to determine the efficacy of drugs or evaluate tissue susceptibility.[74] Therapeutic attenuation of CSD, in some instances has a track record for translation into headache therapeutics[75] and is consequently a translationally relevant model. Interestingly, tonabersat, a gap junction inhibitor, which effectively inhibits CSD. has demonstrated mixed results both as an acute and prophylactic treatment.[76]

Despite the utility of these models, *in vivo* investigation of CSD has multiple drawbacks. Often these models require craniotomy and cortical exposure to allow delivery of agents or stimuli, which introduce confounding effects such as non-specific tissue damage. Moreover, the use of anaesthetic has been shown to alter CSD characteristics.[77] However, *in vitro* systems, such as acute brain slices, eliminate these factors while still mirroring numerous aspects of *in vivo* biological conditions.

Acute brain slices have emerged as invaluable models for comprehending cortical function, as they maintain the structural and functional characteristics of *in vivo* neural networks.[78 79] These platforms grant easier manipulation of tissue conditions, the ability to adjust susceptibility, and the validation of drug targets that might otherwise be impeded by the blood-brain barrier.[80] Slice models have played a pivotal role in examining the function of CGRP and precisely identifying its receptors,[52] in addition to investigating the mechanisms of TBI,[81 82] and stroke.[83 84] Modelling CSD in acute brain slices in the context of headache may help uncover molecular and metabolic pathways which contribute towards headache susceptibility.

1.1.5 Metabolism in headache

An imbalance between energy supply and demand in the brain has been hypothesized as a potential factor in the development and susceptibility of migraine.[85-87] Numerous studies have additionally indicated a primary malfunction of mitochondria as a contributing factor.[88] Various clinical trials have evaluated the effectiveness of nutraceuticals. For example, riboflavin, and coenzyme Q10, precursors and co-factors of the mitochondrial respiratory chain, respectively, have both exhibited the ability to reduce migraine attack frequency and severity, suggesting supplementing mitochondrial function is therapeutic.[89-92] However, often nutraceutical trials are small [89] with limited generalizability, lack appropriate placebo-control groups,[90 91] and have resulted in conflicting outcomes.[93 94] Therefore the use of supplementation or nutraceuticals for headache intervention has been hindered by the challenge of pinpointing dysfunctional metabolic pathways and targets.

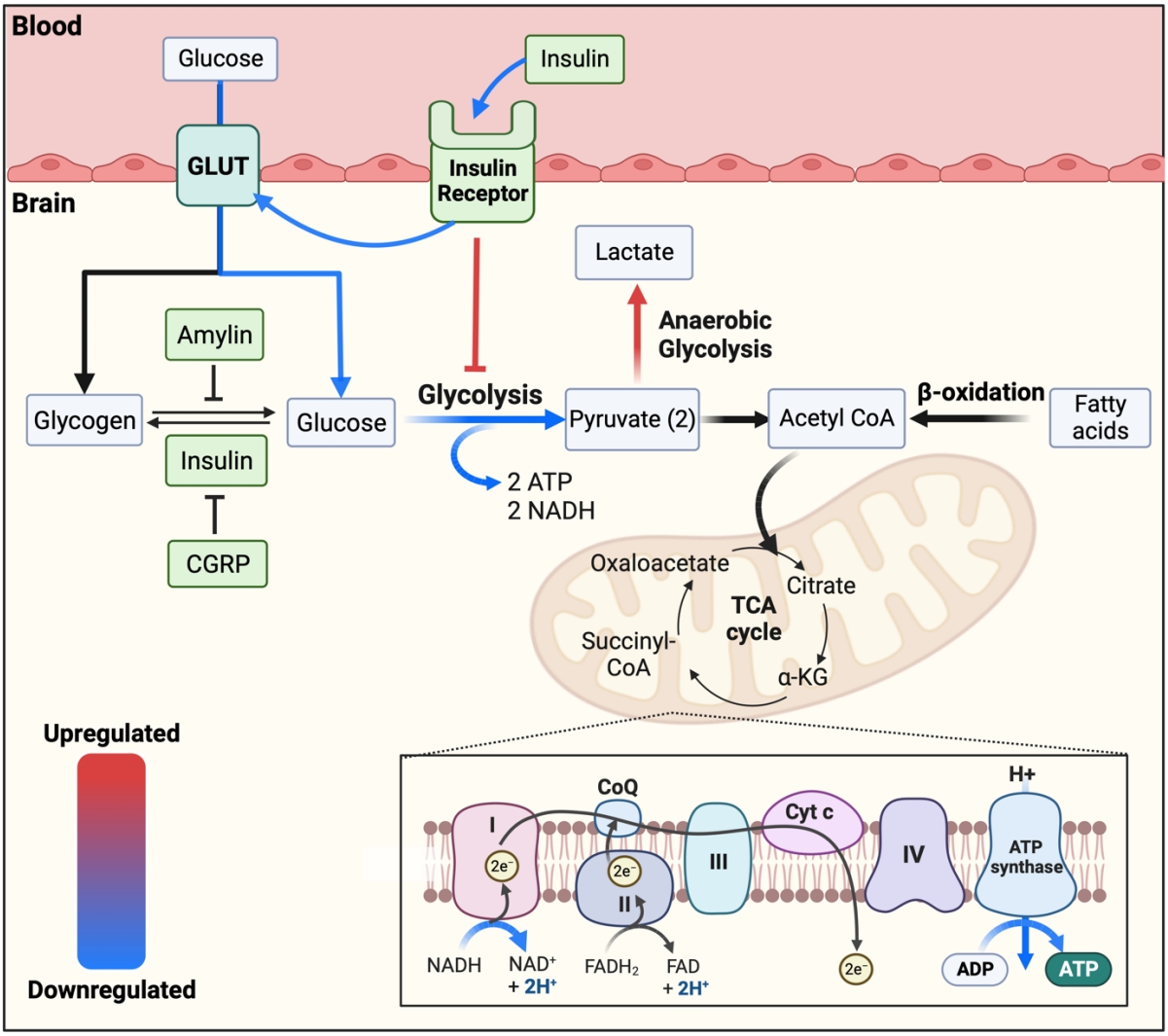

Figure 4. Hypothesised alterations in metabolic flux which may contribute to migraine pathophysiology.

The activity of numerous metabolic pathways is altered in migraine patients. Colour of arrows indicates upregulation (red) or downregulation (blue). Glucose hypometabolism has been exhibited in migraine in addition to upregulated lactate production. Reduced NADH oxidation and increased levels of ADP have additionally been recorded. α-KG: alpha-ketoglutarate, ADP; adenosine diphosphate, ATP; adenosine triphosphate, CoQ; coenzyme q, Cyt c; cytochrome c, FAD; flavin adenine dinucleotide, GLUT; glucose transporter, H+; hydrogen, NAD; nicotinamide adenine dinucleotide, TCA; tricarboxylic acid cycle. Figure created with BioRender.

1.1.5.1 Glucose metabolism

Glucose is the brain's primary energy source, and its metabolism is shared between neurons and astrocytes. Although neurons can facilitate both glycolytic and oxidative metabolism, they switch to glycolysis for rapid ATP production during increased energy demands.[95] Astrocytes are thought to have a metabolically supportive role and the astrocyte-neuron lactate shuttle (ANLS) theory suggests that although neurons primarily produce lactate from pyruvate, astrocytes convert pyruvate to facilitate oxidative phosphorylation. Neuronal lactate can be transported to astrocytes, converted back into pyruvate, and used for oxidative phosphorylation to produce ATP during increased energetic demand.[96]

Fasting is thought to be a strong headache precipitator,[97] and the triggering of migraine by fasting or skipping meals may relate to premonitory symptoms.[97 98] A study found that 58% of patients experiencing frequent migraines or tension-type headaches reported headaches linked to food deprivation.[99] The metabolism of glucose is of particular interest, as impaired insulin sensitivity and high fasting insulin has been observed in patients with migraine.[100 101] ^{18}F-Fluorodeoxyglucose PET (^{18}F-FDG PET) studies in episodic migraine have exhibited glucose hypometabolism in temporal[102] and fronto-temporal[103] regions involved in pain processing compared to controls.[104] Hypometabolism was also associated with disease duration,[102 104] suggesting that repeated migraine attacks and activation of nociceptive regions may lead to abnormalities in glucose metabolism (Figure 4). Moreover, treatment with trigeminal nerve stimulation not only decreased migraine attack frequency, but additionally improved hypometabolism, suggesting that improving glucose metabolism may be prophylactic in migraine.[103]

In rodent studies, inducing hypoglycaemia via food deprivation or insulin administration demonstrated a decrease in CSD thresholds and increased CSD duration.[105] [106] Spontaneous depolarisation events, have also been recorded in hypoglycaemic rats.[107] Conversely, hyperglycaemia increased CSD thresholds and decreased their frequency, thereby providing a protective effect.[105] These studies propose that glucose and glycolysis is imperative to maintaining adequate normal cortical excitability and increased CSD thresholds.

1.1.5.2 Lactate metabolism

Anaerobic glycolysis occurs in the absence of sufficient oxygen, resulting in lactate production which is often utilised as a pathological marker of hypoxia. Proton magnetic resonance spectroscopy (^{1}H-MRS) studies have highlighted elevated lactate in brains of FHM[108] and migraine with aura patients during interictal periods.[109] [110] Moreover, upregulated lactate has been measured interictally in the serum and plasma of migraine patients (Figure 4).[111-113] Excess lactate in headache sufferers may indicate mitochondrial dysfunction and further support the hypothesis of aberrant glycolysis.

Results of animal studies also suggest that lactate excess may be related to headache and CSD. During CSD in rats, ^{1}H-MRS measurements indicate a 2.8 fold increase in lactate.[114] Since CSD is highly oxygen-demanding, neuronal tissue may switch to the preferential use of anaerobic processes to produce ATP.[115] Moreover, studies have demonstrated that lactate is produced in excess by astrocytes and used as an energy substrate by neurons during recovery periods following CSD.[116] Although healthy neuronal tissue demonstrates plasticity to changes in energetic flux,

anaerobic respiration is less efficient at ATP production than aerobic. Therefore, permanent switches to anaerobic methods may contribute to pathology of migraine chronification.

1.1.5.3 Mitochondrial function and oxidative phosphorylation

Neurons rely primarily on oxidative phosphorylation for energy, a process hosted by mitochondria. ^{31}Phosphorus MRS (^{31}P-MRS) studies in migraine have consistently highlighted mitochondrial dysfunction. These studies exhibit increased ADP, the precursor to ATP,[88 117 118] and decreased reduced available free energy,[86 119 120] which are consistent with findings of mitochondrial cytopathies.[121 122] The peripheral blood transcriptome of migraine patients has also revealed alterations in oxidative phosphorylation-linked pathways.[113] These studies suggest an imbalance between energy demand and production which may underlie inability to maintain ionic milieu, thereby reducing threshold for CSD or migraine attack.

Preclinical models have demonstrated an initial surge in NADH oxidation and ATP production, followed by an extended period of reduced oxidation during CSD.[115 123 124] Recurring CSD events have resulted in changes in the oxidative capacity of neural tissue, suggesting enduring metabolic shifts.[123] CSD also leads to reduced mitochondrial membrane potential and thus diminished ATP synthase activity.[125] Biochemical investigations have highlighted fragmented structure and modified biogenesis of mitochondria in trigeminal ganglion neurons following repetitive dural sensitization in rats.[126]

Evidence of mitochondrial alterations have additionally been identified in secondary headache disorders such as IIH. Lactate:pyruvate ratio was altered in the CSF and

serum of IIH patients, which is a marker characteristic of oxidative phosphorylation disorders and pyruvate dehydrogenase deficiency.[127 128] This ratio has additionally been identified in TBI,[129] subarachnoid hemorrhage,[130] and hydrocephalus,[131] suggesting that this may be characteristic of elevated ICP.

Differentiating between migraine-specific metabolic changes and the effects of chronic disease on mitochondrial dysfunction, however, is difficult. Oxidative damage is a key pathogenic pathway involved in numerous neurodegenerative disorders, including Alzheimer's and Huntington's.[132 133] In parallel with migraine, obesity and type 2 diabetes, lowered rates of oxidative phosphorylation and excessive reactive oxygen species production have been reported.[134] Additionally, reduced glucose metabolism and excess lactate production are markers not only in migraine,[103 111-113] but also in Huntington's.[135 136] Diminished oxidative phosphorylation has been recorded in the basal ganglia of Huntington's patients, suggesting that brain excitotoxicity may lead to mitochondrial dysfunction.[137] Collectively, these studies suggest functional deficiencies in mitochondria shared across migraine, secondary headache and other chronic disorders which may be potential avenues for therapeutic intervention.

1.1.6 Current therapeutics for migraine

Recent decades have led to the development of migraine therapeutics which offer improved specificity to headache pain and migraine symptoms compared to non-steroidal anti-inflammatory drugs. Noteworthy classes of medications include acute therapies 5-$HT_{1B/1D}$ receptor agonists (triptans) and CGRP drugs which are used as preventative treatments including receptor antagonists (gepants) and antibodies.

1.1.6.1 5-HT$_{1B/1D}$ receptor agonists

Triptans are serotonin 5-HT$_{1B/1D}$ receptor agonists which have multiple modes of actions to treat migraine. Vascular studies have demonstrated that triptans were able to vasoconstrict abnormally dilated vessels which were associated with migraine.[138]

Triptans are additionally believed to have central activity, since they can inhibit neurotransmitter release from trigeminal nerves[139] and reduce trigeminal nerve activation,[140] thus preventing nociceptive transmission. In addition to aborting headache pain, triptans have demonstrated efficacy in treating migraine related symptom such as photophobia and nausea.[141]

Triptans are not, however, effective for all patients. Only 30-40% experience freedom from pain at 2 hours,[142] and in a third of patients who don't respond, headache reoccurs within 24 hours.[143] Due to their vasoconstrictive properties, triptans also have contraindications in those with cardiovascular diseases.[144] Since migraine is a risk factor for development these disorders, this prevents a large proportion of patients from using these drugs.[145 146]

1.1.6.2 CGRP receptor antagonists and antibodies

The emergence of CGRP therapies has brought about a ground-breaking shift in the management of migraines. These medications circumvent vasoactive effects[147] and represent the first class of drugs designed to target the trigeminal system.[148] CGRP therapies can be classified into two main categories: antagonists, known as gepants, which act at the CGRP receptor,[148] and monoclonal antibodies (mAbs) that can either target CGRP molecules directly or the canonical CGRP receptor.

Gepants, block the binding of CGRP to its receptor, preventing cAMP production and vasodilation.[149] Clinical trials have found that olcegepant for example, can induce freedom from pain and sustain response for over 24 hours in migraine patients.[150] Moreover intravenous olcegepant was also able to improve related migraine symptoms such as photophobia and nausea.[150] Preclinical models have additionally demonstrated the efficacy of gepants to target several aspects of migraine pathophysiology. Studies demonstrate the ability to prevent hyperalgesia and trigeminal sensitization,[151 152] as well as inhibit release of pro-inflammatory cytokines, thereby preventing downstream neuroinflammation.[152] Only a small percentage of gepants cross the blood-brain barrier,[153] which has led to debate regarding the most efficacious location of action for migraine drugs.

MAbs are additionally used as preventative treatments for episodic[154] and chronic migraine.[155] MAbs are much larger than gepants and are believed to have limited access across the blood brain barrier.[153] Antibodies targeting CGRP itself result in reduced free ligand, and the percent of binding has been correlated with clinical efficacy.[156] Erenumab, is currently the only CGRP mAb which targets the receptor and was the first medication approved in the United States to prevent migraines.[154] Combining gepants and mAbs may provide a multi-faceted approach to attenuating CGRP signalling and thereby preventing trigeminal nociception.

1.2 Idiopathic Intracranial Hypertension

IIH is a neurological disorder characterized by raised ICP with unknown etiology.[157] Patients suffer a risk of visual loss due to compression of the optic nerve, however headache is the principal driver of IIH morbidity and is present in up to 95% of

patients.[158] IIH is considered a secondary headache disorder, however, the mechanisms underlying headache due to raised ICP remain unknown, and therefore targeted therapies are lacking.

1.2.1 Epidemiology

The prevalence of IIH is approximately 2.2 cases per 100,000 in the general population.[159] However, among women who are obese, this prevalence rises significantly to 21.4 cases per 100,000.[159] Despite being previously considered a rare condition, IIH is closely intertwined with obesity rates and is rising in parallel with the global obesity epidemic.[160] [161] Notably, in the United Kingdom, the incidence of IIH has increased by 118% from 2002 to 2016, rising from 3.53 to 7.69 cases per 100,000 within the female population.[162] This surge is accompanied by a 442% increase in hospital admissions, including emergency visits and inpatient stays.[162]

This upward trajectory poses a growing concern for public health, given that IIH inflicts a significant economic burden on healthcare systems. In England, the annual hospital costs escalated from £9.2 million to £49.9 million between 2002 and 2014, with projections anticipating costs to increase to £462 million by 2030.[162] Hospital admissions have also increased in the United States, with costs surpassing $444 million including loss of work-related income.[163] Recurring hospital admissions may be indicative of the social disadvantages linked with IIH, [164] shedding light on the historical inefficacy of treatment approaches for this condition.

1.2.2 Pathophysiology

The exact mechanisms driving IIH remain elusive; nevertheless, several proposed pathways contribute to increased ICP. These encompass modifications in cerebral spinal fluid (CSF) dynamics, such as hypersecretion or drainage obstruction, as well as the involvement of obesity and androgens,[165] [166] in addition to dysfunctional metabolism.[167]

1.2.2.1 Disturbances in CSF dynamics

While IIH is believed to be a multifaceted disorder, altered CSF dynamics serves as a pivotal converging pathway. The choroid plexus is the centre of CSF production and secretion. This structure is composed of specialized epithelial cells with Na^+/K^+ ATPase ion pumps which establish osmotic gradients and oversee CSF movement.[168] CSF plays a pivotal role in clearing proteins and metabolites from within the central nervous system, via the glymphatic system. The underlying causes of IIH are thought to revolve around either increased CSF section or the impairment of CSF drainage pathways.[169] Evidence to support this hypothesis include reduction in CSF protein levels,[170] and delayed uptake of radio-labelled tracer into the CSF, implicating compromised drainage in intracranial hypertension patients.[171] Moreover, diversion of CSF via lumbar puncture or surgery can be therapeutic for both headache and vision in patients with IIH,[172] implicating the role of excess CSF.

1.2.2.2 Androgen excess

The principal risk factors associated with IIH; female sex, obesity, and reproductive age,[173] point to a possible involvement of sex hormones in the pathophysiology of

IIH. Given the epidemiological profile, it is unsurprising that the prevalence of polycystic ovary syndrome (PCOS) is notably high in IIH, with rates ranging from 8.7% to 57%.[174-176] Interestingly, in comparison with women with PCOS or obesity alone, IIH patients exhibit higher levels of testosterone in the CSF and serum.[166] Heightened levels of androgens correlate with earlier onset in women.[177] Additionally there are instances of IIH developing in female-to-male transgender patients undergoing testosterone therapy,[178] with symptoms resolving upon discontinuation of testosterone.[178-180] *In vivo* studies of choroid plexus cells demonstrated that testosterone enhanced Na^+/K^+ ATPase activity, a surrogate for CSF secretion.[181] Moreover, the discovery of androgen receptors on the human choroid plexus[166] provides evidence for the involvement of androgen excess in heightened CSF secretion.[182]

Further exploration of endocrine patterns in IIH patients holds potential for shedding light on the connection between IIH and obesity, considering that adipose tissue may have an endocrine role in pathology.[182] Adipose tissue is a source of neuroendocrine and inflammatory molecules, which have shown differential regulation in IIH.[183] The functional consequences of these variations are yet to be fully understood.

1.2.2.3 Metabolic dysfunction

It is well established that IIH occurs almost exclusively (>90%) in women with obesity and weight gain and truncal adiposity are established risk factors for IIH development.[183-185] Recent metabolic studies have supported the notion that IIH is no longer considered an exclusively central nervous system disease, with mounting evidence suggesting systemic metabolic perturbations.[166 183 186]

Individuals with IIH exhibit heightened insulin resistance in the context of hyperleptinemia and excessive secretion of leptin from adipocytes.[183] Additionally, the omental and subcutaneous adipose tissues of IIH patients display a distinctive lipogenic profile which is genetically and metabolically primed to store more calories.[183] Individuals diagnosed with IIH also experience a twofold increase in the risk of cardiovascular disease in comparison to those with obesity.[164] NMR spectroscopy has additionally identified a metabolic profile in the CSF, serum and urine of IIH participants, which is indicative of global metabolic dysregulation.[167] This profile featured a perturbed lactate:pyruvate ratio, alterations in the hyperosmolar metabolite urea which may influence CSF dynamics and headache, and elevated CSF acetate, which was associated with headache morbidity.[167]

Therapeutic interventions in IIH have been shown to improve metabolism.[167] [187] Additionally, drugs which recover metabolic function are beneficial in IIH. Blocking the cortisol generating enzyme 11β hydroxysteroid dehydrogenase type 1 demonstrated the ability to reduce ICP in IIH.[188] Improving perturbations in metabolism in IIH may provide a novel therapeutic target for lowering ICP and alleviating related symptoms.

1.2.3 Headache pathophysiology

While raised ICP in IIH poses a significant risk of permanent visual impairment, headaches constitute the predominant feature and significantly reduces the quality of life for those affected.[189-191] Raised ICP headaches often fulfil migraine criteria,[192] and patients report related symptoms including photophobia, phonophobia, nausea and allodynia.[190] [193] Similarly to migraine, post traumatic headache, which also

features raised ICP, can be triggered by CGRP infusion.[194] Moreover, clinical studies have showcased the efficacy of CGRP antibodies in alleviating headaches in IIH.[58 61] Despite sharing many characteristics with migraine headaches, the precise mechanisms underlying IIH-related headaches remain elusive. Increasingly, off-label migraine treatments are used to manage headache in IIH, although formal evidence of effectiveness is lacking.[172] Excessive use of common analgesics, opiates, and non-steroidal anti-inflammatory drugs is prevalent in IIH, potentially leading to medication-overuse headaches.[195] Moreover, headache is evidently refractory in IIH, with twice as many women prescribed opiates compared to migraineurs, and a greater number of headache preventatives were prescribed.[195] Understanding the pathophysiology of raised ICP headaches helps unveil the therapeutic targets for drug development and thereby avoid medication overuse headache.

1.2.4 Animal models

1.2.4.1 IIH-specific animal models

Modelling IIH has so far proven difficult. This is mostly because the cause of raised ICP is idiopathic and the aetiology is likely to involve a complex interplay of androgen excess, perturbed metabolism, weight gain and dysfunction CSF dynamics. Consequently, there is currently no perfect IIH model, and instead, researchers have recapitulated IIH drivers in animals to better understand their pathology.

Weight gain and androgen excess are risk factors for the development of IIH, [166 183-185] therefore some studies have employed high fat diets and testosterone exposure to recreate this aspect of IIH. Consistently in these investigations, high fat fed animals have exhibited increased ICP (55-65%),[196-198] whilst exposing female

animals to testosterone excess led to a similar increase in ICP (55%).[197] These models reciprocate some of the aetiology of IIH and are capable of inducing changes in ICP independent of tissue damage or infection, therefore producing a more 'idiopathic' model. However not all obese women have raised ICP, and observed changes in ICP in obese animals may not represent the severity of ICP elevations demonstrated in patients. Moreover, although these models do demonstrate some changes in the retinal nerve fibre layer, papilledema, a hallmark of IIH is yet to be detected in obese animal models.[196]

There are limited *in vitro* models which allow for the investigation of raised ICP and IIH. Choroid plexus cell cultures have provided important insight into the mechanistic drivers of CSF in IIH and have demonstrated their usefulness as tools for therapeutic testing.[199] However investigating changes in ICP, requires a multifaceted interplay of CSF and vascular dynamics within an enclosed volume, which necessitates the use of animal models.

1.2.4.2 Raised ICP animal models

Other *in vivo* models are less specific to IIH and more broadly model raised ICP. These include methods which increase CSF volume within the ventricles and skull or prevent the drainage of CSF.

Hydrostatic fluid reservoirs can be used to introduce liquid into the ventricles by increasing the height of the reservoir and therefore utilising gravity to increase the speed and volume of infusion.[200 201] A cannula is implanted in the cisterna magna or lateral ventricles of rodents, often in conjunction with a ICP recording probe, facilitating both the introduction of raised pressure and its immediate recording. This system allows the manipulation of the severity of ICP in real time by altering the

reservoir height, in addition to rapid return to baseline allowing assessment of prior, during and after ICP fluctuations. However, such methods can only be used to investigate relatively acute increases in pressure, since long term maintenance of the reservoir in a freely moving awake animal is difficult.

Hydrocephalus is a neurological disorder which also features dysfunctional CSF dynamics and raised ICP. Experimental modelling of hydrocephalus *in vivo* provides a robust, model of moderately increased ICP.[199 202] This can be achieved by injecting a suspension of kaolin clay into the cisterna magna and depositing in the fourth ventricle.[203 204] This suspension often spreads into the subarachnoid space and leads to obstruction of CSF pathways and ventricular enlargement.[205-207] This model is advantageous as hydrocephalus typically develops quickly following kaolin injection (>24 hours),[208 209] meaning the effects of raised ICP can be investigated imminently. In comparison to fluid reservoirs this is also a moderately less invasive procedure, as kaolin injection can be performed percutaneously depending on species and age. Although this allows for the investigation of the direct consequences of raised ICP, this method induces an inflammatory response and structural changes to the brain (ventricle dilation)[202] which are not observed in IIH, thereby reducing the translational value of the model.

1.2.5 Therapeutics for IIH

A Cochrane review on IIH management concluded that there was an absence of evidence to recommend or reject the efficacy of treatments currently available for IIH.[210] A targeted therapy for headache due to raised ICP does not exist. Currently

there are three main categories for treatment of IIH: weight loss, surgical interventions, and pharmaceutical agents.

1.2.5.1 Therapeutic weight loss for IIH

Weight loss is therapeutic in IIH,[211 212] and is recommended to all typical IIH patients within the consensus guidelines.[172] Weight loss has proven to decrease ICP, reduce papilledema and alleviate headache.[211 212] In addition to improvement in clinical symptoms, weight loss also results in metabolic changes in IIH patients, signifying that this is a disease modifying intervention.[167]

A loss of between 3-24% of body weight is required to accomplish disease remission,[211 213] which is unlikely to be achieved without bariatric surgery. Furthermore, a recent study revealed that bariatric surgery was superior at lowering ICP compared to community weight loss interventions.[212] Bariatric surgery patients also exhibited a sustained reduction in ICP and improvement in quality of life after 2 years.[212] A direct association was identified between the change in weight and reduction in ICP in those following bariatric surgery.[214] Maintaining this level of weight loss however is difficult, and regain is associated with disease relapse.[215] Therefore, combining weight loss with pharmacological attenuation of CSF dynamics may provide an effective method at achieving remission.

1.2.5.2 CSF surgical interventions

Preserving vision is a priority for management of IIH, and in those who present with rapid loss of visual function surgical intervention may be required.[172 216] The aim of surgical methods is to remove CSF and thereby pressure on the optic nerve. These

interventions include diversion of CSF via ventriculoperitoneal or lumboperitoneal shunt, optic nerve sheath fenestration and frequent lumbar punctures.[217] However, determining the most effective method is difficult since there is a lack of trials evaluating each surgical intervention for IIH. Moreover, there is limited long-term efficacy and safety informing clinical practise of CSF diversion surgery and a third of patients require multiple revision surgeries.[218] This further highlights the need for effective therapeutics to lower ICP, which avoid multiple highly invasive surgeries.

1.2.5.3 Pharmacological targeting the choroid plexus

The choroid plexus is composed of epithelial cells which form the blood-CSD barrier, movement of ions across the epithelium creates an osmotic gradient driving movement of water. The activity of the Na^+/K^+ ATPase pump is closely associated with the secretion of CSD in the choroid plexus, in addition to the transport of HCO_3- and regulation via the Na^+/H^+ exchangers.[219] Glucagon-like peptide 1 (GLP-1) receptors are additionally found on the choroid plexus and agonism leads to conversion of ATP to cAMP via adenylate cyclase which has downstream effects on CSF pathways (Figure 5). Reducing CSF production by targeting transporters on the apical surface of the choroid plexus is a common goal for pharmacological IIH treatments such as carbonic anhydrase inhibitors acetazolamide[220] and topiramate (Figure 5).[221]

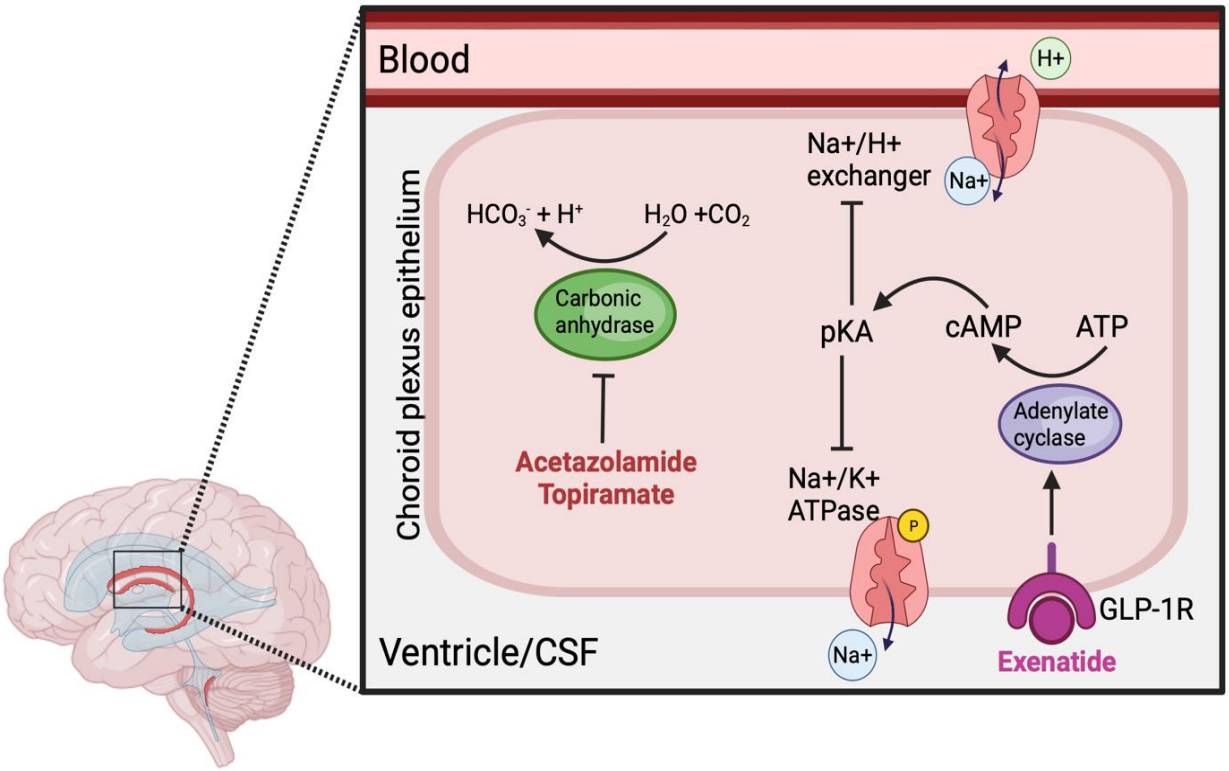

Figure 5. Mode of action of CSF altering drugs which target receptors on the choroid plexus epithelium.

Na^+/K^+ ATPase and Na^+/H^+ exchangers are transporters involved in CSF secretion which can be altered with agonism of the GLP-1 receptor via pKA. Acetazolamide and topiramate target carbonic anhydrase and production of HCO_3^- which is pivotal in CSF secretion (Adapted from [222]). ATP; adenosine triphosphate, cAMP; Cyclic adenosine monophosphate, CO_2; carbon dioxide, CSF; cerebrospinal fluid, GLP-1R; glucagon-like peptide 1 receptor, H+; hydrogen, HCO_3-; bicarbonate, K+; potassium, Na+; sodium, pKA; protein kinase A. Figure created with BioRender.

1.2.5.3.1 Carbonic anhydrase inhibitors

Acetazolamide is commonly the first line treatment for IIH.[220] It is a carbonic anhydrase inhibitor and although its action on CSF dynamics is not fully clear, it is able to prevent $HCO3^-$ production and reduce Na^+/K^+ ATPase activity (Figure 5).[223] Acetazolamide is however used off-label for IIH, and has only demonstrated a small improvement in visual field outcomes in patients with mild visual loss.[224] Moreover,

acetazolamide is not well tolerated, with previous trials reporting high discontinuation rates in IIH patients due to adverse effects such as tingling sensation, metallic taste and vomiting and diarrhoea.[225] [226]

Topiramate is also a carbonic anhydrase inhibitor and offers the added advantage of promoting weight loss potentially via appetite suppression and altering energy utilization.[227] There have been reports of topiramate alleviating symptoms in IIH,[228] [229] with more significant effects on ICP compared to acetazolamide.[230] In spite of these promising outcomes, topiramate is associated with undesirable side effects, including low mood, which is prevalent in IIH patients at baseline, cognitive side effects, nausea and anorexia.[231]

1.2.5.3.2 Glucagon like peptide 1

The GLP-1 receptor is a member of the class B GPCR family, similar to CGRP receptors. Upon activation of the receptor, there is a cascade of downstream signalling pathways mediated by G proteins. Agonist-activation of GLP-1 receptors increases levels of cAMP through activation of adenylate cyclase via Gαs signalling,[232] and initiates the phospholipase C pathway via Gαq signalling.[233] Downstream signalling can lead to alterations in membrane potential and induction of transcriptional changes depending on their location within the body.

GLP-1 receptor mRNA is expressed in a range of organs including the lung, stomach, adipose tissue, heart, kidneys, ovary and brain.[234] GLP-1 signalling is responsible for 70% of meal-stimulated insulin secretion.[235] Upon binding to receptors on pancreatic β-cells, GLP-1 initiates transcription of insulin likely thought

to be mediated by the family of CREB kinases.[236] GLP-1 receptor agonists (GLP-1RA) are existing therapies for diabetes.[237 238]

There is also widespread expression of GLP-1 receptor in the central nervous system where it governs various processes including regulation of gastric emptying, hepatic glucose production heart rate and blood pressure and specific neuroendocrine and behavioural responses to stress.[239] GLP-1 receptors are in high in the hypothalamus, central nucleus of the amygdala, anterodorsal thalamic nucleus,[240] which relates to its role in regulation of food intake and energy metabolism.[241 242] This function has been utilised in new licensed therapies for obesity, since GLP-1 agonists can lead to satiety.[243 244]

Receptors have additionally been located at the choroid plexus and increases in cAMP contribute towards inhibition of Na^+/H^+ exchangers, preventing Na^+ re-absorption from the blood, and Na^+/K^+ ATPase, diminishing Na^+ excretion into ventricles (Figure 5).[222] Together these reductions in Na^+ movement prevents the secretion of CSF.[199] Trials in animal models of raised ICP demonstrated the ability of GLP-1RA, exenatide, to reduce ICP with effects sustained for up to 2 weeks.[199] This reduction in ICP was greater than in comparison to other drugs commonly used in IIH.[245] Translation to clinical studies has also revealed the ability of exenatide to significantly lower ICP in IIH patients 24 hours, 2 weeks and 12 weeks following treatment.[246] GLP-1-R agonism has also exhibited therapeutic effects on headache, reducing monthly headache days in patients with IIH,[192 246] suggesting its suitability as a headache therapeutic in raised pressure.

1.3 Hypothesis and aims

Two related hypotheses were explored in this project. The first considered the therapeutic potential of understanding the metabolic disturbances following headache-related disruptions in neuronal function. The second explored the idea of shared mechanisms between ICP-related headache and migraine and the therapeutic potential of lowering ICP or blocking CGRP.

Hypothesis I:

There is a wealth of evidence to suggest that metabolic perturbations are involved in the pathophysiology of headache. Better understanding of the factors which increase the susceptibility to headache attack would provide novel therapeutic targets and in the context of altered metabolism may prove the benefits of using nutraceuticals. CSD is an energetically demanding event, therefore it is hypothesized that a plethora of metabolic changes will be detectable during and following a CSD event that may help explain the susceptibility of migraine patients to attack. To test this hypothesis the project explored the following aims:

- To establish and validate a *in vitro* brain slice CSD model, amenable to metabolic readouts at precise time-points during and after CSD.
- To use the CSD-based slice model to probe mitochondrial and metabolic function during CSD.
- Subject the brain slice model to glucose deprivation to investigate the role of glucose metabolism on the metabolic response to CSD.

Hypothesis II:

Considering the phenotype of raised ICP headache, and the evidence showing they can be both provoked, and alleviated with CGRP agents suggests, it was hypothesized a shared pathophysiology exists between raised ICP headache and migraine. To explore this hypothesis this project also aimed to:

- Establish a model of raised ICP that would facilitate both electrophysiological and behavioural measurements of headache.
- Investigate the effects of raised ICP on cortical activity and neurovascular responses to evoked CSD in addition to pain behaviours, which are models of migraine pathophysiology.
- Explore the effects of GLP-1R agonism on ICP and the consequences on cortical activity, neurovascular responses, and pain behaviours.
- Examine the results of blocking CGRP on ICP, CSD parameters and pain behaviours in the setting of raised ICP.

CHAPTER 2 MATERIALS AND METHODS

2.1 Animal Husbandry

Animals were used for experiments at two different licensed establishments. *Ex vivo* mouse work was conducted at the Biomedical Services Unit at the University of Birmingham, and *in vivo* rat work at the Hodgkin Biological Services at King's College London. All procedures complied with the UK Animals (Scientific Procedures) Act 1986 and in agreement with the ARRIVE guidelines under PPLs PP9890223 (King's College London) and PP1816482 (University of Birmingham).

2.1.1 *Ex vivo* experimental mice

Thy1-ChR2-YFP mice (B6.Cg-Tg(Thy1-COP4/EYFP)18Gfng/J Jackson Laboratories), were used for the majority of *ex vivo* experiments. The transgene features channelrhodopsin (ChR2) a light activated cation-selective ion channel fused to a yellow fluorescent protein (YFP) (Figure 6).[247] Mouse antigen thymus 1 (Thy1) drives protein expression in random subsets of neurons, resulting in ChR2-YFP in neurons of the brainstem, cerebellum, hippocampus, cortex and olfactory bulb.[247] Although this provides a non-invasive model to investigate CSD, by initiating action potential firing in cortical neurons with focal photostimulation,[248] it was not optimised in this thesis.

Male homozygous Thy1-ChR2-YFP animals were obtained from Jackson Laboratories and bred in-house with wild type (WT) females. To identify the genotype of animals, 2-10mg of ear tissue was taken with an ear punch sterilized with 70%

ethanol and stored in a 1ml Eppendorf tube. Ear tissue was sent to Transnetyx for automated genotyping using protocols from Jackson Laboratories.

Mice were housed in sex and litter matched groups in standard IVC cages in a climate-controlled room, kept on a 12:12 light/dark cycle and fed with standard rodent chow (EURodent Diet 14%, Labdiet). All animal handling and procedures were performed according to the guidelines specified by the UK Home Office and approved by the University of Birmingham's University Animal Welfare and Ethical Review Body (PP1816482).

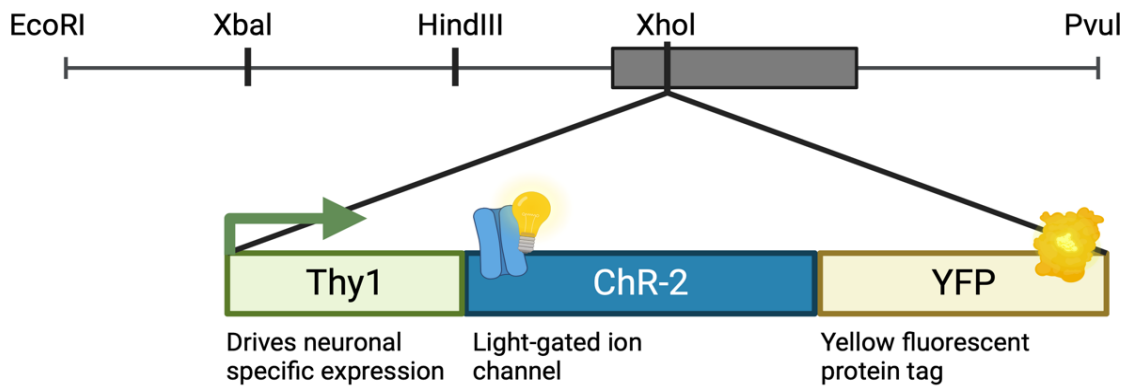

Figure 6. The Thy1-ChR2-YFP transgene construct.

ChR2; Channelrhodopsin-2, Thy1; Thymus 1, YFP; Yellow fluorescent protein. EcoRI, Xbal, HindIII, Xhol, Pvul denote restriction enzyme sites. Figure created with BioRender.

2.1.2 *In vivo* experiment rats

Since androgens and gender have a role in IIH, male Sprague Dawley rats (Enivgo) were used for *in vivo* raised pressure model experiments.[166] Rats were housed in litter matched same-sex groups in a climate-controlled room and kept on a 12:12

light/dark cycle with free access to food and water. All animal handling and procedures were performed according to the guidelines specified by the UK Home Office and approved by King's College University Animal Welfare and Ethical Review Body (PP9890223).

2.2 *Ex vivo* brain slice techniques

Optimizing an *ex vivo* platform capable of modelling headache mechanisms would help uncover metabolic pathways that contribute to brain hyperexcitability and trigeminal activation. Therefore, an acute brain slice platform which modelled CSD and allowed probing of metabolic function was optimized.

2.2.1 Acute brain slice preparation

Acute brain slices were prepared from Thy1-ChR2-YFP mice (male and female aged 10-27 weeks, both WT and heterozygous genotypes). Animals were euthanized by cervical dislocation and death confirmed by cessation of heartbeat. Animals were decapitated and the head sterilized with 70% ethanol. A sagittal midline incision was made through the fur, skin and skull, following which the brain was removed. The brain was placed in ice cold modified slicing artificial cerebrospinal fluid (SaCSF, Table 1) and the cerebellum removed to allow even coronal mounting onto a tissue specimen holder (Campden Instruments) using superglue (Gorilla Glue). Coronal slices were generated using a vibratome (Campden Instruments, 7000SMZ-2 Vibratome) fitted with a ceramic blade which created slices of 350μm thickness using a vibration frequency of 80Hz, amplitude 1.25 frequency and a blade advance speed

of 0.20mm/s. The brain and subsequent slices were collected in the vibratome tissue bath in ice-cold SaCSF which was bubbled with 95% O_2 and 5% CO_2.

Slices were immediately transferred using a cut pasture pipette to a submerged slice recovery chamber (tissue slice recovery chamber Model 7470, Campden Instruments) maintained at 35°C with an integrated gas bubbler supplying 95% O_2 and 5% CO_2. Slices were kept on netted sub-chambers in artificial cerebrospinal fluid (aCSF, Table 1). This allowed recovery of tissues following slicing and maintained the viability of the slices until the end of experiments. Slices were allowed to recover for 1 hour before proceeding (summarized in Figure 7).

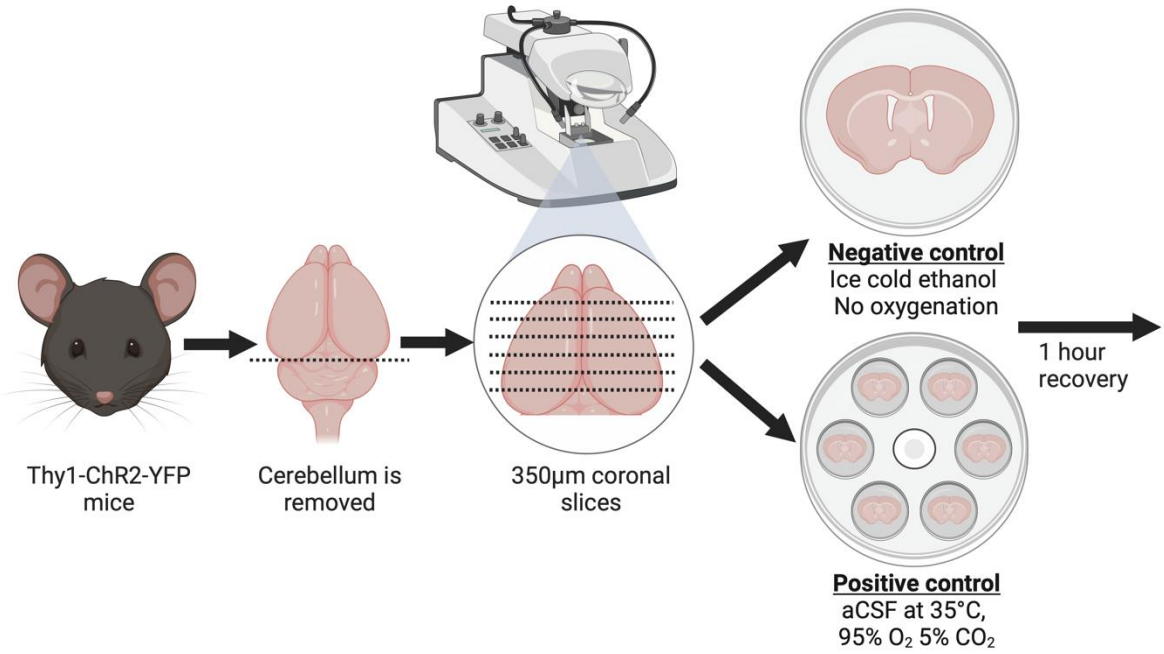

Figure 7. Overview of the workflow of the acute brain slice model.
After slicing with a vibratome the viability of slices was assessed by comparing those incubated in standard aCSF for 1 hour after slicing (positive control), to those exposed to 100% ethanol (negative viability control). aCSF; artificial cerebrospinal fluid, CO_2; carbon dioxide, O_2; oxygen, Thy1-ChR2-YFP; thymus-1, channel rhodopsin 2, yellow fluorescent protein transgenic animals. Figure created with BioRender.

2.2.1.1 Negative control slices

To ascertain results of metabolic investigation were due to CSD changes and not a reflection of the declining viability of the tissue following slicing, negative control slices were also assayed. Brain slices were moved directly from the vibratome to ice cold 100% ethanol and kept on ice without oxygenation for >1 hour (**Error! Reference source not found.**).

2.2.1.2 Acute brain slice solutions

Table 1. Chemical components of aCSF solutions dissolved in 1L dH_2O.
$CaCl_2$; calcium chloride, $MgCl_2$; magnesium chloride, KCl; potassium chloride, $NaHCO_3$; sodium bicarbonate, NaCl; sodium chloride, NaH_2PO_4; sodium phosphate monobasic.

Solution	**Chemical compound (mM)**						
aCSF	$NaHCO_3$ (26)	NaH_2PO_4 (1.25)	NaCl (125)	KCl (3)	$CaCl_2$ (0.002)	Glucose (10)	
SaCSF	$NaHCO_3$ (26)	NaH_2PO_4 (1.25)	NaCl (125)	KCl (3)	$CaCl_2$ (0.002)	Glucose (10)	$MgCl_2$ (5)
aCSF-glc	$NaHCO_3$ (26)	NaH_2PO_4 (1.25)	NaCl (125)	KCl (3)	$CaCl_2$ (0.002)		

2.2.2 CSD induction *ex vivo*

Topical application of KCl to cortical surfaces is a commonly utilised method of inducing a CSD both *ex* and *in vivo* in animal models.[73] [249] [250] Therefore CSD

induction was achieved by applying 1µL of KCl (2M) to the cortical region of acute forebrain slices.

2.2.3 Fluorescent labelling

2.2.3.1 Propidium iodide staining

To determine the viability of tissues and confirm negative controls, a membrane impermeable stain Propidium Iodide (PI, Sigma Aldrich) was used to label membrane rupture and cell viability in brain slices. Vibratome slices of forebrain (350µm) were incubated in either aCSF or 100% ethanol for 1 hour (described in 2.2.1.1). Slices were fixed in 4% paraformaldehyde (PFA) for 30 minutes at room temperature (RT) before incubation in 5µg/ml PI (in PBS) for 30 minutes at RT. Slices were washed three times in PBS and mounted onto slides using Aqua-Poly mount (Polysciences). Slides were stored at 4°C overnight to set before imaging a Zeiss LSM780 Confocal Microscope equipped with a 10x 0.45NA Water Immersion C-ACHROMAT Lens.

2.2.3.2 Caspase 3/7 labelling

NucView 488 (NucView® 488 Caspase-3 Assay Kit for Live Cells, Biotium), a fluorescence label of caspase 3/7 activity, was used to compare the viability of brain slices. Following incubation in either aCSF or 100% ethanol for 1 hour as described in 2.2.1.1, slices were incubated in 5µg/ml of NucView® 488 Caspase-3 Substrate for 30 minutes in oxygenated aCSF at 35°C. Slices were then washed three times with PBS and fixed in 4% PFA for 30 minutes. Following fixation, slices were mounted onto slides using Aqua-Poly mount (Polysciences, Inc.) and stored overnight at 4°C

to set. Subsequently, slices were imaged on a Zeiss LSM780 Confocal Microscope using a 10x 0.45NA, Water Immersed C-ACHROMAT Lens.

2.2.3.2.1 Caspase 3/7 imaging analysis

Z-stacks of 12 images were captured and analysed with ImageJ Fiji.[251] A 2D projection of the stack was made by taking the maximum intensity of each pixel and subtracting the background using a rolling ball radius of 40 pixels. The background was made white, and the image converted to a binary mask. A median filter was applied to reduce noise with a radius of 3.5 pixels and a watershed segmentation to separate overlapping cells. Finally, the Analyse Particles function was used to detect cells between 35-350 pixels^2 of 0-1.00 circularity. Data from two images per slice were averaged to give a single value for each slice.

2.2.3.3 Calcium indicators

The fluorescent calcium (Ca^{2+}) indicator Fluo-4-AM (Invitrogen™) was used to measure intracellular Ca^{2+} flux during CSD events. Fluo-4-AM was reconstituted with Pluronic acid (Pluronic™ F-127 (20% Solution in DMSO) Invitrogen™) to aid entry into cells. Slices were incubated in 2.5µM/ml Fluo-4-AM for 30 minutes in oxygenated (35°C, 95% O_2 5% CO_2) aCSF, and then washed in fresh warmed aCSF and transferred to a 35mm imaging dish (MatTek, P35GC-0-14-C) on a microscope stage.

2.2.3.3.1 Calcium imaging and analysis

Slices were imaged using an inverted microscope (Zeiss Axiovert200) equipped with a differential spinning disk module (Andor Technology, DSD Revolution) and a 10x 0.25NA dry objective. Fluo-4-AM signals were imaged with excitation at 488nm and emission at 520nm and images captured with a monochrome CCD camera (Andor Technologies, Clara).

During experiments a time series of images were captured at 2Hz. Following a baseline of 200 frames, 1µL KCl (2M) was added at the cortical edge and imaging was repeated for 400 frames. ImageJ Fiji was used to analyse Nuview488 signals.[251] 10 regions of interest (ROI) were manually selected approximately 200µm from the slice edge. The fluorescent intensity of all 10 ROI was averaged at each frame. The first 5 frames of both control and CSD recordings were averaged to calculate a baseline fluorescence (F0), and F/F0 was calculated to represent change in fluorescence over time.

2.2.3.4 Mitochondrial potential dyes

Rhodamine-123 (RH-123, Sigma) is a cell permeant fluorescent dye that is sequestered into active mitochondria. Brain slices were incubated in 1µM RH-123 in aCSF (35°C, 95% O_2 5% CO_2) for 15 minutes then washed three times in fresh aCSF. A single baseline image was taken, following which 1µL KCl (2M) was added to cortical edges. Changes in fluorescence were recorded in slices using a Zeiss

LSM780 Confocal Microscope using a 10x 0.45NA, Water Immersed C-ACHROMAT Lens. A stack of 230 images were captured with one frame every 3.87s.

2.2.3.4.1 Mitochondrial potential imaging and analysis

ImageJ Fiji was used to analyse image stacks.[251] 10 ROI were manually selected approximately 200µm from the area of stimulation. The fluorescent intensity of all 10 ROI was averaged at each frame. The mean of the first 3 frames was calculated to provide a baseline fluorescence (F0). F/F0 to represent change in fluorescence over time compared to baseline.

2.2.4 Respirometry

2.2.4.1 High resolution respirometry – Oroboros

The Oroboros Oxygraph-2K (O2k) oxygen system (OROBOROS Instruments, Innsbruck) was used to assess the mitochondrial activity of intact brain slices by measuring oxygen consumption rates in closed respirometry chambers. The O2k measures the rate of oxidative phosphorylation in tissues, in which oxygen is required as the final electron acceptor. By incubating slices with various combinations of respiratory substrates and mitochondrial complex inhibitors, respiratory states can be experimentally induced and interrogated.

Initially, chambers were oxygenated to 380-400 nmol/ml O_2 via injection of 3µL 200µM H_2O_2. Following a minimum of 1-hour recovery in the tissue slice recovery chamber, brain slices were weighed to normalise O_2 flux. Slices were then transferred to a calibrated Oroboros respirometer chamber containing 2.5ml of aCSF with 280 units/ml catalase warmed to approximately 37°C. Tissues were allowed to

equilibrate for 10 minutes without the presence of substrates and baseline respiration was measured.

2.2.4.1.1 Oroboros SUIT protocol

Once baseline oxygen flux had stabilised, a substrate-uncoupler-inhibition titrate (SUIT) protocol was used, in which a series of substrates were added in succession to investigate respiratory control (Table 2, Figure 8). Substrates were added using a Hamilton syringe (Hamilton Company) in the following order: 0.05mM malate, 0.2mM octanoyl-carnitine, 5mM ADP, 2.05mM malate, 10mM glutamate, 10mM succinate, 0.25µM FCCP, 0.5µM rotenone and finally 2.5µM antimycin A.

H_2O_2 was added to both chambers when oxygen concentrations decreased to lower than atmospheric levels (approx. 180µM), to prevent tissues experiencing hypoxia. Oxygen consumption and flux rates were normalised to tissue weight and calculated using DatLab 7.4 (Oroboros Instruments) by averaging the stable response of slices following addition of substrates.

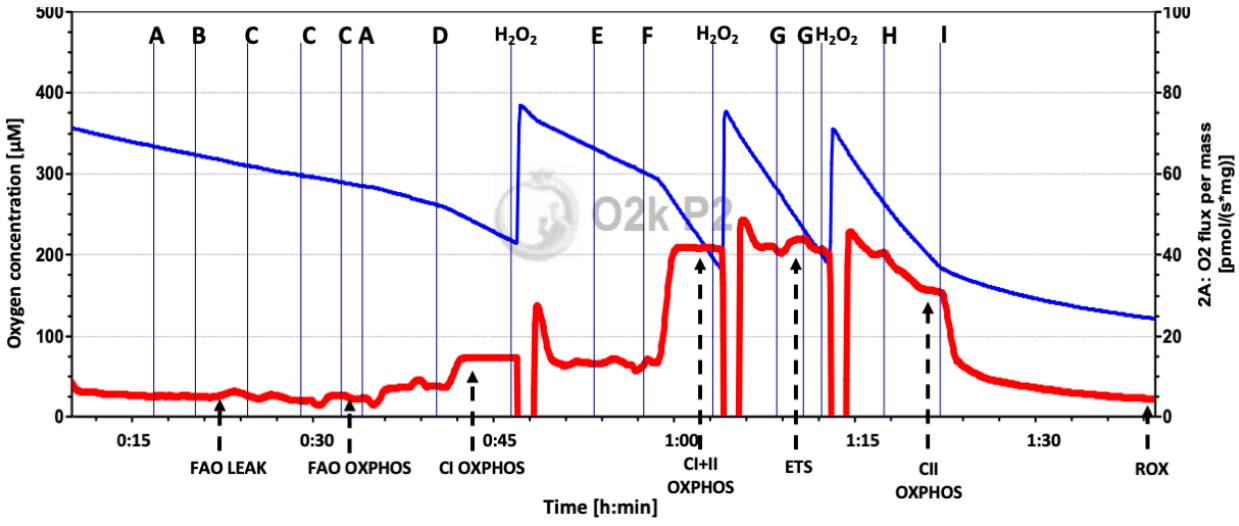

Figure 8. Example trace of a Oroboros measurement using a SUIT protocol.

The blue line indicates absolute O_2 concentration (μM) while the red line represents O_2 flux (pmol $O_2/s^{-1}/mg^{-1}$). A – malate, B – octanoyl carnitine, C – ADP, D – glutamate, E- cytochrome C, F – succinate, G- FCCP, H - rotenone, I – antimycin A. CI OXPHOS; complex I oxidative phosphorylation, CII OXPHOS; complex II oxidative phosphorylation, CI + II OXPHOS; complex I and II oxidative phosphorylation, ETS; electron transfer state, FAO LEAK; fatty acid oxidation leak, FAO OXPHOS; fatty acid oxidative flux ROX; residual, non-mitochondrial respiration.

Table 2. Substrates and their site of action used in the SUIT protocol.

Listed in the order of which they were added and the pathways they are involved. ADP; adenosine diphosphate, ATP; adenosine triphosphate, FCCP; carbonyl cyanide-p-trifluoromethoxyphenylhydrazone, NAD+; nicotinamide adenine dinucleotide. CI OXPHOS; complex I oxidative phosphorylation, CII OXPHOS; complex II oxidative phosphorylation, CI + II OXPHOS; complex I and II oxidative phosphorylation, ETS; electron transfer state, FAO LEAK; fatty acid oxidation leak, FAO OXPHOS; fatty acid oxidative flux ROX; residual, non-mitochondrial respiration.

Substrate	Site of action	Pathway	Measures
Malate	Complex I	Donates electron for NAD+ via malate dehydrogenase in complex I.	**FAO LEAK** Proton leakage from fatty acid β-oxidation
Octanoyl Carnitine	Electron-Transferring Flavoprotein	Fatty acid conjugate.	
ADP	Complex V, adenine nucleotide translocase	Final product of oxidative phosphorylation pathways.	**FAO OXPHOS** Maximal oxidative phosphorylation capacity
Glutamate	Complex I	Donates electron for NAD + and complex I.	**CI OXPHOS** Complex I specific respiration

Succinate	Complex II	Substrate to complex II succinate dehydrogenase. (CI+II OXPHOS)	**CI + II OXPHOS** Total OXPHOS capacity from complex I and II
Cytochrome C	Mitochondrial membrane	Assesses the intactness of the outer mitochondrial membrane and therefore its integrity.	
FCCP		Uncoupler of mitochondrial oxidative phosphorylation, maximum capacity of the ETS. (ETS)	**ETS** Electron transfer state
Rotenone	Complex I	Inhibitor of complex I, inhibits mitochondrial ATP production.	**CII ETS** Contribution of electron flow from complex II
Antimycin A	Complex III	Inhibitor of complex II, inhibits mitochondrial ATP production. (CII ETS)	**ROX** Residual, non-mitochondrial respiration

2.2.4.2 High throughput respirometry – Seahorse XF

The Seahorse Extracellular Flux (XF) analyser (Agilent Technologies) is a high-throughput method for interrogating mitochondrial respiration and glycolysis by measuring oxygen consumption rate (OCR), extracellular acidification rate (ECAR) and proton efflux rate (PER). Data extraction was performed by a metabolic technician.

2.2.4.2.1 Tissue preparation

Brain slices of 200μm thickness were created using a vibratome as described in 2.2.1. Before transferring to submerged slice recovery chamber (tissue slice recovery chamber Model 7470, Campden Instruments), 2mm round discs were cut from the slices using a biopsy punch (Integra™ Miltex™ Standard Biopsy Punch 2mm) to fit in the 24 well XFe24 Islet Capture Microplate (Agilent Technologies). Tissue was then transferred to the slice recovery chamber and incubated for 1 hour in seahorse modified aCSF (20mM NaCl, 3.5mM KCl, 1.3mM $CaCl^2$, 1mM $MgCl^2$ hexahydrate, 0.4mM KH^2PO^4, and 5mM HEPES with 10mM glucose, 35°C, 95% O_2 5% CO_2). 500μL of pre-warmed seahorse modified aCSF was added to each well in the microplate.

Brain discs were transferred using a paintbrush and secured in the well by placing capture screens (small circular nets, Agilent Technologies) in the wells. Within the well plate, 13 slices, assigned to the experimental group, were exposed to 1μl KCl (2M), while 7 control slices were treated with aCSF instead of KCl. In addition, 4 wells were used to measure background rates of OCR and ECAR and contained no slices.

2.2.4.2.2 Assay protocol

Compounds to be injected into the well (Table 3) were loaded into the ports prior to loading the microplate into the XF analyser. A modified XF Glycolytic Rate Assay was run in which substrates were added in the sequence detailed in Table 3. The assay is composed of cycles which comprise of a mixing period (3 minutes), a wait period (2 minutes) and a measure period (3 minutes). During measurements 7μL of the well volume is sampled to measure oxygen and pH giving rise to OCR and ECAR.

2.2.4.2.3 OCR, ECAR and GlycoPER analysis

The Agilent Seahorse XF Glycolytic Rate Assay report generator was used to automatically calculate parameters from assay data. Glycolysis is not the only process contributing to ECAR in the media, and can in part be driven by mitochondrial-derived CO_2.[252] Therefore glycoPER was calculated to decipher the contribution of glycolytic activity from ECAR and OCR measurements. To achieve this, a measured buffer factor of 0.1 mpH/pmol H^+ was applied to initially transform ECAR to PER. Additionally, sources of acidification not associated with glycolysis were corrected for by the following formula pmol H^+/min/well = 1* (H^+ total – 0.60*OCR_{mito}) – where; 1 = average lactate:H^+, 0.60 = average H^+:O_2 and OCR_{mito} is basal mitochondrial respiration to reflect lactate efflux rate. Percentage OCR and PER were calculated by normalising results to the mean baseline rates.

Table 3. Compounds in the induced XF Glycolytic Rate Assay, pathways which are measured, the concentration and cycles of measurement.

aCSF; artificial cerebrospinal fluid, CSD; cortical spreading depression, KCl; potassium chloride.

	Compound		
	None	KCl (aCSF control)	Rotenone + Antimycin A
Measurement	Basal respiration	Impact of CSD	Non-mitochondrial respiration
Concentration	-	500µM	50µM
Cycles	4	6	8

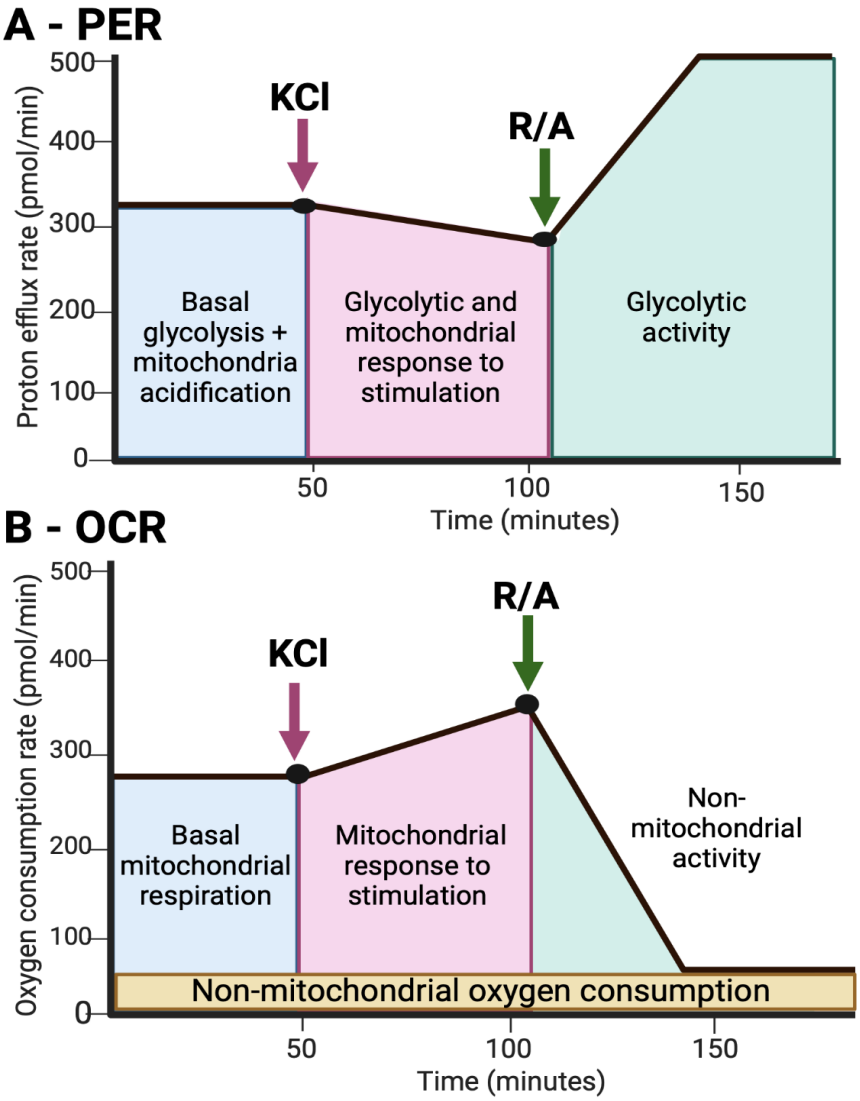

Figure 9. The metabolic processes which can be interrogated using the induced glycolytic assay kit.

A - Proton efflux measurements encompasses both glycolytic and mitochondrial-derived acidification. By inhibiting mitochondrial function with rotenone and antimycin A (R/A), it is possible to decipher glycoPER by subtracting mitochondrial acidification from the total PER. **B** – OCR allows the probing of mitochondrial oxidative respiration at baseline and in response to KCl. R/A allows the investigation of non-mitochondrial oxygen consumption. glycoPER; glycolysis driven proton efflux rate, OCR; oxygen consumption rate, PER; proton efflux rate. Figure created with BioRender.

2.3 *In vivo* techniques

2.3.1 Cisterna magna injection

Injection of kaolin to the cisterna magna was used to prevent CSF movement leading to obstructive hydrocephalus and thereby increasing ICP.[204] Animals were anaesthetised with isoflurane gas in an induction chamber (5% in 0.1% O_2 0.3% air mix) and maintained in a mask at 2% isoflurane and placed on a heating pad (Harvard Biosciences). The posterior of the animal's head was shaved and cleaned with an alcohol wipe. The neck was flexed over a padded cardboard tube to maximise foramen magnum exposure (Figure 10). The skin was pulled taut over the foramen magnum and the rhomboid atlanto-occipital membrane above the cisterna magna was marked with a permanent marker. A 0.5ml 30-gauge insulin needle was used to inject 250mg/ml kaolin suspension or equal volume 0.9% saline into the cisterna magna percutaneously.

Animals were then injected subcutaneously with 5mg/kg carprofen (Rimadyl, Zoetis) and 1ml/100g 0.9% saline to prevent dehydration, then placed in a heated recovery chamber for 30 minutes. Following the day of surgery, animals were weighed and monitored daily, and 5mg/kg carprofen and 1ml/100g 0.9% saline was administered subcutaneously as needed.

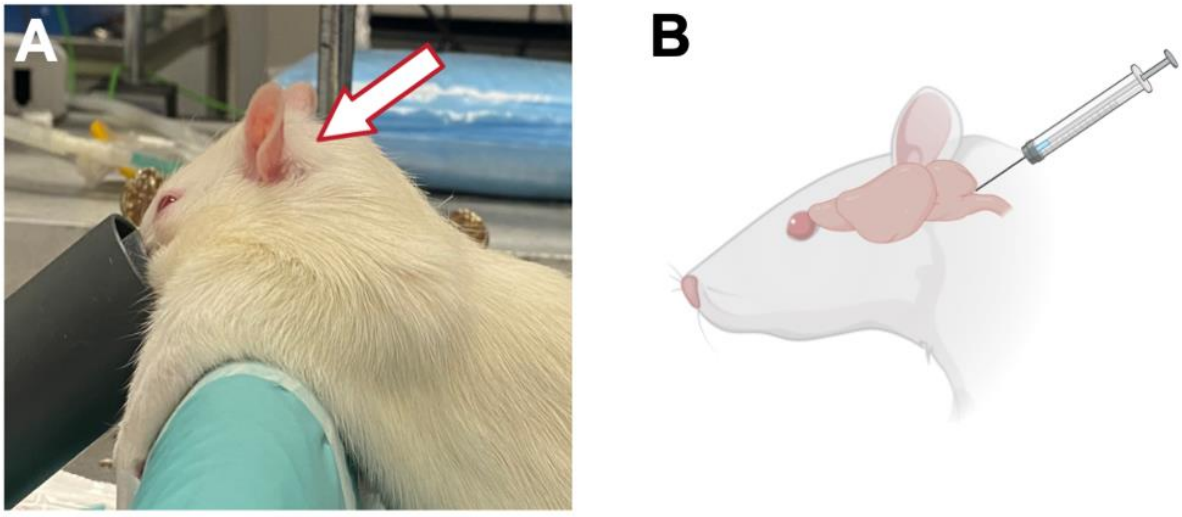

Figure 10. Methodology for injection into the cisterna magna.

A - Rats were positioned in a flexible nose cone and angled at 45° to allow the neck to be flexed and expose the anti-occipital membrane. Arrow indicates area and angle of needle insertion. **B** - Anatomical representation of the angle and region of injection.

2.3.1.1 Animal surgical preparation

Rats were prepared for surgery and anesthetized prior to ICP and CSD assessments as follows. Rats were anaesthetised with isoflurane gas in an induction chamber (5% in 0.1% O_2 0.3% air mix) and maintained in a mask at 2% isoflurane. The left femoral vein was cannulated to maintain anaesthesia with intravenous propofol (PropoFlo Plus, Abbott, 30 – 50mg/kg/hr) with a polythene cannula (external diameter, 0.96mm, Portex Ltd.). Anaesthetic depth was confirmed by lack of the withdrawal response from pinching the hind paw. Rats were then tracheotomized to allow ventilation of the animal with oxygen-enriched air and monitoring of the tidal CO_2 which was maintained at 3-3.5% through a connected ventilator (Harvard Apparatus, small animal ventilator) and end-tidal CO_2 monitor (Kent Scientific). A rectal probe

connected to a heating pad was used to monitor body temperature and maintain it at 36.5-37ºC (Harvard apparatus).

2.3.1.2 Intracranial pressure measurements

A solid state ICP catheter was inserted into the epidural space to directly measure ICP in the rat. 30 minutes prior to use, a 2 French (2F) rat pressure catheter (Millar) was left to soak in room temperature saline to prevent variations when recording *in vivo*. The catheter was connected to a single-channel bridge amplifier with a catheter interface cable (AEC-10D, AD Instruments). Data was acquired using a Powerlab 4SP (AD Instruments) and recorded and analysed using LabChart software (LabChart 7 v7.3.8, AD Instruments).

First the ICP catheter was kept still and 'zero-ed' in the LabChart software. The catheter was then calibrated using a pressure gauge kit (AD Instruments), requiring the recording of two pressures of known values, within the expected range of data. The catheter was enclosed in tubing with a pressure gauge and a syringe to allow the increase of pressure by pushing air into the tubing. Whilst recording in the LabChart software r the pressure was increased briefly to 5mmHg then 50mmHg. The software was used to convert the voltage units originally outputted by the bridge amp recorded at 5 and 50mmHg to their corresponding to units of pressure.

Following preparation, the head of the animal was fixed in a stereotactic frame (Kopf Instruments) and a medial incision was made expose the skull. A small hole was drilled into the parietal bone of the skull, taking care to ensure the dura remained intact. The catheter was slowly introduced into the epidural space and secured with bone wax (Ethicon) to create a sealed volume. The jugular vein of the animal was compressed to confirm that the catheter was inserted correctly and accurately

measuring ICP. The recording was allowed to settle until a consistent signal was obtained and the mean and SD of a 5 minute recording was calculated from the Labchart software. ICP values were rounded to the nearest whole number due to the inability to calibrate the software to decimal places using the pressure gauge.

2.3.2 *In vivo* CSD assessment

2.3.2.1 Electrode preparation

Prior to electrophysiology experiments, micropipettes were created from single barrel borosilicate glass capillaries (World Precision Instruments) using a horizontal pipette puller (P-97 Flaming/Brown type micropipette puller, Sutter Instruments). The tip of the glass micropipette was checked using a light microscope to ensure that it was intact, and that the diameter of the opening was between 5-10μm.

The glass micropipette was filled with 3M NaCl, ensuring there were no bubbles and connected to a micropipette holder (MEH1S20, World Precision Instruments) also filled with 3M NaCl. A silver/silver chloride (Ag/AgCl) pellet half-cell (World Precision Instruments) was soldered to a small length of wire connected to a pin (NL976 NL102G Headstage Accessory Kit, Digitimer) allowing connection to the head stage (NL102G DC Pre Amplifier Headstage, Digitimer). The micropipette holder was connected to the Ag/AgCl half-cell via crocodile clips and the tips of both were inserted in a beaker filled with 3M NaCl to equalise for approximately 45 minutes prior to recordings.

2.3.2.2 Surgical procedure

Following preparation, the head of the animal was fixed in a stereotactic frame (Kopf Instruments). To assess CSD, a medial incision was made to expose the skull and neck muscles and a hemi-cranial window was drilled into the left or right parietal bone using a saline-cooled drill. The parietal bone was removed to create a cranial window, with care taken to keep the dura mater intact. The micropipette was secured on a micromanipulator (Kopf Instruments) and placed 800µm below the cortical surface with the use of the fine adjustment manipulator to record cortical steady state potential (direct current (DC) shift, Figure 11). The Ag/AgCl pellet electrode was placed subcutaneously in contact with the neck muscle and connected to a high-impedance head stage. The signal was fed through a DC preamplifier (gain x 1000, NL102G DC Pre Amplifier, Digitimer), filtered (NL125/6 Band Pass Filter, Digitimer), and then passed through a second stage amplifier (NL106 AC/DC Amplifier, Digitimer), through an analogue-to-digital converter (Power 1401plus, Cambridge Electronic Design Limited) and displayed on a personal computer where it was processed and stored (Spike5 v8.04, Cambridge Electronic Design Limited).

CBF was additionally monitored via laser Doppler (Moor Instruments). The laser Doppler probe was placed on the cortical surface in parallel with the microelectrode with a micromanipulator (Kopf Instruments). A cranial window was also made using a saline-cooled drill posterior to the recording window to allow placement of a cotton ball soaked with KCl (1M) (Figure 11).

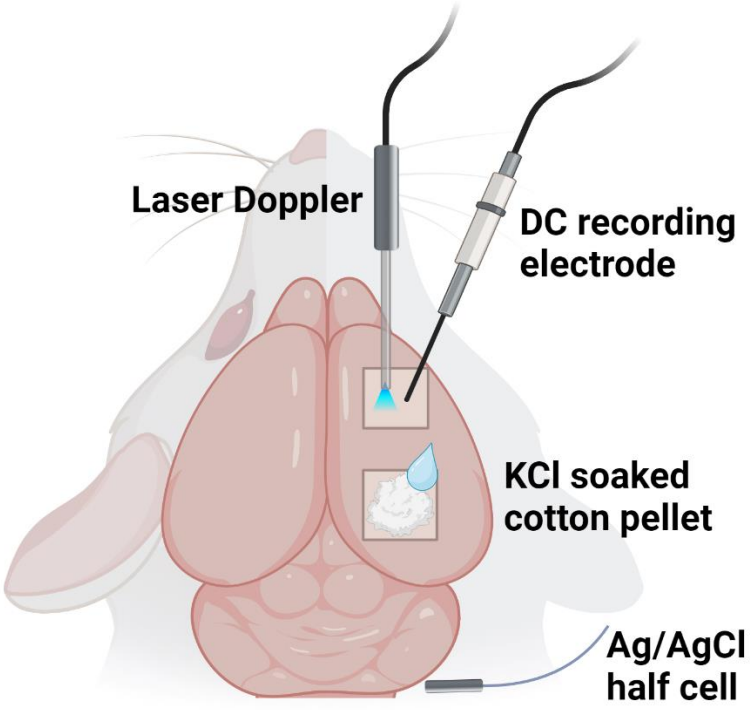

Figure 11. Placement of CBF and DC recording electrodes during CSD measurements.

CBF and DC was recorded at the cortical surface of rodents in response to KCl stimulation. Ag; silver, AgCl; silver chloride, DC; direct current, KCl; potassium chloride. Figure created with BioRender.

2.3.2.3 CSD induction and recording

After surgical preparation, the cortex was left to rest for approximately 30 minutes after any potential activity induced by the electrode placements. During this period baseline activity was recorded. A cotton pellet soaked in 1M KCl was placed on the cortical surface in the cortical window posterior to the recording electrodes and the shift in DC currents and CBF were recorded. 5µL of 1M KCl was added to the pellet every 15 minutes for 1 hour.

At the end of recordings, rats were euthanised with an overdose of intraperitoneal pentobarbitone sodium 200mg/ml 0.1ml/100g bodyweight (Pentoject Animalcare Ltd). They were then transcardially perfused with 1ml/g bodyweight of 0.01M heparinised (1:10) PBS, followed by 1ml/g bodyweight of 4% PFA in 0.01M PBS using a peristaltic pump (Watson Marlow). Brains were dissected and post-fixed in PFA for 1 week.

2.3.2.4 CSD data analysis

The DC and CBF changes were quantified in CSD recordings using Spike2 software (v8.04, Cambridge Electronic Design Limited) (Figure 12). The depolarisation latency describes the duration, in seconds, between KCl application and the beginning of the first depolarisation (as indicated by a sharp negative change in the DC signal). The depolarisation duration was defined as the time in seconds between the beginning of the negative DC signal change and when the signal reaches the most negative apex. The repolarisation duration describes the time in seconds between the most negative apex DC signal and when the signal returns to baseline DC. The % change in CBF is calculated using the formula: (highest CBF response during the CSD – the baseline CBF)/baseline CBF x 100. The number of CBF peaks coupled to depolarisation events were also counted and displayed as whole numbers.

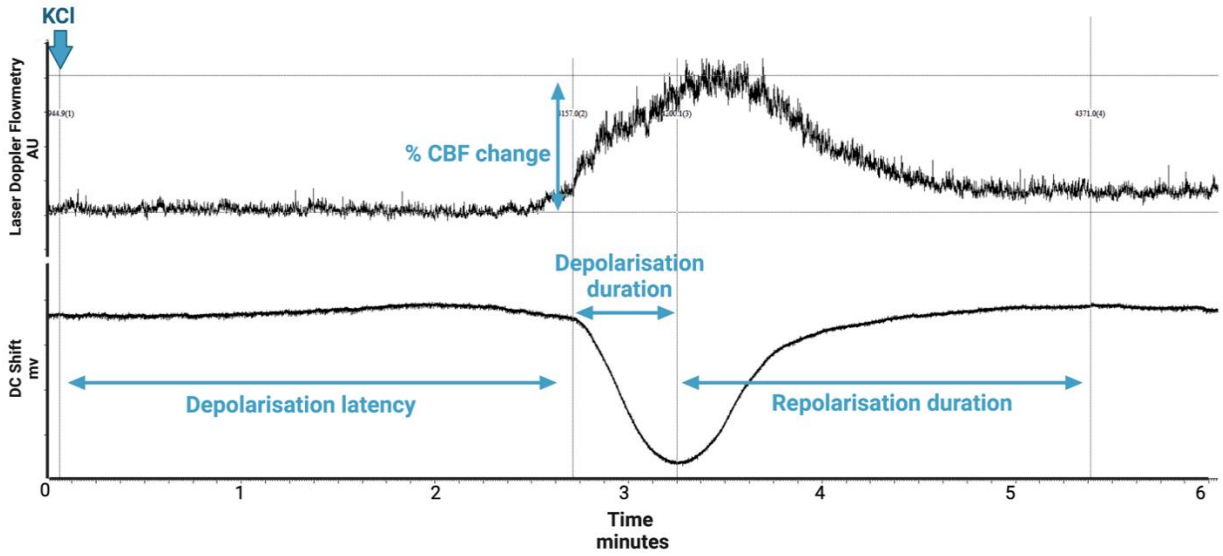

Figure 12. Quantification of cortical and CBF changes during CSD.

Depolarisation latency described the duration between stimulation and initiation of the first depolarisation. Depolarisation duration was defined as the time between the depolarisation initiation and the negative apex of the signal. Repolarisation duration was the time between the most negative DC signal and returns to baseline. % CBF change was calculated via (highest CBF response during the CSD – the baseline CBF)/baseline CBF x 100, AU; arbitrary units, CBF; cortical blood flow, DC; direct current.

2.3.3 Mechanical threshold behavioural studies

Measuring both periorbital and hind paw mechanical threshold is a commonly utilized method in preclinical migraine models to assess hyperalgesia,[253 254] and can indicate changes in trigeminal sensory processing.[72 255] To determine changes in mechanical thresholds the Up-and-Down method which uses calibrated von Frey filaments to determine the threshold at which animals respond 50% of occasions (50% mechanical withdrawal threshold).[256] The Up-and-Down method was originally formulated by Dixon to determine the median lethal dose (LD50).[256] A modified

method was then applied to rodents by Chaplan et al. as a quantitative allodynia assessment technique.[257]

The following formula was used to calculate mechanical thresholds:

$$50\%\ \text{g threshold} = (10^{[Xf + k\partial]})/1000$$

In which: Xf = value (in log units) of the final von Frey hair used

k = tabular value for the pattern of responses (Appendix Table 1)

∂ = the average interval (in log units) between stimuli (0.354).

2.3.3.1 Pretesting habituation

The behavioural testing room was maintained between 30-50 lux and ~21°C and testing was conducted at the same time (within-1 hour) each day to avoid circadian variation. Rats were habituated to the von Frey apparatus on 2 occasions prior to and baseline assessments and additionally prior to each assessment by placing them in the apparatus (a clear Perspex box on a raised wire platform, Figure 13A) without testing for 1 hour. Rats were always placed in the same box during each habituation and testing event. After 1-hour rats were returned to their home cages.

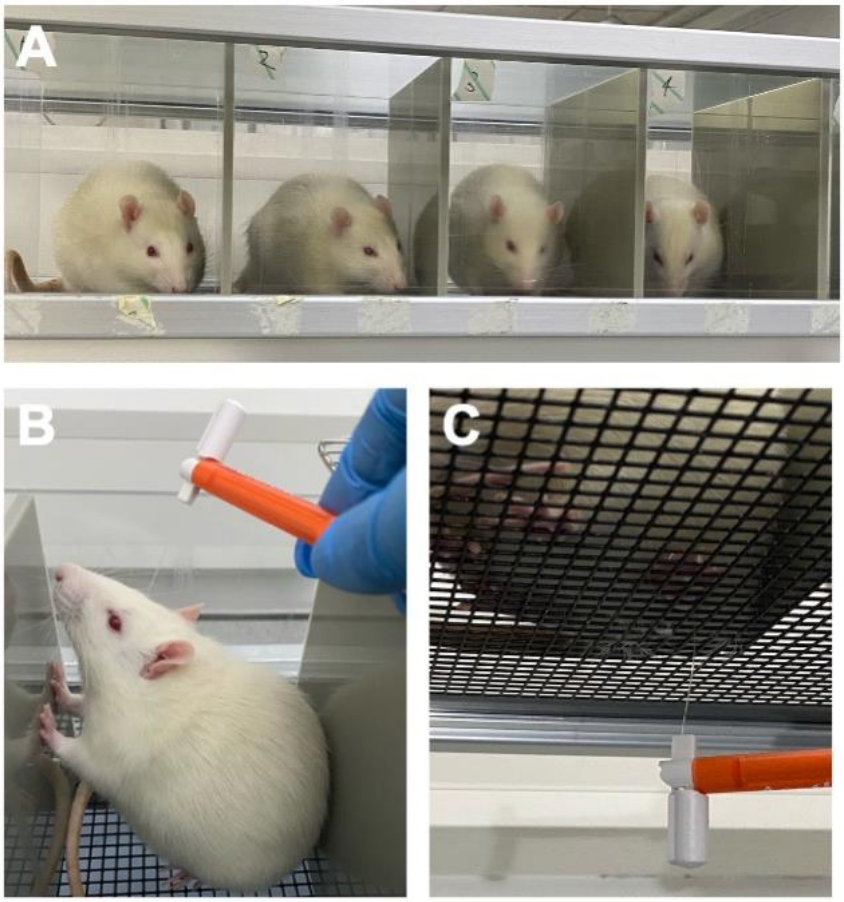

Figure 13. Von Frey mechanical threshold testing apparatus and methodology. **A** – Perspex enclosure and raised wire platform in which animals were habituated and tested within. Rats were always placed in the same box. **B** – Demonstration of periorbital testing, **C** – Hind paw testing using von Frey filaments.

2.3.3.2 von Frey mechanical threshold testing

Prior to testing, rats were habituated to the testing apparatus for 1-hour. Periorbital sensitivity was tested using von Frey graded filaments of the following pressures: 0.4, 0.60, 1.0, 2.0, 4.0, 6.0, 8.0g. A filament was applied perpendicular to the periorbital region ensuring the filament would bend with the aim to elicit a positive response (Figure 13B). Positive responses included: sharp movement of the head away from the filament, bowing or burrowing of the head or grooming the head repeatedly with

paws. Absence of behaviours were recorded as a negative response. Von Frey testing was performed using the Up-Down method.[257] Animals were tested with the first filament (always 1g) if the animal did not respond, the next higher filament was used. Conversely if the animal did respond the next lower filament was tested. This was performed a further 4 times following the first positive response or until the minimum (0.16g) or maximum (8g) weight filament was tested.

Hind paw testing was conducted similarly to periorbital testing; however, filaments were instead applied to the plantar surface of the hind paw (Figure 13C). The left hind paw was assessed in all rats. Positive responses included: immediately moving the paw, grooming or licking the paw.

Baseline measurements were repeated twice with a minimum of 3 days between assessments and an average taken of the two measurements. Day 7 measurements were 7 days after cisterna magna injection and conducted twice within the assessment and an average calculated.

2.3.4 Drugs

2.3.4.1 GLP-1 receptor agonist

GLP-1 receptor agonist (GLP-1RA) exenatide (Byetta, AstraZeneca) was used to investigate the impact of lowering ICP in animals. 1 day after cisterna magna injection, all animals were given analgesia subcutaneously (5mg/kg carprofen). Animals were then injected daily for 6 days with 20µg/kg exenatide or equal volume saline subcutaneously, a dosage previously used in our group.[199] On the final day, exenatide was administered 1 hour before end-point experiments.

2.3.4.2 CGRP antagonist

CGRP antagonist olcegepant (BIBN4096BS, Sigma) was used to explore the impact of blocking the CGRP receptor in animals with raised ICP. One day after cisterna magna injection, all animals were given analgesia subcutaneously (5mg/kg carprofen). Animals were then injected daily for 6 days with 1mg/kg olcegepant (0.02% DMSO) or equal volume 0.02% DMSO intraperitoneally, a dosage which is commonly utilised in other studies.[151] [258] On the final day, olcegepant was administered 1 hour before end-point experiments.

2.3.5 Histochemistry methods

2.3.5.1 Ventricle dilation measurements

Whole brains were collected from rats following CSD assessments after transcardial perfusion and a portion of the brain approximately 1-3cm anterior to bregma (Figure 14A) was isolated and placed into PFA. Following post-fixation for 1 week, brains was washed with PBS and sliced using a stainless-steel large rat brain matrix with 1mm wide coronal divisions and a single edge razor blade. Coronal slices were imaged using a flatbed scanner (Epson Perfection V7000 Photo). Images were analysed using ImageJ Fiji.[251] The ventricle:brain ratio was calculated using the formula (A+B/C) in which A and B denote the widths of the lateral ventricles and C denotes the width of the entire brain slice across the ventricles (Figure 14B).

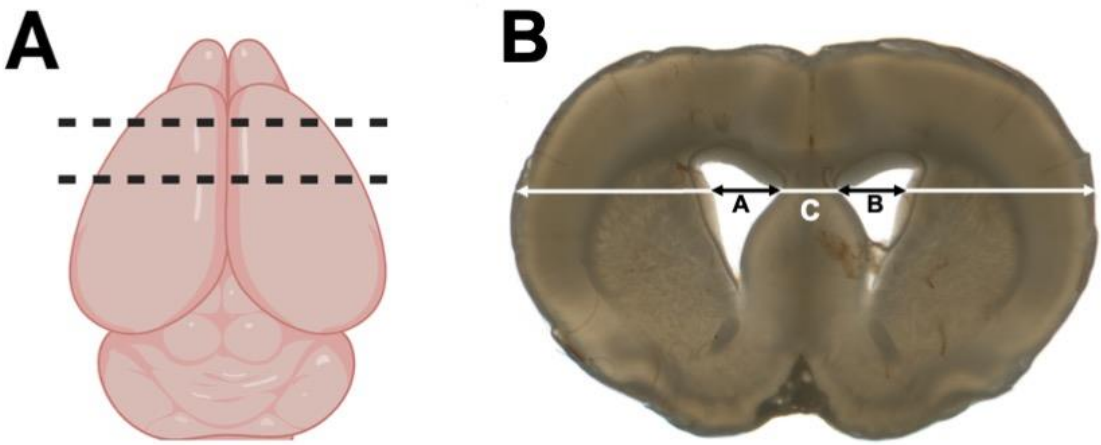

Figure 14. Method of measuring ventricle enlargement in rat brains.
A - Area of the brain approximately 1-3cm anterior to bregma which was sliced to quantify ventricle dilation. **B** - Coronal brain slice from a raised ICP animal in which ventricle:brain ratio is calculated by A+B/C.

2.4 Analytical techniques used for *ex vivo* and *in vivo* experiments.

2.4.1 Protein analysis

2.4.1.1 Protein extraction and quantification

Ice cold radioimmunoprecipitation assay (RIPA) extraction buffer supplemented with protease and phosphatase inhibitors (1 tablet per 10ml buffer, both ThermoFisher Scientific) was added to tissue samples (16.67µL per mg of tissue). Samples were manually homogenized using a TissueLyser II (QIAGEN) at 30 cycles per second for 2 minutes. Homogenized samples were then freeze-thawed twice at -80°C to ensure thorough lysis, vortexed for 10 seconds and centrifuged at 13,000 x g at 4°C for 10 minutes to pellet debris. The supernatant was stored at -80°C until further use.

Protein was quantified in samples using the bicinchoninic acid assay (Pierce™ BCA Protein Assay Kit, ThermoFisher Scientific). This relies on the reduction of copper by proteins in an alkaline solution, leading to a colorimetric result which is correlated to the concentration of protein in a sample.

Samples were tested in 25µL triplicates, 200µL of the BCA working reagent was added to each well, and thoroughly mixed on a plate shaker for 30 seconds. The plate was incubated at 37°C for 30 minutes following which the absorbance was measured at 562 nm on a plate reader (Molecular Devices SpectraMax). To calculate sample protein content the average absorbance of the blank standard replicates was subtracted from sample and standard measurements. A standard curve constructed from serial dilutions of bovine serum albumin was generated, facilitating the determination of the protein concentration for each unknown sample.

2.4.1.2 CGRP quantification

To determine changes in α-CGRP, an enzyme-linked immunoassay (ELISA) (S-1167 BMA-Biomedicals) was used. Due to their high protein content, trigeminal ganglion samples were diluted 1:5 for the assay. Samples were tested in 50µL duplicates and 25µL of antiserum was added into each well and incubated at RT for 1 hour. 25µL biotinylated tracer was added to each well and incubated for a following 2 hours. The plate was washed with ELISA buffer five times and subsequently 100µL of streptavidin-horse radish protein was added to all wells and incubated for 1 hour. The plate was washed again with ELISA buffer then incubated with 100µL of 3,3′,5,5′-Tetramethylbenzidine (TMB) chromogenic solution for 30 minutes. The colorimetric reaction was terminated by adding 100µL hydrogen chloride and absorbance was read at 450nm. To calculate α-CGRP concentrations, the average absorbance of the

blank standard replicates was subtracted from sample and standard measurements. A standard curve was generated, facilitating the determination of the protein concentration for each unknown sample.

2.4.2 Metabolomics

2.4.2.1 Metabolite extraction

Tissues samples were pulverised using a cooled pestle and mortar and weighed in pre-cooled sample tubes in a calibrated microbalance (Accuris Instruments Analytical Series W3100-210, Dublin, Ireland). High-performance liquid chromatography (HPLC) grade methanol, 500µl at -20°C, was added to pulverised tissue to quench metabolism followed by 200µl 2.5µg/ml glutaric acid in dH_2O as an internal standard. A 5mm steel bead (QIAGEN) was added, and samples were placed into a cassette cooled to -20°C and homogenised using a TissueLyser II (QIAGEN) at 30 cycles per second for 2 minutes. Samples were centrifuged and the supernatant moved to a 13x100mm glass tube, the remaining tissue pellet was dried overnight and weighed for results normalisation.

Protein contaminants were precipitated by adding 1.4ml 2:1 acetone:isopropanol solution at -20°C, vortexing for 10s then agitating for 10 minutes on an orbital shaker at 750rpm (ThermoFisher Scientific). Samples were centrifuged at 3220 x g for 5 minutes to pellet protein. Supernatant was transferred to a fresh glass tube and the protein pellet was left to dry overnight. HPLC grade water 1ml with 500µl chloroform at -20°C was added to the supernatant to aid separation of non-polar metabolites. Samples were agitated as before then centrifuged at 4000rpm for 5 minutes. The fractions separated with the polar aqueous layer on the top and the non-polar at the

bottom, separated by a thin protein interface. The polar fraction was transferred to a new tube, 2ml for NMR and 200µL for gas chromatography mass spectrometry (GCMS), then evaporated to dryness using a SpeedVac (ThermoFisher Scientific) at 30ºC for 4-5 hours and stored at -80ºC until further analysis.

2.4.2.2 Nuclear magnetic resonance spectroscopy

2.4.2.2.1 Pellet resuspension

NMR spectroscopy was utilized as an untargeted method to detect and quantify metabolites in samples. Dried sample pellets were resuspended in 60µL of 100mM sodium phosphate buffer (1L dH_2O (mM): Na_2HPO_4 (57.8), NaH_2PO_4 (42.2), D4-TMSP (0.5mM) pH 7.0) then briefly vortexed and sonicated for 5 minutes. Resuspended samples of 50µL were pipetted into champagne vials and a Gilson liquid handling robotic system (Cortecnet) transferred 35µL into 1.7mm NMR tubes.

NMR tubes were then loaded into Bruker Neo 800 MHz NMR spectrometer, equipped with a 1.7mm z-PFG TCI Cryoprobe. A NOESY1d pulse sequence was used to achieve water suppression. Automatic tuning and matching were used, and samples were shimmed to a TMSP linewidth of <1Hz. In total 128 transients with 16384 complex data points (1.31s FID acquisition time) were recorded for each sample, with a total of 16 steady-state scans per sample. The interscan relaxation delay was set to 4 seconds and the spectral width of 12500Hz (15.63ppm). Data acquired was in the form of 1H-NMR spectra.

2.4.2.2.2 Nuclear magnetic resonance data analysis

1H-NMR spectra were analysed using MetaboLabPy (version 0.6.35, Ludwig 2020). The D4-TMSP internal standard signal was set at 0.0ppm followed by manual phase correction and batch baseline correction using a spline baseline. The area under each peak of interest was integrated and compared to the TMSP peak to calculate the mM concentration. Dried tissue weight was used for normalisation.

2.4.2.3 Gas chromatography mass spectrometry

2.4.2.3.1 Chemical derivatisation

Chemical derivatisation and data acquisition was conducted by a metabolomic technician. Samples were treated with 40µL of methoxamine in pyridine (2%) for 1 hour at 60°C and 50µL of N-tertbutyldimethylsilyl-N-methyltrifluoroacetamide with 1% (w/v) tertbutyldimethyl-chlorosilane. This was then incubated for another hour at 60°C in closed tubes before being transferred to a chromatography vial with a glass insert (ThermoFisher Scientific) for GC-MS analysis.

2.4.2.3.2 Data acquisition and analysis

Derivatised samples were analysed using an Agilent 8890 GC and 5977B MSD (Agilent Technologies) after 1µL of sample was injected in splitless mode with helium carrier gas at a rate of 1.0mL min^{-1}. Initially GC oven temperature was set at 100°C for 1 minute, then increased to 170°C at a rate of 10°C min^{-1}, followed by an increase to 200°C at a rate of 5°C min^{-1} before finally reaching 320°C at a rate of 10°C min^{-1} with a 5 minute hold. Metabolites were then detected in scan mode with

the subsequent total ion count of each metabolite being normalised to the internal standard D6-Glutaric acid. This data was then normalised according to sample type.

2.5 Statistical analysis

All statistical analysis was performed using Graphpad Prism (GraphPad Software, Version 8). The normality of data was assessed using the Shapiro-Wilk test. Data which were normally distributed were analysed using parametric tests (*t* tests, Pearson's correlation coefficient) and reported as mean and standard deviation (SD). Non-normally distributed data were analysed using non-parametric tests (Mann-Whitney test, Spearman rank correlation test) and reported as median (range).

Graphs were also created using Graphpad Prism (GraphPad Software, Version 8). Normally distributed data were displayed as bar charts displaying mean ± standard error of the mean (SEM). Non-normally distributed data were displayed as box and whisker plots, representing the median ± maximum and minimum values (whiskers).

2.5.1 Sample size calculations

Power calculations were utilised to determine sample sizes using STPLAN software (MD Anderson Cancer Center, University of Texas). Sample sizes were calculated using $\alpha = 0.05$ and power = 0.80, and effect sizes which reflected previous pilot data and published studies.

For mechanical withdrawal thresholds, assessment was based on published studies,[253] in which an adequately powered behavioural study requires at least $n = 8$ rats per group. For electrophysiology, an adequately powered study requires $n = 10$-

12 per group.[259] Previous use of the raised ICP model and investigation of GLP-1RA within the group,[199] demonstrated a powered study requires *n* = 6-9 animals per group.

CHAPTER 3 EXPLORING METABOLISM IN A BRAIN SLICE MODEL OF CORTICAL SPREADING DEPRESSION

3.1 Introduction

The pathophysiology of migraine involves altered brain excitability, sensitization of the trigeminal system, and neurovascular changes, yet the precise mechanisms underlying headache generation remain elusive.[15] The high prevalence of migraine in both mitochondrial (lifetime prevalence of 61%)[260] and metabolic disorders (1-year prevalence of 11.9% in men and 22.5% in women)[261] also suggests mitochondrial alterations may be a characteristic of migraine.[262] The ability of fasting to precipitate migraine attack also implicates the role of glucose metabolism in headache pathology.[263] [264] Altering the glycaemic state of animal models has led to alterations in CSD susceptibility.

CSD is a highly energy-intensive event and induces a distinct pattern of changes in CBF which also contribute towards unbalanced energy production.[265] Rapid oxygen consumption occurs in response to heightened energy demands, often leading to localized hypoxia in regions of high activity.[115] This, combined with underlying mitochondrial dysfunction, results in reduced oxidative ATP production impeding recovery from CSD and prolonging depolarization.[115] [116] Supplementation with vitamins or antioxidants which grossly target brain metabolism have been trialled, however the results have been variable and seem to depend on patient's individual deficiencies.[93] [94] Pinpointing exactly which pathways are implicated has hampered the success of nutraceutical targeting and requires *in vivo* investigation.

To experimentally induce CSD *in vivo*, mechanical or thermal stimulation, administration of inflammatory substances, or KCl to cortex is employed.[54] [73] However, these methods often require a craniotomy and cortical exposure,

introducing the confounding effects of tissue damage and anaesthesia, which can alter CSD characteristics.[77] *Ex vivo* brain slice platforms offer a solution by removing these confounding effects while largely preserving the *in vivo* biology. Thus, they enable in-depth investigation of pathophysiology at the cell and molecular level within relevant neuronal circuits. Furthermore, this provides a context where drugs, that would typically be impeded by the blood-brain barrier, may be applied with a temporal and spatial precision which would be unachievable *in vivo*.[78 79]

Acute brain slices have proven to be valuable models for cortical function, retaining the structural and functional characteristics of neuronal networks.[78 79] They have also been employed to model pathophysiological events associated with TBI and stroke.[81-84] Extending their application to modelling CSD in the context of headaches could provide insights into metabolic dysfunction potentially underlying brain hyperexcitability and trigeminal activation. Such models could facilitate the exploration of therapeutic targets and validation of pathogenic pathways involved in headaches.

3.1.1 Aims

Accumulating evidence has suggested that metabolic disturbances play a role in headache pathology and susceptibility, however supplement trials in migraine have exhibited varying success.[93 94] Exploring metabolism in an *ex vivo* 3-dimensional tissue model of headache may identify and validate potential therapeutic targets, such as nutraceutical interventions. Therefore, this chapter aimed to:

1. Establish and validate an acute brain slice model capable of CSD induction and metabolic investigation within relevant neural circuits.

2. Probe metabolic consequences associated with headache-related events by investigating the metabolite profiles, mitochondrial activity and calcium influx in brain slices following CSD induction.
3. Explore the metabolic pathways which contribute toward pathology of fasting headache, by challenging the slice model with glucose deprivation.

3.2 Methods

3.2.1 Animal husbandry

This chapter utilised the optogenetic mouse strain Thy1-ChR-YFP. As discussed in 2.1.1 these mice express a ChR2 gene fused with the YFP coding sequence under the control of the Thy1 promoter. The transgene is expressed in a range of neuronal cell types including layer 5 cortical neurons. This optogenetic line offers clear advantages for the study of CSD since temporal and spatial activation of ChR2 can be controlled precisely.[248] However, for practical reasons, the ChR2 system was not optimised in this chapter and CSD induction relied on conventional approaches involving KCl application. Since expression of CHR2-YFP transgenes are not expected to influence performance of the KCl stimulations, both WT and heterozygous Thy1-ChR2-YFP mice aged 9-20 weeks, and of both sexes, were used in this chapter.

Mice were group housed in sex and litter matched groups in standard IVC cages in a climate-controlled room, kept on a 12:12 light/dark cycle and fed with standard rodent chow (EURodent Diet 14%, Labdiet).

3.2.2 Brain slice preparation

Acute brain slices were prepared from animals as described in 2.2.1. Briefly, animals were culled via cervical dislocation, decapitated, and the brain rapidly removed and placed into oxygenated cooled SaCSF. 350μm coronal slices were prepared using a vibratome whilst perfused with 95% O_2 5% CO_2 SaCSF on ice.

3.2.2.1 Incubation conditions of slices

To evaluate the viability of the model, slices incubated with standard aCSF (containing 10mM glucose; positive controls) were compared to slices incubated in 100% ethanol (negative controls) as described in 2.2.1.1 (Table 4). To examine the role of glucose on the metabolic consequences of CSD, slices maintained with standard levels of glucose (+glc, 10 mM) were compared with slices deprived of glucose (-glc, 0mM) (Table 4). After slice preparation, tissues were immediately incubated for 1 hour in aCSF with 10mM glucose, before incubation for an additional hour in either the glc+ or glc- conditions (Table 4). Both -/+glc conditions were incubated at 35°C and perfused with 95% O_2 5% CO_2. A workflow of -/+ glc experiments is outlined in Figure 15.

Table 4. Incubation media of different slice conditions.

Each incubation was performed for 1 hour.

Condition	1st Incubation	2nd Incubation
Positive control	aCSF +10mM glucose	-
Negative control	100% ethanol -O_2/CO_2 -37oC	
+Glc	aCSF +10mM glucose	aCSF +10mM glucose
-Glc	aCSF +10mM glucose	aCSF + 0mM glucose

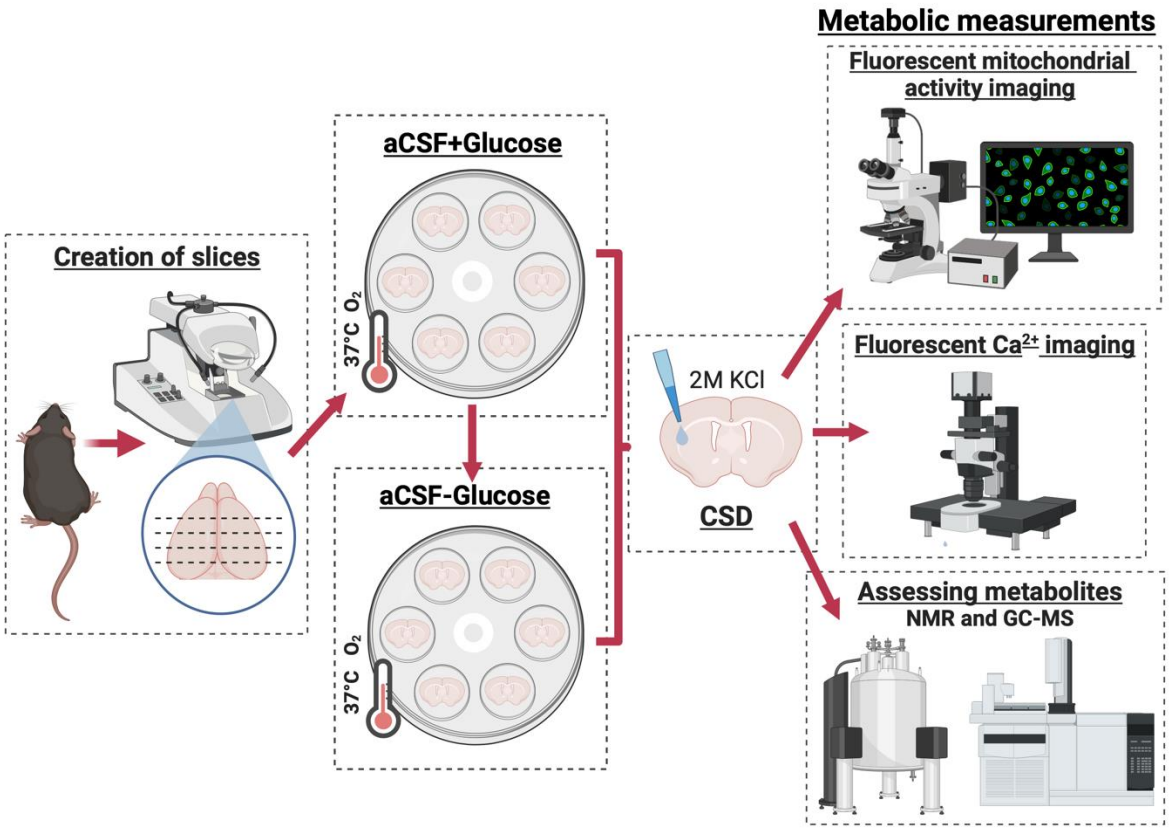

Figure 15. Workflow of experiments assessing the impact of glucose on metabolic readouts following CSD.

aCSF; artificial cerebrospinal fluid, Ca^{2+}; calcium, CSD; cortical spreading depression, GCMS; gas chromatography mass spectroscopy, KCl; potassium chloride, NMR; nuclear magnetic resonance spectroscopy. Note, for clarity, viability control groups (+/- ethanol) are not shown. Figure created with BioRender.

3.2.2.2 CSD induction in brain slices

CSD was induced in slices using topical application of KCl. A droplet of 1µL of 2M KCl was added to the cortical area of slices to stimulate depolarization.

3.2.3 Fluorescent labelling in slices

3.2.3.1 Propidium iodide staining

To assess the viability of slices, PI, a cell impermeable stain was used in to label positive and negative control slices. Following incubation in their respective conditions (aCSF or 100% ethanol), slices were fixed in 4% PFA for 30 minutes at RT. Fixed slices were then incubated for 30 minutes in 5µg/ml PI as described in 2.2.3.1.

3.2.3.2 Caspase 3/7 labelling

NucView 488 fluorescently labels activity of caspase 3/7 and was used to compare apoptotic activity in positive and negative control slices. Following recovery in their respective conditions (aCSF or 100% ethanol), slices were incubated in 5µg/ml of Nucview488 caspase-3 substrate for 30 minutes then fixed in 4% PFA for 30 minutes at RT. Slices were mounted and a z-stack of 12 images captured and analysed as described in 2.2.3.2.1.

3.2.3.3 Calcium indicators

Fluorescent Ca^{2+} indicators were used to indicate movement of Ca^{2+} following CSD stimulation using Fluo-4-AM. Slices were incubated in 2.5µM/ml Fluo-4-AM for 30 minutes in aCSF as described in 2.2.3.3. Slices were then transferred to an imaging dish on a microscope stage and a baseline recording of 200 frames was captured at 2Hz. Imaging was repeated following addition of 1µL KCl (2M) to the cortical edge of the slice for 400 frames. Images were captured and F/F0 was calculated to represent change in fluorescence over time in comparison to baseline as described in 2.2.3.3.1.

3.2.3.4 Mitochondrial potential dyes

To assess changes in mitochondrial potential during CSD slices were incubated in RH-123 as described in 2.2.3.4. A single baseline image was taken prior to KCl addition, following which 1µL 2M KCl was added to the cortical edges. Slices were imaged and F/F0 was calculated as detailed in 2.2.3.4.1.

3.2.4 Respirometry methods in brain slices

3.2.4.1 High resolution respirometry

Oroboros oxygraphy chambers were prepared as specified in 2.2.4.1. After incubation in their respective conditions brain slices were weighed transferred to a calibrated Oroboros chamber and allowed to equilibrate prior to the addition of substrates as discussed in 2.2.4.1. A SUIT protocol was then initiated in which a series of substrates were added in succession to investigate respiratory control

(Table 2., Figure 8). Oxygen consumption and flux rates were normalised to tissue weight and calculated using DatLab 7.4 by averaging the stable response of slices following addition of substrates.

3.2.4.2 High throughput respirometry

The Seahorse XF analyser was used to measure OCR and ECAR from brain slice tissue. Brain slices were prepared as described in 0 from one animal, and a total of *n* = 20 brain slices were assayed in parallel. Slices were incubated in a Seahorse XF24 Cell Culture microplate and secured in the well with a capture screen with seahorse-modified aCSF at 37°C. The microplate was then loaded onto the XF analyser. During the assay each compound from the mitochondrial stress kit was subsequently released from its cartridge following a specified programme as described in 2.2.4.2.2 (Table 3).

3.2.5 Metabolomics

Following Ca^{2+} imaging to confirm CSD, brain slices were snap frozen in liquid nitrogen and stored in -80°C until required for analysis. Slices were pulverised as described in 2.4.2.1 and typically, approximately 30-40mg of tissue were weighed out for metabolomic analysis. In some instances, it was necessary to combine multiple brain slices from the same animal to achieve this minimum weight. The absolute concentration of metabolites was measured in samples using GCMS using the parameters listed in 2.4.2.3.

3.2.6 Statistical analysis

The normality of data was assessed using the Shapiro-Wilk test. Positive NucView stained cells, metabolite concentrations and respiratory flux as assessed by high resolution (Oroboros) and high throughput (Seahorse) were compared between conditions using unpaired two-tailed *t* test. To compare changes in fluorescent Ca^{2+} and mitochondrial activity, the area under the curve (AUC) was calculated and compared between conditions using unpaired two tailed *t* test. Results were considered statistically significant when *P* values were * $P<0.05$, ** $P<0.01$, *** $P<0.001$, and **** $P<0.0001$.

3.3 Results

3.3.1 Assessing the viability of the brain slice model

3.3.1.1 Markers of cell death

Slices incubated in 100% ethanol were utilised as negative controls to confirm the viability of experimental brain slices and verify that results did not reflect tissue death. Both negative and positive controls exhibited a high percentage of relatively dim PI labelling distributed evenly throughout the slice (Figure 16A). In negative controls clusters of intensely stained cells were observed at the cortical edges, and in some deeper cortical layers. In contrast intensely PI positive cells were not observed in positive controls.

To assess apoptotic activity in slices NucView 488 was utilised to visualise caspase-3 activity. The negative controls demonstrated abundant positively labelled cells, in contrast to positive controls, which showed a sparse distribution of labelled cells

(Figure 16A). Quantification demonstrated a significantly higher number of positive cells in negative control slices compared to positive (100% ethanol mean (SD) = 1150 cells (188) *n* = 8 slices, aCSF = 410 cells (234) *n* = 10 slices, *P*<0.0001, Figure 16B).

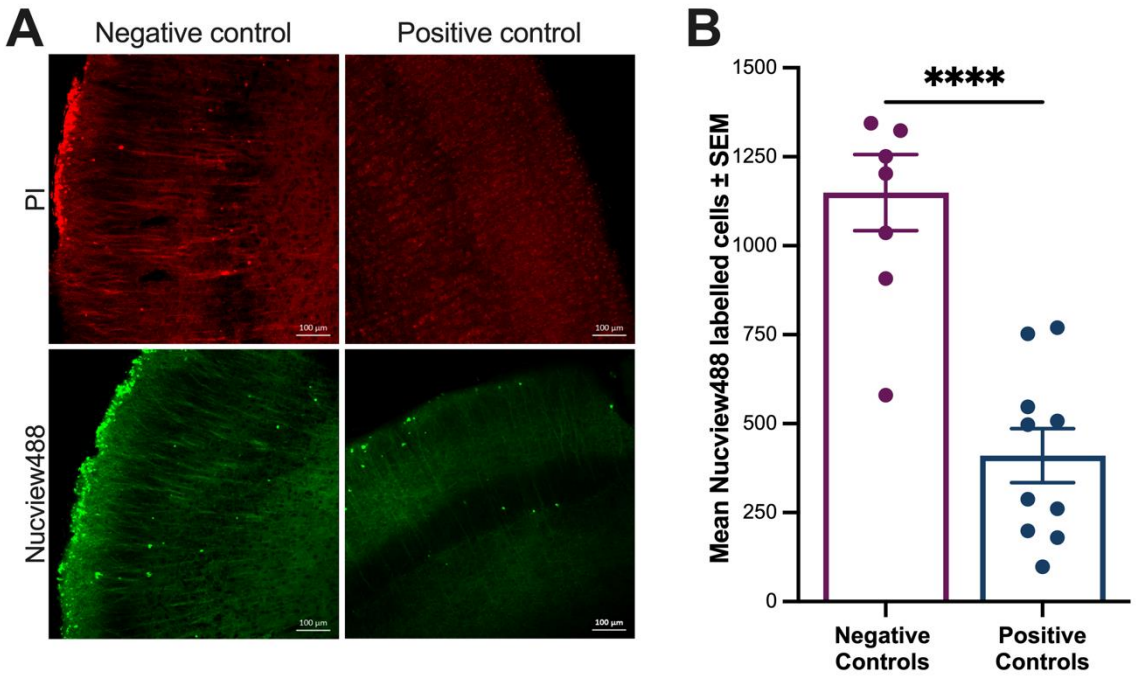

Figure 16. Assessing the viability of negative and positive viability controls.
A - Immunofluorescent labels of cell viability. Left panels 100% ethanol, right aCSF incubated, top PI staining, bottom NucView488 labelling. **B** – Quantification of Nucview488 labelled cells. Data presented as mean ± SEM 100% ethanol *n* = 7 slices, aCSF *n* = 10 slices. aCSF; artificial cerebrospinal fluid. Significance determined by unpaired *t* test **** *P*<0.0001

3.3.1.2 Baseline respiratory function

High resolution respirometry-based measurements of mitochondrial function were used to probe the metabolic health of the brain slice model. Positive control slices had a mean (SD) basal respiratory flux of 13.73pmol $O_2/s^{-1}/mg^{-1}$ (4.87) and exhibited minimal changes in respiratory flux when assessing FAO LEAK and OXPHOS

(Figure 17). Glutamate administration resulted in an increase in CI OXPHOS respiratory flux (mean (SD) = 13.71pmol $O_2/s^{-1}/mg^{-1}$ (3.11)). However, the most significant increase in respiratory flux resulted from succinate addition, which instigated CI and CII OXPHOS (mean (SD) = 27.53pmol $O_2/s^{-1}/mg^{-1}$ (7.73)). Peak respiratory flux was achieved when assessing the ETS (mean (SD) = 30.03pmol $O_2/s^{-1}/mg^{-1}$ (5.26)).

In comparison to positive controls, negative slices demonstrated a significantly lower respiratory flux throughout the SUIT protocol, signifying reduced mitochondrial respiratory capacity. Moreover, negative controls failed to respond to the addition of any substrates throughout the protocol. (Figure 17B, Table 5).

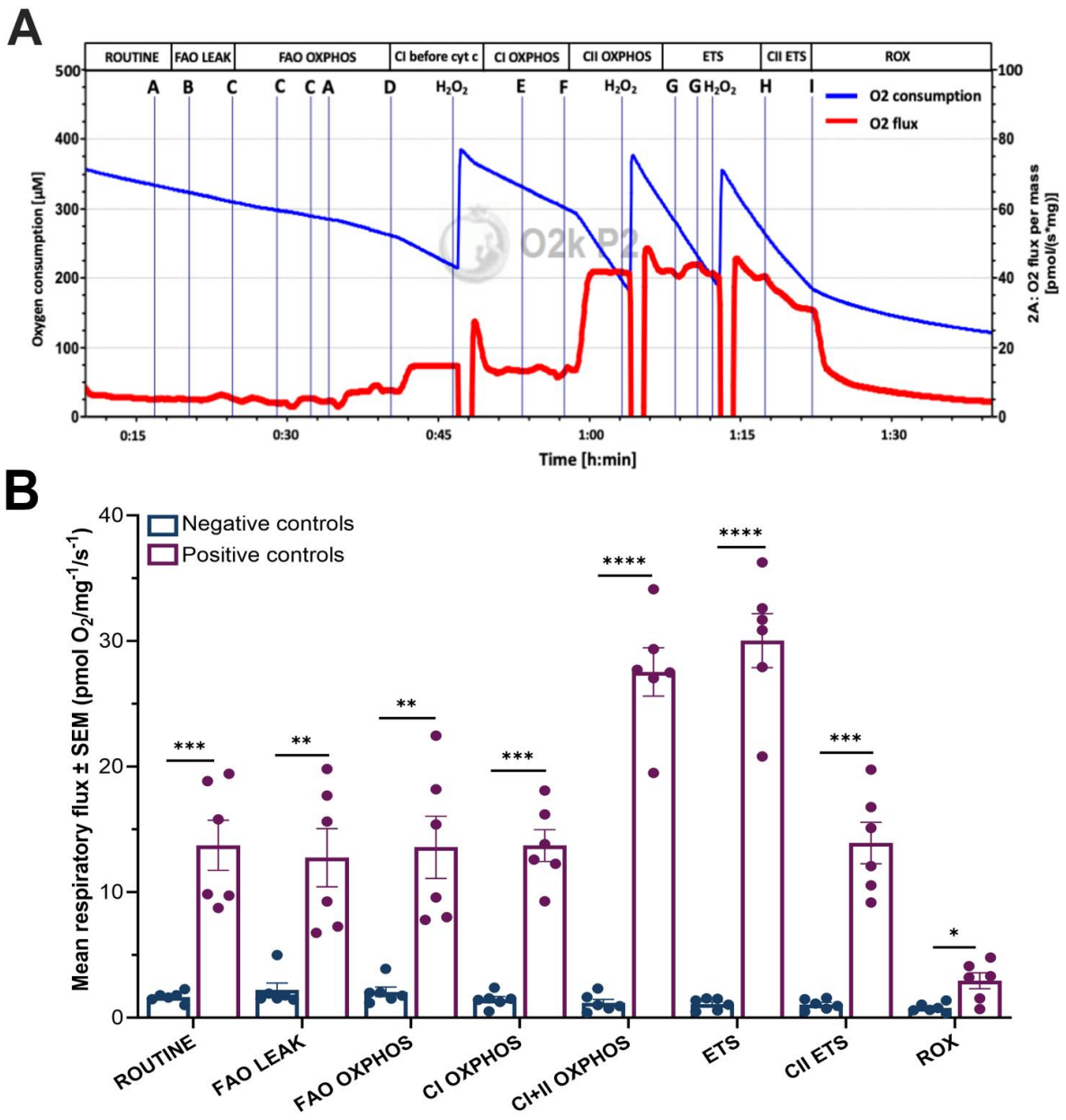

Figure 17. Respiratory flux was significantly higher in positive control slices.

A - Example trace of respiratory flux from a positive control slice (blue trace**;** oxygen concentration within the chamber (µM), red trace**;** respiratory flux of the slice (pmol $O_2/s^{-1}/mg^{-1}$**)** A – malate, B – octanoyl carnitine, C – ADP, D – glutamate, E- cytochrome c F – succinate, G- FCCP, H - rotenone, I – antimycin. **B** – Comparison of respiratory flux in negative and positive control slices. CI OXPHOS; complex I oxidative phosphorylation, CII OXPHOS; complex II oxidative phosphorylation, CI + II OXPHOS; complex I and II oxidative phosphorylation, ETS; electron transfer state, FAO LEAK; fatty acid oxidation leak, FAO OXPHOS; fatty acid oxidative flux ROX;

residual, non-mitochondrial respiration. Data presented as mean ± SEM 100% negative controls *n* = 6 slices, positive controls *n* = 6 slices. Significance determined by paired *t* test * *P*<.05, ** *P*<.01, *** *P*<.001, **** *P*<.0001.

Table 5. Mitochondrial state respiratory flux in negative and positive controls.
CI OXPHOS; complex I oxidative phosphorylation, CII OXPHOS; complex II oxidative phosphorylation, CI + II OXPHOS; complex I and II oxidative phosphorylation, ETS; electron transfer state, FAO LEAK; fatty acid oxidation leak, FAO OXPHOS; fatty acid oxidative flux ROX; residual, non-mitochondrial respiration. Negative controls *n* = 6 slices, positive controls *n* = 6 slices. Significance determined by paired *t* test.

Respiratory State	**O_2 flux per mass (pmol O_2/s^{-1}/mg^{-1}) Mean (SD)**		***P***
	Negative controls	**Positive controls**	
FAO LEAK	2.20 (1.38)	12.74 (5.67)	0.0036
FAO OXPHOS	2.06 (0.95)	13.57 (6.07)	0.0034
CI OXPHOS	1.43 (0.59)	13.71 (3.11)	0.0001
CI + II OXPHOS	1.04 (0.47)	27.53 (4.73)	<0.0001
ETS	0.99 (0.43)	30.03 (5.26)	<0.0001
CII ETS	1.03 (0.43)	13.91 (4.03)	0.0006
ROX	0.80 (0.41)	2.94 (1.55)	0.019

3.3.2 The effect of KCl stimulation on metabolic function

Whilst Oroboros provides insight into oxidative respiration from the mitochondria, the OCR and ECAR were recorded in slices from a wild type animal to calculate changes in both glycolysis and mitochondrial respiration during CSD. OCR and ECAR were measured following the addition of KCl (500 µM; *n* = 13 slices) or aCSF (*n* = 7 slices) as a control.

Baseline OCR was similar between control and KCl slices (Figure 18C). Stimulation with KCl led to a decrease in OCR, with rates significantly lower than control slices ((control = 221.40% (48.21), KCl = 175.60% (42.49), *P* = 0.0414, Figure 18A, C). Non-mitochondrial OCR was significantly lower in control slices than those stimulated with KCl ((control = 56.48 (9.79), KCl = 81.41 (26.21), *P* = 0.0276, Figure 18D).

Using the OCR and ECAR it was possible to calculate PER which is attributed to glycolysis (glycoPER). Baseline glycoPER was slightly lower in control slices compared to those which would be stimulated with KCl (control = 60.36pmol H+/min, KCl = 108.03pmol H+/min, Figure 18F). KCl injection led to a significantly increased glycoPER (258.82pmol H+/min), whereas aCSF addition led to reduction in glycoPER (1.11pmol H+/min, Figure 18G). glycoPER following rotenone and antimycin A addition to inhibit mitochondria indicates compensatory glycolysis. This was higher in control slices compared to those stimulated with KCl (control = 537.60pmol H+/min, KCl = 248.20pmol H+/min, Figure 18H).

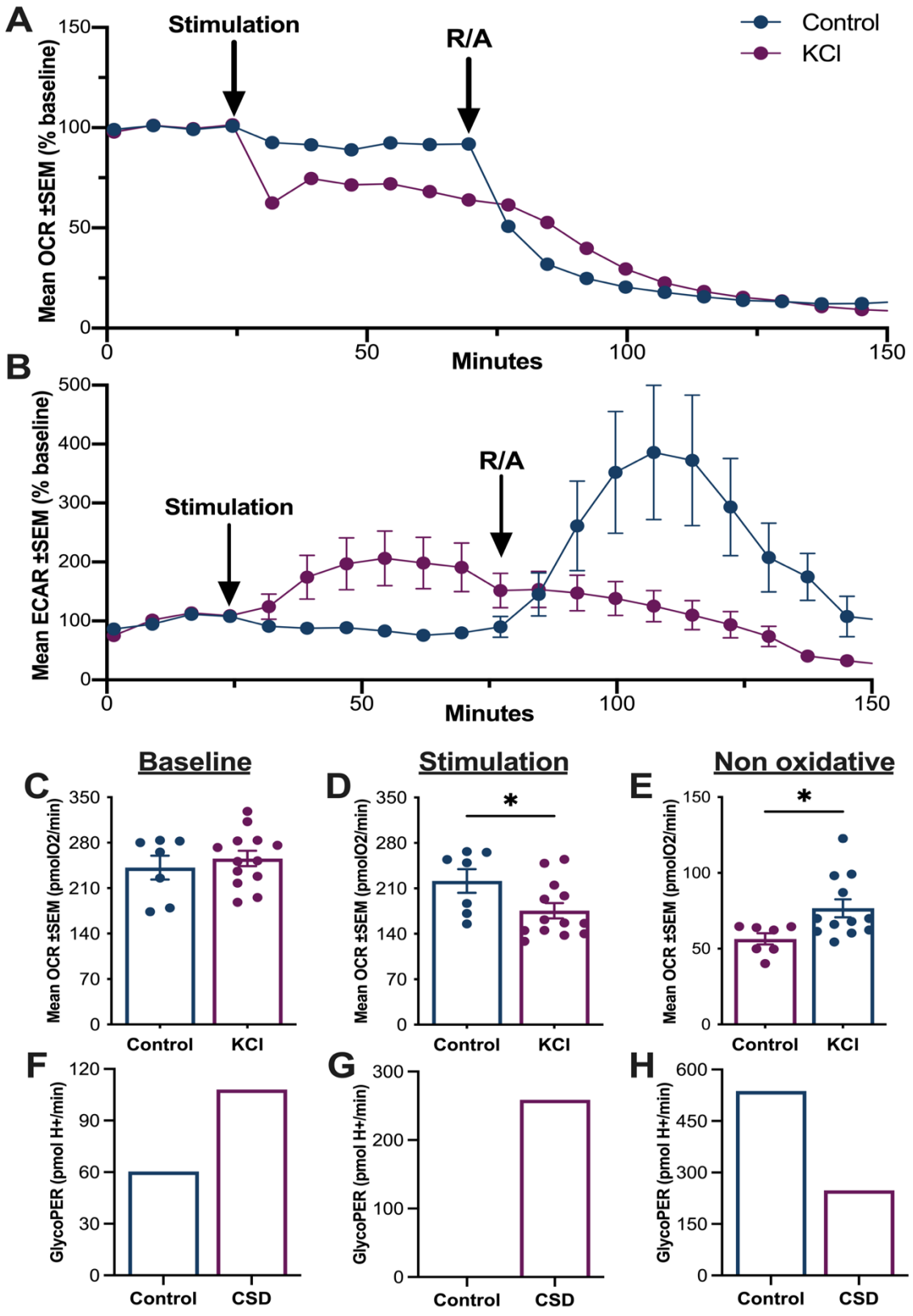

Figure 18. OCR, ECAR and glycoPER in brain slices following CSD induction.

A – Average OCR and **B**- ECAR from slices stimulated with KCl and control slices treated with aCSF alone. **C-D** – quantification of OCR at **C -** baseline**, D** - following KCl/aCSF stimulation and **E** - after the addition of rotenone and antimycin A to block mitochondrial function. **F-G** - glycoPER calculated from slices at **F –** baseline, **G** - following stimulation**, H** - and after the addition of rotenone and antimycin A. Data represent mean ± SEM, significance is determined by unpaired *t* test * *P*<0.05.

3.3.3 The impact of glucose deprivation on responses to CSD

3.3.3.1 KCl stimulation increases Ca^{2+} fluorescence

Fluorescent Ca^{2+} was measured in brain slices in response to KCl stimulation in slices both in the presence (+glc) and absence (-glc) of glucose. Prior to KCl addition, there was minimal Ca^{2+} movement with almost no change in fluorescence (Figure 19A and B). Following the addition of KCl, fluorescence significantly increased in +/- glc slices (mean AUC (SD) +glc control = 2.26 (10.87), KCl = 11.40 (18.04) *P*<0.0001 *n* = 8 mice; -glc control =4.81 (10.08), KCl = 11.10 (8.80) *P*<0.0001 *n* = 7 mice). Ca^{2+} fluorescence continued to increase over the 200 second recordings, plateauing at t150 seconds after KCl addition (-glc *n* = 11, +glc *n* = 11 mice, Figure 19C). Change in F/F0 was faster in –glc slices than +glc (F/F0 =1.10 in –glc =24s *n* =11 mice, +glc = 37.5s *n* = 11 mice Figure 19C) and continued to increase to a higher maximum F/F0 than +glc (maximum F/F0 +glc =1.20, -glc = 1.28, Figure 19D). All animals used to investigate the impact of glucose on Ca^{2+} activity were transgenic. However, there were no differences in the activity of Ca^{2+} in the absence of glucose between genotypes (AUC mean (SE) wild type = 275.9 (0.77), transgenic = 276.7 (0.97), Appendix Figure 1).

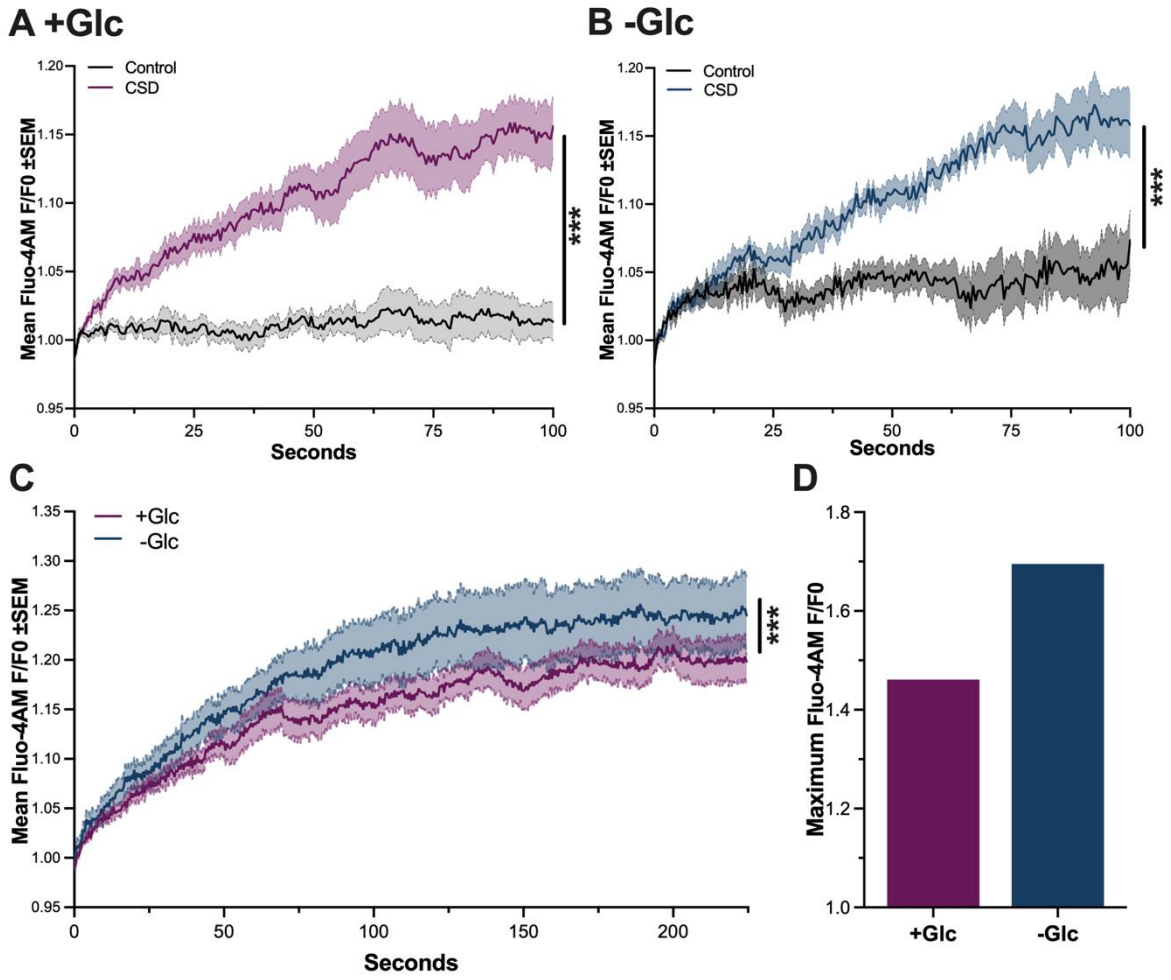

Figure 19. KCl induced changes in Ca^{2+} movement in the presence and absence of glucose.

A - Fluo-4AM F/F0 in +glc slices following KCl versus controls (*n* = 7 mice) **B -** F/F0 in -glc slices following KCl versus controls (*n* = 8 mice). **C -** F/F0 following KCl in +glc (*n* = 11 mice) and -glc (*n* = 11 mice)**. D -** Maximum F/F0 in -/+ glc slices. CSD; cortical spreading depression, Glc; glucose. Data presented as mean ± SEM. Significance determined by unpaired *t* test *** *P*<0.001.

3.3.3.2 KCl increases RH123 fluoresce in presence of glucose

RH-123 was used to assess the spatial response of mitochondrial activity in brain slices following CSD, both in the presence and absence of glucose. In +glc slices, KCl stimulation led to a significant increase in RH123 fluorescence (mean AUC (SD) control = 0.16 (0.38), KCl = 1.12 (1.56), *n* = 5 mice, *P*<0.0001 Figure 20A). In -glc slices however, there was no changes in RH123 fluorescence following KCl (control = 0.05 (0.19), KCl = 0.06 (0.41), *n* = 5 mice, Figure 20B). Change in RH123 fluorescence is significantly higher in +glc than -glc following KCl (+glc = 13.00 (17.36) *n* = 9 mice, -glc = 0.34 (4.13) *n* = 8 mice p <0.0001, Figure 20C). Both transgenic (TG) and WT animals were used for these investigations. The impact of genotype on mitochondrial activity was explored and there were no significant differences in responses between wild type and transgenic slices in the presence of glucose (AUC mean (SE) wild type = 24.26 (0.41), transgenic = 24.69 (0.45), Appendix Figure 1). Additionally, there were no significant differences in responses between wild type and transgenic slices in the absence of glucose (AUC mean (SE) wild type = 12.23 (0.10), transgenic = 12.34 (0.08), Appendix Figure 1).

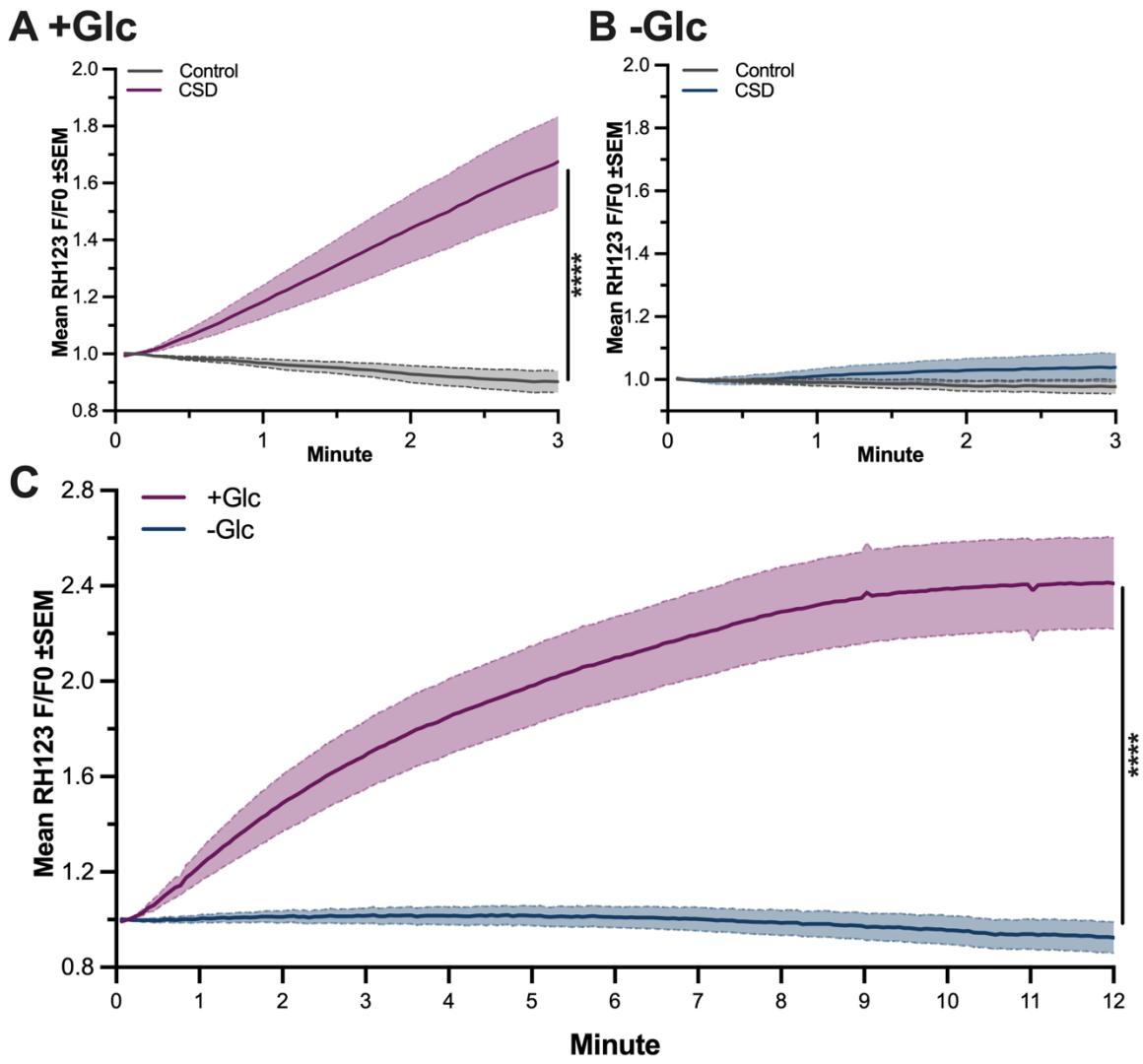

Figure 20. KCl induced changes in RH123 fluorescence in the presence of glucose.

A - F/F0 in control (pre-stimulation) and after KCl in +glc slices (*n* = 5 mice) **B -** F/F0 in control (pre-stimulation) and after KCl in -glc slices (*n* = 5 mice) **C -** F/F0 in +glc (*n* = 9 mice) and -glc (*n* = 8 mice) slices after KCl. CSD; cortical spreading depression, Glc; glucose, RH123; rhodamine 123. Data presented as mean ± SEM. Significance determined by unpaired *t* test **** *P*<0.0001.

3.3.3.3 Metabolites were altered following CSD in the presence and absence of glucose

Metabolites were quantified in brain slices following induction of CSD in both the absence and presence of glucose. In +glc slices, a number of metabolites were significantly altered following CSD. Notably, lactate was found to be increased (mean (SD) control = 148.52 (52.71) *n* = 10 slices, CSD = 457.16 (221.13) *n* =13 slices, *P* = 0.0006, Figure 21E), in addition to malate (control = 8.01 (1.53), CSD = 11.89 (3.90), *P* = 0.0099, Figure 21F) and pyruvate (control = 3.09 (0.93), CSD = 3.98 (0.91), *P* = 0.0315, Figure 21H). Several metabolites demonstrated a trend towards significance increase following CSD (Table 6).

The metabolic profile of slices following a CSD differed depending on the presence of glucose. Notably alanine, glutamate, lactate and malate were significantly lower in -glc compared to +glc slices after CSD (Table 6, Figure 22A,D,E,F). Aspartate, proline and succinate were found to be significantly higher in -glc slices compared to +glc slices following CSD (Table 6, Figure 22B,G,I).

Metabolites were measured in slices from both wild type and transgenic animals in both the presence and absence of glucose. The metabolites were compared between genotypes following CSD (Appendix Table 2) citrate in the presence of glucose was the only metabolite which demonstrated a higher concentration in transgenic animals (wild type mean (SD) = 2.50 (0.48) *n* = 4, transgenic = 7.25 (1.05) *n* = 9, *P* = 0.014).

Table 6. Metabolites quantified in control and CSD, +glc and -glc slices.

CSD; cortical spreading depression, Glc; glucose, SD; standard deviation. Significance determined by unpaired *t* test, * *P*<0.05, ** *P*<0.01, *** *P*<0.001, **** *P*<0.0001

Metabolite	**Concentration Mean (SD)**		**p**	**Concentration Mean (SD)**	**p**
	+Glc Control *n* = 10	**+Glc CSD *n* = 13**		**-Glc CSD *n* = 13**	
Alanine	12.55 (5.41)	19.22 (10.17)	0.0749	6.83 (3.30)	0.0003 ***
Aspartate	186.46 (59.66)	205.40 (88.22)	0.5664	285.35 (103.69)	0.0448 *
Citrate	3.58 (1.24)	5.79 (3.47)	0.0693	5.99 (3.92)	0.894
Fumarate	4.83 (1.41)	5.48 (1.75)	0.3528	5.03 (1.54)	0.4978
Glutamate	372.87 (131.48)	511.72 (234.31)	0.1085	213.74 (78.99)	0.0002 ***
Glycine	37.50 (20.57)	47.42 (24.14)	0.3176	32.88 (8.60)	0.0531
Isoleucine	0.85 (0.26)	1.12 (0.44)	0.107	0.83 (0.19)	0.0418 *
Lactate	148.52 (52.71)	457.16 (221.13)	0.0006 ***	98.34 (67.02)	<0.0001 ****
Leucine	0.91 (0.35)	1.39 (0.86)	0.1106	0.92 (0.33)	0.0789
Malate	8.01 (1.53)	11.89 (3.90)	0.0099 **	9.06 (2.32)	0.050 *
Pyruvate	3.09 (0.93)	3.98 (0.91)	0.0315 *	3.81 (1.39)	0.7116
Succinate	11.83 (4.30)	16.17 (7.00)	0.0997	38.96 (14.12)	<0.0001 ****

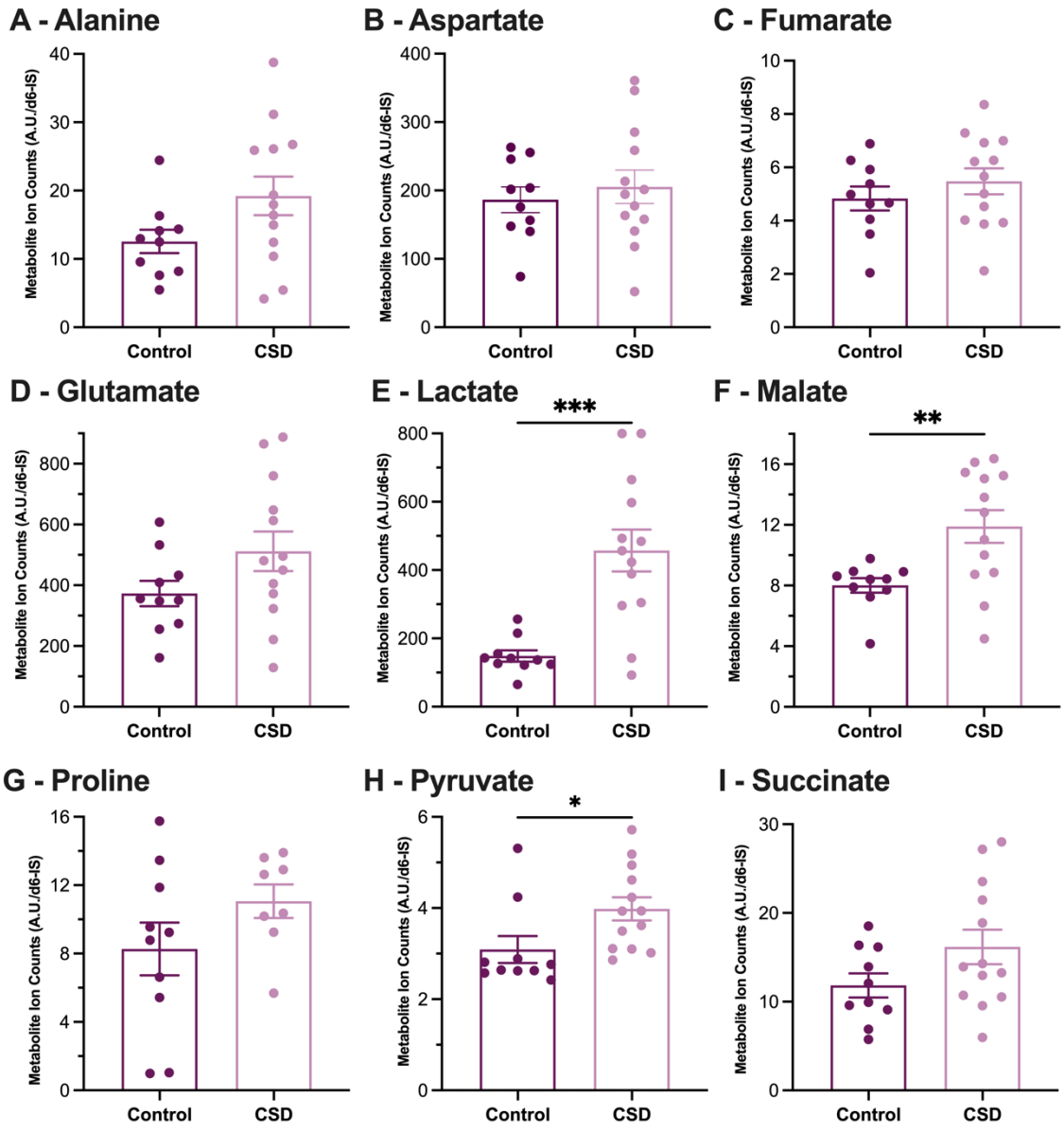

Figure 21. Metabolite quantification in brain slices following CSD stimulation. AU; arbitrary units, CSD; cortical spreading depression. Data presented as mean ± SEM. Significance determined by unpaired *t* test * *P*<0.05, ** *P*<0.01, *** *P*<0.001.

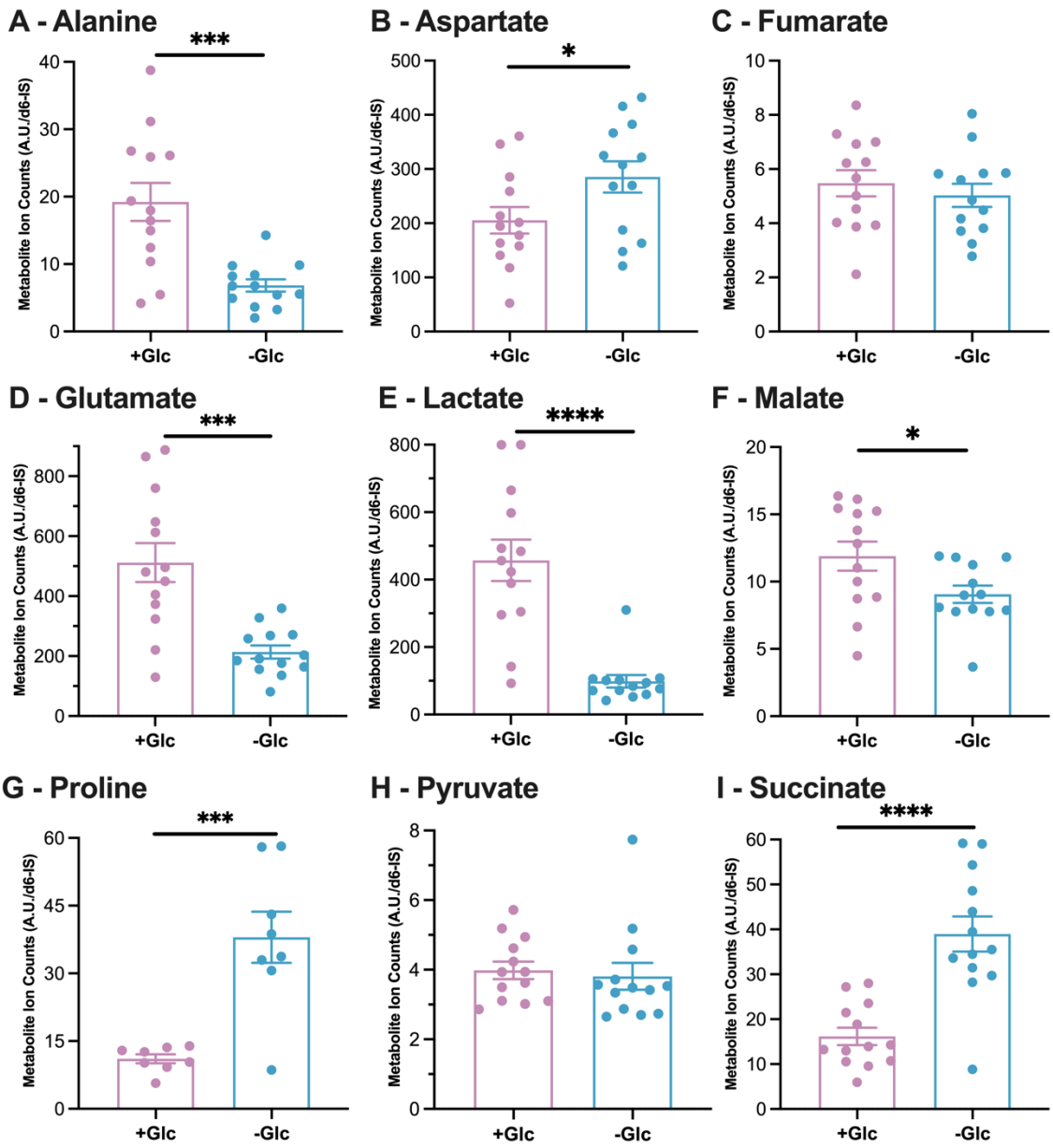

Figure 22. Metabolite quantification in brain slices following CSD stimulation in the presence and absence of glucose.

AU; arbitrary units, Glc; glucose. Data presented as mean ± SEM. Significance determined by unpaired *t* test * $P<0.05$, ** $P<0.01$, *** $P<0.001$. **** $P<0.0001$.

3.4 Discussion

This chapter established a viable, acute brain slice platform capable of providing readouts of CSD induced changes in metabolism. Moreover, investigating the impact

of glucose on responses to CSD has demonstrated differential metabolic responses, perhaps to mitigate the absence of a major energetic substrate. These changes suggest that brain slices exhibit metabolic plasticity in response to stimulation, to utilise alternative pathways to generate ATP and rescue ionic gradients.

3.4.1 Slices in the model exhibited low apoptotic activity

Acute slices demonstrated reduced apoptotic activity in comparison to negative control (100% ethanol) slices, proving their suitability as a model for metabolic investigation. Creation of the acute brain slices involves unavoidable exposure of the tissue to hypoxia while the brain is isolated and prepared for slicing. Moreover, the slicing procedure necessarily involves a degree of physical injury. Therefore, it was important to assess the viability of slices following the slicing procedure. Negative control slices exposed to hypoxia and incubated in ethanol without oxygenation demonstrated significant caspase-3 activity. Evaluation of caspase-3 activity has also demonstrated increases indicative of apoptosis in cerebral organoids exposed to increasing ethanol concentrations,[266] demonstrating the validity of this assessment. In comparison, positive control slices exhibited sparse caspase-3 activity, which may be due to the initial trauma caused during slicing. Previous investigation of acute brain slices has demonstrated spontaneous activity of neurons up to 3 hours after creation,[267 268] thereby determining the viability of slices during this period.

We also evaluated the rupture of cell membranes via the PI assay, since this method is a well-established readout of cell death.[269] Considering tissues had undergone significant mechanical trauma following slicing, it is unsurprising positively PI stained neurons were abundant throughout both positive and negative controls. This is a

similarly found by other groups utilising acute brain slices, which show positive PI staining in tissue deemed viable to assay.[269] Nevertheless, some differences in PI staining were evident between 100% ethanol and aCSF treatments, with ethanol treated slices showing clusters of intensely PI positive cells that were not observed in the aCSF group. 350μm is a typical thickness for acute brain slices investigations, in part because it allows retention of a reasonable volume of viable cells and circuits above and below the cut surfaces, which are the primary sites of mechanical trauma. Observations of CSD events in this study, and those of others [270], indicate preservation of viable neural circuits despite anatomical damage arising from the slicing procedure. Interestingly, in this study, NucView488 may have been more suitable for assessing the health and viability of acute brain slices, since other studies have revealed that PI mediated disparities are not demonstrated until after 6 hours following slicing.[268]

A future investigation of the changes in apoptotic activity over time following slices may provide the ideal window of investigation in this model. An alternative solution to combat apoptotic activity due to the trauma of slicing is the use of organotypic brain slice cultures, particularly from younger animals. Acute adult mouse slices were chosen for the present studies in an attempt to develop a model closer to adult headache while avoiding potential limitations associated with culture artefacts. However, the use of organotypic cultures brings advantages since they tend to demonstrate higher plasticity and greater resistance to mechanical trauma. Slice cultures are typically obtained from young post-natal pups, and are maintained at a liquid medium / air interface on a porous membrane interface that sustains the slices for many weeks.[271] Importantly slice cultures continue to exhibit robust spontaneous network activity over a number of weeks to months[272] highlighting a greater viability

and functionality in comparison to acute slice models, and their suitability for future studies of CSD-related events.

3.4.2 Characterizing mitochondrial activity in slices at baseline

Utilizing high-resolution respirometry, the findings indicate that under normal conditions, acute brain slices primarily depend on oxidative phosphorylation rather than fatty acid oxidation. This is evident from the observed increase in respiratory flux when transitioning to CI and CII OXPHOS states. There are no existing studies which have assayed whole intact forebrain slices using high resolution respirometry. Comparable procedures have been applied to whole mouse brain samples and homogenized distinct brain regions, revealing a consistent pattern of responses and peak oxygen flux rates during complex I and II oxidative phosphorylation.[273 274]

Other studies using homogenate samples have higher fluxes at approximately 100-110pmol $O_2/mg^{-1}/s^{-1}$ during electron transfer state evaluation, whereas brain slices in this study achieved a mean 30.03pmol $O_2/mg^{-1}/s^{-1}$. Discrepancies in respiratory flux amplitude may be due to variation in tissue preparation. Intact brain slices maintain tissue architecture and interactions between organelles, while homogenization of tissue disrupts this architecture and permeabilizes the plasma membrane of cells. Permeabilization and isolation of mitochondria may aid the delivery of substrates to the mitochondria. However, this method may not be suitable for future investigation of the consequences of CSD, since it prevents the immediate assessment of neural circuit function following stimulation. In support of this, assays using non-permeabilised hippocampal slices exhibit oxygen flux rates which are more comparable to the brain slice values in this study.[275] ETS stimulated values in

hippocampal slices were on average 11pmol $O_2/mg^{-1}/s^{-1}$ and although lower than whole brain slices, the selection of brain region may underlie discrepancies.[275]

Comparing the respirometry responses of positive and negative control slices provides further evidence of the disparity in viability of the controls. Negative slices exhibited significantly depleted mitochondrial activity and failed to respond to the addition of substrates in the SUIT protocol, indicating a diminished activity across all mitochondrial complexes and respiratory states. Cerebral organoids exposed to ethanol also exhibited mitochondrial dysfunction as evidenced by decreased mitochondrial respiratory flux, similarly to the effects in 100% ethanol slices in this thesis.[266] Interestingly, organoid consumption rates were not depressed to the levels seen in the ethanol slices in this thesis, a discrepancy that may be due to the combination of a lower temperature, and exposure to hypoxia in the present study. This model thereby provides a useful tool for future investigation of metabolic and ionic pathways involved in CSD.

3.4.3 Glycolysis is upregulated in response to KCl

Measuring OCR and glycoPER allowed the monitoring of oxidative respiration and glycolysis in brain slices in response to KCl. The findings revealed that in response to KCl stimulation, slices upregulate glycolytic activity and reduce mitochondrial respiration. This shift favouring glycolysis over oxidative phosphorylation could be an adaptive response to rapidly produce ATP in response to depolarization. Previous studies of the metabolic effects of CSD have demonstrated an early breakdown of glycogen in response to increased energy demand,[116] supporting the finding that glycolysis plays an important role in supporting the energy demands of cortical tissue

during the initial period following CSD. It was also observed that KCl addition reduced mitochondrial oxidative respiration (OCR), below that of baseline. This may be due to the preference of glycolysis during this energetically demanding period.

Inhibiting mitochondrial activity to a higher level of OCR in KCl stimulated slices compared to controls. This was unexpected but may indicate non-specific oxygen consumption driven by reactive oxygen species (ROS) or nitric oxide production. ROS has been found to be consistently upregulated by CSD,[276] [277] and nitric oxide has multiple roles in migraine pathophysiology including cranial blood flow and nociceptive processing.[278] This highlights a metabolic response to CSD which may contribute towards headache pathophysiology.

Previous studies have also suggested that this process of non-mitochondrial OCR is utilized to recycle NADH for glycolysis.[279] This supports the finding of glycolysis in response to CSD but indicates slices are limited by the supply of energetic substrates to sustain adequate ATP production via glycolysis.

aCSF addition to control slices diminished glycoPER, to below that of baseline activity. The reasons for this are unknown however OCR is increased, indicating high mitochondrial activity, potentially suggesting a preference of metabolic processes. This is also supported by the finding that inhibition of mitochondrial respiration with rotenone and antimycin A led to increased glycoPER in control slices. This measurement of glycoPER represents compensatory glycolysis and is likely higher as there is more of a mitochondrial ATP supply to compensate for.

Although only the effects of a single injection of KCl were investigated, this sustained an increased concentration of K+ in the media for the remainder of the recording. This may have resulted a sustained depolarisation with conduction block and may relate to the finding of lower glycolytic activity in KCl slices compared to controls

towards the end of the recording. Repeated CSD events and the resulting prolonged depletion in glycolytic activity may contribute towards headache pathophysiology and suggests a therapeutic target. It should be noted that this method was only performed on slices from one animal. Although the methodology allows the simultaneous recording from multiple slices in separate wells, the results only represent the metabolic response of one animal.

3.4.4 Ca^{2+} movement increases in response to KCl stimulation

Focal application of KCl to the cortical edges of brain slices resulted in a significant increase in Ca^{2+} fluorescence in cortical regions. These changes in Ca^{2+} demonstrate temporal and spatial characteristics similar to the spread of depolarization recorded by intrinsic optical signals and electrophysiology.[280] Other brain slice models also utilising fluorescent Ca^{2+} indicators, illustrated that CSD was associated with wave-like movements of increased intracellular Ca^{2+} thar preceded the onset of changes in intrinsic optical signals.[281] Moreover, *in vivo* models utilising genetically encoded fluorescent Ca^{2+} plasmids exhibited associations between electrically recorded CSD events and increases in Ca^{2+} fluorescence, which both moved in waves across the cortical surface of the brain.[282]

Waves of Ca^{2+} flux are predominantly facilitated by astrocytes during depolarisation spreading.[281] Hence, the analysis of Ca^{2+} fluctuations offer a proxy for measuring the propagation of depolarization within neurons and, possibly provides further insights into the astrocytic response during CSD. Interestingly, voltage gated Ca^{2+} channels are present in the dura mater, trigeminal ganglion and TNC in which Ca^{2+} signalling is thought to regulate CGRP release.[283] Although CGRP was not measured in these

slices, Ca^{2+} signalling may provide a map of CGRP release and may contribute towards the relationship between CSD and headache nociception.

The role of Ca^{2+} signalling during CSD remains unclear but could potentially elicit a neuroprotective response. Previous studies have shown that increased cytoplasmic Ca^{2+} levels prior to oxygen-glucose deprivation can prevent neuronal death in hippocampal neurons. [284] This phenomenon might explain the heightened intensity of signals in slices deprived of glucose, as Ca^{2+} signals peaked faster and higher compared to those with glucose. Previous investigation demonstrated that glucose deprivation led to oxidative stress and mitochondrial dysfunction in neurons but not astrocytes. As results demonstrate the facilitation of Ca^{2+} movements in astrocytes this may support the resilience of astrocytes to glucose deprivation.[285] Moreover, cell models have demonstrated an upregulation of Ca^{2+} signalling during glucose deprivation, activating the PI3K/Akt survival signalling pathway.[286] This provides further evidence for the protective role of Ca^{2+} in response to CSD.

Elevated Ca^{2+} levels may however induce neuronal injury if levels persistently remain elevated after CSD.[287] While longitudinal measurements were not taken to observe changes during CSD recovery, previous studies on oxygen and glucose deprivation have demonstrated prolonged increases in Ca^{2+} levels, suggesting possible membrane damage. Aberrant Ca^{2+} accumulation may therefore contribute to neuronal damage and increase susceptibility to CSD.

3.4.5 Mitochondrial activity following CSD is dependent on glucose availability

Mitochondrial activity was upregulated in response to KCl stimulation in the presence of glucose, indicating that CSD induces an increase in energetic demand. However, in the absence of glucose, there was no change in mitochondrial activity, highlighting an inability to respond to heightened energetic demands and potentially suggesting mitochondrial exhaustion.

It is somewhat surprising that even in the absence of glucose, mitochondrial activity is not upregulated, considering these pathways rely on other substrates such as fatty acid oxidation and glutamate. It's possible that oxidative respiration was being utilized to maintain the baseline activity of brain slices but may not have been sufficient to support a dramatic increase in energetic demand following CSD. In a NTG mouse model of migraine, low-glucose resulted in decreased levels of ATP production, which were accompanied by an increased production of ROS.[288] Although the production of ROS was not measured, alanine, a metabolite involved in antioxidation[289] [290] was significantly lower in -glc slices following CSD. Reduced mitochondrial activity in the absence of glucose may be indicative of upregulated ROS which may exacerbate nociception in conditions of fasting headache.[278] This may also indicate that slices in the absence of glucose are unable to counteract increasing levels of ROS as a result of depolarisation.

3.4.6 Differential metabolism is upregulated in the absence of glucose

We measured changes in metabolites following CSD in brain slices in the presence of glucose and found increases in pyruvate, lactate and malate. Pyruvate is a product of glycolysis which correlates with findings of increased glycolytic activity in response to KCl-mediated depolarisation. An increase in lactate, an anaerobic product of glycolysis, was also discovered. This is a common finding both *in vivo* in rodent models[291] and human tissues,[292] in which glucose is rapidly utilized and lactate increases in response to stimulation. *In vivo*, CSD is often accompanied by neurovascular changes which may struggle to provide adequate oxygen to highly metabolic active tissue, leading to hypoxia.[115] [123] This failure to meet oxygen demands may result in anaerobic respiration, as demonstrated by the observation of increased pyruvate and lactate. Moreover, in conditions of metabolic stress, neuronal tissue may resort to lactate as an alternative energy substrate.[116]

In the absence of glucose, several metabolites were altered. Alanine, a metabolite involved in antioxidation[289] [290] was lower following CSD, further supporting the hypothesis that ROS production may be upregulated in the absence of glucose. Lactate was also found to be reduced compared to slices with glucose, this is likely because the starting substrate of anaerobic respiration is not available. Moreover, previous investigation of the effects of low glucose have exhibited NADH/NAD+ redox imbalance leading to reduced lactate dehydrogenase activity.[293]

Interestingly a lower concentration of glutamate was also identified in glucose deprived slices. Previous investigation in brain slices found that inhibiting pyruvate uptake drives neurons to switch to glutamate as a fuel for the TCA cycle.[294] This not

only supplies substrates for oxidative phosphorylation, but since neurons are believed to take up and utilize glutamate, may prevent the accumulation of glutamate consequently exocytotic injury.[294]

Succinate was found to be significantly higher in slices without glucose. Evidence has demonstrated that succinate is sensitive to tissue hypoxia, and is often a signal of ischemia.[295] For example, oxygen-glucose deprivation led to accumulation of succinate in neural cells.[296] Succinate accumulation is additionally thought to be responsible for mitochondrial ROS production during reperfusion,[297] and may contribute towards ROS production during CSD. Although not significant in slices with glucose, there is a slight increase in succinate following CSD. In conditions of glucose deprivation, oxygen consumption may be higher in an increased attempt to support alternative metabolic pathway, therefore leading to hypoxia. Oxygen supply in tissue slices was not monitored during and after a CSD, changes in metabolic markers were observed which suggest an upregulation of ROS and hypoxia.

3.4.7 Limitations and future directions

The work in this chapter does have some limitations which should be considered.

Both wild type and transgenic animals were used in these experiments, however there were no significant differences identified in the metabolic results between genotypes. Although Ca^{2+} movement was utilised as a surrogate of CSD in brain slices, this project did not utilise a method of electrophysiological measurement of CSD in response to KCl stimulation. Therefore, it was not possible to correlate the metabolic findings with the exact electrophysiological responses. Future experiments aim to record CSD events temporally and spatially in brain slices with the use of

multi-electrode assays. This would allow the exploration of the cellular impact of metabolic deficiency and assessment of the benefits of nutraceuticals on CSD characteristics. This model would additionally lend itself to investigating the impacts of secondary headache disorders on CSD. In the context of IIH, obtaining brain slices from animals with raised ICP or alternatively exposed to risk factors such as obesity and testosterone excess would be valuable to investigate the impact of these mechanisms on CSD.

The extracellular Ca^{2+} concentrations employed in aCSF within this thesis were notably lower than the levels typically used in other studies. Established brain slice models commonly utilize Ca^{2+} concentrations ranging from 1.2 to 2mM. Nevertheless, the results obtained in this thesis support the validity of the experiments conducted. Even with reduced Ca^{2+} levels, KCl was still effective in influencing changes in intracellular Ca^{2+} flux, as recorded with Fluo4AM. Additionally, the metabolic effects observed following KCl stimulation indicate the induction of cellular signalling events, despite the lower Ca^{2+} concentration.

In rats, the intracellular Ca^{2+} concentration is estimated to be 36-57nM, and it is reasonable to assume similar levels in mice. Under these conditions, an extracellular Ca^{2+} concentration of 2µm (as used in our experiments) would have provided a reasonable chemical driving force to facilitate Ca^{2+} influx via L-type voltage-operated Ca^{2+} channels. In conclusion, it is justifiable to believe that the Ca^{2+} concentration employed in this study was adequate to support CSD, and the observed Ca^{2+} signals can be attributed to depolarization-induced Ca^{2+} influx.

Although brain slices models are valuable tools for investigating CSD, they lack CBF which is a central component of the characteristic response to CSD. Brain slices were incubated with oxygen to prevent tissue hypoxia however the results of these

investigations must take into consideration this facet of the physiological response is lacking. Moreover, the impact of complete glucose deprivation was chosen as a model of metabolic stress, which may not be fully translational to fasting headache. However, this was chosen to investigate a proof of concept, and demonstrated via Ca^{2+} imaging that there is still a physiological response to CSD. Future investigations of a dose-dependent response to decreasing glucose concentrations may more fully recapitulate the triggers in patients.

This study employed both male and female animals to create acute brain slices. Recent evidence has highlighted sex-related differences in CSD, particularly demonstrating increased susceptibility in females.[298 299] Although the methods did not allow us to investigate this, there were no overt differences found in metabolic responses between slices from sexes. However this model would allow further in depth exploration of the role of sex and hormones on the role of metabolism and CSD, since oestrogen is thought to contribute towards modulation of electrophysiological responses.[298]

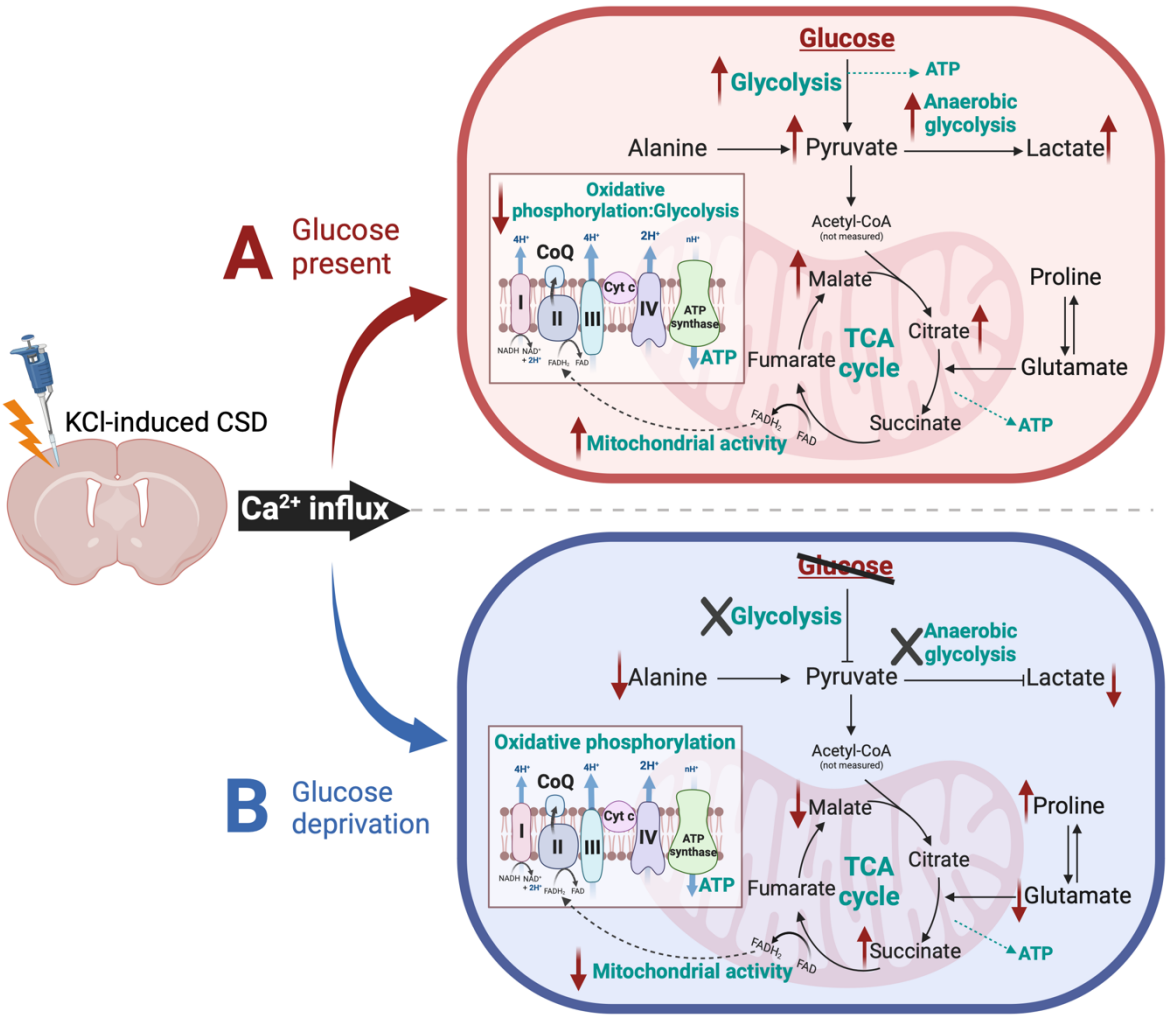

Figure 23. Summary of metabolic results in brain slices in the presence and deprivation of glucose.

In the presence of glucose; glycolysis and markers of anaerobic glycolysis were upregulated in response to CSD. Although there were markers of increased mitochondrial activity, seahorse analysis demonstrated a higher rate of glycolysis versus oxidative phosphorylation. In the absence of glucose; markers of glycolysis are reduced and there was no change in mitochondrial activity in response to KCl stimulation. Green text alludes to metabolic pathways, red arrows indicate upregulation or downregulation as indicated by results. ATP; adenosine triphosphate, Ca2+; calcium, CSD; cortical spreading depression, CoQ; coenzyme q10, Cyt c; cytochrome c, FAD+; flavin adenine dinucleotide, KCl; potassium chloride, NAD+; nicotinamide adenine dinucleotide, TCA; tricarboxylic acid. Figure created with BioRender.

CHAPTER 4 INVESTIGATING MECHANISMS OF HEADACHE IN ANIMAL MODELS OF RAISED INTRACRANIAL PRESSURE

4.1 Introduction

Raised ICP is a feature of several conditions driving headache including IIH,[300] TBI,[301] stroke,[302] hydrocephalus[303] and subarachnoid haemorrhage. Headache is the principal driver of morbidity in IIH,[57] and is highly refractory compared to migraine.[195] Current ICP lowering therapies exhibit poor efficacy[304] and tolerability,[305] underscoring the need for targeted headache therapeutics in IIH. However, developments are hindered by lack of knowledge of the mechanisms driving raised ICP headache. Raised ICP headaches are often migraine-like.[192] Allodynia has been observed in both migraine and in IIH, [57 72] and mechanical thresholds are noted to be abnormal in animal models of pain behaviour.[71]

The impact of raised ICP on headache pathways in animal models has not been extensively explored. Previous evidence of raised ICP in diet induced obesity models resulted in cephalic cutaneous allodynia and increased expression of α-CGRP in trigeminal ganglion.[196] Allodynia was however correlated with abdominal fat, making it difficult to decipher the role of raised ICP independently. Employing hydrocephalus models to study the influence of elevated ICP on headache would minimise the impact of secondary factors such as obesity.

4.1.1 Aims

The gap in knowledge regarding the role of raised ICP on headache mechanisms hinders the development of targeted therapeutics. Therefore, the aim of this chapter was to:

1. Validate and optimise a model of raised ICP using intracisternal injection of kaolin.
2. Investigate the influence of raised ICP on mechanical pain threshold behaviour.
3. Explore the impact of raised ICP on cortical excitability and CBF by recording evoked CSD responses.

4.2 Methods

4.2.1 Animal husbandry

Male Sprague Dawley rats (Enivgo) (n=64) aged 11-22 weeks weighing 228g-460g were used. Rats were housed in sex and litter matched groups in a climate-controlled room and kept on a 12:12 light/dark cycle with free access to food and water. All animal handling and procedures were performed according to the guidelines described in 2.1.2.

4.2.2 Cisterna magna injection

Injection of kaolin to the cisterna magna was used to impede CSF movement and thereby increase ICP.[204] Animals were anesthetized with isoflurane gas in an induction chamber and injected with saline (control) or kaolin (raised ICP) in the cisterna magna of animals as described in 2.3.1.

5mg/kg carprofen and 1ml/100g 0.9% saline was administered as needed in the days following injection. During behavioural studies, animals were injected with carprofen

on day 1 and day 4 following injection. For CSD studies, animals were given carprofen as necessary with a 48-hour wash out before the day of assessment.

4.2.3 Confirming raised ICP

The ICP was measured in the epidural space of the skull of animals for up to 30 minutes as detailed in 2.3.1.2. Following ICP measurements, some animals were used for CSD studies. In these animals, a cortical window was drilled in the parietal bone of the opposite hemisphere to avoid any effects of the ICP catheter placement on cortical responses.

4.2.4 Measuring CSD responses

CSD responses were recorded 7 days after cisterna magna injection. Animals were anesthetized with isoflurane gas and intravenous administration of anaesthesia was conducted as described in 2.3.1.1. Animals were also tracheostomized and mechanically ventilated as described in 2.3.1.1. Animals were secured in a stereotaxic frame and 2 cortical windows were created in the parietal bone of the skull as detailed in 2.3.2.3. A cotton pellet soaked in KCl was placed on the cortical surface of the brain and 5µL of KCl was added to the pellet every 15 minutes over 1 hour in accordance with other CSD studies.[259] DC and CBF responses to KCl stimulation were recorded using Spike2 software and analysed as described in 2.3.2.4.

4.2.5 Mechanical pain threshold testing

Mechanical pain thresholds were assessed at baseline (pre-injection) and 7 days after intracisternal injection (Figure 24). All animals were habituated to the testing room as described in 2.3.3.1. von Frey filaments were applied to the periorbital and hind paw regions to measure mechanical thresholds using the Up-Down method,[257] as detailed in 2.3.3.2. ICP was measured in animals following mechanical threshold testing as described in 2.3.1.2.

4.2.6 Tissue collection

At the end of experiments, animals were culled with an overdose of pentobarbital (Euthatal 0.1ml/kg). In pilot studies of kaolin volume optimisation and CSD investigations, animals were transcardially perfused with PFA, and the brain collected and fixed as described in 2.3.2.3. In animals used for mechanical pain threshold testing a coronal section of the brain central to bregma was cut and post-fixed in PFA for 1 week on an orbital shaker. The remaining brain tissue and trigeminal ganglia were snap frozen in liquid nitrogen for further at -80°C until further analysis.

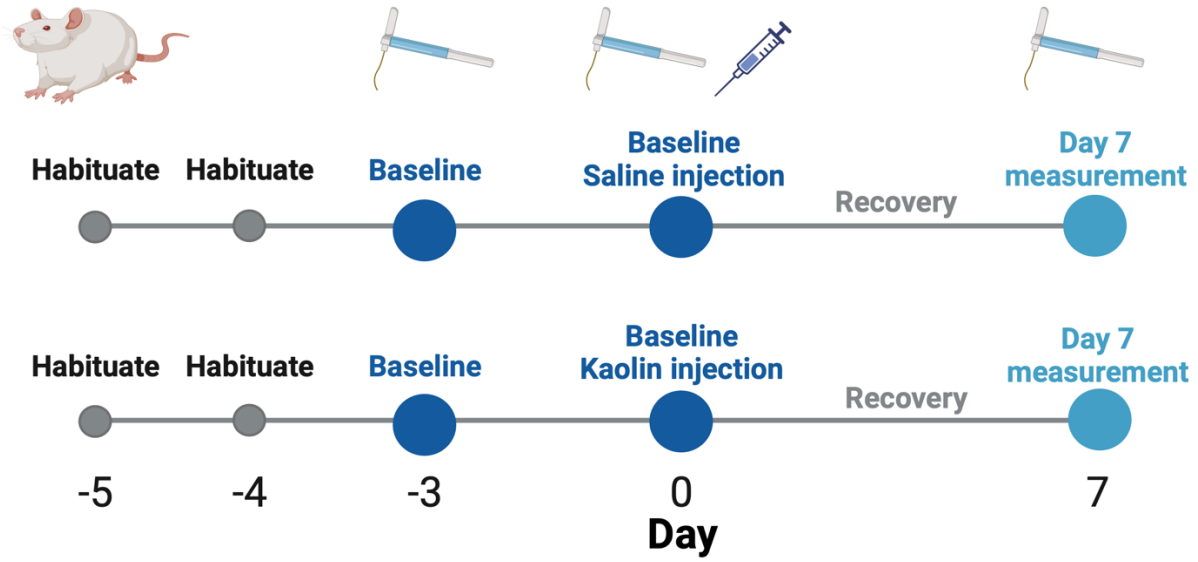

Figure 24. Timeline of raised ICP model and mechanical threshold testing. Timeline of behavioural experiments which assessed mechanical pain thresholds of animals with raised ICP (kaolin) versus controls (saline). Animals were habituated prior to baseline testing which was conducted prior to intracisternal injection and 7 days after injection. Figure created with BioRender.

4.2.7 Confirming hydrocephalus induction

To confirm hydrocephalus induction, fixed brain samples were sliced, and ventricle dilation was quantified in all animals as described in 2.3.5.1.

4.2.8 CGRP quantification in trigeminal ganglion

Protein was extracted and quantified from snap frozen trigeminal ganglion as described in 2.4.1.1. α-CGRP was quantified using an ELISA as described in 2.4.1.2. and expressed as normalized protein content.

4.2.9 Metabolite quantification

Snap frozen whole brain samples were pulverized, and the metabolites were extracted as described in 2.4.2.1. The absolute concentration of metabolites was measured in samples using NMR as detailed in 2.4.2.2. Metabolite content was normalised to the dry weight of each sample.

4.2.10 Statistical analysis

The normality of data was assessed using the Shapiro-Wilk test. Data which were normally distributed were analysed using parametric tests (*t* tests, Pearson's correlation coefficient) and reported as mean and standard deviation (SD). Non-normally distributed data were analysed using non-parametric tests (Mann-Whitney test, Spearman rank correlation test) and reported as median and range. Results were considered statistically significant when p values were * $P<0.05$, ** $P<0.01$, *** $P<0.001$, and **** $P<0.0001$.

4.3 Results

4.3.1.1 Confirming optimal kaolin volume for hydrocephalus induction

Pilot studies aimed to establish the optimal volume of a 250mg/ml kaolin suspension for creating a moderately increased ICP model within 7 days. Three volumes were tested: 40µL, 70µL, and 80µL and the ventricle:brain ratio was measured to confirm the development of hydrocephalus. Each kaolin volume resulted in moderate ventricle dilation (Figure 25A). However, only 40µL resulted in was significantly

higher ventricle:brain ratio than saline-injected controls (mean (SD) ratio saline = 0.01 (0.07), *n* = 6, 40µL kaoli*n* = 0.14 (0.07), *n* = 9, p=0.008; Table 7). Moreover, there were no significant differences observed between different volumes of kaolin (Table 7, Figure 25B).

Table 7. Ventricle:brain ratio of animals injected with 40µL, 70µL or 80µL kaolin suspensions compared to 40µL saline.

SD; standard deviation. Significance determined by unpaired t-test comparing results to 40µL saline.

Vol (µL)	Substance	n	Ventricle:brain ratio Mean (SD)	*p* vs 40µL saline
40	Saline	6	0.01 (0.07)	0.008
	Kaolin	9	0.14 (0.07)	
70	Kaolin	2	0.11 (0.03)	0.095
80	Kaolin	3	0.22 (0.14)	0.071

4.3.1.2 Adverse effects of increasing kaolin volumes

Animals injected with 70µL and 80µL kaolin volumes experienced significant weight loss over the 6-day recovery (Figure 25C). Moreover, animals exhibited severe side effects, including ataxia, inability to groom, and severe piloerection. In contrast, animals injected with 40µL of kaolin also lost weight compared to saline-injected animals, but this weight loss began to stabilize by day 3 post-injection. Moreover, animals injected with 40µL of kaolin displayed milder side effects, primarily mild ataxia, and piloerection. Subsequently 40µL kaolin was injected to create a model of raised ICP due to its capacity to induce significant hydrocephalus with minimal adverse effects.

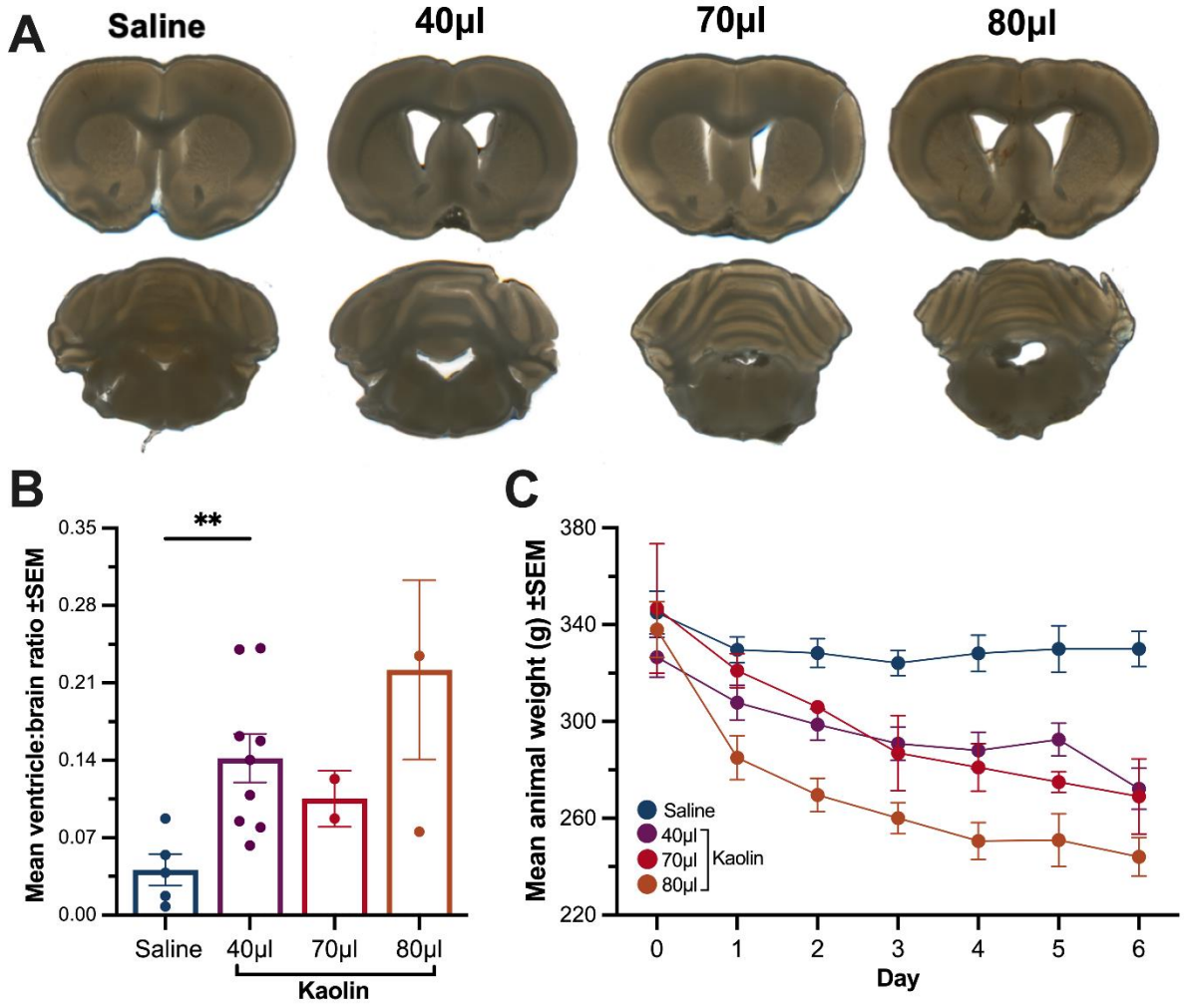

Figure 25. Optimisation of kaolin volume to create a model of raised ICP.

A - Coronal brain regions of animals injected with 40µL saline, 40µL, 70µL and 80µL of kaolin. **B** – Quantification of ventricle:brain ratio. **C –** Mean weight change of animals injected with 40µL saline versus 40µL, 70µL and 80µL of kaolin over 6 days post injection.

4.3.2 Ventricle dilation in the raised ICP model

Ventricle dilation was used to confirm successful induction of the hydrocephalus model. Ventricle:brain ratio was significantly higher in raised ICP animals compared

to controls (median (range) raised ICP = 0.17 (0.21) *n* = 24, control = 0.04 (0.10) *n* = 21, p <0.0001, Figure 26A and B).

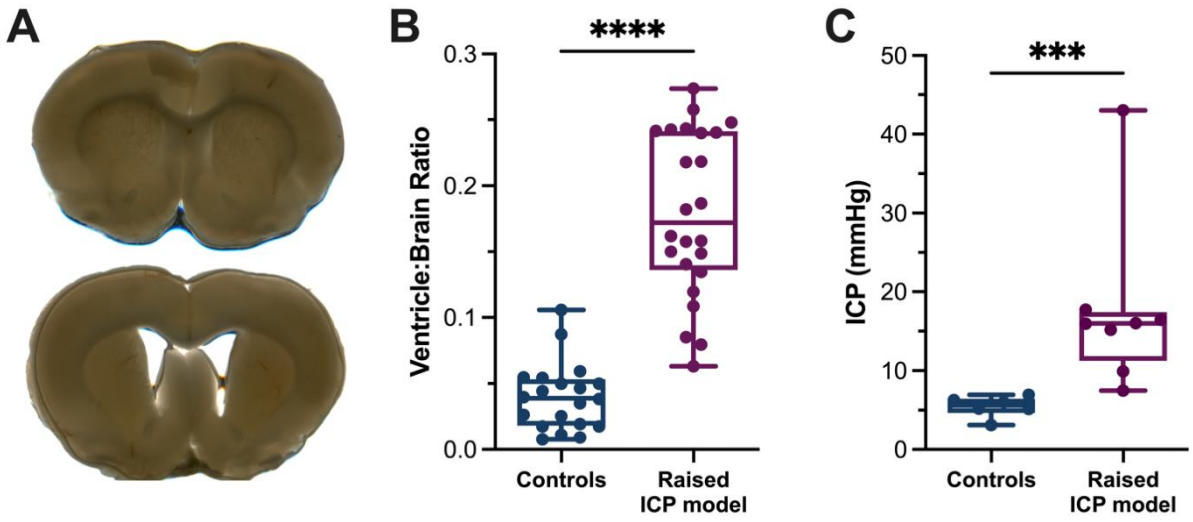

Figure 26. Kaolin injection induced ventricle dilation and raised ICP.

A – Coronal slices from control (top) and raised ICP animals (bottom). **B** – The ventricle:brain ratio was significantly higher in animals with raised ICP versus controls. **C** – ICP was significantly higher in the raised ICP model compared to controls. ICP; intracranial pressure, mmHg; millimetres of mercury. Data presented as median ± range. Significance determined by Mann Whitney U test *** *P*<0.001 , **** *P*<0.0001.

4.3.3 Confirmation of raised ICP in the model

To confirm the model featured increased ICP, epidural pressure was measured in control animals versus raised ICP animals. ICP was significantly higher in raised ICP animals compared to controls (median (range) raised ICP =16mmHg (9) *n* = 6, controls = 6mmHg (2) *n* = 8, *P*<0.001, Figure 26C). There was no association between the ventricle:brain ratio and ICP in either control or raised ICP animals.

4.3.4 Cortical responses to stimulation were altered in raised ICP

Cortical excitability is altered in migraine. Measuring evoked CSD responses in animals exposed to raised ICP can indicate alterations in neuronal function and excitability. In control animals, cortical stimulation induced a rapid decline in the DC signal which was coupled with an increase in CBF characteristic of CSD (% CBF change mean (SD) = 217.65% (37.70), *n* = 8, Figure 27A and F). Repolarisation of the signal was coupled with CBF and DC signals which returned quickly to baseline (repolarisation duration median (range) = 86.96s (140.05), *n* = 9, Figure 27A and D). During the 1-hour recording, controls exhibited mean (SD) 12 (3) CBF peaks which were coupled to depolarisation events.

Cortical responses to stimulation were drastically altered in animals with raised ICP (Figure 27B). Depolarisation duration was significantly increased (median (range) raised ICP = 108.81s (222.12) *n* = 11, controls = 37.54s (108.38) *n* = 9, *P* = 0.038, Figure 27C). Repolarisation duration was markedly increased in raised ICP animals, (median (range) raised ICP = 1824.26s (3499.54) *n* = 12, control = 86.96s (140.05) *n* = 9, p <0.0001, Figure 27D). There was also a significantly lower change in CBF during depolarisation (mean (SD) raised ICP = 85.55% (30.84) *n* = 9, control = 217.64% (37.70) *n* = 8, *P*<0.0001, Figure 27F) During the 1-hour recording, raised ICP exhibited a lower number of CBF peaks compared to normal ICP (mean (SD) raised ICP = 5 (2) *n* = 8, controls = 12 (3) *n* = 8, p=0.005, Figure 27G). Cortical responses in animals with raised ICP were markedly altered, exhibiting a delayed hyperpolarization following initial depolarisation and a loss of neurovascular coupling.

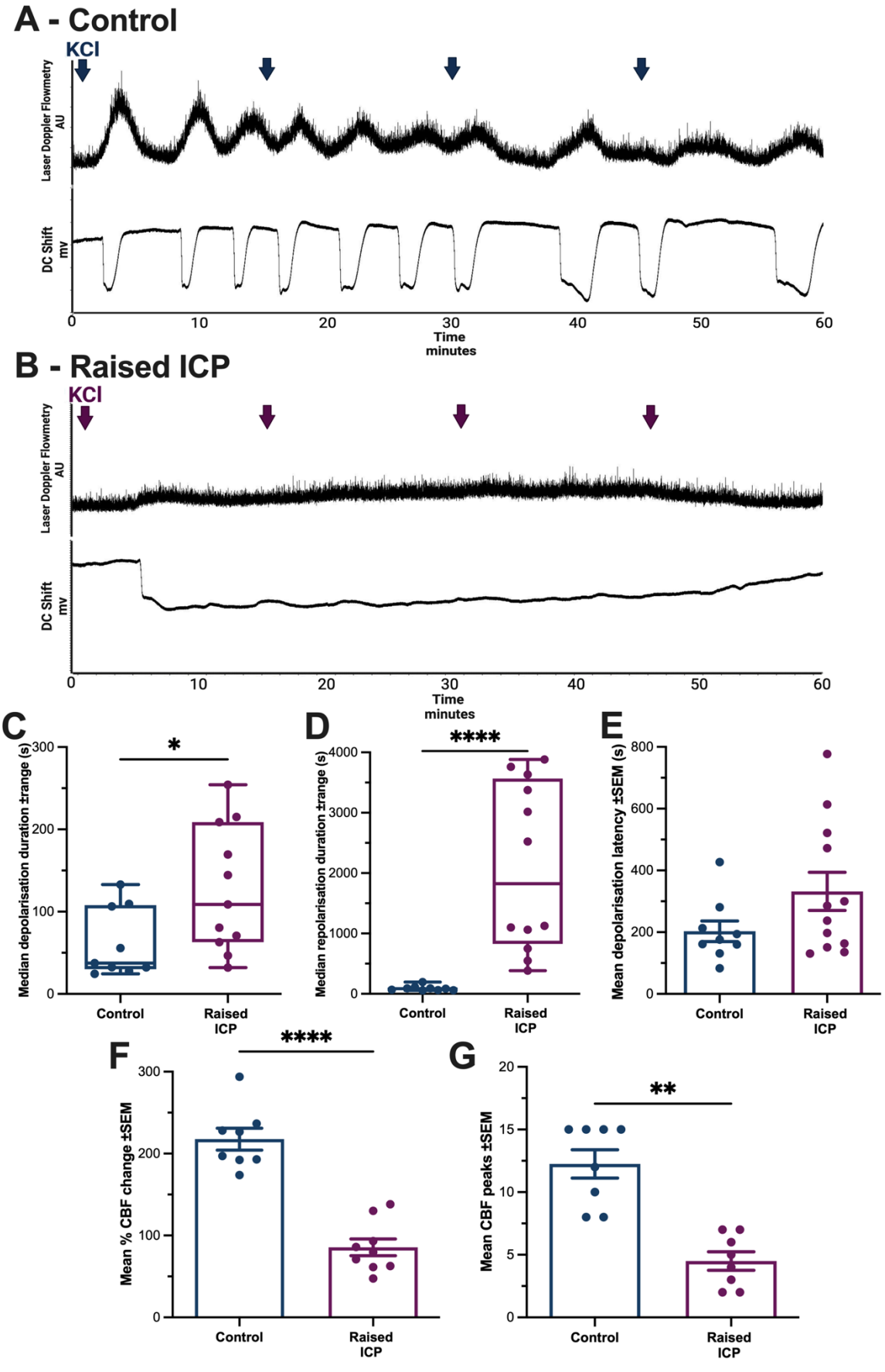
A - Control
KCl
Laser Doppler Flowmetry AU
DC Shift mv
0
10
20
30
40
50
60
Time minutes
B - Raised ICP
KCl
Laser Doppler Flowmetry AU
DC Shift mv
0
10
20
30
40
50
60
Time minutes
C
Median depolarisation duration ±range (s)
300
200
100
0
*
Control
Raised ICP
D
Median repolarisation duration ±range (s)
4000
3000
2000
1000
0
****
Control
Raised ICP
E
Mean depolarisation latency ±SEM (s)
800
600
400
200
0
Control
Raised ICP
F
Mean % CBF change ±SEM
300
200
100
0
****
Control
Raised ICP
G
Mean CBF peaks ±SEM
20
15
10
5
0
**
Control
Raised ICP

Figure 27. Direct cortical responses were altered in raised ICP animals compared to controls.

CSD responses in control **A** - and raised ICP animals. **B** - Arrows indicate addition of 5µL KCl. **C –** Depolarisation duration was higher in raised ICP animals. **D –** Repolarisation duration increased in raised ICP**. E** – Depolarisation latency was similar between controls and raised ICP. **F -** % change in CBF was lower in raised ICP. **G** – Number of CBF peaks was lower in raised ICP animals. AU; arbitrary units, CBF; cortical blood flow, DC; direct current, ICP; intracranial pressure, KCl; potassium chloride, s; seconds. Data in bar charts presented as mean ± SEM, box and whisker represent median ± range. Significance determined by unpaired *t* test or Mann Whitney U test * $P<0.05$, ** $P<0.01$, **** $P<0.0001$.

4.3.5 Raised ICP animals exhibited altered periorbital and hind paw mechanical thresholds

Testing mechanical thresholds in hind paw and periorbital regions elucidates to changes in extracephalic and cephalic cutaneous sensitivity. Control and raised ICP animals exhibit similar baseline mechanical thresholds (mean (SD) hind paw; control = 6.51g (1.44) $n = 10$, raised ICP = 5.78g (1.66) $n = 12$ $P = 0.289$, periorbital control = 5.71g (2.81) $n = 10$, raised ICP = 6.13g (2.07) $n = 12$, $P = 0.687$). Hind paw thresholds did not differ in controls between baseline and day 7 assessments (baseline = 6.51g (1.44), day 7 = 5.16g (1.40), $n = 10$ $P = 0.106$, Figure 28A). In animals with raised ICP however, mechanical thresholds were significantly reduced at day 7 (baseline = 5.78g (1.66), day 7 = 3.34g (2.22), $n = 12$ $p < 0.001$, Figure 28A). Periorbital thresholds also did not differ in controls between baseline and day 7 assessments (baseline = 5.71g (2.81), day 7 = 6.43g (1.88), $n = 10$, Figure 28B). Periorbital thresholds were reduced at day 7 compared in raised ICP animals (baseline = 6.13g (2.07), day 7 = 2.35g (1.91), $n = 12$ $p < 0.001$, Figure 28B). These

studies demonstrate that animals exhibit changes in cephalic and extracephalic sensitivity following 7 days exposure to raised ICP.

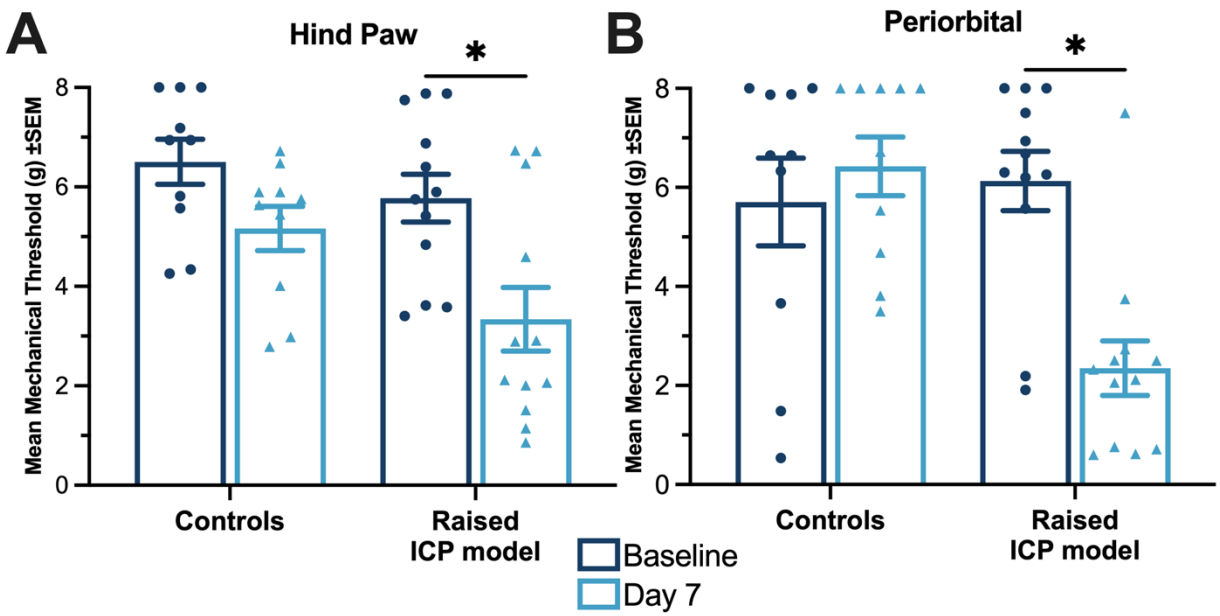

Figure 28. Raised ICP led to reduced hind paw and periorbital mechanical thresholds.

A – Hind paw and **B –** periorbital mechanical thresholds at baseline (dark blue) and day 7 (light blue) in controls and raised ICP. g; grams, ICP; intracranial pressure. Data presented as mean ± SEM. Significance determined by paired *t* test * = *P*<0.05.

4.3.6 CGRP expression in raised ICP

CGRP was quantified in trigeminal ganglion to determine if there were altered levels of CGRP signalling in nociceptive structures. However, there were no significant differences in between controls and raised ICP (median (range) controls = 0.003pg/ml (0.002) *n* = 8, raised ICP = 0.003 pg/ml (0.002) *n* = 10, Figure 29A).

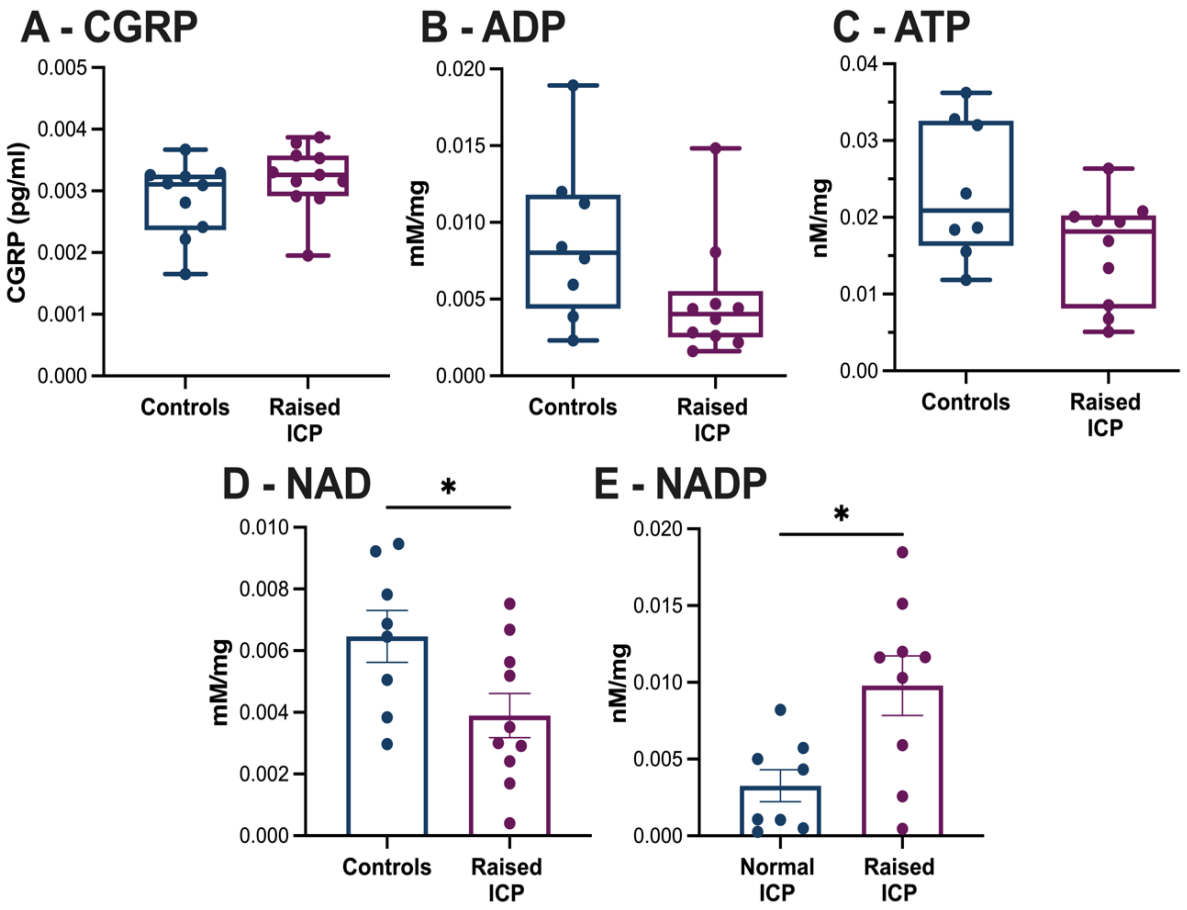

Figure 29. CGRP and metabolic profile of animals with normal and raised ICP.

A –CGRP protein in the trigeminal ganglion of control and raised ICP animals. Quantification of metabolites; **B** – ADP, **C** – ATP, **D** – NAD, **E** – NADP in normal versus raised ICP animals. ADP; adenosine diphosphate, ATP; adenosine triphosphate, CGRP; calcitonin gene-related peptide, ICP; intracranial pressure, NAD; nicotinamide adenine dinucleotide, NADP; nicotinamide adenine dinucleotide phosphate. Data in bar charts presented as mean ± SEM, box and whisker represent median ± range. Significance determined by unpaired *t* test or Mann Whitney U test * $P<0.05$.

4.3.7 Metabolic changes following raised ICP

Metabolic perturbations have been reported in IIH; therefore, metabolites were measured in brain tissue from control animals (n = 8) compared to raised ICP (n =

10). Metabolites which demonstrated either a significant or trend towards change include ADP, which exhibited a trend towards decrease in raised ICP animals (median (range) raised ICP = 0.004 mM/mg (0.013), controls = 0.008mM/mg (0.017), *P* = 0.083, Figure 29B). ATP also demonstrated a trend towards decrease in raised ICP (median (range) controls = 0.021 (0.024), raised ICP = 0.018 (0.021), *P* = 0.173, Figure 29C). NAD was significantly lower in animals with raised ICP (mean (SD) raised ICP = 0.004 (0.002), controls = 0.007 (0.002), *P* = 0.033, Figure 29D). NADP however was significantly increased in animals with raised ICP (mean (SD) raised ICP = 0.010 (0.006), controls = 0.003 (0.003) *P* = 0.012, Figure 29E).

Table 8. Metabolite measurements in control and raised ICP animals.

ADP; adenosine diphosphate, ATP; adenosine triphosphate, ICP; intracranial pressure, NAD; nicotinamide adenine dinucleotide, NADP; nicotinamide adenine dinucleotide phosphate. * denotes non-parametric data which is displayed as median (range). Significance determined by unpaired *t* test or Mann Whitney U test.

Metabolite	**Concentration mM/mg**		***p***
	Controls	**Raised ICP**	
ADP *	0.008 (0.017)	0.004 (0.013)	0.083
Acetate	0.037 (0.014)	0.029 (0.013)	0.204
ATP *	0.021 (0.024)	0.018 (0.021)	0.173
Creatine	0.101 (0.036)	0.083 (0.037)	0.309
Fumarate	0.002 (0.001)	0.002 (0.001)	0.653
Glutamate	0.138 (0.018)	0.131 (0.015)	0.421
Lactate	1.448 (0.486)	1.334 (0.676)	0.694
NAD	0.007 (0.002)	0.004 (0.002)	0.033
NADP	0.003 (0.003)	0.010 (0.006)	0.012
Phosphocreatine	0.935 (0.284)	0.737 (0.344)	0.210

Pyruvate	0.160 (0.049)	0.132 (0.060)	0.305

4.4 Discussion

The mechanisms contributing to headache in raised ICP have previously remained elusive. This work optimised and validated an animal model of raised ICP, in addition to demonstrating that raised ICP features altered pain behaviour (mechanical thresholds), disrupted cortical responses to evoked CSD and neurovascular uncoupling. Despite the risk factor of weight gain in IIH, this does not apply to all raised ICP disorders, highlighting the need for a model of moderately elevated ICP which minimises secondary factors.

4.4.1 Optimizing a model of hydrocephalus

The characterization of headache mechanisms in a model of raised ICP has not previously been accomplished. This chapter aimed to induce obstructive hydrocephalus in adult rats by injecting kaolin into the cisterna magna, with the goal of creating a model that accurately simulates raised ICP.

Previous research of modelling raised ICP to investigate the characteristics of IIH has utilized kaolin volumes ranging from 80 to 90µL.[199 306] Although the use of 80µL of kaolin in pilot experiments led to ventricle dilation, this volume also resulted in significant adverse effects, including substantial weight loss and severe symptoms such as ataxia and inability to groom. This not only renders the model unsustainable but also fails to accurately represent the physiology of moderate increases in ICP seen in IIH.[57]

Similarly, injecting 70µL of kaolin produced similar adverse effects, making this volume unsuitable for these purposes. It is worth noting that previous studies have not extensively discussed the effects of injecting larger volumes (80µL to 90µL) of kaolin on mortality or adverse outcomes.[199 306] Moreover, the measurements in these earlier studies were only conducted for up to 7 days, suggesting that animals injected with larger kaolin volumes may not be viable for experiments extending beyond this timeframe.

Injection of kaolin into the cisterna magna is a commonly employed method in young animals (3 weeks old) for the purpose of modelling hydrocephalus.[203 205 307 308] Reported mortality rates in these models are relatively low, ranging from 5% to 12.5%, and hydrocephalic animals have been successfully maintained for up to 4 weeks following injection.[203 205 307 308] In contrast, when working with adult animals, prior studies have employed 30-50µL of kaolin to induce hydrocephalus.[309-312] Ventricle enlargement becomes apparent at 2 weeks post-injection with 30µL of kaolin,[309 312] and between 2-7 days for animals injected with 50µL.[310 311] To create a model that exhibited ventricle dilation after 7 days with low mortality in adult animals 40µL volume was trailed.

While the injection of 40µL of kaolin minimized the severity of weight loss in animals, it's important to note that all kaolin-injected animals experienced weight reduction and a delay in regaining weight. This outcome aligns with other kaolin studies, which have consistently shown a failure to gain weight compared to control groups.[313] Animals injected with 40µL of kaolin exhibited significant ventricle dilation compared to saline controls. Additionally, there were no discernible differences in the ventricle-to-brain ratio between the 40µL group and those injected with larger volumes. Consequently, it was determined that 40µL effectively restricted CSF flow without

causing severe weight loss or moderate ataxia and was equally effective at inducing hydrocephalus in this model. [306]

4.4.2 ICP was raised in the model of hydrocephalus

40µL of kaolin also resulted in a significant increase in ICP after 7 days and aligns with ICP elevations observed in patients with IIH.[57] This is in agreement with other studies of kaolin models of hydrocephalus that also record increased ICP after 5-7 days.[199 208 209] Control saline-injected animals exhibited ICP values ranging from 3.12 to 6.96 mmHg, which aligns with previously reported epidural ICP measurements in adult rats.[314 315]

Previous studies utilizing 90µL of kaolin reported a significant increase in ICP just 1 day after injection, which then normalized by the 7th day.[306] It was hypothesized that this reduction in ICP at 1 week might be attributed to an adaptive response to ventricle dilation, potentially involving changes in aquaporin-4 distribution.[306] It is plausible in the model used in this thesis; a lower volume of kaolin facilitated a more gradual increase in ICP thereby preventing an adaptative response and resulting in sustained elevated ICP after 1-week. In support of this, studies of mice injected with 10µL of kaolin showed a gradual increase in ICP over 5 days,[209] and other small animal models using smaller volumes (30µL) have also demonstrated ICP increases after 7 days.[208] Although daily ICP monitoring were not feasible in this study, analysing pressure changes by using implanted ICP monitors would allow insights into the development and adaptation of pressure in this model.

In conclusion, the injection of 40μL of kaolin into the cisterna magna led to the development of hydrocephalus, as confirmed by ventricle dilation and elevated ICP observed 7 days after injection.

4.4.3 Raised intracranial pressure altered CSD responses

Evoked CSD responses in raised ICP animals show significant alterations, including neurovascular uncoupling and a failure of neuronal hyperpolarization following depolarization. It was originally hypothesised that elevated ICP may increase tissue susceptibility to hyperexcitability and therefore incidence of CSD events. In TBI rat models employing fluid percussion injury, raised ICP was found to be associated with an increase in CSD cycles.[316] This effect was sustained for up to 4.5 hours following injury, which may elucidate to the acute effects of ICP on cortical function. The drastically prolonged depolarised period demonstrated in this study may be the result of more chronic exposure to raised ICP, since responses were measured following 7 days of exposure. Future investigation of the acute effects of raised ICP on CSD responses may indicate a threshold of ICP which leads to altered responses. Migraine aura is not a prominent characteristic of raised ICP headaches or IIH.[192] This observation might elucidate the lack of a higher occurrence of CSD events in animals with increased ICP.

Our data implies that in raised ICP, cortical tissue is unable to hyperpolarise following stimulation, which may indicate that raised ICP alters the ability to restore ionic gradients. The metabolic profile of IIH patients features altered lactate:pyruvate ratios,[167] characteristic of mitochondrial dysfunction and pathological mitochondria have been identified in astrocytes and neurons of IIH patients.[317] Inability to support

the highly energetically demanding ionic homeostasis following stimulation may explain the significant delay in hyperpolarisation exhibited in this study. In support of this, alterations in NAD^+ and NADH metabolites in animals with raised ICP were identified, further supporting mitochondrial and energetic failure as a contributing factor to altered cortical responses. Previous characterisation of kaolin models have demonstrated restricted CSF flow into the cranial subarachnoid space,[209] and reduced lymphatic clearance,[310] which has also been demonstrated in IIH patients.[318] Prevention of waste clearance could additionally contribute towards the inability of cortical tissue to recover from depolarisation events.

In animals with elevated ICP, CBF responses to CSD were altered, showing an atypical lack of increase in blood flow.[319] This suggests neurovascular uncoupling, potentially indicating a hypoxic response in cortical tissue due to heightened energetic demands. Under normal, healthy conditions, cerebral autoregulation mechanisms work to maintain sufficient CBF. While studies specifically exploring cerebral perfusion in IIH are limited, research involving ICP manipulation has shown a decrease in CBF at higher pressure levels.[320] Furthermore, animal models of TBI have revealed a negative correlation between ICP and CBF, [316] [321] implying a possible connection between ICP and neurovascular responses. At elevated ICP and cerebral perfusion pressure, blood vessels may become fully constricted or dilated, impairing local vascular responses to neural activity.[322]

In animals with raised ICP, there might be a loss of CBF autoregulation due to mechanical compression of vasculature, resulting in an inability to support cerebrovascular responses to cortical stimulation.[323] This combination of energetic insufficiency and neurovascular uncoupling in the context of elevated ICP may hinder the ability of cortical tissue to recover adequately from stimulation.

4.4.4 Raised ICP led to changes in pain behaviour

Animals with raised ICP exhibit increased trigeminal sensitivity as demonstrated by reductions in mechanical pain thresholds in both cephalic and extra-cephalic regions. Cutaneous allodynia is present in over 50% of the migraine population and is associated with migraine symptoms.[324] Allodynia has also been reported in IIH patients and reduction in ICP after 12 months was found to be associated with improved markers of allodynia.[57]

The direct effects of ICP on trigeminal afferents have not been extensively explored, however raised ICP has been recorded in 47.4% of patients with trigeminal neuralgia,[325] and several case reports have diagnosed IIH in patients with trigeminal neuralgia,[326 327] suggesting a causative role of ICP in trigeminal-mediated pain. TBI animal models also exhibit both reduced periorbital and hind paw mechanical thresholds, however ICP was not measured in these studies.[328 329] The extent of ICP elevations in this chapter could potentially affect trigeminal pathways within the trigeminocervical complex, leading to sensitization of both ascending and descending pain pathways. Elevated ICP and ventricular dilation might also activate trigeminal afferents innervating the cranial meninges through vascular stretching.

4.4.5 Limitations and future directions

The current data has certain limitations. Androgens and gender have a major role in the pathophysiology of IIH,[166] and migraine.[330] In relation to these methods in particular, recent studies have highlighted differences in CSD responses between

male and female rats.[298] To minimize the impact of female gender on investigations and better understand the direct relationship between ICP and headache mechanisms, a male rat model was used. While this choice may limit the translational applicability of the findings to IIH, it makes these results more broadly relevant to secondary headache disorders characterized by raised ICP, which may not be influenced by gender. Future research examining the influence of gender and androgens in this raised ICP model could provide insights into how these risk factors exacerbate headaches. Hormonal fluctuations also occur in female rats, following a four-phase oestrus cycle. Conducting experiments in each of these phases would explore the effects of hormones and gender on headache pathways in the context of raised ICP.

It is important to note that an obstructive hydrocephalus model was employed, which is not exclusively representative of IIH. This is a significant consideration since the cause of raised ICP in IIH is idiopathic. Nonetheless, a dedicated model for IIH does not currently exist. IIH is characterized by disturbed metabolism, androgen excess, and female gender as prominent features. Future investigations into the impact of these factors on the raised ICP model could provide a more comprehensive understanding of the pathogenic mechanisms of headache in IIH. Additionally, exposing this raised ICP model to androgen excess via slow-release implanted pellets or a high-fat diet may reveal the effects of these risk factors on headache mechanisms, particularly within the context of IIH.

In conclusion, the findings from this chapter shed light on the previously unknown mechanisms underlying headaches raised ICP. An animal model unveiled heightened trigeminovascular sensitivity, disrupted cortical responses to stimulation, and impaired neurovascular coupling as key features of raised ICP.

CHAPTER 5 EXAMINING THE EFFECTS OF PHARMALOGICAL INTERVENTIONS IN AN *IN VIVO* MODEL OF RAISED INTRACRANIAL PRESSURE

5.1 Introduction

Currently, there are no targeted therapies for headaches related to elevated ICP. A 2015 Cochrane review concluded that there is insufficient evidence to support the recommendation of current drugs for IIH.[331] Amiloride, furosemide, spironolactone, and topiramate are frequently used off-label for ICP reduction. Nonetheless, prior trials have indicated that these medications had only a minimal impact on ICP, with no noticeable distinctions among them.[332] Moreover, these agents are often associated with adverse side effects, such as worsening cognition impairment,[333 334] anorexia, and fatigue, leading to low tolerability.[335] Consequently, there is an unmet need for therapeutics that can result in a clinically meaningful reduction in ICP without causing side effects.

Although some IIH studies have presented an relationship between ICP and headache morbidity,[57] this association is not consistent across all studies, as some have shown no improvement in headache symptoms when reducing ICP.[190] The relationship between pressure and headache is therefore complex and it remains unclear whether reducing ICP would be therapeutic for headaches.

New clinical studies have revealed that the GLP-1-RA exenatide was able to lower ICP in IIH patients.[246] GLP-1-RA administration has also demonstrated the ability to reduce the number of monthly headache days in IIH patients,[192 246] suggesting its potential as a therapeutic for headaches associated with elevated pressure. Open-label studies have highlighted the efficacy of CGRP antibodies in treating headache in IIH patients.[58 60] Erenumab reduced the frequency headache in patients with recurrent papilledema, a marker of raised ICP, indicating that attenuating CGRP

signalling was effective in the presence of elevated ICP.[61] The role of CGRP signalling in raised ICP however, has not previously been explored. Investigating the effects of lowering ICP or attenuating CGRP pathways specifically on headache mechanisms may provide a basis for their use as therapeutics for raised ICP headache.

5.1.1 Aims

In the previous chapter, raised ICP resulted in altered mechanical pain thresholds, disrupted cortical activity and loss of CBF coupling in response to evoked CSD. Therefore, this chapter progressed to explore therapeutic manipulation of this relationship and aimed to:

1. Investigate the effects of reducing ICP with GLP-1RA exenatide on mechanical pain thresholds, cortical and neurovascular responses to evoked CSD.
2. Examine the consequences of blocking CGRP with CGRP-receptor antagonist (CGRP receptor antagonist) olcegepant on mechanical pain thresholds, cortical and neurovascular responses to stimulation in the setting of raised ICP.

5.2 Methods

5.2.1 Animals used for drug experiments

Male Sprague Dawley rats (Enivgo) (n=76) aged 10-17 weeks weighing 226g-404g were used. Rats were housed in sex and litter matched groups in a climate-controlled room and kept on a 12:12 light/dark cycle with free access to food and water. All

animal handling and procedures were performed according to the guidelines described in 2.1.2.

5.2.2 Cisterna Magna Injection

All animals used in this chapter had intracisternal injection of kaolin to model raised ICP. Animals were anesthetized with isoflurane gas in an induction chamber and injected in the cisterna magna with kaolin as described in 2.3.1.

5.2.3 Pharmacological agents

GLP-1RA exenatide (Byetta, AstraZeneca UK Limited) was used to investigate the impact of lowering ICP in animals. 1 day after cisterna magna injection, all animals were given analgesia (5mg/kg carprofen). On days 2-6 animals were injected daily with 20ug/kg GLP-1RA or equal volume saline subcutaneously (Figure 30, Table 9). On day 7 animals were injected with the final dose of exenatide or vehicle 1 hour prior to CSD or mechanical threshold assessment.

CGRP receptor antagonist olcegepant (BIBN4096BS, Sigma) was used to explore the impact of blocking CGRP in animals with raised ICP. 1 day after cisterna magna injection, all animals were given analgesia (5mg/kg carprofen). On days 2-6 animals were injected daily with 1mg/kg olcegepant (0.02% DMSO) or equal volume 0.02% DMSO intraperitoneally (Figure 30, Table 9). On day 7 animals were injected with the final dose of olcegepant or vehicle 1 hour prior to CSD or mechanical threshold assessment.

In both exenatide and olcegepant trials, animals used for behavioural studies were given analgesia (5mg/kg carprofen) on day 1 and day 4 following injection to reduce the impact of analgesia on assessments.

Table 9. Purpose, concentration, and dosage of drugs.

CGRP-R; calcitonin gene related peptide receptor, CSF; cerebrospinal fluid, GLP-1RA; glucagon like peptide-1 receptor.

Drug	Purpose	Conc	Dosage	Delivery	Ref
GLP-1RA: Exenatide	Reduce CSF secretion	20ug/kg	Daily	Subcutaneous	199
CGRP receptor antagonist: olcegepant	Block CGRP signalling	1mg/kg	Daily	Intraperitoneal	151 258

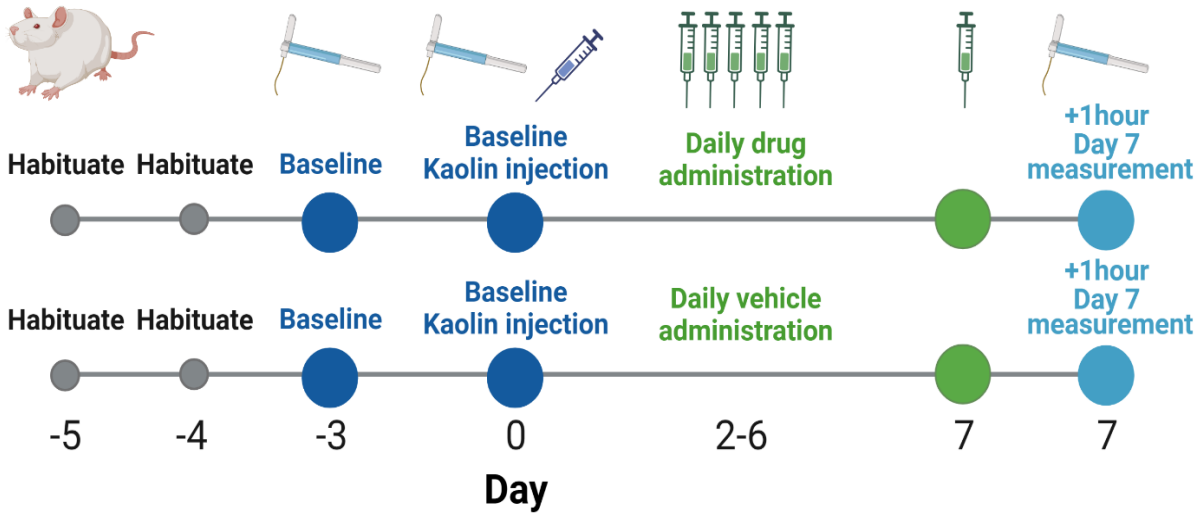

Figure 30. Timeline of behavioural mechanical threshold testing in animals injected with drug or vehicle.

Following habituation and baseline testing all animals were injected intracisternally with kaolin, animals were administered daily with vehicle or drug and the day 7 measurement was conducted 1 hour after the final administration.

5.2.4 Measuring ICP following drug treatment

ICP was measured in the epidural space of the skull in all animals following vehicle or drug administration. On day 7 animals were anesthetized with isoflurane gas in an induction chamber and epidural ICP was measured as detailed in 2.3.1.2.

In CSD cohorts, ICP was measured 1 hour following drug or vehicle administration and prior to initiating CSD induction. Following ICP measurements, a cortical window was drilled in the parietal bone of the opposite hemisphere to avoid any effects of the ICP catheter placement on CSD responses.

5.2.5 Measuring CSD responses after pharmacological intervention

To investigate the effects of reducing ICP and blocking CGRP on cortical activity, CSD responses were recorded in raised ICP animals of GLP-1RA or olcegepant treated animals versus vehicle.

Animals were anesthetized with isoflurane gas and the femoral vein was cannulated to allow intravenous administration of anaesthesia described in 2.3.1.1. Animals were also tracheostomized and mechanically ventilated as described in 2.3.1.1.

Animals were secured in a stereotaxic frame and 2 cortical windows were created in the parietal bone of the skull as detailed in 2.3.2.3. CSD was induced using 1M KCl and the resulting steady state potential (DC) and cBF changes were measured as per 2.3.2.3. A cotton pellet soaked in KCl was placed on the cortical surface of the brain and 5µL of KCl was added to the pellet every 15 minutes over 1 hour. DC and cBF responses to KCl stimulation were recorded using Spike2 software and analysed as described in 2.3.2.4.

5.2.6 Assessing the impact of pharmacological agents on mechanical thresholds

Mechanical thresholds were assessed at baseline (pre-kaolin injection) and after kaolin injection and 6 days of injection of drug or vehicle (Figure 30). All animals were habituated to the testing room and conditions on two occasions prior to baseline testing as described in 2.3.3.1. von Frey filaments were applied to the periorbital and hind paw regions (Figure 13B) to measure mechanical thresholds as detailed in 2.3.3.2. Two baseline measurements were conducted with a minimum of 3 days between measurements. Mechanical thresholds were repeated on day 7 1 hour after final administration of drug or vehicle (Figure 30).

5.2.7 CGRP quantification in trigeminal ganglion

Following mechanical threshold testing, the trigeminal ganglion was collected from animals and snap frozen in liquid nitrogen. Protein was extracted and quantified from ganglion as described in 2.4.1.1. CGRP was quantified in trigeminal ganglion using an ELISA as described in 2.4.1.2. and expressed as normalized protein content using the quantity of total protein within each sample.

5.2.8 Statistical analysis

The normality of data was assessed using the Shapiro-Wilk test. Data which were normally distributed were analysed using parametric tests (*t* tests, Pearson's correlation coefficient) and reported as mean and standard deviation (SD). Non-

normally distributed data were analysed using non-parametric tests (Mann-Whitney test, Spearman rank correlation test) and reported as median and range. Results were considered statistically significant when p values were * $P<0.05$, ** $P<0.01$, *** $P<0.001$, and **** $P<0.0001$.

5.3 Results

5.3.1 The effects of reducing ICP with GLP-1 receptor agonist

5.3.1.1 GLP-1R agonism reduced ICP

Using a model of a raised ICP the impact of GLP-1RA exenatide on ICP and headache was investigated. Daily GLP-1RA administration resulted in a significantly lower ICP compared to those with vehicle (mean (SD) GLP-1RA = 9.74mmHg (6.09) n = 19, vehicle = 18.27mmHg (6.67) n = 16, P = 0.004, Figure 31A). GLP-1RA lowered ICP within a range of normal ICP values, as measurements was not significantly different between raised ICP animals treated with GLP-1RA and controls (Figure 31B). Vehicle ICP were not significantly different to raised ICP model animals not injected with vehicle (Figure 31B). GLP-1RA treatment did not reduce ventricle:brain ratio, as there was no difference to vehicle injected animals (mean (SD) vehicle = 0.13 (0.05) n = 11, GLP-1RA = 0.14 (0.05), n = 13). There were no differences between percentage weight change in animals treated with GLP-1RA versus vehicle (Figure 31C).

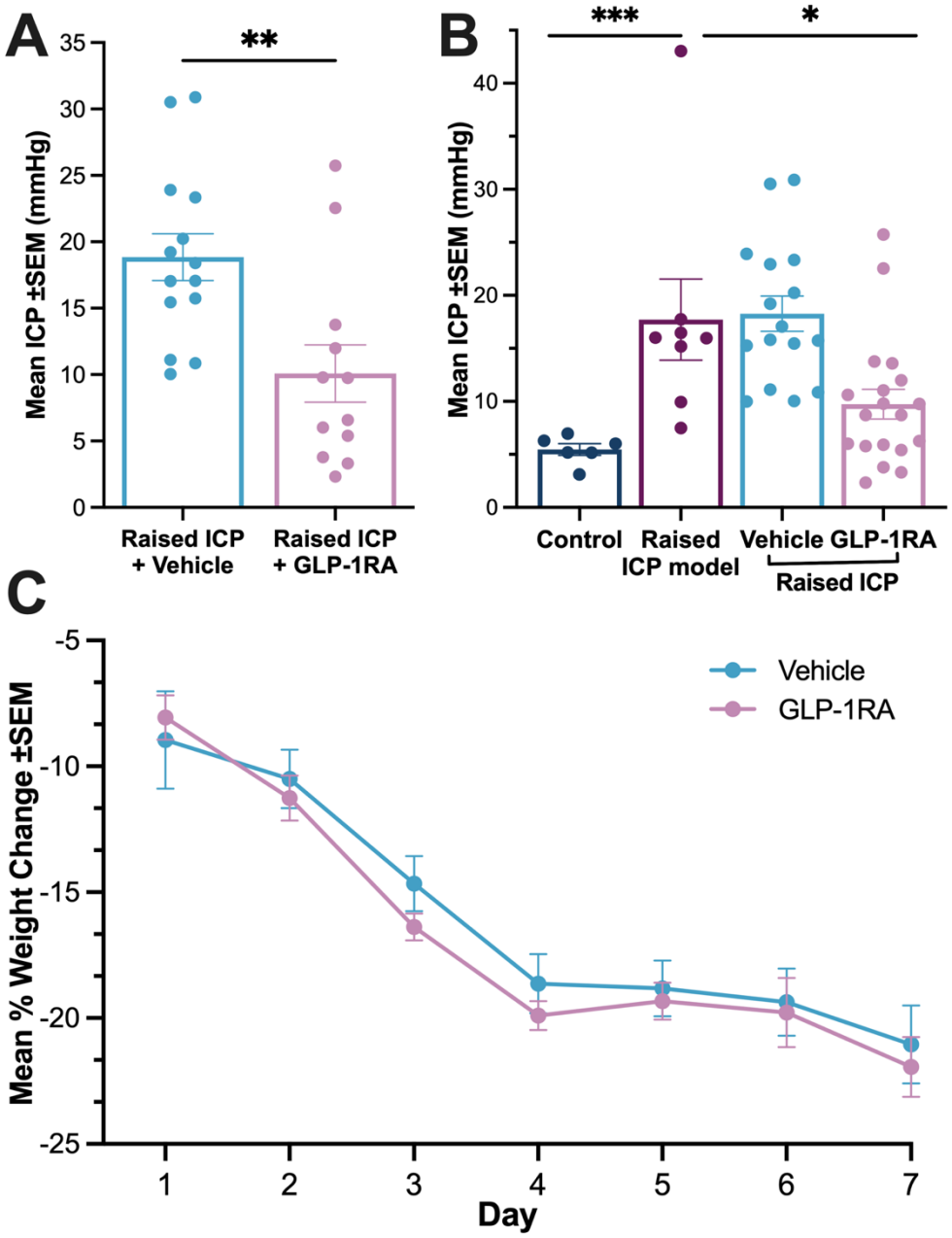

Figure 31. GLP-1RA exenatide reduced ICP in the raised ICP model.

A – ICP was lower in animals injected daily with GLP-1RA compared to vehicle. **B** – ICP in animals injected with GLP-1RA was not significantly different to controls. **C –** Mean percentage weight change different between animals injected with vehicle or GLP-1RA. GLP-1RA; glucagon like peptide-1 receptor agonist, ICP; intracranial pressure. Data in presented as mean ± SEM. Significance determined by unpaired *t* test * $P<0.05$, ** $P<0.01$, **** $P<0.0001$.

5.3.1.2 GLP-1R agonism prevented reductions in mechanical thresholds

We investigated the impact of reducing ICP on mechanical pain thresholds. Hind paw thresholds were significantly reduced at day 7 in vehicle treated animals (mean (SD)

baseline = 7.15g (0.95), day 7 = 2.99g (1.97), *n* = 12, *P*<0.0001,

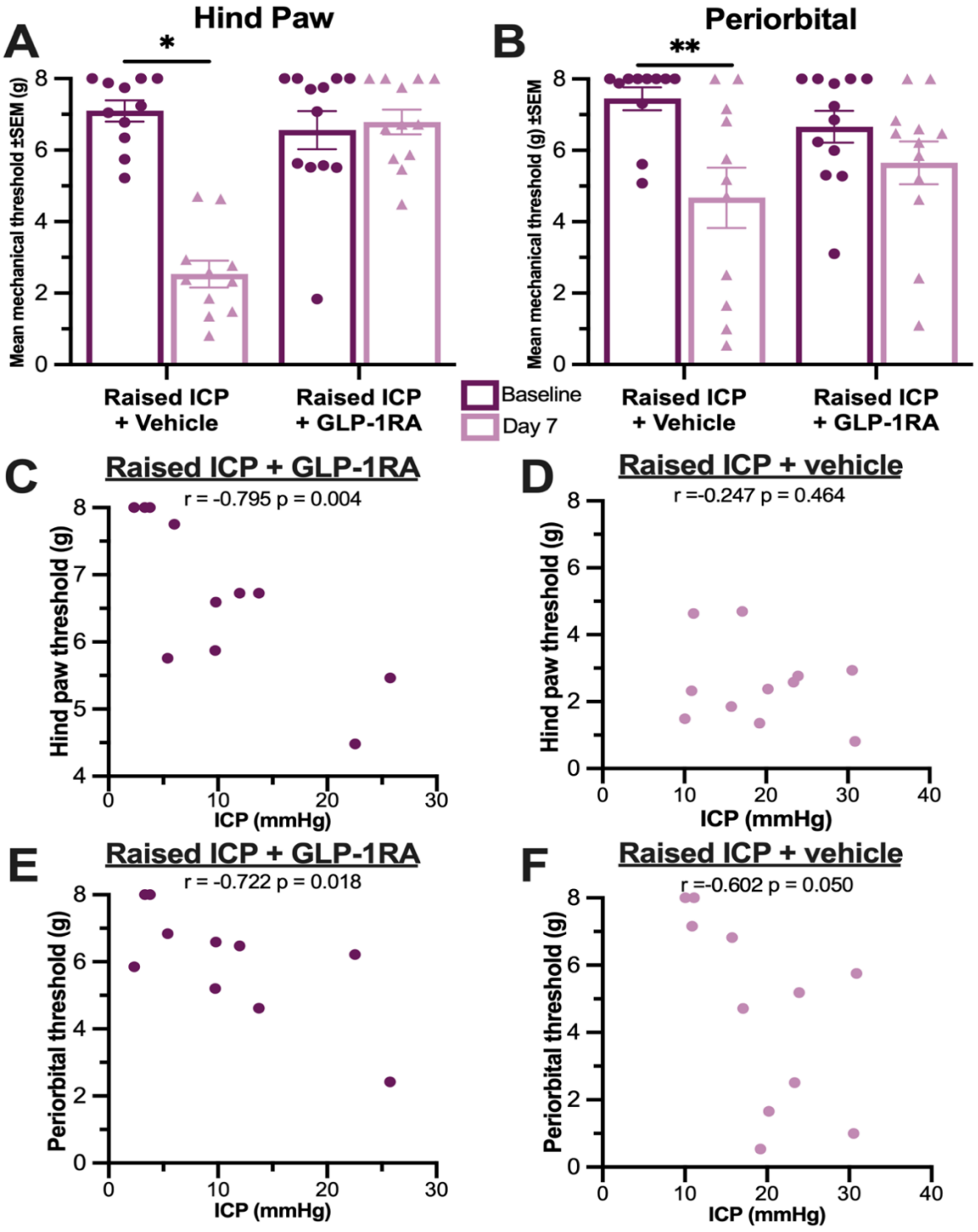

Figure 32A). However, there were no differences in hind paw thresholds in animals treated with GLP-1RA between baseline and day 7 (baseline = 6.36g (1.92), day 7 =

6.86g (1.22), *n* = 11,

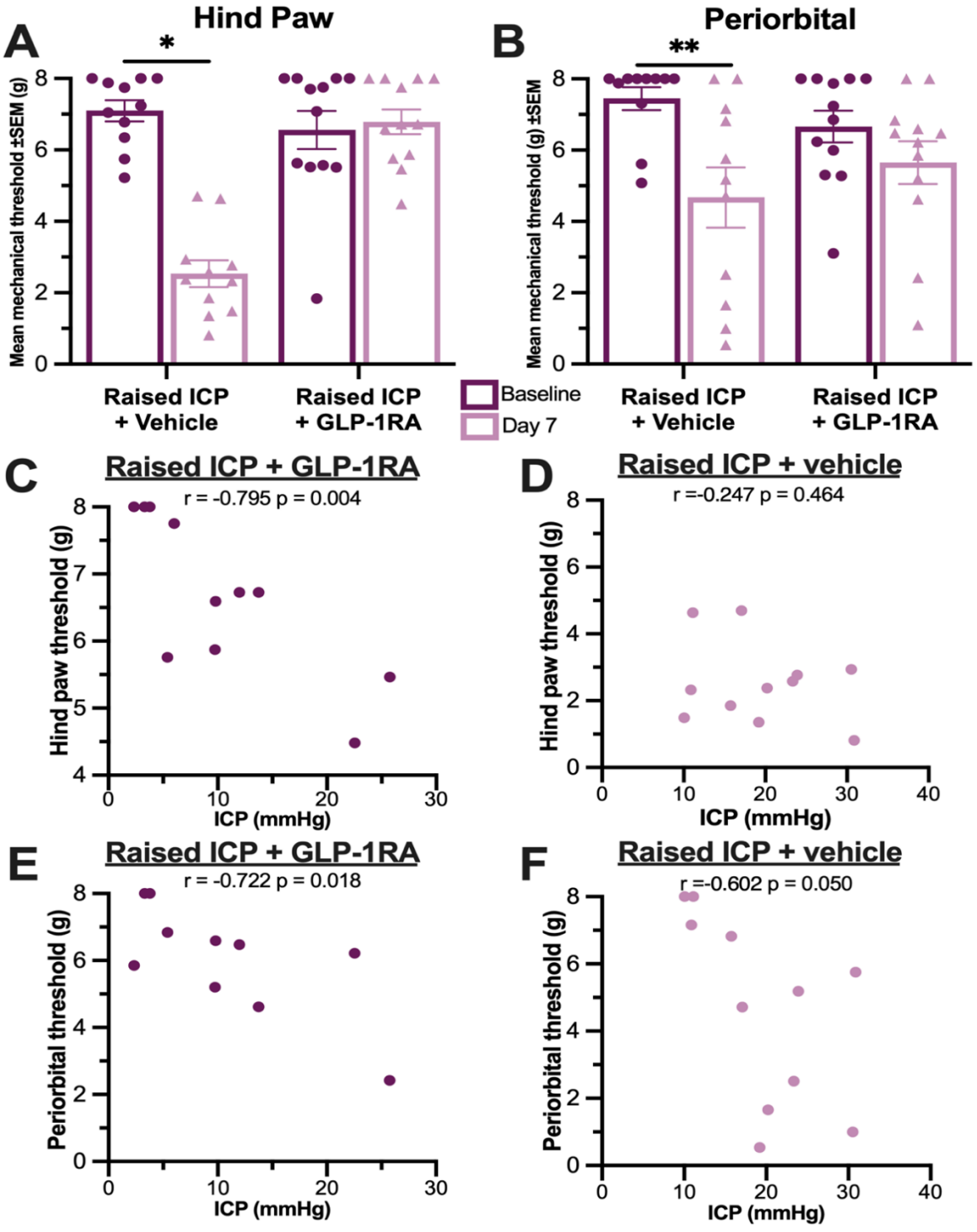
A
Hind Paw
*
Mean mechanical threshold ±SEM (g)
Raised ICP + Vehicle
Raised ICP + GLP-1RA
B
Periorbital
**
Mean mechanical threshold (g) ±SEM
Baseline
Day 7
C
Raised ICP + GLP-1RA
r = -0.795 p = 0.004
Hind paw threshold (g)
ICP (mmHg)
D
Raised ICP + vehicle
r =-0.247 p = 0.464
E
Raised ICP + GLP-1RA
r = -0.722 p = 0.018
Periorbital threshold (g)
F
Raised ICP + vehicle
r =-0.602 p = 0.050

Figure 32A). There was also a significant negative correlation in GLP-1RA animals between ICP and hind paw thresholds (r = -0.795, p=0.004,

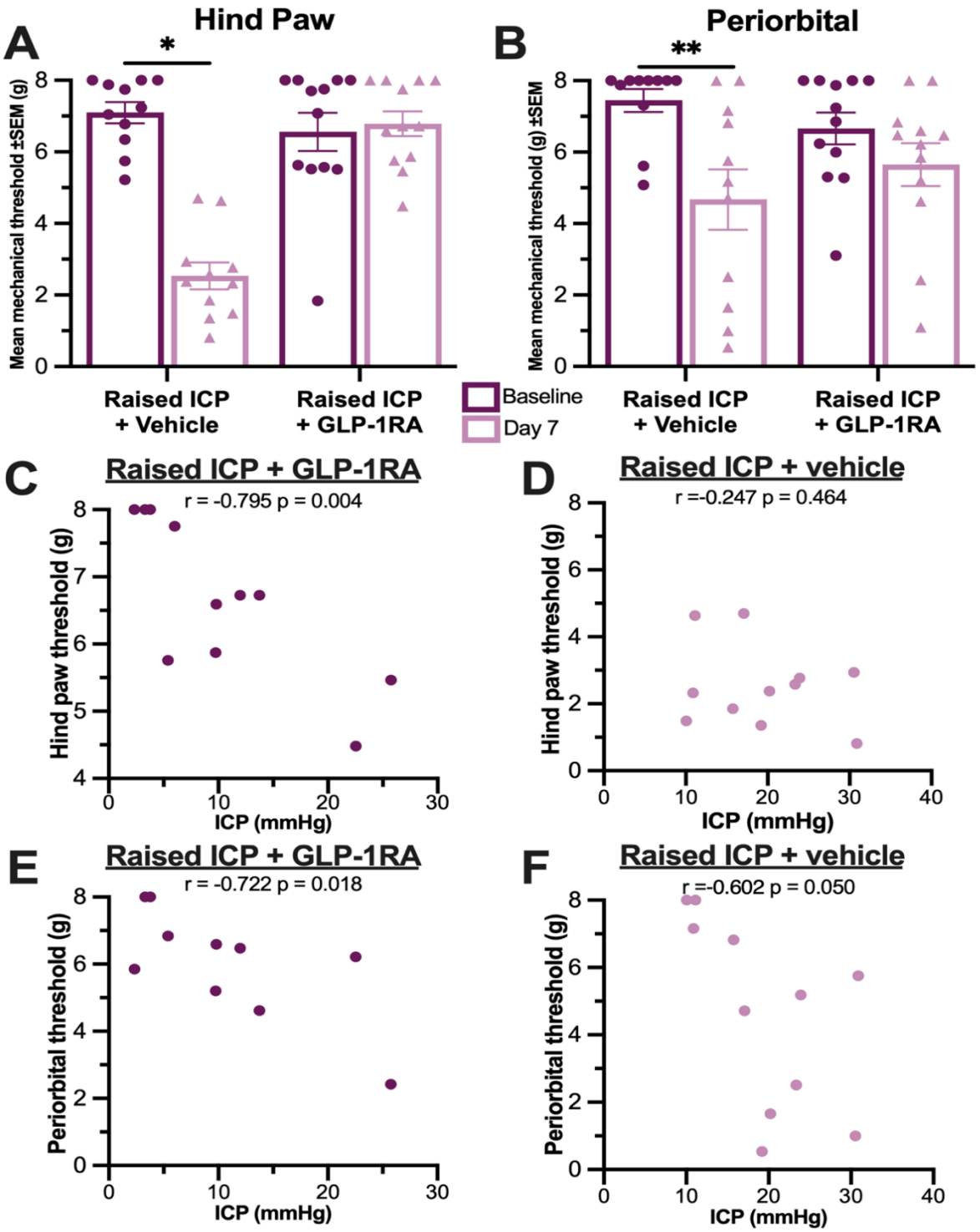

Figure 32C). No associations were found between vehicle treated ICP and mechanical thresholds

(

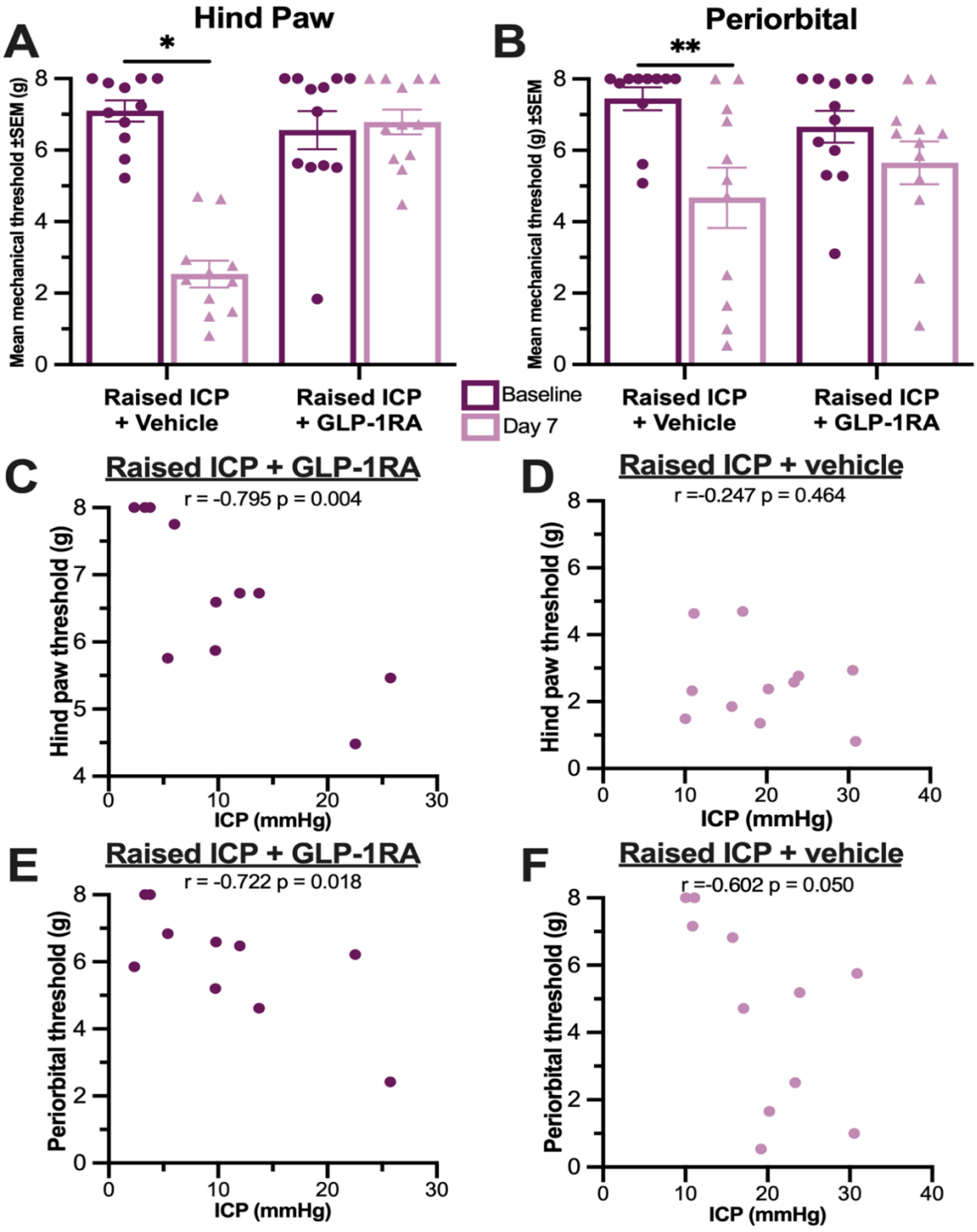
A
Hind Paw
*
Mean mechanical threshold ±SEM (g)
Raised ICP + Vehicle
Raised ICP + GLP-1RA
B
Periorbital
**
Mean mechanical threshold (g) ±SEM
Baseline
Day 7
C
Raised ICP + GLP-1RA
r = -0.795 p = 0.004
Hind paw threshold (g)
ICP (mmHg)
D
Raised ICP + vehicle
r =-0.247 p = 0.464
E
Raised ICP + GLP-1RA
r = -0.722 p = 0.018
Periorbital threshold (g)
F
Raised ICP + vehicle
r =-0.602 p = 0.050

Figure 32D).

Periorbital thresholds were reduced at day 7 in animals treated with vehicle (baseline= 7.02g (1.78), day 7 = 4.95g (2.84), *n* = 12 *P*<0.01,

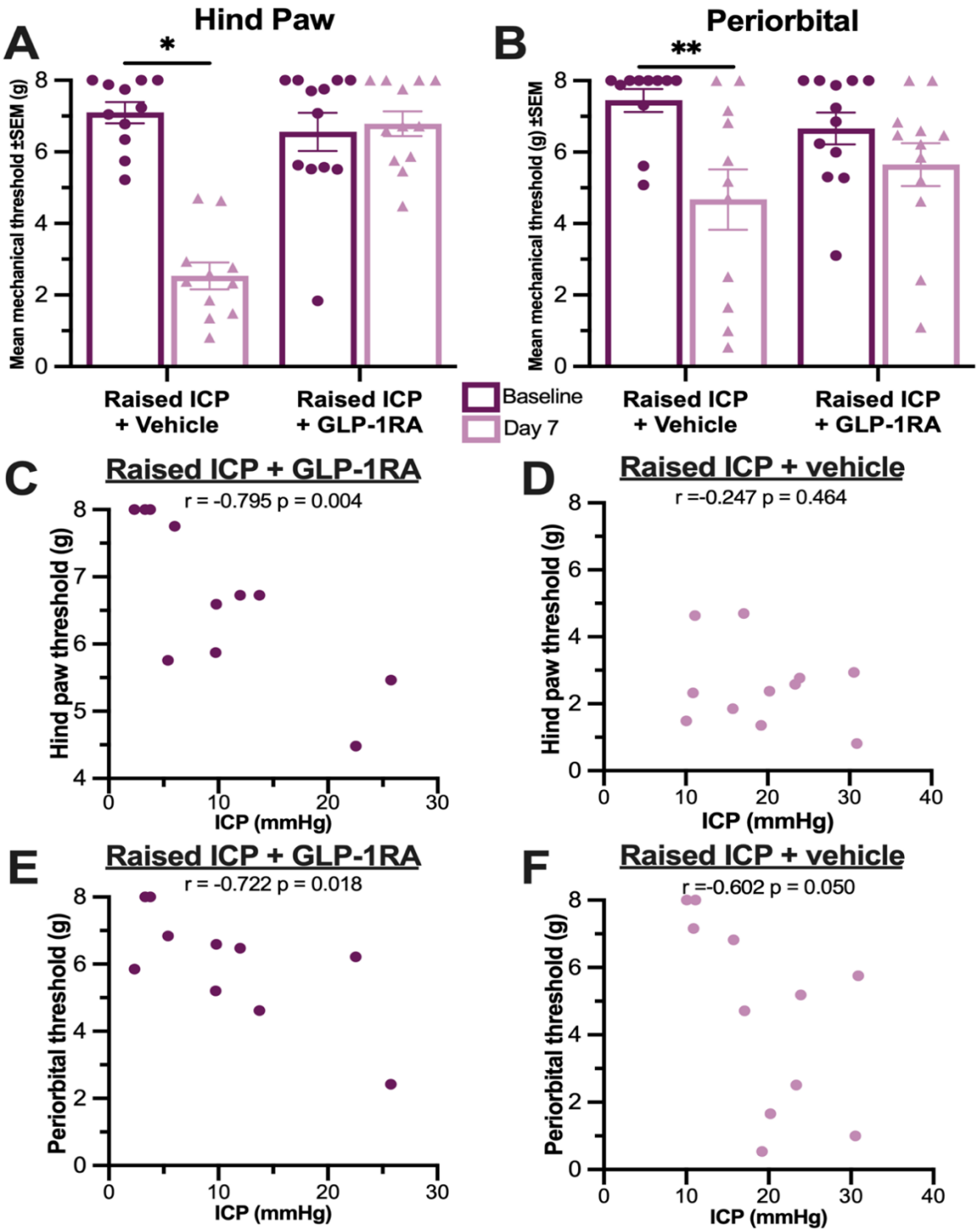

Figure 32B). GLP-1RA treated animals, however, did not exhibit changes in periorbital thresholds between baseline and day 7 (baseline = 6.98g (1.11), day 7 =

5.69g (2.17), *n* = 11,

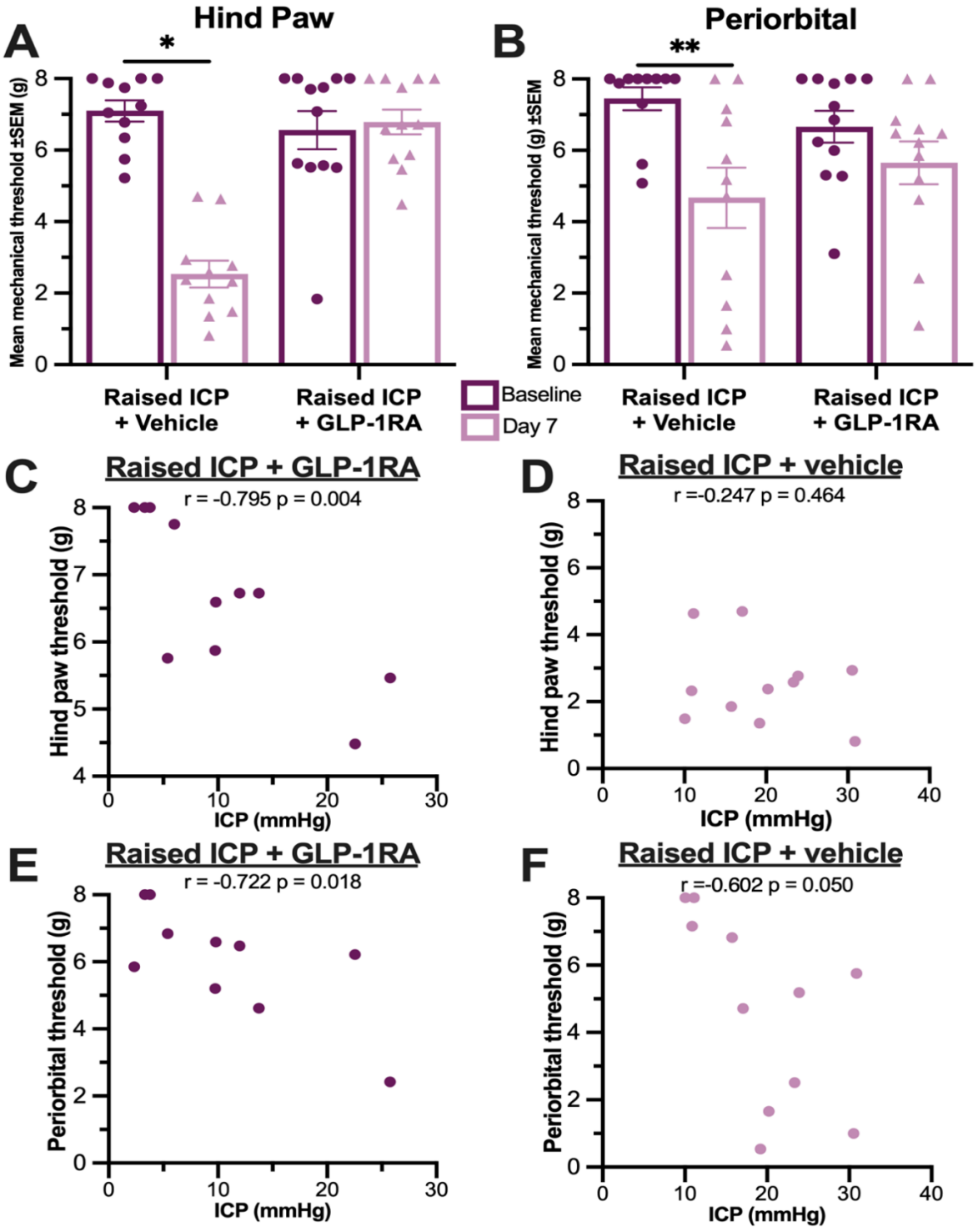

Figure 32B). Both animals treated with vehicle and GLP-1RA demonstrate a negative association between ICP and periorbital mechanical thresholds at day 7

(GLP-1RA r = -0.722 *P* = 0.018

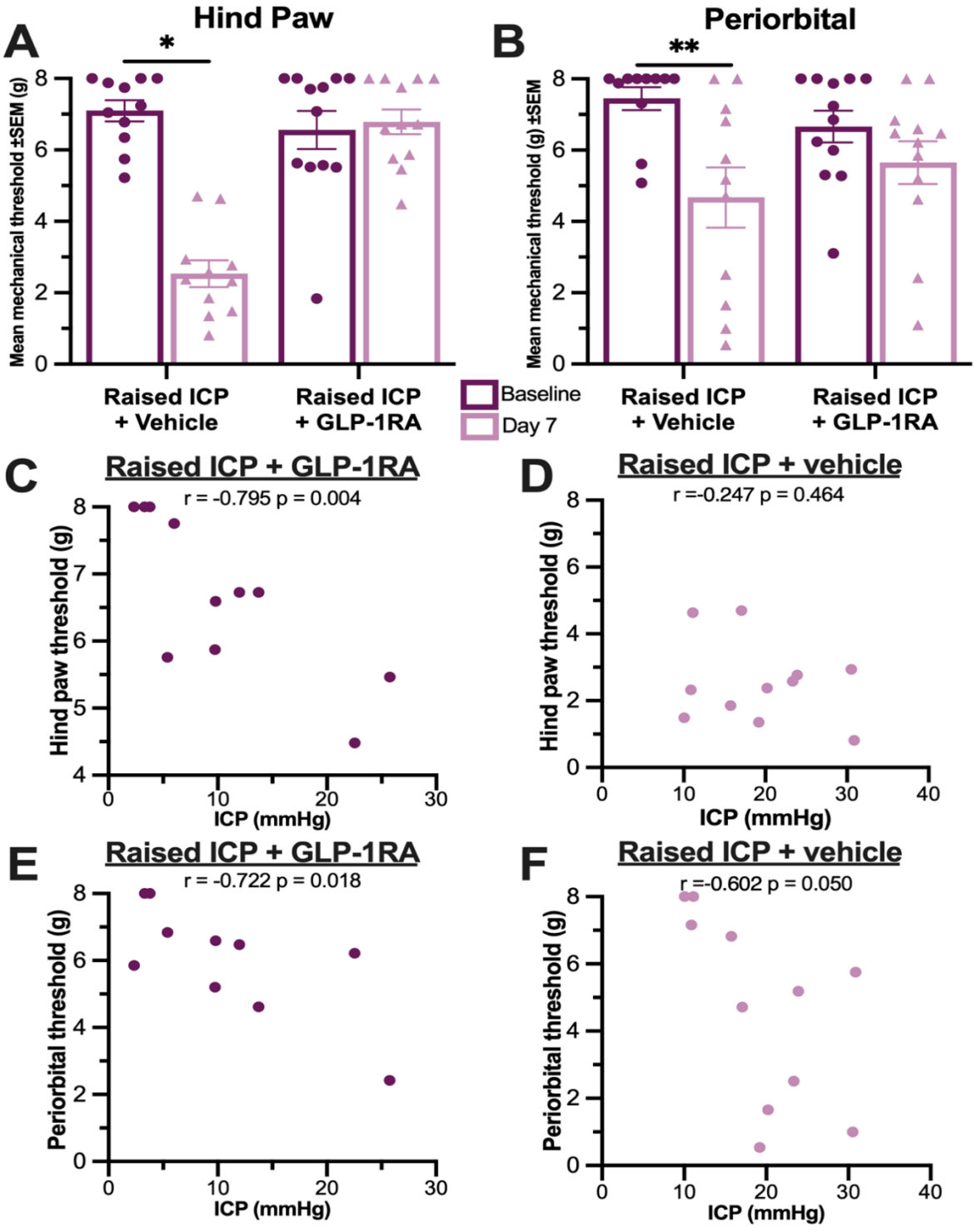

Figure 32E, vehicle r = -0.602 *P* = 0.050

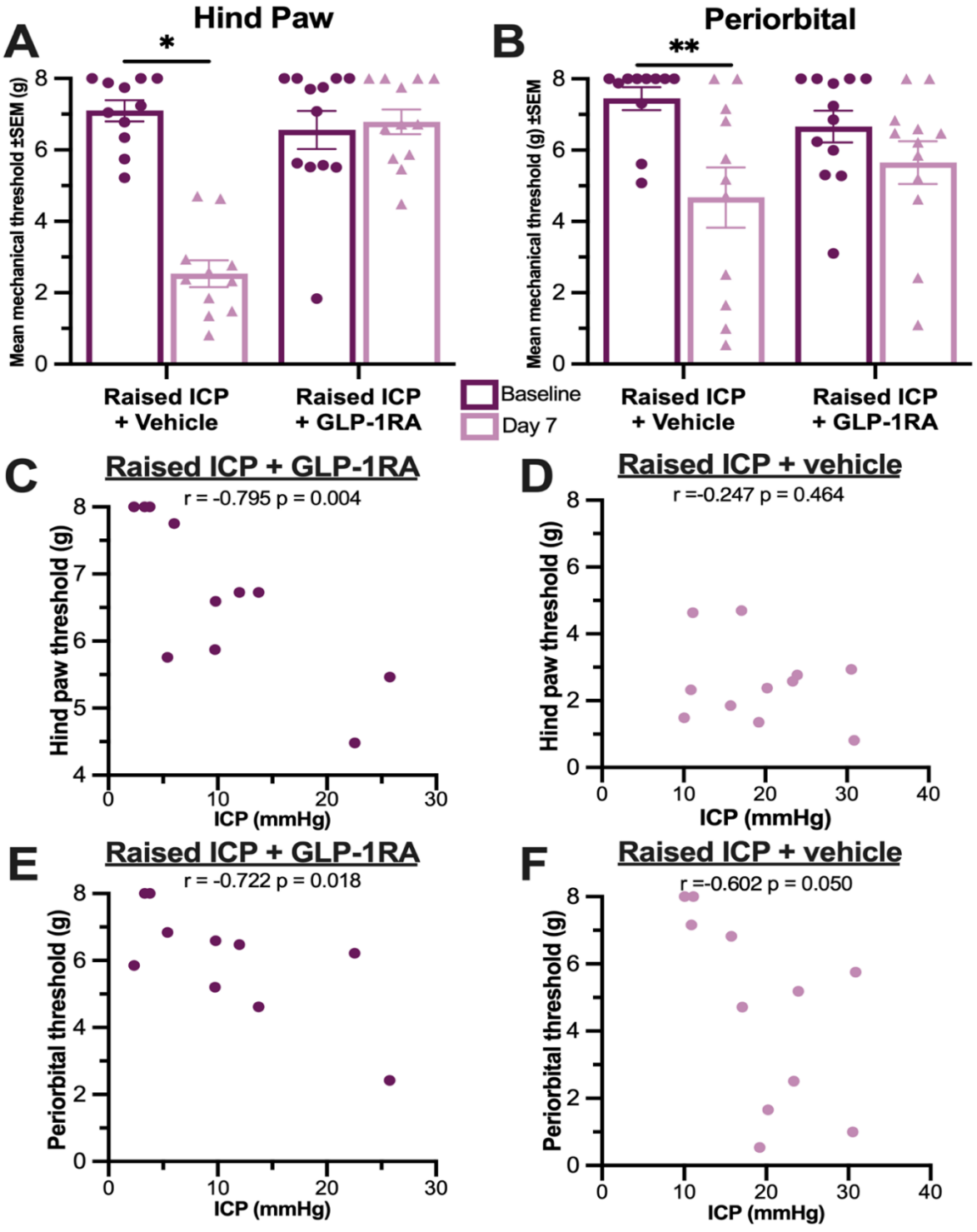

Figure 32F).

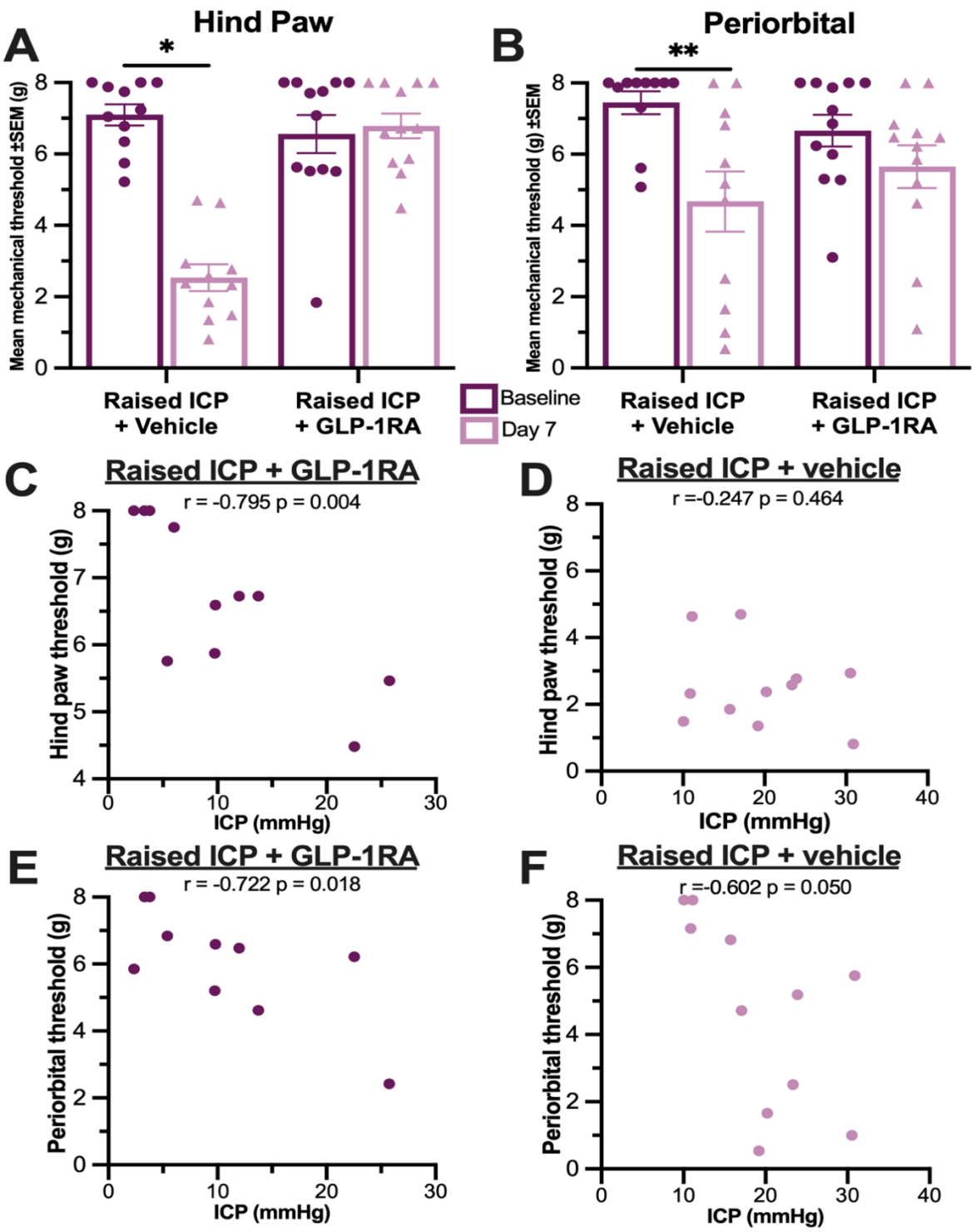

Figure 32. GLP-1RA rescued changes in hind paw and periorbital mechanical thresholds and were associated with ICP.

A- Hind paw and **B –** Periorbital mechanical thresholds were reduced at day 7 in vehicle but not GLP-1RA. **C -** Association between hind paw thresholds and ICP in vehicle **D** – and GLP-1RA animals. **E –** Periorbital thresholds were associated with

ICP in both animals with vehicle and **F -** GLP-1RA**.** GLP-1RA; glucagon-like peptide 1 receptor agonist ICP; intracranial pressure, mmHg; millimetres of mercury. Data in bar charts presented as mean ± SEM, box and whisker represent median ± range. Significance determined by unpaired *t* test or Mann Whitney U test * $P<0.05$ ** $P<0.01$.

5.3.1.3 GLP-1R agonism improved evoked CSD cortical and neurovascular responses

Evoked CSD responses were measured in raised ICP animals treated with vehicle or GLP-1RA to explore the impact of reducing ICP. In raised ICP animals treated with vehicle, cortical responses were similar to those demonstrated by raised ICP (Figure 33A). Repolarisation duration was significantly delayed (median (range) = 800.85s (1988.67) $n = 6$, Figure 33D) and CBF change was low (mean (SD) = 70.62% (47.75) $n = 6$ Figure 33F).

GLP-1RA treatment improved cortical function and neurovascular coupling following stimulation (Figure 33B). Depolarisation duration was significantly reduced (mean (SD) GLP-1RA = 56.57s (25.10) $n = 7$, vehicle = 115.98s (58.80) $n = 6$, $P = 0.033$ Figure 33C). Repolarisation duration was also markedly decreased (median (range) GLP-1RA = 177.55s (562.88) $n = 7$, vehicle = 800.85s (1988.67) $n = 6$, $P = 0.002$, Figure 33D). Percentage change in CBF responses were improved with GLP-1RA treatment although did not reach significance (mean (SD) GLP-1RA = 138.50% (116.80), $n = 7$, vehicle = 70.62% (47.75), $n = 6$, $P = 0.212$, Figure 33F). The number of CBF peaks was significantly higher in animals treated with GLP-1RA versus vehicle (mean (SD) GLP-1RA = 11 (4), vehicle = 3 (2) $n = 5$, $n = 6$, $P = 0.0021$, Figure 33G).

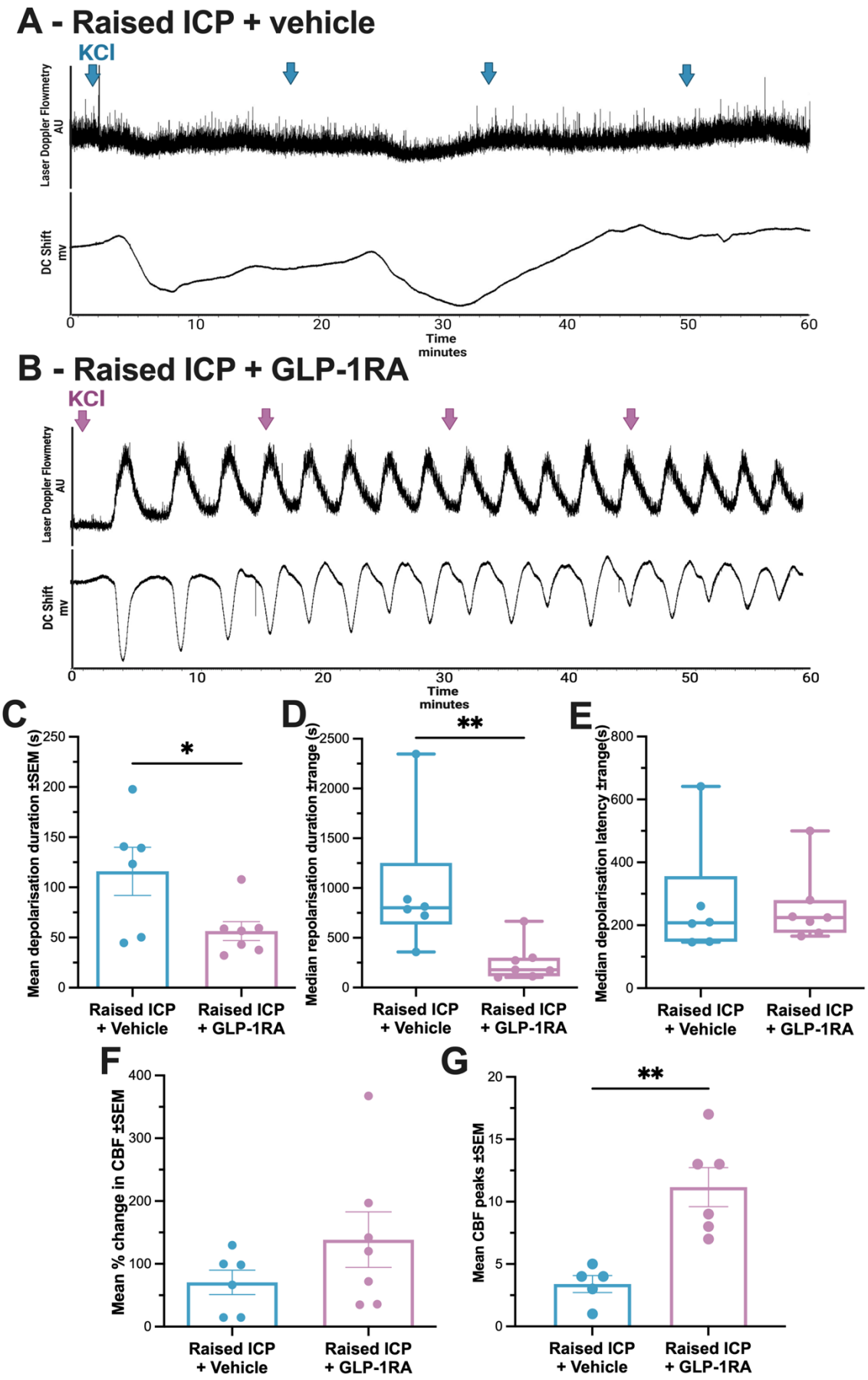
A - Raised ICP + vehicle
KCl
Laser Doppler Flowmetry AU
DC Shift mv
0
10
20
30
40
50
60
Time minutes
B - Raised ICP + GLP-1RA
KCl
Laser Doppler Flowmetry AU
DC Shift mv
0
10
20
30
40
50
60
Time minutes
C
Mean depolarisation duration ±SEM (s)
*
Raised ICP + Vehicle
Raised ICP + GLP-1RA
D
Median repolarisation duration ±range (s)
**
Raised ICP + Vehicle
Raised ICP + GLP-1RA
E
Median depolarisation latency ±range(s)
Raised ICP + Vehicle
Raised ICP + GLP-1RA
F
Mean % change in CBF ±SEM
Raised ICP + Vehicle
Raised ICP + GLP-1RA
G
Mean CBF peaks ±SEM
**
Raised ICP + Vehicle
Raised ICP + GLP-1RA

Figure 33. GLP-1RA restored cortical responses to stimulation.
Representative steady state potential (DC) and CBF response to KCl stimulation in raised ICP animals with **A** - vehicle and **B** - GLP-1RA. Arrows indicate addition of 5µL KCl to the cotton pellet every 15 minutes. **C** – Depolarisation duration was reduced in GLP-1RA animals. **D** – Repolarisation duration showed a trend towards reduction in GLP-1RA animals. **E** – Depolarisation latency was similar between animals injected with vehicle and GLP-1RA. **F** - % change in CBF, **G** – Number of CBF peaks in the hour recording is higher in GLP-1RA animals. AU; arbitrary units, CBF; cortical blood flow, KCl; potassium chloride, ICP; intracranial pressure, GLP-1RA; glucagon like peptide-1 receptor agonist. Data in bar charts presented as mean ± SEM, box and whisker represent median ± range. Significance determined by unpaired *t* test or Mann Whitney U test * $P<0.05$, ** $P<0.01$.

5.3.2 The effects of attenuating CGRP in raised ICP

5.3.2.1 CGRP receptor antagonism did not reduce ICP

Daily administration of CGRP receptor antagonist olcegepant allowed the investigation of the impact of blocking CGRP in the setting of raised ICP. ICP was similar between vehicle and olcegepant treated animals (mean (SD) olcegepant = 20.84mmHg (7.35) *n* = 18, vehicle = 20.47mmHg (6.37) *n* = 15, Figure 34A). Change in weight over 7 days was not significantly different between vehicle or olcegepant animals (Figure 34B).

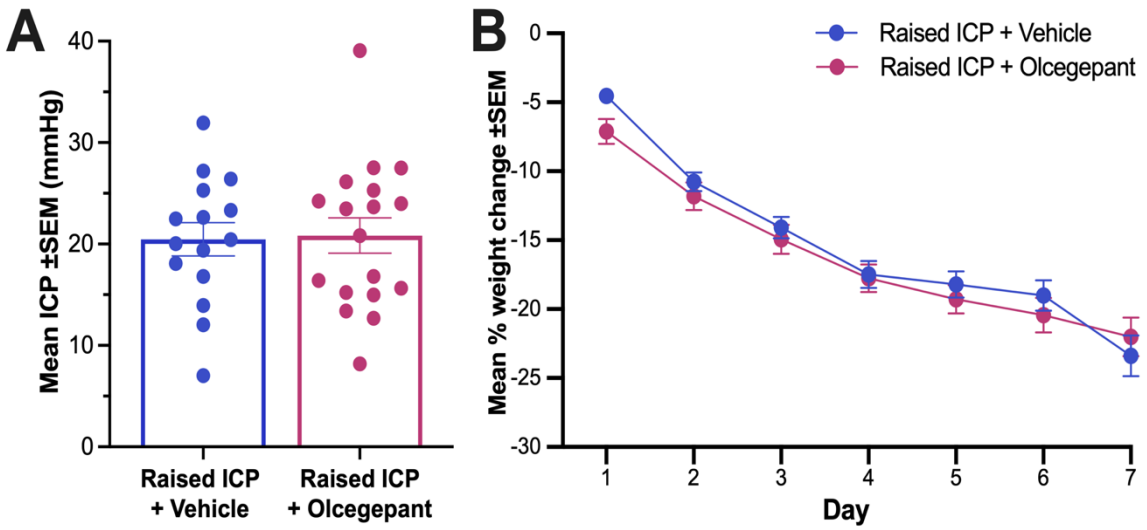

Figure 34. Olcegepant did not influence ICP in raised ICP animals.

A – ICP is similar between animals treated with vehicle and olcegepant. **B -** Percentage weight change over 7 days is similar between vehicle and olcegepant. ICP; intracranial pressure. Data in presented as mean ± SEM.

5.3.2.2 CGRP receptor antagonism rescued periorbital sensitivity in raised ICP

Mechanical pain thresholds were measured at baseline and 7 days following vehicle or olcegepant administration in raised ICP animals. Vehicle injected animals exhibited a significant decrease in hind paw thresholds at day 7 compared to baseline (baseline mean (SD) = 5.31g (1.68), day 7 = 2.83g (1.23), n = 10 P<0.01, Figure 35A). Hind paw thresholds were also reduced in animals treated with olcegepant at day 7 (baseline = 5.96g (1.12), day 7 = 2.49g (1.30), n =10 P<0.0001, Figure 35A).

Periorbital thresholds were decreased in vehicle treated animals at day 7 versus baseline (baseline = 6.83g (1.00), day 7 = 3.29g (2.39), n = 9 P = 0.003, Figure 35B). However, in animals treated with olcegepant, there were no significant differences

between mechanical thresholds at baseline and day 7 (baseline = 7.69g (0.71), day 7 = 6.35g (2.32), *n* = 10, Figure 35B).

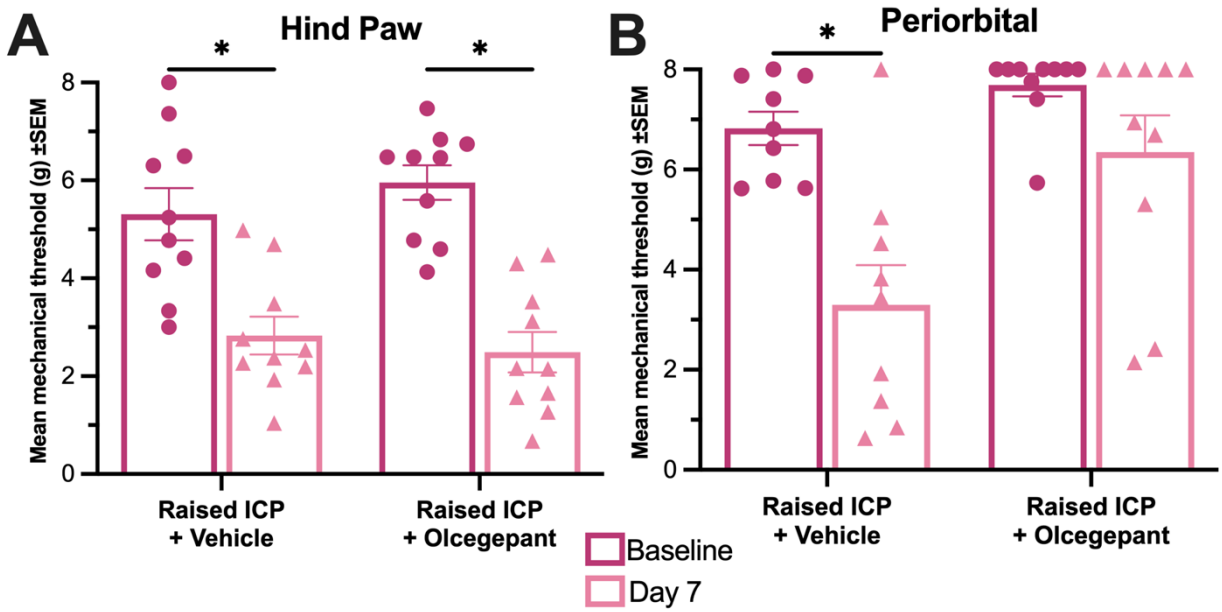

Figure 35. Olcegepant rescued changes in periorbital mechanical thresholds. **A** – Hind paw and **B** – Periorbital mechanical thresholds at day 7 compared to baseline in animals treated with vehicle and olcegepant. g; grams, ICP; intracranial pressure. Data in presented as mean ± SEM. Significance determined by paired *t* test ** *P*<0.01, *** *P*<0.001.

5.3.2.3 CGRP receptor antagonism did not influence evoked CSD responses cortical responses to stimulation

Evoked CSD responses were measured in animals with raised ICP following olcegepant treatment to determine the effects on cortical excitability in the setting of raised ICP. Cortical responses were similar between animals treated with vehicle or olcegepant (Figure 36A, B). Depolarisation duration and latency were also not significantly different between groups (Figure 36C, E). Both exhibited a lag in

hyperpolarisation (vehicle mean (SD) = 1503.19s (1132.18) *n* = 5, olcegepant = 1561.23s (1206.01) *n* = 9, Figure 36D) olcegepant did not impact CBF (vehicle mean (SD) = 69.02% (72.68) *n* = 5, olcegepant = 73.06% (42.66) *n* = 9, Figure 36F). The number of CBF peaks were also not different between vehicle and olcegepant animals (vehicle mean (SD) = 3 (2) *n* = 5, olcegepant = 4 (2), *n* = 10, Figure 36G).

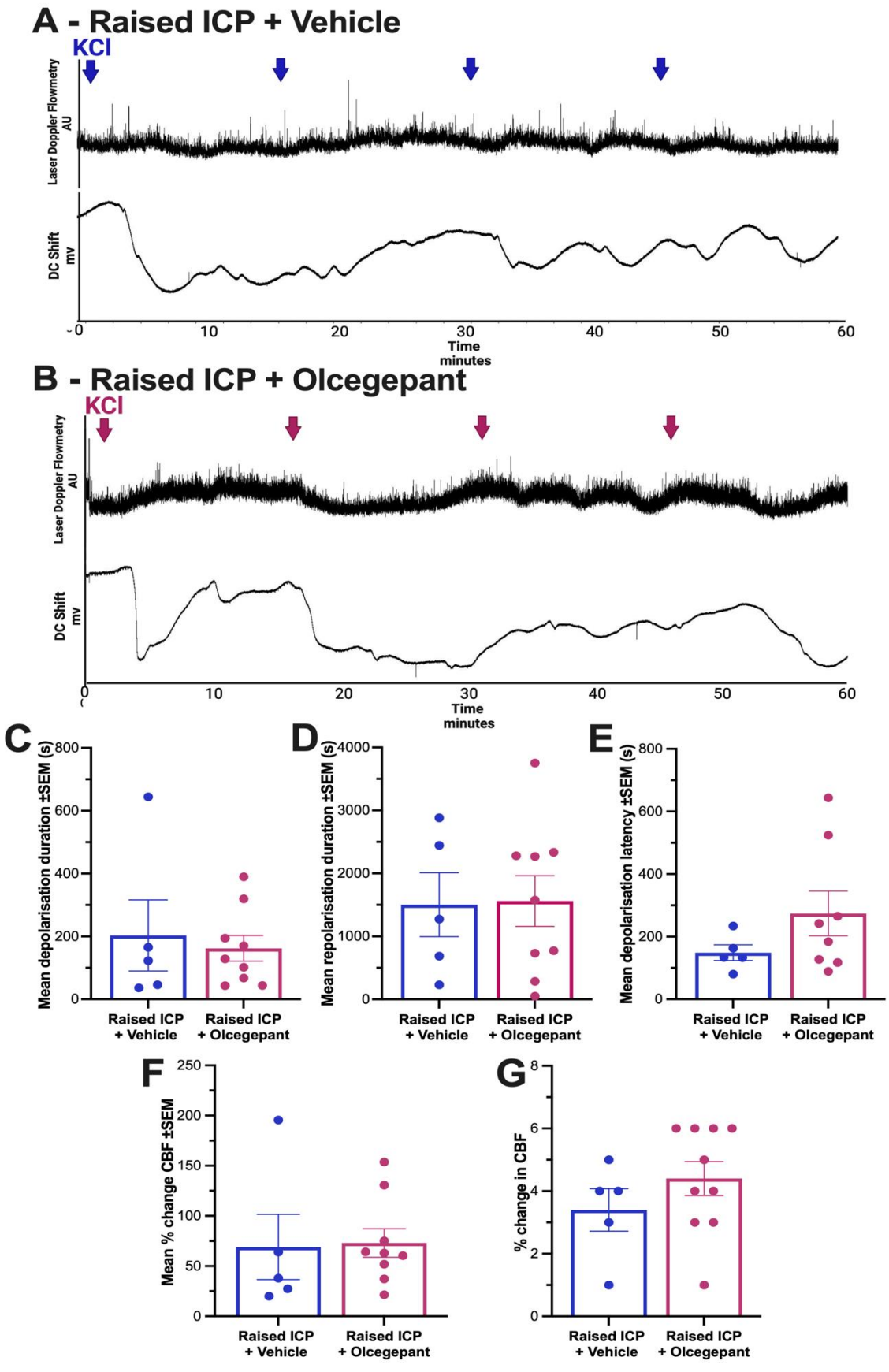
A - Raised ICP + Vehicle
KCl
Laser Doppler Flowmetry AU
DC Shift mv
0
10
20
30
40
50
60
Time minutes
B - Raised ICP + Olcegepant
KCl
Laser Doppler Flowmetry AU
DC Shift mv
0
10
20
30
40
50
60
Time minutes
C
Mean depolarisation duration ±SEM (s)
0
200
400
600
800
Raised ICP + Vehicle
Raised ICP + Olcegepant
D
Mean repolarisation duration ±SEM (s)
0
1000
2000
3000
4000
Raised ICP + Vehicle
Raised ICP + Olcegepant
E
Mean depolarisation latency ±SEM (s)
0
200
400
600
800
Raised ICP + Vehicle
Raised ICP + Olcegepant
F
Mean % change CBF ±SEM
0
50
100
150
200
250
Raised ICP + Vehicle
Raised ICP + Olcegepant
G
% change in CBF
0
2
4
6
8
Raised ICP + Vehicle
Raised ICP + Olcegepant

Figure 36. Cortical responses were not altered by olcegepant.

Representative steady state potential (DC) and CBF response to KCl stimulation in **A** - vehicle and **B –** olcegepant treated animals. Arrows indicate addition of 5µL KCl. **C** – Depolarisation duration **D** – Repolarisation duration **E –** Depolarisation latency **F** - % change in CBF and **G –** number of CBF peaks within the hour recording was similar between raised ICP animals exposed to vehicle or olcegepant. AU; arbitrary units, CBF; cortical blood flow, KCl; potassium chloride, ICP; intracranial pressure. Data in presented as mean ± SEM.

5.3.2.4 CGRP in the trigeminal ganglion was not altered by pharmacological treatment

CGRP protein was measured in the trigeminal ganglion of animals with raised ICP treated with GLP-1RA, olcegepant or vehicle to investigate if CGRP is more abundant in nociceptive structures. There were no significant differences in animals treated with vehicle or exenatide, or animals treated with vehicle or olcegepant (Table 10).

Table 10. CGRP concentration in the trigeminal ganglion of controls and raised ICP treated with vehicle versus GLP-1RA and olcegepant.

* denotes non-parametric data which are presented as median (range). Significance was determined by unpaired *t* test or Mann Whitney u test.

ICP	**Drug**	**Normalized trigeminal ganglion CGRP** Mean (SD) pg/ml	***n***	***P***
Normal *		0.0033 (0.0085)	12	0.0931
Raised *		0.0031 (0.0020)	10	
Raised	Vehicle	0.0034 (0.0012)	12	0.3363
	Exenatide	0.00297 (0.0008)	12	
	Vehicle	0.0052 (0.0023)	10	

	Olcegepant	0.0053 (0.0019)	9	0.946

5.4 Discussion

5.4.1 GLP-1 receptor agonism reduced ICP

Targeted therapeutics for headache in IIH and other conditions of raised ICP are lacking. To determine the effects of reducing ICP on pain behaviour and CSD responses, animals were treated with GLP-1RA exenatide. GLP1-RA significantly reduced ICP in the raised pressure model, similarly to previous studies demonstrating its efficacy in both kaolin injected animals[199] and IIH patients.[246] ICP in GLP-1RA treated animals returned to levels similar to those of control animals, exhibiting the reversal of the effects of CSF blockage with kaolin. This emphasises the therapeutic potential of GLP-1RA for the use in patients with conditions of raised ICP and highlights that increases in ICP were reversible in this model.

GLP-1R agonism in choroid plexus cells resulted in reduction of Na^+/K^+ specific ATPase activity, thereby reducing CSF secretion.[199] Similar ventricle dilation was observed between raised ICP animals treated with vehicle and GLP-1RA, indicating that drug treatment is not able to reverse this effect but may act on lowering ICP via CSF secretion. It is unlikely that GLP-1R agonism would have been able to eliminate blockage caused by kaolin at the injection site. Since GLP-1RA administration commenced one day after kaolin injection, the dilatory effects of hydrocephalus were likely to have occurred within this period prior to drug administration. Exenatide is a fast acting formulation of a GLP-1RA, with a half-life of 2.4 hours, which may have led to a rapid effect on raised ICP animals.[336] Since animals used were adults, the

plasticity of neuronal tissue is reduced, thereby the reversibility of this dilation may be prevented. Measurement of CSF secretion using tracers in the CSF perfused and collected from the cisterna magna would be interesting to better understand the mechanistic role of GLP-1RA in this model.

GLP-1RA has a role in appetite and satiety and has recently been licensed for the treatment of obesity due to their ability to reduce appetite and drive weight loss.[337 338] In IIH, weight loss was similar between placebo and GLP-1RA arms, indicating that the reduction in ICP was independent of changes in weight.[246] This study also highlighted that weight change was similar between animals treated with vehicle and GLP-1RA suggesting changes in ICP were independent of changes in weight.

5.4.2 Reducing ICP improved cortical function and cerebrovascular responses

Reduction of ICP with GLP-1RA was accompanied by improved neuronal activity and cerebrovascular during evoked CSD. In addition to its effects on ICP, a large proportion of GLP-1R in the brain are found in cortical regions.[339] Exendin-4 was also able to reduce cortical cell death, preserve dopaminergic neurons and improve functional behaviour in an animal model of Parkinson's disease.[340] GLP-1R agonism may potentially protect against cell death induced by pathological ICP, thereby improving the neural CSD responses as indicated in the current study. These results demonstrate the metabolic and neurovascular benefits of exenatide as a potential therapeutic for raised ICP headache.

In *ex vivo* brain slice models, GLP-1R agonism with exendin-4 was able to exert a dilatory effect on cortical arterioles reversing constrictions induced by ischaemic

stroke.[341] *In vivo* exendin-4 also improved brain tissue PO_2 providing a protective effect against the hypoxic damage of ischaemia.[341] This data in this chapter suggest that GLP-1RA exenatide may have a similar effect, reversing the neurovascular uncoupling induced by raised ICP. By reducing ICP to control values, it is possible that autoregulation can facilitate CBF increases to respond to neuronal activity following stimulation. However, ventricles remained dilated in animals treated with GLP-1RA suggesting there may remain compression between dural layers and the skull.

The ability to increase CBF in response to stimulation may prevent hypoxia, thereby allowing the cortical tissue to respond adequately to increased energetic demand. Regulation of glial responses may also contribute towards recovered neurovascular function. In previous studies GLP-1RA liraglutide was able to inhibit microglial activation, prevent brain oedema and blood-brain-barrier breakdown and reduce brain injury in an animal model of subarachnoid haemorrhage.[342] The prevention of inflammatory responses may aid in rescuing of neuronal function and cerebrovascular changes in response to evoked CSD as demonstrated in this thesis.

5.4.3 Reducing ICP prevented pain behaviour associated with trigeminal sensitivity

Reducing ICP with GLP-1RA prevented reductions in cephalic and extra-cephalic mechanical sensitivity. There was also an association between ICP and periorbital and hind paw thresholds in animals treated with exenatide. Alleviating ICP via weight loss or surgical shunt has beneficial effects on improving headache outcomes in IIH.[191 212 343] An association between reduction in ICP and improvement in markers of

allodynia has also been identified in IIH patients,[57] highlighting the translational relevance of these results. In IIH patients, GLP-1RA liraglutide reduced monthly headache days, however ICP was not measured and therefore it was not possible to attribute changes in ICP.[344] GLP-1R have been identified at the trigeminal nucleus and therefore may directly play a role in nociception.[345] [346] Liraglutide has also exhibited the ability to attenuate trigeminal allodynia in a nitroglycerin-induced chronic migraine model.[347] Upregulation of interleukin-10 in the TNC was able to supress central sensitization, indicating that GLP-1RA may potentially prevent trigeminal sensitization by also downregulating inflammation.[346]

Evidence of GLP-1R expression adjacent to afferent renal nerve fibres immunoreactive to CGRP has suggested cross talk between these molecules.[348] Both GLP-1 and CGRP have roles in lipid metabolism,[349] [350] therefore suggesting a role of GLP-1 in CGRP mediated pathways. In addition to its role in lowering ICP, GLP-1 may act by modulating CGRP,[351] thereby exerting antinociceptive effects. The direct effects of GLP-1R agonism on CGRP pathways have not been explored, however this poses a dual action of GLP-1RA on headache pathways and may contribute to the preventative effects on pain behaviour.

5.4.4 Attenuating CGRP signalling did not influence CSD responses

In this model of raised ICP, olcegepant did not influence ICP. This is an important finding since the relationship between CGRP signal attenuation and ICP has not previously been investigated.

CGRP-R antagonism did not recover the prolonged depolarised state or improve neurovascular uncoupling in animals with raised ICP. Previous studies have

exhibited similar findings.[53] [352] Although olcegepant was able to block CSD induced trigeminal sensitivity in other migraine models, it was not able to modify CSD responses.[352] Moreover, use of CGRP-RA MK-8825 also did not attenuate DC shifts changes or accompanied hemodynamic response.[53] Since the crossing of CGRP-RA across the blood-brain barrier is still thought to be poor,[353] it is possible that it is unable to prevent neuronal changes caused by raised ICP, unlike GLP-1RA which readily crosses the blood-brain barrier. [354] [355] However, in animal models with blood-brain-barrier damage, CGRP monoclonal antibodies persistently failed to abolish CSD initiation, suggesting CSD mechanisms may not be entirely CGRP-dependant.[356]

In addition, there has been no previous evidence of olcegepant demonstrating any impact on the hemodynamic in migraine patients following infusion of migraine inducing agent glyceryl trinitrate.[357] *In vivo*, investigation of the effects of CGRP infusion found that olcegepant was not able to prevent vasodilatory effects.[358] Moreover in animal models of ischemic stroke, CGRP-R antagonism reduced reperfusion success and doubled infarct volume, supporting its inability to improve neurovascular function in conditions of poor perfusion.[359] These studies support findings that olcegepant did not improve neurovascular uncoupling found in raised ICP responses to CSD.

5.4.5 CGRP-R antagonism rescued cranial nociception in the setting of raised ICP

CGRP receptor antagonism prevented cranial nociception in the model of raised ICP. Numerous *in vivo* studies have confirmed the efficacy of olcegepant at attenuating

changes in periorbital sensitivity.[151 360-362] CGRP-RA act on peripheral trigeminal sensory afferents involved in nociceptive signalling in migraine, suggesting that these pathways may also contribute towards cranial nociception in raised ICP.

There were no beneficial effects of olcegepant on hind paw sensitivity which has been demonstrated by some other groups.[151 361] Most studies of the effect of CGRP-RA on trigeminal sensitivity have been conducted in migraine models. In this model of raised ICP, the effects on peripheral sensitization may be mediated by non-CGRP dependant pathways, preventing the beneficial effects of olcegepant. However, there is still debate regarding whether the activity of spinal trigeminal neurons is governed by CGRP receptor activation.[363 364] Animal studies have identified that inhibition of CGRP receptors with olcegepant in the trigeminal ganglion did not impact the neuronal activity in peripheral regions governed by spinal trigeminal neurons.[363 364] Our results may be due to the ability of CGRP-RA to block receptors on trigeminal sensory afferents but not dorsal root ganglion.[363 364]

Other clinical studies have highlighted the ability of CGRP targeting with mAbs to alleviate headache in conditions of raised ICP including IIH and post traumatic headache.[58 60] This is in line with the effectiveness of CGRP therapeutics to treat migraine, but not currently peripheral chronic pain disorders, which aligns with the data which demonstrates olcegepant is not able to alleviate peripheral sensitivity. Evidently additional studies are needed to clarify the role of CGRP inhibition in raised ICP models.

5.4.6 Limitations and future directions

There are some limitations which are applicable to this work. Due to the invasiveness of ICP measurements, it was not possible to measure ICP before and after drug treatment. This would have provided change measurements in ICP, and additionally confirm that kaolin injection resulted in raised ICP before drug initiation. However, comparisons instead were made between animals injected with vehicle versus drug, allowing the evaluation the effect of therapeutic agents.

We also only used male rats for these investigations. This is important to consider when interpreting results, since female sex has been found to alter pain promotion of CGRP and response to CGRP-RA in mice.[66] Although sex different responses between GLP-1RA treatment have not been accessed future evaluation of the impact of these drugs in both male and female animals would explore this.

The work in this chapter demonstrated the therapeutic effects of GLP-1R agonism on pain behaviours, suggesting reducing ICP may improve nociception. Reducing ICP also improved cortical function in response to stimulation and rescued coupling to CBF activity, proposing an improvement on physiological function. The experiments in this chapter also signify that CGRP antagonism is beneficial in managing cranial nociception in raised ICP. These results provide pre-clinical evidence of the efficacy of therapeutics for the management of headache behaviours and pathways which will help inform clinical trials, since targeted therapies are lacking in raised ICP.

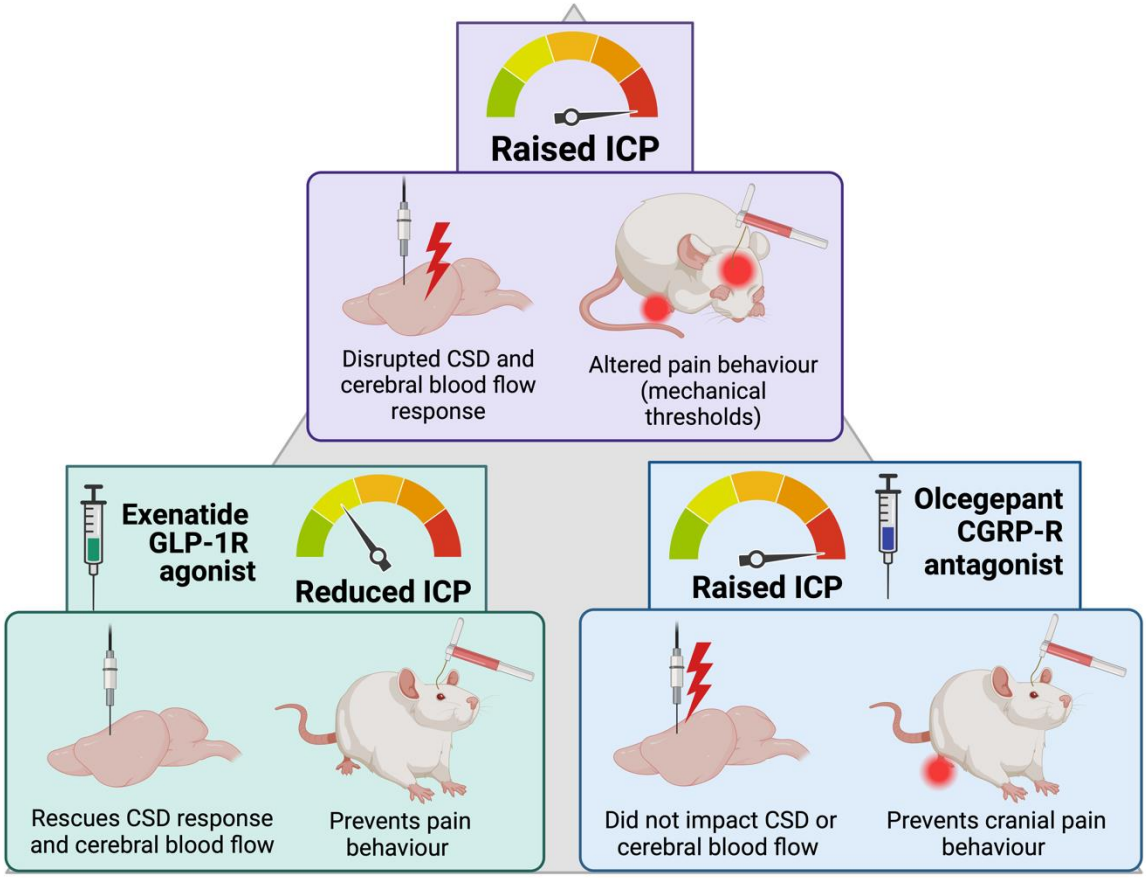

Figure 37. Summary of the effects of raised ICP and pharmacological manipulation on headache mechanisms.

Raised ICP rodents exhibit disrupted CSD and CBF responses in addition to altered mechanical pain thresholds. Reducing ICP with GLP-1RA rescued CSD responses and prevented changes in mechanical pain thresholds. In the setting of raised ICP, CGRP-R antagonism prevented changes in cranial pain thresholds but did not impact CSD responses. CGRP; calcitonin gene related peptide, CSD; cortical spreading depression, GLP-1R; glucagon like peptide 1 receptor, ICP; intracranial pressure.

CHAPTER 6 DISCUSSION

6.1 Key findings

To summarise key metabolic findings, studies demonstrated that KCl stimulation led to a wave-like movement of Ca^{2+} across acute brain slices, characteristic of the astrocytic response during CSD.[281] In response to CSD, there was a shift towards glycolysis, which is replicated by other studies of the characterised metabolic response to CSD.[116] Although a local increase in mitochondrial activity using fluorescent labels was exhibited in response to stimulation, globally, this rate was lower than glycolytic activity. Increased lactate was also recorded, a marker of anaerobic respiration following CSD, emphasizing the increased oxygen demand of neuronal tissue in response to depolarization.[115] [123] Characterizing the metabolic response to spreading depolarization under 'healthy' conditions establishes a foundational reference point for identifying changes in disease states. These findings offer numerous targets for therapeutic development and serve as a baseline against which disease-state responses can be compared to.

Secondly, glucose deprivation drastically altered the metabolic responses to CSD in brain slices, which may have indicated the upregulation of compensatory metabolic mechanisms. For instance, this data revealed that KCl stimulation still resulted in increased Ca^{2+} signalling, which may represent a typical astrocytic CSD response that is not impacted by glucose availability. However, since Ca2+ signalling was incrementally increased, this may also signify a neuroprotective response.[284] There was a complete absence in the upregulation of mitochondrial activity in glucose deprived slices, which may indicate mitochondrial exhaustion. This finding, in addition to a reduced antioxidative metabolite alanine, suggests ROS may contribute towards

the depressed metabolic response to CSD.[365] Reduced glutamate was also discovered following CSD in the absence of glucose potentially suggesting alternative substrate use under metabolic stress. Although together these results demonstrate that in the absence of energetic substrates, neuronal tissue demonstrates metabolic plasticity, mitochondrial exhaustion may contribute towards fatigue following migraine attack.

This thesis additionally investigated the influence of elevated ICP on headache pathways. This work demonstrated the successful optimisation and utilization of an adult rodent model of raised ICP, previously this has not been utilised in the context of headache studies. This model illustrated that raised ICP led to altered pain behaviour; namely reductions in mechanical pain thresholds, suggesting changes in trigeminal sensitivity. Raised ICP also led to dramatically altered evoked CSD responses, featuring a prolonged depolarization period and loss of cerebrovascular responses.

This model also replicated previous findings that GLP-1RA exenatide can reduce ICP.[199] Interestingly it was determined that this had therapeutic effects on pain behaviours and was able to prevent changes in mechanical thresholds as a result of raised ICP. GLP-1R agonism was also able to inhibit the effects of raised ICP on cortical and cerebrovascular function so that CSD responses resembled that of control animals. These findings suggest that reducing ICP and via agonism of the GLP-1 pathways is beneficial at reducing markers of headache mechanisms.

CGRP receptor antagonists are effective migraine therapeutics, however their use in raised ICP headache has not previously been investigated. Experiments in this research reveal that CGRP antagonism reduced cranial nociception, preventing changes in periorbital mechanical pain thresholds in the setting of raised ICP. In

agreement with previous studies CGRP antagonism did not influence CSD characteristics,[352] nor did it impact ICP. Taken together these results suggest the utility of CGRP therapeutics for patients with raised ICP headache to reduce cranial nociception.

6.2 General discussion

The research presented in this thesis has yielded important advancements, notably the development and validation of an *ex vivo* brain slice model. This model enabled metabolic analysis of the impact of CSD, a mechanism important to the pathophysiology of headaches. By unravelling the metabolic dynamics during CSD recovery, invaluable insights have been gained into upregulated metabolic pathways. Additionally, utilizing this model, the effects of fasting on energetic flux were explored, shedding light on metabolic alterations implicated in fasting-induced headaches. Future employment of this model would allow us to investigate the impact of raised ICP on headache mechanisms at a molecular and cellular level.

The observed prevented glycolytic and mitochondrial pathways due to the absence of glucose hints at potential brain energy depletion during stimulation. This could offer a compelling explanation for why fasting individuals are more susceptible to headaches, suggesting a lack of upregulation in energy production pathways. Moreover, these findings indicate that supplementing the oxidative respiratory pathways to support depleted mitochondrial activity may improve CSD recovery or outcomes. These findings not only advance our comprehension of the metabolic role in CSD but also reveal disruptions in energetic pathways, pinpointing potential targets for therapeutic interventions. Given that IIH also involves metabolic

disturbances, these insights shed light on how altered metabolic profiles due to raised ICP might exacerbate challenges in headache mechanisms.

Additionally, this research has provided valuable insights into headaches attributed to increased ICP a condition for which targeted therapies are currently lacking due to a limited understanding of its causes. By optimising an animal model to mimic moderate ICP, this work uncovered how elevated ICP influences mechanisms related to headache nociception and physiology. The observed alterations in cortical and CBF responses, in addition to altered pain behaviours characteristic of allodynia, represent the first preclinical investigation into headaches linked with raised ICP. These findings suggest a potential shared mechanism with migraine, offering a steppingstone towards understanding and addressing these challenging conditions.

Furthermore, the study highlighted promising therapeutic directions. GLP-1R agonism with exenatide showed a positive impact in reducing evoked pain behaviours and improving cortical and CBF responses during CSD. This hints at the potential use of GLP-1R agonists in alleviating headache nociception due to increased ICP, while also positively affecting critical neurovascular functions. Similarly, the preventive effect of CGRP receptor antagonism on cranial nociception in the context of raised ICP suggests a plausible therapeutic approach involving CGRP therapeutics for managing raised ICP headaches.

This research advances knowledge of how elevated pressure relates to headaches. By demonstrating the potential efficacy of certain therapeutics in addressing headache measures in raised ICP, this work holds promise for improved patient care and adds to the scientific knowledge, potentially guiding the development of targeted treatments.

6.3 Limitations and future investigations

The experiments conducted in this thesis have yielded valuable mechanistic insights into the metabolic implications of CSD. However, it's important to acknowledge the limitations associated with using brain slices as a model for headache physiology. Changes in blood flow and neuroinflammatory responses, which are well-documented in CSD,[115 366 367] can influence the metabolism and functionality of cells within the slices. While brain slice results may not fully replicate the metabolic changes that occur *in vivo*, the testing conditions, which included oxygen-perfused aCSF, may have mitigated some of these effects. Future validation of the impact of CSD on metabolism *in vivo* is necessary to ensure that the findings remain unaffected by vascular changes.

Emerging data has also revealed that CSD responses are different between male and female animals.[298] Both sexes were used in the brain slice model, which may have led to different metabolic responses between animals.[330] The differences in metabolic function between sexes has not been examined in the context of headache and CSD, however this would be a topic of interest for future investigation.

It should also be acknowledged that investigation of the impact of raised ICP has been carried out exclusively in male animals. Since there are differences in CSD responses between different sexes,[330] investigations in males only eliminated the need to analyse the effect of not only raised ICP but also sex, and menstrual cycle phase . This allowed us to directly investigate relationship between raised ICP and headache. As IIH mostly effects women, this model is less translational to the disorder, and may not take into consideration this aspect on headache pathophysiology. Moreover, this model more accurately represents obstructive

hydrocephalus rather than a truly idiopathic cause of raised ICP. Taken together this is more a broad model of raised ICP rather than specifically of IIH, which should be considered when interpreting results. Repeating investigations in female animals would help us understand the interaction of sex hormones on raised ICP headache and would be of future interest.

Because of the selected methodology and the constraints of the animal licensing, it was only possible to obtain absolute ICP measurements in animals after 7 days. While comparisons were made of the effects of drugs on pressure using a control group, this necessitated relying on ventricle dilation measurements to confirm the model's success before administering the drugs. The utilization of telemetric or fully implantable ICP monitors would enable repeated sampling of ICP, thereby providing measurements of changes and allowing the use of animals as their own controls.

As this thesis has demonstrated the utility of a rodent model of raised ICP which is able to facilitate headache measurements, this opens the possibility to numerous future drug studies. Although this has demonstrated the efficacy of GLP-1RA exenatide the reduce ICP and have benefits on headache measurements, it may give rise to the question of other existing GLP-1RA. Exenatide has a short half-life and is able accumulate to a therapeutic concentration much faster than other GLP-1RA formulations such as liraglutide.[246 368] Assessing the effects of other GLP-1RA which are available for reducing ICP and associated headache markers may provide more options for IIH patients with drugs which may be more accessible.

6.4 Clinical translation

Altered metabolism can contribute to various aspects of headache disorders, such as food cravings before headache onset,[369] fasting as a trigger,[1] and post-headache fatigue.[15] Despite these associations, the understanding of metabolism's role in response to headache mechanisms has remained limited. Our data has shed light on pathways that undergo differential regulation in response to stimulation, offering potential targets for future therapeutic investigations. For instance, supplementing oxidative respiration in fasting headache may address the lack of mitochondrial response to CSD demonstrated in this research. These findings support the use of riboflavin[91 92] and coenzyme Q10[89 90] which supply these pathways and therefore may be beneficial for fasting headache.

Unlike pharmaceuticals, supplements are cost-effective, non-prescription, readily available, and associated with fewer side effects. Nutraceuticals may serve as a means to bolster metabolic pathways, potentially mitigating headache susceptibility, expediting recovery, or preventing post-effects. This research has revealed the neural tissue's metabolic adaptability following CSD, including the utilization of alternative energy pathways and substrates. Furthermore, it suggests that anaerobic respiration may occur after a CSD, hinting at the possibility of enhancing tissue oxygenation to expedite recovery from headache mechanisms. This insight may also contribute to a better understanding of the heightened risk of ischemic stroke in individuals with migraine with aura. [370]

The pathophysiology of raised ICP headache remains unknown, however the data from this thesis contributes information to the knowledge of pathways which are involved in headache nociception. Moreover, these findings reveal that raised ICP

headache may share pathophysiology with migraine, since changes in mechanical pain thresholds and altered cortical excitability are also features of migraine.[57 72 371] These observations align with the reports from patients with elevated ICP who experience allodynia and describe their headaches as migraine-like.[57 193] This suggests that patients with elevated ICP headaches may benefit from treatment approaches similar to those used for migraine patients. However, further investigation is warranted to gain a deeper understanding of the interplay between migraine and the mechanisms underlying elevated ICP headaches.

There are currently no targeted treatments for headache attributed to raised ICP and limited evidence suggesting the efficacy of migraine therapeutics. Although CGRP therapeutics have been highly effective in migraine, without mechanistic understanding of the role of blocking CGRP there is limited data to recommend its use in IIH. This has limited the availability of these drugs to IIH patients. The data in this thesis supports the use of CGRP antagonist to treat cranial nociception in headache attributed to raised ICP. This is important since recent studies have demonstrated high opiate use in IIH patients,[195] which suggests IIH patients are at risk of medication overuse headache. CGRP therapeutics may avoid this in IIH patients.

In addition to emerging clinical studies,[246] these results support the use of GLP-1RA in conditions of raised ICP. These results illustrate the therapeutic effects of exenatide on ICP, which were notably correlated to reduced pain-related behaviours. While previous trials in IIH patients have not consistently shown the benefits of reducing ICP on headache outcomes,[190] the data from this thesis suggests that the specific reduction of ICP, particularly through GLP-1R agonism, can ameliorate pain behaviours associated with allodynia. Thus, GLP-1 receptor agonists may offer

therapeutic potential for patients with elevated ICP headache by simultaneously addressing ICP reduction and the associated symptoms, while also mitigating cranial nociception linked to headaches.

Data from this thesis implies that combining GLP-1RA and olcegepant may provide a method of reducing ICP and headache nociception. CGRP receptor antagonism did not exhibit an ICP lowering effect, therefore ICP should be treated independently, and vision monitored to prevent worsening in the absence of headache.

6.5 Conclusions

This thesis has successfully established a platform for investigating metabolism within the context of CSD as a model of headache. These studies have comprehensively characterized the mitochondrial and glycolytic responses in neural tissue during CSD, enabling the identification of potential targets for nutraceutical development. Moreover, our findings suggest the involvement of glucose metabolism in CSD susceptibility and its associated energetic consequences. Additionally, this research has delved into the impact of elevated ICP on headache, while also highlighting the favourable outcomes associated with both lowering ICP through GLP-1R agonism and blocking CGRP via receptor antagonism. These insights hold significant promise for the translational aspect of the research, offering promising avenues for more effective headache management strategies for patients suffering from elevated ICP-related headaches.

CHAPTER 7 APPENDIX

7.1 NucView imaging parameters

```
run("Z Project...", "start=3 projection=[Max Intensity]");

run("Subtract Background...", "rolling=40");

setOption("BlackBackground", false);

run("Convert to Mask");

run("Median...", "radius=3.5");

run("Watershed");

run("Analyze Particles...", "size=35-350 circularity=0.0-1.00 summarize");
```

7.2 von Frey threshold calculations

Appendix Table 1. Tabular value for *k* based on response pattern to calculate 50% mechanical withdrawal threshold using the up-down von Frey method. Originally modified from [372] and adapted in a model of neuropathy by [257].

Pattern	Value for *k*	Pattern	Value for *k*	Pattern	Value for *k*	Pattern	Value for *k*
OX	-0.500	OOOXOOOO	-0.547	XO	0.5	XXXOXXXX	0.547
OOX	-0.388	OOOOXOOOO	-0.547	XXO	0.388	XXXXOXXXX	0.547
OOOX	-0.378	OXOOOX	-1.250	XXXO	0.378	XOXXXO	1.25
OOOOX	-0.377	OOXOOOX	-1.247	XXXXO	0.377	XXOXXXO	1.247
OXO	0.842	OOOXOOOX	-1.246	XOX	-0.842	XXXOXXXO	1.246
OOXO	0.890	OOOOXOOOX	-1.246	XXOX	-0.89	XXXXOXXXO	1.246
OOOXO	0.894	OXOOXO	0.372	XXXOX	-0.894	XOXXOX	-0.372
OOOOXO	0.894	OOXOOXO	0.380	XXXXOX	-0.894	XXOXXOX	-0.38
OXX	-0.178	OOOXOOXO	0.381	XOO	0.178	XXXOXXOX	-0.381
OOXX	0.000	OOOOXOOXO	0.381	XXOO	0	XXXXOXXOX	-0.381
OOOXX	0.026	OXOOXX	-0.169	XXXOO	-0.026	XOXXOO	0.169
OOOOXX	0.028	OOXOOXX	-0.144	XXXXOO	-0.028	XXOXXOO	0.144
OXOO	0.299	OOOXOOXX	-0.142	XOXX	-0.299	XXXOXXOO	0.142
OOXOO	0.314	OOOOXOOXX	-0.142	XXOXX	-0.314	XXXXOXXOO	0.142
OOOXOO	0.315	OXOXOO	0.022	XXXOXX	-0.315	XOXOXX	-0.022
OOOOXOO	0.315	OOXOXOO	0.039	XXXXOXX	-0.315	XXOXOXX	-0.039
OXOX	-0.500	OOOXOXOO	0.040	XOXO	0.5	XXXOXOXX	-0.04
OOXOX	-0.439	OOOOXOXOO	0.040	XXOXO	0.439	XXXXOXOXX	-0.04
OOOXOX	-0.432	OXOXOX	-0.500	XXXOXO	0.432	XOXOXO	0.5
OOOOXOX	-0.432	OOXOXOX	-0.458	XXXXOXO	0.432	XXOXOXO	0.458
OXXO	1.000	OOOXOXOX	-0.453	XOOX	-1	XXXOXOXO	0.453
OOXXO	1.122	OOOOXOXOX	-0.453	XXOOX	-1.122	XXXXOXOXO	0.453
OOOXXO	1.139	OXOXXO	1.169	XXXOOX	-1.139	XOXOOX	-1.169
OOOOXXO	1.140	OOXOXXO	1.237	XXXXOOX	-1.14	XXOXOOX	-1.237
OXXX	0.194	OOOXOXXO	1.247	XOOO	-0.194	XXXOXOOX	-1.247
OOXXX	0.449	OOOOXOXXO	1.248	XXOOO	-0.449	XXXXOXOOX	-1.248
OOOXXX	0.500	OXOXXX	0.611	XXXOOO	-0.5	XOXOOO	-0.611
OOOOXXX	0.506	OOXOXXX	0.732	XXXXOOO	-0.506	XXOXOOO	-0.732
OXOOO	-0.157	OOOXOXXX	0.756	XOXXX	0.157	XXXOXOOO	-0.756
OOXOOO	-0.154	OOOOXOXXX	0.758	XXOXXX	0.154	XXXXOXOOO	-0.758
OOOXOOO	-0.154	OXXOOO	-0.296	XXXOXXX	0.154	XOOXXX	0.296
OOOOXOOO	-0.154	OOXXOOO	-0.266	XXXXOXXX	0.154	XXOOXXX	0.266
OXOOX	-0.878	OOOXXOOO	-0.263	XOXXO	0.878	XXXOOXXX	0.263
OOXOOX	-0.861	OOOOXXOOO	-0.263	XXOXXO	0.861	XXXXOOXXX	0.263
OOOXOOX	-0.860	OXXOOX	-0.831	XXXOXXO	0.86	XOOXXO	0.831
OOOOXOOX	-0.860	OOXXOOX	-0.763	XXXXOXXO	0.86	XXOOXXO	0.763
OXOXO	0.701	OOOXXOOX	-0.753	XOXOX	-0.701	XXXOOXXO	0.753
OOXOXO	0.737	OOOOXXOOX	-0.752	XXOXOX	-0.737	XXXXOOXXO	0.752
OOOXOXO	0.741	OXXOXO	0.831	XXXOXOX	-0.741	XOOXOX	-0.831
OOOOXOXO	0.741	OOXXOXO	0.935	XXXXOXOX	-0.741	XXOOXOX	-0.935
OXOXX	0.084	OOOXXOXO	0.952	XOXOO	-0.084	XXXOOXOX	-0.952
OOXOXX	0.169	OOOOXXOXO	0.954	XXOXOO	-0.169	XXXXOOXOX	-0.954
OOOXOXX	0.181	OXXOXX	0.296	XXXOXOO	-0.181	XOOXOO	-0.296
OOOOXOXX	0.182	OOXXOXX	0.463	XXXXOXOO	-0.182	XXOOXOO	-0.463
OXXOO	0.305	OOOXXOXX	0.500	XOOXX	-0.305	XXXOOXOO	-0.5
OOXXOO	0.372	OOOOXXOXX	0.504	XXOOXX	-0.372	XXXXOOXOO	-0.504
OOOXXOO	0.380	OXXXOO	0.500	XXXOOXX	-0.38	XOOOXX	-0.5
OOOOXXOO	0.381	OOXXXOO	0.648	XXXXOOXX	-0.381	XXOOOXX	-0.648
OXXOX	-0.305	OOOXXXOO	0.678	XOOXO	0.305	XXXOOOXX	-0.678
OOXXOX	-0.169	OOOOXXXOO	0.681	XXOOXO	0.169	XXXXOOOXX	-0.681
OOOXXOX	-0.144	OXXXOX	-0.043	XXXOOXO	0.144	XOOOXO	0.043
OOOOXXOX	-0.142	OOXXXOX	0.187	XXXXOOXO	0.142	XXOOOXO	-0.187
OXXXO	1.288	OOOXXXOX	0.244	XOOOX	-1.288	XXXOOOXO	-0.244
OOXXXO	1.500	OOOOXXXOX	0.252	XXOOOX	-1.5	XXXXOOOXO	-0.252
OOOXXXO	1.544	OXXXXO	1.603	XXXOOOX	-1.544	XOOOOX	-1.603
OOOOXXXO	1.549	OOXXXXO	1.917	XXXXOOOX	-1.549	XXOOOOX	-1.917

7.3 The effect of genotype on metabolite results

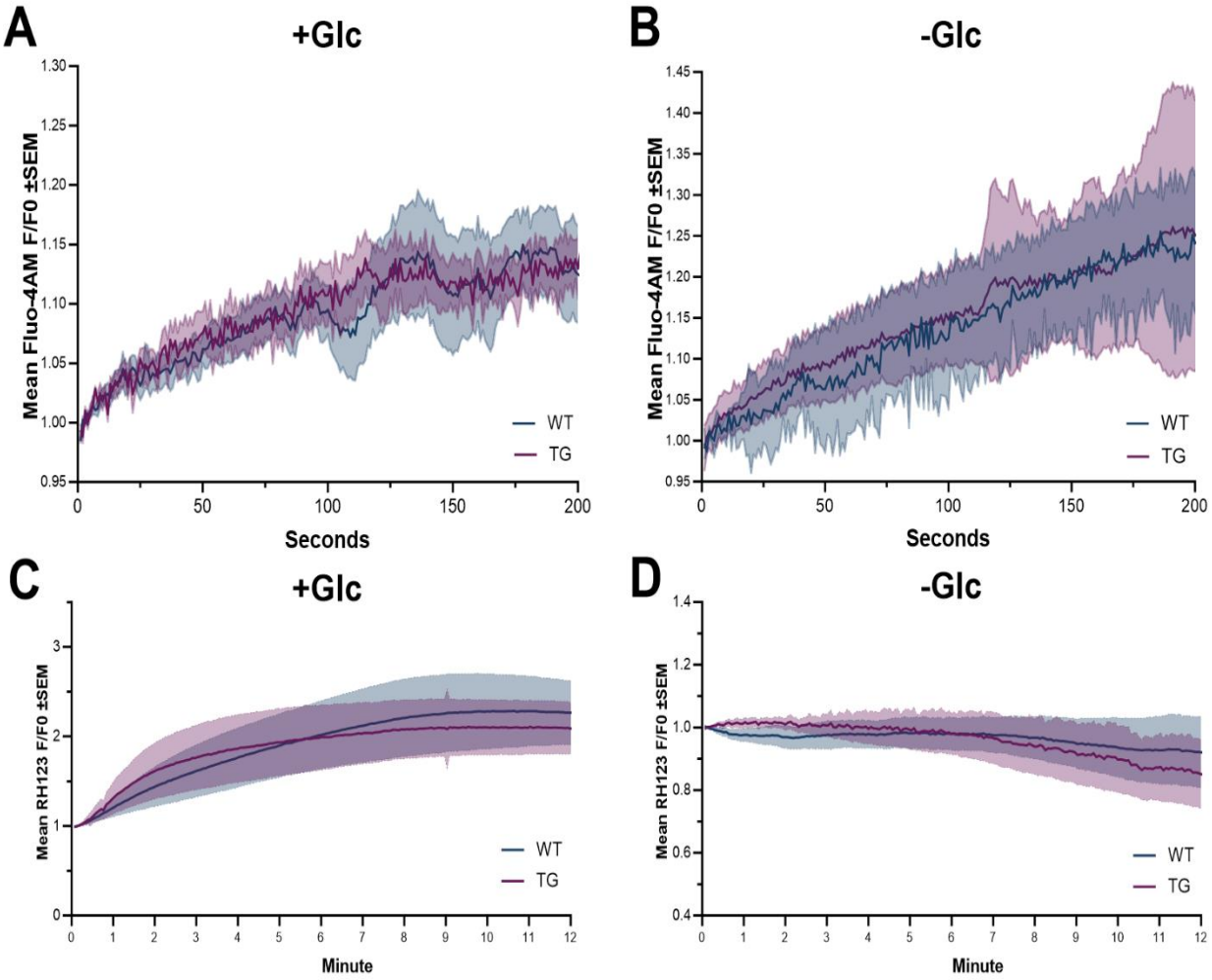

Appendix Figure 1. Animal genotype did not influence changes in metabolic fluorescent measurements. There were no significant differences between changes in Ca2+ signalling between WT and TG animals in the presence **-A** or absence **-B** of glucose. There were no significant differences between changes in mitochondrial activity between WT and TG animals in the presence **-A** or absence **-B** of glucose. CSD; cortical spreading depression, Glc; glucose, SEM; standard error. TG; transgenic animal, WT; wild type animal.

Appendix Table 2. Metabolites compared between +glc and -glc slices from wild type and transgenic animals following CSD.

CSD; cortical spreading depression, Glc; glucose, SD; standard deviation. TG; transgenic animal, WT; wild type animal. Significance determined by unpaired t test, * = *P* <0.05.

Metabolite	**Concentration Mean (SD)**		***P***	**Concentration Mean (SD)**		***P***
	+Glc			**-Glc**		
	WT ***N* = 4**	**TG** ***N* = 9**		**WT** ***N* = 2**	**TG** ***N* = 11**	
Alanine	22.05 (6.06)	17.97 (3.23)	0.527	6.02 (2.38)	6.98 (1.03)	0.723
Aspartate	227.93 (65.83)	195.38 (23.11)	0.562	370.08 (62.32)	269.94 (30.79)	0.223
Citrate	2.50 (0.48)	7.25 (1.05)	0.014 *	3.43 (1.56)	6.45 (1.22)	0.337
Fumarate	4.97 (1.08)	5.70 (0.54)	0.508	5.84 (1.35)	4.88 (0.46)	0.446
Glutamate	591.96 (162.65)	476.06 (64.99)	0.434	224.64 (33.78)	211.76 (25.64)	0.843
Glycine	56.13 (14.81)	43.07 (7.70)	0.403	32.23 (6.57)	33.00 (2.70)	0.9123
Isoleucine	1.29 (0.26)	2.04 (0.13)	0.378	0.79 (0.19)	0.84 (0.06)	0.721
Lactate	551.08 (142.68)	415.42 (63.63)	0.328	77.08 (17.53)	102.21 (21.79)	0.646
Leucine	1.56 (0.40)	1.32 (0.31)	0.661	0.86 (0.03)	0.93 (0.10)	0.773
Malate	10.64 (2.31)	12.45 (1.23)	0.464	9.90 (1.92)	8.91 (0.71)	0.603
Pyruvate	3.75 (0.45)	4.09 (0.32)	0.562	2.68 (0.02)	4.02 (0.43)	0.224
Succinate	19.54 (4.67)	14.68 (1.90)	0.265	42.91 (11.43)	38.24 (4.36)	0.686

CHAPTER 8 REFERENCES

1. Society HCCotIH. The International Classification of Headache Disorders, 3rd edition. *Cephalalgia* 2018;38(1):1-211. doi: 10.1177/0333102417738202 [published Online First: 2018/01/26]
2. Stovner LJ, Hagen K, Linde M, et al. The global prevalence of headache: an update, with analysis of the influences of methodological factors on prevalence estimates. *J Headache Pain* 2022;23(1):34. doi: 10.1186/s10194-022-01402-2
3. World Health O. Atlas of headache disorders and resources in the world 2011. Geneva: World Health Organization, 2011.
4. Collaborators GDaIIaP. Global, regional, and national incidence, prevalence, and years lived with disability for 354 diseases and injuries for 195 countries and territories, 1990-2017: a systematic analysis for the Global Burden of Disease Study 2017. *The Lancet* 2018;392(10159):1789-858. doi: 10.1016/s0140-6736(18)32279-7 [published Online First: 2018/11/30]
5. Stovner LJ, Nichols E, Steiner TJ, et al. Global, regional, and national burden of migraine and tension-type headache, 1990-2016: a systematic analysis for the Global Burden of Disease Study 2016. *Lancet Neurol* 2018;17(11):954-76. doi: 10.1016/S1474-4422(18)30322-3
6. Collaborators GBDN. Global, regional, and national burden of neurological disorders, 1990-2016: a systematic analysis for the Global Burden of Disease Study 2016. *Lancet Neurol* 2019;18(5):459-80. doi: 10.1016/S1474-4422(18)30499-X [published Online First: 20190314]
7. Steiner TJ, Stovner LJ, Jensen R, et al. Migraine remains second among the world's causes of disability, and first among young women: findings from GBD2019. *J Headache Pain* 2020;21(1):137. doi: 10.1186/s10194-020-01208-0
8. WorkFoundation. Migraine's impact on employment in Europe. What can be done to improve work outcomes for people with migraine? https://www.lancaster.ac.uk/media/lancaster-university/content-assets/documents/lums/work-foundation/Migraines-impact-on-employment-in-Europe-FINAL-pub-vA-accessible.pdf: Lancaster University

2019:54.
9. Hu XH, Markson LE, Lipton RB, et al. Burden of Migraine in the United States: Disability and Economic Costs. *Archives of Internal Medicine* 1999;159(8):813-18. doi: 10.1001/archinte.159.8.813
10. Lipton RB, Hamelsky SW, Kolodner KB, et al. Migraine, quality of life, and depression. *Neurology* 2000;55(5):629. doi: 10.1212/WNL.55.5.629
11. Hamelsky SW, Lipton RB. Psychiatric comorbidity of migraine. *Headache* 2006;46(9):1327-33. doi: 10.1111/j.1526-4610.2006.00576.x [published Online First: 2006/10/17]
12. Steiner TJ, Stovner LJ, Birbeck GL. Migraine: the seventh disabler. *J Headache Pain* 2013;14(1):1-1. doi: 10.1186/1129-2377-14-1
13. Schwedt TJ, Shapiro RE. Funding of research on headache disorders by the National Institutes of Health. *Headache* 2009;49(2):162-9. doi: 10.1111/j.1526-4610.2008.01323.x [published Online First: 2009/02/19]
14. Collaborators GH. Global, regional, and national burden of migraine and tension-type headache, 1990-2016: a systematic analysis for the Global Burden of

Disease Study 2016. *Lancet Neurol* 2018;17(11):954-76. doi: 10.1016/s1474-4422(18)30322-3
15. Charles A, Brennan KC. The neurobiology of migraine. *Handb Clin Neurol* 2010;97:99-108. doi: 10.1016/S0072-9752(10)97007-3
16. Ruthirago D, Julayanont P, Kim J. Chapter 7.2 - Translational Correlation: Migraine. In: Conn PM, ed. Conn's Translational Neuroscience. San Diego: Academic Press 2017:159-65.
17. Noseda R, Jakubowski M, Kainz V, et al. Cortical projections of functionally identified thalamic trigeminovascular neurons: implications for migraine headache and its associated symptoms. *J Neurosci* 2011;31(40):14204-17. doi: 10.1523/jneurosci.3285-11.2011
18. Penfield W, Mcnaughton F. Dural headache and innervation of the dura mater. *Archives of Neurology & Psychiatry* 1940;44(1):43-75. doi: 10.1001/archneurpsyc.1940.02280070051003
19. Dodick DW. A phase-by-phase review of migraine pathophysiology. *Headache* 2018;58:4-16.
20. Strassman AM, Raymond SA, Burstein R. Sensitization of meningeal sensory neurons and the origin of headaches. *Nature* 1996;384(6609):560-4. doi: 10.1038/384560a0 [published Online First: 1996/12/12]
21. Burstein R, Noseda R, Borsook D. Migraine: multiple processes, complex pathophysiology. *J Neurosci* 2015;35(17):6619-29.
22. Burstein R, Yamamura H, Malick A, et al. Chemical stimulation of the intracranial dura induces enhanced responses to facial stimulation in brain stem trigeminal neurons. *J Neurophysiol* 1998;79(2):964-82. doi: 10.1152/jn.1998.79.2.964 [published Online First: 1998/04/18]
23. Moulton EA, Burstein R, Tully S, et al. Interictal dysfunction of a brainstem descending modulatory center in migraine patients. *PLoS One* 2008;3(11):e3799-e99. doi: 10.1371/journal.pone.0003799 [published Online First: 2008/11/24]
24. Benemei S, De Cesaris F, Fusi C, et al. TRPA1 and other TRP channels in migraine. *J Headache Pain* 2013;14(1):71. doi: 10.1186/1129-2377-14-71
25. Meng J, Ovsepian SV, Wang J, et al. Activation of TRPV1 mediates calcitonin gene-related peptide release, which excites trigeminal sensory neurons and is attenuated by a retargeted botulinum toxin with anti-nociceptive potential. *J Neurosci* 2009;29(15):4981-92. doi: 10.1523/jneurosci.5490-08.2009 [published Online First: 2009/04/17]
26. Deen M, Correnti E, Kamm K, et al. Blocking CGRP in migraine patients – a review of pros and cons. *J Headache Pain* 2017;18(1):96. doi: 10.1186/s10194-017-0807-1
27. Walker CS, Conner AC, Poyner DR, et al. Regulation of signal transduction by calcitonin gene-related peptide receptors. *Trends in pharmacological sciences* 2010;31(10):476-83.
28. Hay DL, Poyner DR, Smith DM. Desensitisation of adrenomedullin and CGRP receptors. *Regulatory Peptides* 2003;112(1):139-45. doi: https://doi.org/10.1016/S0167-0115(03)00032-6
29. Drissi H, Lasmoles F, Le Mellay V, et al. Activation of phospholipase C-β1 via Gαq/11during calcium mobilization by calcitonin gene-related peptide. *Journal of Biological Chemistry* 1998;273(32):20168-74.

30. Brain SD, Grant AD. Vascular Actions of Calcitonin Gene-Related Peptide and Adrenomedullin. *Physiological Reviews* 2004;84(3):903-34. doi: 10.1152/physrev.00037.2003
31. Wallrapp A, Burkett PR, Riesenfeld SJ, et al. Calcitonin gene-related peptide negatively regulates alarmin-driven type 2 innate lymphoid cell responses. *Immunity* 2019;51(4):709-23. e6.
32. Mulderry P, Ghatki M, Spokks R, et al. Differential expression of α-CGRP and β-CGRP by primary sensory neurons and enteric autonomic neurons of the rat. *Neuroscience* 1988;25(1):195-205.
33. Iyengar S, Ossipov MH, Johnson KW. The role of calcitonin gene-related peptide in peripheral and central pain mechanisms including migraine. *Pain* 2017;158(4):543-59. doi: 10.1097/j.pain.0000000000000831 [published Online First: 2017/03/17]
34. Goadsby PJ, Edvinsson L, Ekman R. Vasoactive peptide release in the extracerebral circulation of humans during migraine headache. *Ann Neurol* 1990;28(2):183-7. doi: 10.1002/ana.410280213 [published Online First: 1990/08/01]
35. Lassen LH, Haderslev PA, Jacobsen VB, et al. CGRP may play a causative role in migraine. *Cephalalgia* 2002;22(1):54-61. doi: 10.1046/j.1468-2982.2002.00310.x [published Online First: 2002/05/08]
36. Aurora SK, Wilkinson F. The brain is hyperexcitable in migraine. *Cephalalgia* 2007;27(12):1442-53. doi: 10.1111/j.1468-2982.2007.01502.x
37. Lauritzen M. Cerebral blood flow in migraine and cortical spreading depression. *Acta Neurol Scand Suppl* 1987;113:1-40.
38. Goadsby PJ, Holland PR, Martins-Oliveira M, et al. Pathophysiology of Migraine: A Disorder of Sensory Processing. *Physiol Rev* 2017;97(2):553-622. doi: 10.1152/physrev.00034.2015 [published Online First: 2017/02/10]
39. Fusco MD, Marconi R, Silvestri L, et al. Haploinsufficiency of ATP1A2 encoding the Na+/K+ pump α2 subunit associated with familial hemiplegic migraine type 2. *Nat Genet* 2003;33(2):192-96.
40. Ophoff RA, Terwindt GM, Vergouwe MN, et al. Familial hemiplegic migraine and episodic ataxia type-2 are caused by mutations in the Ca2+ channel gene CACNL1A4. *Cell* 1996;87(3):543-52.
41. Dichgans M, Freilinger T, Eckstein G, et al. Mutation in the neuronal voltage-gated sodium channel SCN1A in familial hemiplegic migraine. *The Lancet* 2005;366(9483):371-77.
42. Leo L, Gherardini L, Barone V, et al. Increased Susceptibility to Cortical Spreading Depression in the Mouse Model of Familial Hemiplegic Migraine Type 2. *PLOS Genetics* 2011;7(6):e1002129. doi: 10.1371/journal.pgen.1002129
43. Hadjikhani N, Sanchez Del Rio M, Wu O, et al. Mechanisms of migraine aura revealed by functional MRI in human visual cortex. *Proc Natl Acad Sci* 2001;98(8):4687-92. doi: 10.1073/pnas.071582498 [published Online First: 04/03]
44. Tozzi A, de Iure A, Di Filippo M, et al. Critical role of calcitonin gene-related peptide receptors in cortical spreading depression. *Proc Natl Acad Sci* 2012;109(46):18985-90.

45. Wang Y, Tye AE, Zhao J, et al. Induction of calcitonin gene-related peptide expression in rats by cortical spreading depression. *Cephalalgia* 2019;39(3):333-41.
46. Kraig RP, Nicholson C. Extracellular ionic variations during spreading depression. *Neuroscience* 1978;3(11):1045-59. doi: 10.1016/0306-4522(78)90122-7 [published Online First: 1978/01/01]
47. Chang JC, Shook LL, Biag J, et al. Biphasic direct current shift, haemoglobin desaturation and neurovascular uncoupling in cortical spreading depression. *Brain* 2010;133(Pt 4):996-1012. doi: 10.1093/brain/awp338 [published Online First: 2010/03/30]
48. Pietrobon D, Moskowitz MA. Chaos and commotion in the wake of cortical spreading depression and spreading depolarizations. *Nat Rev Neurosci* 2014;15(6):379-93. doi: 10.1038/nrn3770
49. Bowyer SM, Aurora KS, Moran JE, et al. Magnetoencephalographic fields from patients with spontaneous and induced migraine aura. *Ann Neurol* 2001;50(5):582-7. doi: 10.1002/ana.1293 [published Online First: 2001/11/15]
50. Chen SP, Ayata C. Spreading Depression in Primary and Secondary Headache Disorders. *Curr Pain Headache Rep* 2016;20(7):44. doi: 10.1007/s11916-016-0574-8 [published Online First: 2016/05/25]
51. Lauritzen M, Dreier JP, Fabricius M, et al. Clinical relevance of cortical spreading depression in neurological disorders: migraine, malignant stroke, subarachnoid and intracranial hemorrhage, and traumatic brain injury. *J Cereb Blood Flow Metab* 2011;31(1):17-35. doi: 10.1038/jcbfm.2010.191 [published Online First: 2010/11/04]
52. Tozzi A, de Iure A, Di Filippo M, et al. Critical role of calcitonin gene-related peptide receptors in cortical spreading depression. *Proc Natl Acad Sci* 2012;109(46):18985-90. doi: 10.1073/pnas.1215435109 [published Online First: 2012/10/29]
53. Filiz A, Tepe N, Eftekhari S, et al. CGRP receptor antagonist MK-8825 attenuates cortical spreading depression induced pain behavior. *Cephalalgia* 2017;39(3):354-65. doi: 10.1177/0333102417735845
54. Zhang X, Levy D, Noseda R, et al. Activation of meningeal nociceptors by cortical spreading depression: implications for migraine with aura. *J Neurosci* 2010;30(26):8807-14. doi: 10.1523/JNEUROSCI.0511-10.2010 [published Online First: 2010/07/02]
55. Ashina H, Iljazi A, Amin FM, et al. Interrelations between migraine-like headache and persistent post-traumatic headache attributed to mild traumatic brain injury: a prospective diary study. *J Headache Pain* 2020;21(1):134. doi: 10.1186/s10194-020-01202-6 [published Online First: 2020/11/21]
56. Mollan SP, Hoffmann J, Sinclair AJ. Advances in the understanding of headache in idiopathic intracranial hypertension. *Curr Opin Neurol* 2019;32(1):92-98. doi: 10.1097/wco.0000000000000651 [published Online First: 2018/12/15]
57. Mollan SP, Wakerley BR, Alimajstorovic Z, et al. Intracranial pressure directly predicts headache morbidity in idiopathic intracranial hypertension. *J Headache Pain* 2021;22(1):118. doi: 10.1186/s10194-021-01321-8
58. Yiangou A, Mitchell JL, Fisher C, et al. Erenumab for headaches in idiopathic intracranial hypertension: A prospective open-label evaluation. *Headache* 2021;61(1):157-69. doi: 10.1111/head.14026

59. Ashina H, Iljazi A, Al-Khazali HM, et al. Hypersensitivity to Calcitonin Gene-Related Peptide in Post-Traumatic Headache. *Ann Neurol* 2020;88(6):1220-28. doi: 10.1002/ana.25915 [published Online First: 2020/09/23]
60. Ashina H, Iljazi A, Al-Khazali HM, et al. Efficacy, tolerability, and safety of erenumab for the preventive treatment of persistent post-traumatic headache attributed to mild traumatic brain injury: an open-label study. *J Headache Pain* 2020;21(1):62. doi: 10.1186/s10194-020-01136-z [published Online First: 2020/06/05]
61. Yiangou A, Mitchell JL, Vijay V, et al. Calcitonin gene related peptide monoclonal antibody treats headache in patients with active idiopathic intracranial hypertension. *J Headache Pain* 2020;21(1):116. doi: 10.1186/s10194-020-01182-7
62. Ashina H, Moskowitz MA. Shared biological foundations of post-traumatic headache and migraine. *Headache* 2021;n/a(n/a) doi: 10.1111/head.14084
63. Rea BJ, Wattiez AS, Waite JS, et al. Peripherally administered calcitonin gene-related peptide induces spontaneous pain in mice: implications for migraine. *Pain* 2018;159(11):2306-17. doi: 10.1097/j.pain.0000000000001337 [published Online First: 2018/07/12]
64. Limmroth V, Katsarava Z, Liedert B, et al. An in vivo rat model to study calcitonin gene related peptide release following activation of the trigeminal vascular system. *Pain* 2001;92(1-2):101-6. doi: 10.1016/s0304-3959(00)00475-9 [published Online First: 2001/04/27]
65. Iversen HK, Olesen J, Tfelt-Hansen P. Intravenous nitroglycerin as an experimental model of vascular headache. Basic characteristics. *Pain* 1989;38(1):17-24. doi: 10.1016/0304-3959(89)90067-5
66. Paige C, Plasencia-Fernandez I, Kume M, et al. A female-specific role for calcitonin gene-related peptide (CGRP) in rodent pain models. *J Neurosci* 2022;42(10):1930-44.
67. Strassman AM, Mineta Y, Vos BP. Distribution of fos-like immunoreactivity in the medullary and upper cervical dorsal horn produced by stimulation of dural blood vessels in the rat. *J Neurosci* 1994;14(6):3725-35. doi: 10.1523/jneurosci.14-06-03725.1994
68. Sugimoto T, He YF, Xiao C, et al. c-fos induction in the subnucleus oralis following trigeminal nerve stimulation. *Brain Research* 1998;783(1):158-62. doi: 10.1016/s0006-8993(97)01176-1
69. Vuralli D, Wattiez AS, Russo AF, et al. Behavioral and cognitive animal models in headache research. *J Headache Pain* 2019;20(1):11. doi: 10.1186/s10194-019-0963-6 [published Online First: 20190131]
70. Farkas S, Bölcskei K, Markovics A, et al. Utility of different outcome measures for the nitroglycerin model of migraine in mice. *J Pharmacol Toxicol Methods* 2016;77:33-44. doi: 10.1016/j.vascn.2015.09.006
71. Pradhan AA, Smith ML, McGuire B, et al. Characterization of a novel model of chronic migraine. *Pain* 2014;155(2):269-74. doi: 10.1016/j.pain.2013.10.004 [published Online First: 2013/10/15]
72. Burstein R, Yarnitsky D, Goor-Aryeh I, et al. An association between migraine and cutaneous allodynia. *Ann Neurol* 2000;47(5):614-24. [published Online First: 2000/05/11]
73. Kobayashi S, Harris VA, Welsh FA. Spreading depression induces tolerance of cortical neurons to ischemia in rat brain. *J Cereb Blood Flow Metab*

1995;15(5):721-7. doi: 10.1038/jcbfm.1995.92 [published Online First: 1995/09/01]
74. Harriott AM, Takizawa T, Chung DY, et al. Spreading depression as a preclinical model of migraine. *J Headache Pain* 2019;20(1):45. doi: 10.1186/s10194-019-1001-4 [published Online First: 2019/05/03]
75. Filiz A, Tepe N, Eftekhari S, et al. CGRP receptor antagonist MK-8825 attenuates cortical spreading depression induced pain behavior. *Cephalalgia : an international journal of headache* 2017:333102417735845. doi: 10.1177/0333102417735845 [published Online First: 2017/10/04]
76. Silberstein S. Tonabersat, A Novel Gap-Junction Modulator for the Prevention of Migraine. *Cephalalgia* 2009;29(2_suppl):28-35. doi: 10.1111/j.1468-2982.2009.01973.x
77. Kudo C, Nozari A, Moskowitz MA, et al. The impact of anesthetics and hyperoxia on cortical spreading depression. *Experimental Neurology* 2008;212(1):201-6. doi: 10.1016/j.expneurol.2008.03.026 [published Online First: 2008/05/27]
78. Yamamoto C, McIlwain H. Electrical activities in thin sections from the mammalian brain maintained in chemically-defined media in vitro. *J Neurochem* 1966;13(12):1333-43. doi: 10.1111/j.1471-4159.1966.tb04296.x [published Online First: 1966/12/01]
79. Li CL, McIlwain H. Maintenance of resting membrane potentials in slices of mammalian cerebral cortex and other tissues in vitro. *J Physiol* 1957;139(2):178-90. doi: 10.1113/jphysiol.1957.sp005885
80. Tang YT, Mendez JM, Theriot JJ, et al. Minimum conditions for the induction of cortical spreading depression in brain slices. *J Neurophysiol* 2014;112(10):2572-9. doi: 10.1152/jn.00205.2014 [published Online First: 2014/08/15]
81. Koshinaga M, Katayama Y, Fukushima M, et al. Rapid and widespread microglial activation induced by traumatic brain injury in rat brain slices. *J Neurotrauma* 2000;17(3):185-92. doi: 10.1089/neu.2000.17.185 [published Online First: 2000/04/11]
82. Church AJ, Andrew RD. Spreading depression expands traumatic injury in neocortical brain slices. *J Neurotrauma* 2005;22(2):277-90. doi: 10.1089/neu.2005.22.277 [published Online First: 2005/02/18]
83. Jarvis CR, Anderson TR, Andrew RD. Anoxic Depolarization Mediates Acute Damage Independent of Glutamate in Neocortical Brain Slices. *Cerebral Cortex* 2001;11(3):249-59. doi: 10.1093/cercor/11.3.249
84. Lipski J, Park TIH, Li D, et al. Involvement of TRP-like channels in the acute ischemic response of hippocampal CA1 neurons in brain slices. *Brain Research* 2006;1077(1):187-99. doi: 10.1016/j.brainres.2006.01.016
85. Grech O, Mollan SP, Wakerley BR, et al. The Role of Metabolism in Migraine Pathophysiology and Susceptibility. *Life* 2021;11(5) doi: 10.3390/life11050415
86. Reyngoudt H, Paemeleire K, Descamps B, et al. 31P-MRS demonstrates a reduction in high-energy phosphates in the occipital lobe of migraine without aura patients. *Cephalalgia* 2011;31(12):1243-53. doi: 10.1177/0333102410394675 [published Online First: 2011/02/04]
87. Boska MD, Welch KMA, Barker PB, et al. Contrasts in cortical magnesium, phospholipid and energy metabolism between migraine syndromes. *Neurology* 2002;58(8):1227. doi: 10.1212/WNL.58.8.1227

88. Uncini A, Lodi R, Di Muzio A, et al. Abnormal brain and muscle energy metabolism shown by 31P-MRS in familial hemiplegic migraine. *J Neurol Sci* 1995;129(2):214-22. doi: 10.1016/0022-510x(94)00283-t [published Online First: 1995/04/01]
89. Sándor PS, Di Clemente L, Coppola G, et al. Efficacy of coenzyme Q10 in migraine prophylaxis: A randomized controlled trial. *Neurology* 2005;64(4):713. doi: 10.1212/01.WNL.0000151975.03598.ED
90. Rozen TD, Oshinsky ML, Gebeline CA, et al. Open Label Trial of Coenzyme Q10 as A Migraine Preventive. *Cephalalgia* 2002;22(2):137-41. doi: 10.1046/j.1468-2982.2002.00335.x
91. Boehnke C, Reuter U, Flach U, et al. High-dose riboflavin treatment is efficacious in migraine prophylaxis: an open study in a tertiary care centre. *Eur J Neurol* 2004;11(7):475-7. doi: 10.1111/j.1468-1331.2004.00813.x [published Online First: 2004/07/20]
92. Schoenen J, Jacquy J, Lenaerts M. Effectiveness of high-dose riboflavin in migraine prophylaxis. A randomized controlled trial. *Neurology* 1998;50(2):466-70. doi: 10.1212/wnl.50.2.466 [published Online First: 1998/03/04]
93. Bigal ME, Bordini CA, Tepper SJ, et al. Intravenous magnesium sulphate in the acute treatment of migraine without aura and migraine with aura. A randomized, double-blind, placebo-controlled study. *Cephalalgia* 2002;22(5):345-53. doi: 10.1046/j.1468-2982.2002.00364.x [published Online First: 2002/07/12]
94. Corbo J, Esses D, Bijur PE, et al. Randomized clinical trial of intravenous magnesium sulfate as an adjunctive medication for emergency department treatment of migraine headache. *Ann Emerg Med* 2001;38(6):621-27. doi: 10.1067/mem.2001.119424 [published Online First: 2001/11/24]
95. Díaz-García CM, Yellen G. Neurons rely on glucose rather than astrocytic lactate during stimulation. *J Neurosci Res* 2019;97(8):883-89. doi: 10.1002/jnr.24374 [published Online First: 2018/12/24]
96. Pellerin L, Magistretti PJ. Neuroenergetics: Calling Upon Astrocytes to Satisfy Hungry Neurons. *The Neuroscientist* 2004;10(1):53-62. doi: 10.1177/1073858403260159
97. Mosek A, Korczyn AD. Yom Kippur headache. *Neurology* 1995;45(11):1953-5. doi: 10.1212/wnl.45.11.1953
98. Giffin NJ, Ruggiero L, Lipton RB, et al. Premonitory symptoms in migraine. *Neurology* 2003;60(6):935. doi: 10.1212/01.WNL.0000052998.58526.A9
99. Martin PR, Seneviratne HM. Effects of food deprivation and a stressor on head pain. *Health Psychology* 1997;16(4):310.
100. Rainero I, Limone P, Ferrero M, et al. Insulin Sensitivity is Impaired in Patients with Migraine. *Cephalalgia* 2005;25(8):593-97. doi: 10.1111/j.1468-2982.2005.00928.x
101. Cavestro C, Rosatello A, Micca G, et al. Insulin Metabolism is Altered in Migraineurs: A New Pathogenic Mechanism for Migraine? *Headache* 2007;47(10):1436-42. doi: 10.1111/j.1526-4610.2007.00719.x
102. Kim JH, Kim S, Suh SI, et al. Interictal metabolic changes in episodic migraine: a voxel-based FDG-PET study. *Cephalalgia* 2010;30(1):53-61. doi: 10.1111/j.1468-2982.2009.01890.x [published Online First: 2009/06/06]

103. Magis D, D'Ostilio K, Thibaut A, et al. Cerebral metabolism before and after external trigeminal nerve stimulation in episodic migraine. *Cephalalgia* 2017;37(9):881-91. doi: 10.1177/0333102416656118 [published Online First: 2016/06/28]
104. Torres-Ferrus M, Pareto D, Gallardo VJ, et al. Cortical metabolic and structural differences in patients with chronic migraine. An exploratory 18FDG-PET and MRI study. *J Headache Pain* 2021;22(1):75. doi: 10.1186/s10194-021-01289-5
105. Hoffmann U, Sukhotinsky I, Eikermann-Haerter K, et al. Glucose modulation of spreading depression susceptibility. *J Cereb Blood Flow Metab* 2013;33(2):191-95. doi: 10.1038/jcbfm.2012.132 [published Online First: 2012/09/12]
106. Bures J, Buresova O. Activation of latent foci of spreading cortical depression in rats. *J Neurophysiol* 1960;23:225-36. doi: 10.1152/jn.1960.23.3.225 [published Online First: 1960/05/01]
107. Astrup J, Norberg K. Potassium activity in cerebral cortex in rats during progressive severe hypoglycemia. *Brain Research* 1976;103(2):418-23. doi: 10.1016/0006-8993(76)90817-9 [published Online First: 1976/02/20]
108. Grimaldi D, Tonon C, Cevoli S, et al. Clinical and neuroimaging evidence of interictal cerebellar dysfunction in FHM2. *Cephalalgia* 2010;30(5):552-9. doi: 10.1111/j.1468-2982.2009.01979.x [published Online First: 2009/08/14]
109. Sándor PS, Dydak U, Schoenen J, et al. MR-spectroscopic imaging during visual stimulation in subgroups of migraine with aura. *Cephalalgia* 2005;25(7):507-18. doi: 10.1111/j.1468-2982.2005.00900.x [published Online First: 2005/06/16]
110. Watanabe H, Kuwabara T, Ohkubo M, et al. Elevation of cerebral lactate detected by localized 1H-magnetic resonance spectroscopy in migraine during the interictal period. *Neurology* 1996;47(4):1093-5. doi: 10.1212/wnl.47.4.1093 [published Online First: 1996/10/01]
111. Proia P, Amato A, Contrò V, et al. Relevance of lactate level detection in migrane and fibromyalgia. *Eur J Transl Myol* 2019;29(2):8202-02. doi: 10.4081/ejtm.2019.8202
112. Okada H, Araga S, Takeshima T, et al. Plasma Lactic Acid and Pyruvic Acid Levels in Migraine and Tension-Type Headache. *Headache* 1998;38(1):39-42. doi: 10.1046/j.1526-4610.1998.3801039.x
113. Aczél T, Körtési T, Kun J, et al. Identification of disease- and headache-specific mediators and pathways in migraine using blood transcriptomic and metabolomic analysis. *J Headache Pain* 2021;22(1):117. doi: 10.1186/s10194-021-01285-9
114. Scheller D, Kolb J, Tegtmeier F. Lactate and pH change in close correlation in the extracellular space of the rat brain during cortical spreading depression. *Neurosci Lett* 1992;135(1):83-6. doi: 10.1016/0304-3940(92)90141-s [published Online First: 1992/01/20]
115. Takano T, Tian GF, Peng W, et al. Cortical spreading depression causes and coincides with tissue hypoxia. *Nat Neurosci* 2007;10(6):754-62. doi: 10.1038/nn1902 [published Online First: 2007/05/01]
116. Feuerstein D, Backes H, Gramer M, et al. Regulation of cerebral metabolism during cortical spreading depression. *J Cereb Blood Flow Metab*

2016;36(11):1965-77. doi: 10.1177/0271678x15612779 [published Online First: 2016/11/03]
117. Barbiroli B, Montagna P, Cortelli P, et al. Abnormal brain and muscle energy metabolism shown by 31P-magnetic resonance spectroscopy in patients affected by migraine with aura. *Neurology* 1992;42(6):1209. doi: 10.1212/WNL.42.6.1209
118. Sacquegna T, Lodi R, De Carolis P, et al. Brain energy metabolism studied by 31P-MR spectroscopy in a case of migraine with prolonged aura. *Acta Neurol Scand* 1992;86(4):376-80. doi: 10.1111/j.1600-0404.1992.tb05104.x [published Online First: 1992/10/01]
119. Schulz UG, Blamire AM, Corkill RG, et al. Association between cortical metabolite levels and clinical manifestations of migrainous aura: an MR-spectroscopy study. *Brain* 2007;130(Pt 12):3102-10. doi: 10.1093/brain/awm165 [published Online First: 2007/10/25]
120. Montagna P, Cortelli P, Monari L, et al. 31P-magnetic resonance spectroscopy in migraine without aura. *Neurology* 1994;44(4):666-9. doi: 10.1212/wnl.44.4.666 [published Online First: 1994/04/01]
121. Barbiroli B, Montagna P, Martinelli P, et al. Defective brain energy metabolism shown by in vivo 31P MR spectroscopy in 28 patients with mitochondrial cytopathies. *J Cereb Blood Flow Metab* 1993;13(3):469-74. doi: 10.1038/jcbfm.1993.61 [published Online First: 1993/05/01]
122. Sassani M, Alix JJ, McDermott CJ, et al. Magnetic resonance spectroscopy reveals mitochondrial dysfunction in amyotrophic lateral sclerosis. *Brain* 2020;143(12):3603-18. doi: 10.1093/brain/awaa340
123. Galeffi F, Somjen GG, Foster KA, et al. Simultaneous monitoring of tissue PO2 and NADH fluorescence during synaptic stimulation and spreading depression reveals a transient dissociation between oxygen utilization and mitochondrial redox state in rat hippocampal slices. *J Cereb Blood Flow Metab* 2011;31(2):626-39. doi: 10.1038/jcbfm.2010.136 [published Online First: 2010/08/26]
124. Carlson AP, Carter RE, Shuttleworth CW. Vascular, electrophysiological, and metabolic consequences of cortical spreading depression in a mouse model of simulated neurosurgical conditions. *Neurol Res* 2012;34(3):223-31. doi: 10.1179/1743132811Y.0000000077 [published Online First: 2012/03/01]
125. Li F, Qiu E, Dong Z, et al. Protection of flunarizine on cerebral mitochondria injury induced by cortical spreading depression under hypoxic conditions. *J Headache Pain* 2011;12(1):47-53. doi: 10.1007/s10194-011-0300-1 [published Online First: 2011/02/26]
126. Dong X, Guan X, Chen K, et al. Abnormal mitochondrial dynamics and impaired mitochondrial biogenesis in trigeminal ganglion neurons in a rat model of migraine. *Neurosci Lett* 2017;636:127-33. doi: 10.1016/j.neulet.2016.10.054 [published Online First: 2016/10/29]
127. Debray FG, Mitchell GA, Allard P, et al. Diagnostic accuracy of blood lactate-to-pyruvate molar ratio in the differential diagnosis of congenital lactic acidosis. *Clin Chem* 2007;53(5):916-21. doi: 10.1373/clinchem.2006.081166 [published Online First: 2007/03/27]
128. Gropman AL. Diagnosis and treatment of childhood mitochondrial diseases. *Curr Neurol Neurosci Rep* 2001;1(2):185-94. doi: 10.1007/s11910-001-0015-9 [published Online First: 2002/03/20]

129. Belli A, Sen J, Petzold A, et al. Metabolic failure precedes intracranial pressure rises in traumatic brain injury: a microdialysis study. *Acta Neurochir (Wien)* 2008;150(5):461-9; discussion 70. doi: 10.1007/s00701-008-1580-3 [published Online First: 2008/04/19]
130. Nagel A, Graetz D, Schink T, et al. Relevance of intracranial hypertension for cerebral metabolism in aneurysmal subarachnoid hemorrhage: Clinical article. *J Neurosurg* 2009;111(1):94-101. doi: 10.3171/2009.1.JNS08587
131. Raisis JE, Kindt GW, McGillicuddy JE, et al. Cerebrospinal fluid lactate and lactate/pyruvate ratios in hydrocephalus. *J Neurosurg* 1976;44(3):337-41. doi: 10.3171/jns.1976.44.3.0337 [published Online First: 1976/03/01]
132. Manczak M, Park BS, Jung Y, et al. Differential expression of oxidative phosphorylation genes in patients with Alzheimer's disease: implications for early mitochondrial dysfunction and oxidative damage. *Neuromolecular medicine* 2004;5:147-62.
133. Nunomura A, Castellani RJ, Zhu X, et al. Involvement of oxidative stress in Alzheimer disease. *Journal of neuropathology & experimental neurology* 2006;65(7):631-41.
134. Wada J, Nakatsuka A. Mitochondrial Dynamics and Mitochondrial Dysfunction in Diabetes. *Acta Med Okayama* 2016;70(3):151-8. doi: 10.18926/amo/54413 [published Online First: 2016/06/25]
135. Jenkins BG, Koroshetz WJ, Beal MF, et al. Evidence for impairment of energy metabolism in vivo in Huntington's disease using localized 1H NMR spectroscopy. *Neurology* 1993;43(12):2689-95. doi: 10.1212/wnl.43.12.2689 [published Online First: 1993/12/01]
136. Trushina E, McMurray C. Oxidative stress and mitochondrial dysfunction in neurodegenerative diseases. *Neuroscience* 2007;145(4):1233-48.
137. Tabrizi SJ, Cleeter MW, Xuereb J, et al. Biochemical abnormalities and excitotoxicity in Huntington's disease brain. *Ann Neurol* 1999;45(1):25-32. doi: 10.1002/1531-8249(199901)45:1<25::aid-art6>3.0.co;2-e [published Online First: 1999/01/23]
138. Asghar M, Hansen AE, Kapijimpanga T, et al. Dilation by CGRP of middle meningeal artery and reversal by sumatriptan in normal volunteers. *Neurology* 2010;75(17):1520-26.
139. Goadsby PJ, Edvinsson L. The trigeminovascular system and migraine: studies characterizing cerebrovascular and neuropeptide changes seen in humans and cats. *Ann Neurol* 1993;33(1):48-56. doi: 10.1002/ana.410330109 [published Online First: 1993/01/01]
140. Cumberbatch MJ, Hill RG, Hargreaves RJ. Rizatriptan has central antinociceptive effects against durally evoked responses. *Eur J Pharmacol* 1997;328(1):37-40. doi: 10.1016/S0014-2999(97)83024-5
141. Group TMOSaCCS. A randomized, double-blind comparison of sumatriptan and Cafergot in the acute treatment of migraine. . *Eur Neurol* 1991;31(5):314-22. doi: 10.1159/000116759
142. Ferrari MD, Roon KI, Lipton RB, et al. Oral triptans (serotonin 5-HT(1B/1D) agonists) in acute migraine treatment: a meta-analysis of 53 trials. *The Lancet* 2001;358(9294):1668-75. doi: 10.1016/s0140-6736(01)06711-3
143. Visser WH, Jaspers NM, de Vriend RH, et al. Risk factors for headache recurrence after sumatriptan: a study in 366 migraine patients. *Cephalalgia* 1996;16(4):264-9. doi: 10.1046/j.1468-2982.1996.1604264.x

144. Diener H-C. The Risks or Lack Thereof of Migraine Treatments in Vascular Disease. *Headache* 2020;60(3):649-53. doi: 10.1111/head.13749
145. Adelborg K, Szépligeti SK, Holland-Bill L, et al. Migraine and risk of cardiovascular diseases: Danish population based matched cohort study. *Bmj* 2018;360
146. Mahmoud AN, Mentias A, Elgendy AY, et al. Migraine and the risk of cardiovascular and cerebrovascular events: a meta-analysis of 16 cohort studies including 1 152 407 subjects. *BMJ Open* 2018;8(3):e020498. doi: 10.1136/bmjopen-2017-020498
147. Petersen KA, Birk S, Lassen LH, et al. The CGRP-antagonist, BIBN4096BS does not affect cerebral or systemic haemodynamics in healthy volunteers. *Cephalalgia* 2005;25(2):139-47. doi: 10.1111/j.1468-2982.2004.00830.x
148. Doods H, Hallermayer G, Wu D, et al. Pharmacological profile of BIBN4096BS, the first selective small molecule CGRP antagonist. *Br J Pharmacol* 2000;129(3):420-23.
149. Edvinsson L, Alm R, Shaw D, et al. Effect of the CGRP receptor antagonist BIBN4096BS in human cerebral, coronary and omental arteries and in SK-N-MC cells. *Eur J Pharmacol* 2002;434(1-2):49-53. doi: 10.1016/s0014-2999(01)01532-1
150. Olesen J, Diener H-C, Husstedt IW, et al. Calcitonin gene–related peptide receptor antagonist BIBN 4096 BS for the acute treatment of migraine. *N Engl J Med* 2004;350(11):1104-10.
151. Christensen SL, Petersen S, Kristensen DM, et al. Targeting CGRP via receptor antagonism and antibody neutralisation in two distinct rodent models of migraine-like pain. *Cephalalgia* 2019;39(14):1827-37. doi: 10.1177/0333102419861726
152. Greco R, Demartini C, Francavilla M, et al. Antagonism of CGRP Receptor: Central and Peripheral Mechanisms and Mediators in an Animal Model of Chronic Migraine. *Cells* 2022;11(19) doi: 10.3390/cells11193092 [published Online First: 2022/10/15]
153. Edvinsson L. CGRP receptor antagonists and antibodies against CGRP and its receptor in migraine treatment. *Br J Clin Pharmacol* 2015;80(2):193-99.
154. Goadsby PJ, Reuter U, Hallström Y, et al. A controlled trial of erenumab for episodic migraine. *N Engl J Med* 2017;377(22):2123-32.
155. Bigal ME, Edvinsson L, Rapoport AM, et al. Safety, tolerability, and efficacy of TEV-48125 for preventive treatment of chronic migraine: a multicentre, randomised, double-blind, placebo-controlled, phase 2b study. *Lancet Neurol* 2015;14(11):1091-100.
156. Kielbasa W, Helton DL. A new era for migraine: pharmacokinetic and pharmacodynamic insights into monoclonal antibodies with a focus on galcanezumab, an anti-CGRP antibody. *Cephalalgia* 2019;39(10):1284-97.
157. Friedman DI, Liu GT, Digre KB. Revised diagnostic criteria for the pseudotumor cerebri syndrome in adults and children. *Neurology* 2013;81(13):1159-65. doi: 10.1212/WNL.0b013e3182a55f17 [published Online First: 2013/08/24]
158. Wall M. Idiopathic intracranial hypertension. *Neurol Clin* 2010;28(3):593-617. doi: 10.1016/j.ncl.2010.03.003 [published Online First: 2010/07/20]
159. Radhakrishnan K, Thacker AK, Bohlaga NH, et al. Epidemiology of idiopathic intracranial hypertension: A prospective and case-control study. *J Neurol Sci*

1993;116(1):18-28. doi: 10.1016/0022-510X(93)90084-C [published Online First: 1993/05/01]
160. McCluskey G, Doherty-Allan R, McCarron P, et al. Meta-analysis and systematic review of population-based epidemiological studies in idiopathic intracranial hypertension. *Eur J Neurol* 2018;25(10):1218-27. doi: 10.1111/ene.13739 [published Online First: 2018/06/29]
161. Kilgore KP, Lee MS, Leavitt JA, et al. Re-evaluating the Incidence of Idiopathic Intracranial Hypertension in an Era of Increasing Obesity. *Ophthalmology* 2017;124(5):697-700. doi: 10.1016/j.ophtha.2017.01.006 [published Online First: 2017/02/12]
162. Mollan SP, Aguiar M, Evison F, et al. The expanding burden of idiopathic intracranial hypertension. *Eye* 2018;33(3):478-85. doi: 10.1038/s41433-018-0238-5 [published Online First: 2018/10/26]
163. Friesner D, Rosenman R, Lobb BM, et al. Idiopathic intracranial hypertension in the USA: the role of obesity in establishing prevalence and healthcare costs. *Obesity Reviews* 2011;12(5):e372-e80. doi: 10.1111/j.1467-789X.2010.00799.x [published Online First: 2010/09/02]
164. Adderley NJ, Subramanian A, Nirantharakumar K, et al. Association Between Idiopathic Intracranial Hypertension and Risk of Cardiovascular Diseases in Women in the United Kingdom. *JAMA Neurol* 2019;76(9):1088-98. doi: 10.1001/jamaneurol.2019.1812 [published Online First: 2019/07/10]
165. Mollan SP, Ali F, Hassan-Smith G, et al. Evolving evidence in adult idiopathic intracranial hypertension: pathophysiology and management. *J Neurol Neurosurg Psychiatry* 2016;87(9):982-92. doi: 10.1136/jnnp-2015-311302 [published Online First: 2016/02/19]
166. O'Reilly MW, Westgate CS, Hornby C, et al. A unique androgen excess signature in idiopathic intracranial hypertension is linked to cerebrospinal fluid dynamics. *JCI Insight* 2019;4(6) doi: 10.1172/jci.insight.125348 [published Online First: 2019/02/13]
167. Grech O, Seneviratne SY, Alimajstorovic Z, et al. Nuclear Magnetic Resonance Spectroscopy Metabolomics in Idiopathic Intracranial Hypertension to Identify Markers of Disease and Headache. *Neurology* 2022;99(16):e1702-e14. doi: 10.1212/wnl.0000000000201007
168. Damkier HH, Brown PD, Praetorius J. Cerebrospinal fluid secretion by the choroid plexus. *Physiol Rev* 2013;93(4):1847-92.
169. Sinclair AJ, Ball AK, Burdon MA, et al. Exploring the pathogenesis of IIH: an inflammatory perspective. *J Neuroimmunol* 2008;201:212-20.
170. Malm J, Kristensen B, Markgren P, et al. CSF hydrodynamics in idiopathic intracranial hypertension: A long-term study. *Neurology* 1992;42(4):851-51.
171. Orefice G, Celentano L, Scaglione M, et al. Radioisotopic cisternography in benign intracranial hypertension of young obese women. A seven-case study and pathogenetic suggestions. *Acta neurologica* 1992;14(1):39-50.
172. Mollan SP, Davies B, Silver NC, et al. Idiopathic intracranial hypertension: consensus guidelines on management. *J Neurol Neurosurg Psychiatry* 2018;89(10):1088-100. doi: 10.1136/jnnp-2017-317440 [published Online First: 2018/06/14]
173. Chen J, Wall M. Epidemiology and risk factors for idiopathic intracranial hypertension. *Int Ophthalmol Clin* 2014;54(1):1-11. doi: 10.1097/IIO.0b013e3182aabf11

174. Thaller M, Homer V, Sassani M, et al. Longitudinal prospective cohort study evaluating prognosis in idiopathic intracranial hypertension patients with and without comorbid polycystic ovarian syndrome. *Eye* 2023 doi: 10.1038/s41433-023-02569-x
175. Avisar I, Gaton DD, Dania H, et al. The prevalence of polycystic ovary syndrome in women with idiopathic intracranial hypertension. *Scientifica* 2012;2012:708042. doi: 10.6064/2012/708042 [published Online First: 20120711]
176. Glueck CJ, Iyengar S, Goldenberg N, et al. Idiopathic intracranial hypertension: associations with coagulation disorders and polycystic-ovary syndrome. *J Lab Clin Med* 2003;142(1):35-45. doi: 10.1016/S0022-2143(03)00069-6 [published Online First: 2003/07/25]
177. Klein A, Stern N, Osher E, et al. Hyperandrogenism is Associated with Earlier Age of Onset of Idiopathic Intracranial Hypertension in Women. *Curr Eye Res* 2013;38(9):972-76. doi: 10.3109/02713683.2013.799214 [published Online First: 2013/05/30]
178. Hornby C, Mollan SP, Mitchell J, et al. What Do Transgender Patients Teach Us About Idiopathic Intracranial Hypertension? *Neuroophthalmology* 2017;41(6):326-29. doi: 10.1080/01658107.2017.1316744 [published Online First: 2017/12/15]
179. Park S, Cheng CP, Lim LT, et al. Secondary intracranial hypertension from testosterone therapy in a transgender patient. *Seminars in ophthalmology* 2014;29(3):156-8. doi: 10.3109/08820538.2013.788678 [published Online First: 2013/06/14]
180. Kapoor KG. Regarding secondary intracranial hypertension from testostereone therapy in a transgender patient. *Seminars in ophthalmology* 2015;30(4):241-2. doi: 10.3109/08820538.2013.847111 [published Online First: 2013/10/30]
181. O'Reilly MW, Westgate CS, Hornby C, et al. A unique androgen excess signature in idiopathic intracranial hypertension is linked to cerebrospinal fluid dynamics. *JCI insight* 2019 doi: 10.1172/jci.insight.125348 [published Online First: 2019/02/13]
182. Markey KA, Uldall M, Botfield H, et al. Idiopathic intracranial hypertension, hormones, and 11beta-hydroxysteroid dehydrogenases. *J Pain Res* 2016;9:223-32. doi: 10.2147/jpr.S80824 [published Online First: 2016/05/18]
183. Westgate CS, Botfield HF, Alimajstorovic Z, et al. Systemic and adipocyte transcriptional and metabolic dysregulation in idiopathic intracranial hypertension. *JCI Insight* 2021;6(10) doi: 10.1172/jci.insight.145346 [published Online First: 2021/04/14]
184. Mollan SP, Tahrani AA, Sinclair AJ. The Potentially Modifiable Risk Factor in Idiopathic Intracranial Hypertension. *Neurol Clin Pract* 2021;11(4):e504. doi: 10.1212/CPJ.0000000000001063
185. Hornby C, Botfield H, O'Reilly MW, et al. Evaluating the Fat Distribution in Idiopathic Intracranial Hypertension Using Dual-Energy X-ray Absorptiometry Scanning. *Neuroophthalmology* 2017;42(2):99-104. doi: 10.1080/01658107.2017.1334218 [published Online First: 2018/03/23]
186. Hornby C, Mollan SP, Botfield H, et al. Metabolic Concepts in Idiopathic Intracranial Hypertension and Their Potential for Therapeutic Intervention. *J Neuroophthalmol* 2018;38(4):522-30. doi: 10.1097/WNO.0000000000000684 [published Online First: 2018/07/10]

187. Alimajstorovic Z, Mollan SP, Grech O, et al. Dysregulation of Amino Acid, Lipid, and Acylpyruvate Metabolism in Idiopathic Intracranial Hypertension: A Non-targeted Case Control and Longitudinal Metabolomic Study. *J Proteome Res* 2023;22(4):1127-37. doi: 10.1021/acs.jproteome.2c00449
188. Markey K, Mitchell J, Botfield H, et al. 11β-Hydroxysteroid dehydrogenase type 1 inhibition in idiopathic intracranial hypertension: a double-blind randomized controlled trial. *Brain Commun* 2020;2(1) doi: 10.1093/braincomms/fcz050
189. Cello KE, Keltner JL, Johnson CA, et al. Factors Affecting Visual Field Outcomes in the Idiopathic Intracranial Hypertension Treatment Trial. *J Neuroophthalmol* 2016;36(1):6-12. doi: 10.1097/wno.0000000000000327 [published Online First: 2015/12/01]
190. Friedman DI, Quiros PA, Subramanian PS, et al. Headache in Idiopathic Intracranial Hypertension: Findings From the Idiopathic Intracranial Hypertension Treatment Trial. *Headache* 2017;57(8):1195-205. doi: 10.1111/head.13153 [published Online First: 2017/07/29]
191. Mulla Y, Markey KA, Woolley RL, et al. Headache determines quality of life in idiopathic intracranial hypertension. *J Headache Pain* 2015;16:521-21. doi: 10.1186/s10194-015-0521-9 [published Online First: 2015/05/15]
192. Sina F, Razmeh S, Habibzadeh N, et al. Migraine headache in patients with idiopathic intracranial hypertension. *Neurol Int* 2017;9(3):7280. doi: 10.4081/or.2017.7280 [published Online First: 2017/10/27]
193. Ekizoglu E, Baykan B, Orhan EK, et al. The analysis of allodynia in patients with idiopathic intracranial hypertension. *Cephalalgia* 2012;32(14):1049-58. doi: 10.1177/0333102412457091 [published Online First: 20120808]
194. Ashina H, Iljazi A, Al-Khazali HM, et al. CGRP-induced migraine-like headache in persistent post-traumatic headache attributed to mild traumatic brain injury. *J Headache Pain* 2022;23(1):135. doi: 10.1186/s10194-022-01499-5 [published Online First: 2022/10/18]
195. Nicola Jaime A, Anuradhaa S, Mary P, et al. Headache, Opiate Use, and Prescribing Trends in Women With Idiopathic Intracranial Hypertension. *Neurology* 2022;99(18):e1968. doi: 10.1212/WNL.0000000000201064
196. Westgate CSJ, Hagen SM, Israelsen IME, et al. The impact of obesity-related raised intracranial pressure in rodents. *Sci Rep* 2022;12(1):9102. doi: 10.1038/s41598-022-13181-6
197. Wardman JH, Jensen MN, Andreassen SN, et al. Modelling idiopathic intracranial hypertension in rats: contributions of high fat diet and testosterone to intracranial pressure and cerebrospinal fluid production. *Fluids and Barriers of the CNS* 2023;20(1):44. doi: 10.1186/s12987-023-00436-1
198. Uldall M, Bhatt DK, Kruuse C, et al. Choroid plexus aquaporin 1 and intracranial pressure are increased in obese rats: towards an idiopathic intracranial hypertension model? *Int J Obes* 2017;41(7):1141-47. doi: 10.1038/ijo.2017.83
199. Botfield HF, Uldall MS, Westgate CSJ, et al. A glucagon-like peptide-1 receptor agonist reduces intracranial pressure in a rat model of hydrocephalus. *Sci Transl Med* 2017;9(404) doi: 10.1126/scitranslmed.aan0972 [published Online First: 2017/08/25]
200. Zhao D, He Z, Vingrys AJ, et al. The effect of intraocular and intracranial pressure on retinal structure and function in rats. *Physiol Rep* 2015;3(8):e12507. doi: 10.14814/phy2.12507

201. Ficarrotta KR, Passaglia CL. Intracranial pressure modulates aqueous humour dynamics of the eye. *J Physiol* 2020;598(2):403-13. doi: 10.1113/jp278768 [published Online First: 2019/11/27]
202. da Silva Lopes L, Slobodian I, Del Bigio MR. Characterization of juvenile and young adult mice following induction of hydrocephalus with kaolin. *Experimental Neurology* 2009;219(1):187-96. doi: 10.1016/j.expneurol.2009.05.015
203. Del Bigio MR, Crook CR, Buist R. Magnetic Resonance Imaging and Behavioral Analysis of Immature Rats with Kaolin-Induced Hydrocephalus: Pre- and Postshunting Observations. *Experimental Neurology* 1997;148(1):256-64. doi: 10.1006/exnr.1997.6644
204. Khan OH DBM. Experimental models of hydrocephalus. In: Tatlisumak T FM, ed. Handbook of Experimental Neurology: Methods and Techniques in Animal Research: Cambridge University Press 2006:457-71.
205. Slobodian I, Krassioukov-Enns D, Del Bigio MR. Protein and synthetic polymer injection for induction of obstructive hydrocephalus in rats. *Cerebrospinal Fluid Research* 2007;4(1):9. doi: 10.1186/1743-8454-4-9
206. Del Bigio MR, Slobodian I, Schellenberg AE, et al. Magnetic resonance imaging indicators of blood-brain barrier and brain water changes in young rats with kaolin-induced hydrocephalus. *Fluids and Barriers of the CNS* 2011;8(1):22. doi: 10.1186/2045-8118-8-22
207. Kondziella D, Lüdemann W, Brinker T, et al. Alterations in brain metabolism, CNS morphology and CSF dynamics in adult rats with kaolin-induced hydrocephalus. *Brain Research* 2002;927(1):35-41. doi: 10.1016/S0006-8993(01)03320-0
208. Azzi GM, Canady AI, Ham S, et al. Kaolin-induced hydrocephalus in the hamster: temporal sequence of changes in intracranial pressure, ventriculomegaly and whole-brain specific gravity. *Acta neuropathologica* 1999;98:245-50.
209. Bloch O, Auguste KI, Manley GT, et al. Accelerated Progression of Kaolin-Induced Hydrocephalus in Aquaporin-4-Deficient Mice. *J Cereb Blood Flow Metab* 2006;26(12):1527-37. doi: 10.1038/sj.jcbfm.9600306
210. Piper RJ, Kalyvas AV, Young AMH, et al. Interventions for idiopathic intracranial hypertension. *Cochrane Database of Systematic Reviews* 2015(8) doi: 10.1002/14651858.CD003434.pub3
211. Sinclair AJ, Burdon MA, Nightingale PG, et al. Low energy diet and intracranial pressure in women with idiopathic intracranial hypertension: prospective cohort study. *Bmj* 2010;341:c2701. doi: 10.1136/bmj.c2701 [published Online First: 2010/07/09]
212. Mollan SP, Mitchell JL, Ottridge RS, et al. Effectiveness of Bariatric Surgery vs Community Weight Management Intervention for the Treatment of Idiopathic Intracranial Hypertension: A Randomized Clinical Trial. *JAMA Neurol* 2021 doi: 10.1001/jamaneurol.2021.0659
213. Kesler A, Hadayer A, Goldhammer Y, et al. Idiopathic intracranial hypertension: risk of recurrences. *Neurology* 2004;63(9):1737-39.
214. Mollan SP, Mitchell JL, Yiangou A, et al. Association of Amount of Weight Lost After Bariatric Surgery With Intracranial Pressure in Women With Idiopathic Intracranial Hypertension. *Neurology* 2022;99(11):e1090-e99. doi: 10.1212/wnl.0000000000200839

215. Ko MW, Chang SC, Ridha MA, et al. Weight gain and recurrence in idiopathic intracranial hypertension: a case-control study. *Neurology* 2011;76(18):1564-7. doi: 10.1212/WNL.0b013e3182190f51 [published Online First: 2011/05/04]
216. Hoffmann J, Mollan SP, Paemeleire K, et al. European headache federation guideline on idiopathic intracranial hypertension. *J Headache Pain* 2018;19(1):93. doi: 10.1186/s10194-018-0919-2 [published Online First: 2018/10/10]
217. Sunderland GJ, Jenkinson MD, Conroy EJ, et al. Neurosurgical CSF Diversion in Idiopathic Intracranial Hypertension: A Narrative Review. *Life* 2021;11(5) doi: 10.3390/life11050393 [published Online First: 20210426]
218. Sinclair AJ, Kuruvath S, Sen D, et al. Is cerebrospinal fluid shunting in idiopathic intracranial hypertension worthwhile? A 10-year review. *Cephalalgia* 2011;31(16):1627-33. doi: 10.1177/0333102411423305 [published Online First: 2011/10/05]
219. Brown PD, Davies SL, Speake T, et al. Molecular mechanisms of cerebrospinal fluid production. *Neuroscience* 2004;129(4):957-70. doi: 10.1016/j.neuroscience.2004.07.003
220. Wall M, McDermott MP, Kieburtz KD, et al. Effect of acetazolamide on visual function in patients with idiopathic intracranial hypertension and mild visual loss: the idiopathic intracranial hypertension treatment trial. *JAMA* 2014;311(16):1641-51. doi: 10.1001/jama.2014.3312 [published Online First: 2014/04/24]
221. Alore PL, Jay WM, Macken MP. Topiramate, pseudotumor cerebri, weight-loss and glaucoma: an ophthalmologic perspective. *Seminars in ophthalmology* 2006;21(1):15-7. doi: 10.1080/08820530500509325 [published Online First: 2006/03/07]
222. Mitchell JL, Mollan SP, Vijay V, et al. Novel advances in monitoring and therapeutic approaches in idiopathic intracranial hypertension. *Curr Opin Neurol* 2019;32(3):422-31. doi: 10.1097/wco.0000000000000690
223. Uldall M, Botfield H, Jansen-Olesen I, et al. Acetazolamide lowers intracranial pressure and modulates the cerebrospinal fluid secretion pathway in healthy rats. *Neurosci Lett* 2017;645:33-39. doi: 10.1016/j.neulet.2017.02.032 [published Online First: 2017/02/22]
224. Wall M, Kupersmith MJ, Kieburtz KD, et al. The idiopathic intracranial hypertension treatment trial: clinical profile at baseline. *JAMA Neurol* 2014;71(6):693-701. doi: 10.1001/jamaneurol.2014.133 [published Online First: 2014/04/24]
225. Ball AK, Howman A, Wheatley K, et al. A randomised controlled trial of treatment for idiopathic intracranial hypertension. *J Neurol* 2011;258(5):874-81. doi: 10.1007/s00415-010-5861-4
226. ten Hove MW, Friedman DI, Patel AD, et al. Safety and Tolerability of Acetazolamide in the Idiopathic Intracranial Hypertension Treatment Trial. *J Neuroophthalmol* 2016;36(1):13-9. doi: 10.1097/wno.0000000000000322 [published Online First: 2015/11/21]
227. York DA, Singer L, Thomas S, et al. Effect of topiramate on body weight and body composition of osborne-mendel rats fed a high-fat diet: alterations in hormones, neuropeptide, and uncoupling-protein mRNAs. *Nutrition* 2000;16(10):967-75. doi: 10.1016/S0899-9007(00)00451-2

228. Celebisoy N, Gokcay F, Sirin H, et al. Treatment of idiopathic intracranial hypertension: topiramate vs acetazolamide, an open-label study. *Acta Neurol Scand* 2007;116(5):322-7. doi: 10.1111/j.1600-0404.2007.00905.x [published Online First: 2007/10/10]
229. Finsterer J, Foldy D, Fertl E. Topiramate resolves headache from pseudotumor cerebri. *J Pain Symptom Manage* 2006;32(5):401-2. doi: 10.1016/j.jpainsymman.2006.07.009 [published Online First: 2006/11/07]
230. Scotton WJ, Botfield HF, Westgate CS, et al. Topiramate is more effective than acetazolamide at lowering intracranial pressure. *Cephalalgia* 2019;39(2):209-18. doi: 10.1177/0333102418776455 [published Online First: 2018/06/15]
231. Jones MW. Topiramate - Safety and Tolerability. *Can J Neurol Sci* 1998;25(S3):S13-S15. doi: 10.1017/S0317167100034855 [published Online First: 2015/09/18]
232. Mayo KE, Miller LJ, Bataille D, et al. International Union of Pharmacology. XXXV. The glucagon receptor family. *Pharmacological reviews* 2003;55(1):167-94.
233. Wheeler MB, Lu M, Dillon JS, et al. Functional expression of the rat glucagon-like peptide-I receptor, evidence for coupling to both adenylyl cyclase and phospholipase-C. *Endocrinology* 1993;133(1):57-62. doi: 10.1210/endo.133.1.8391428
234. Zhao X, Wang M, Wen Z, et al. GLP-1 Receptor Agonists: Beyond Their Pancreatic Effects. *Front Endocrinol (Lausanne)* 2021;12:721135. doi: 10.3389/fendo.2021.721135 [published Online First: 20210823]
235. Miller LJ, Sexton PM, Dong M, et al. The class B G-protein-coupled GLP-1 receptor: an important target for the treatment of type-2 diabetes mellitus. *Int J Obes Suppl* 2014;4(Suppl 1):S9-s13. doi: 10.1038/ijosup.2014.4 [published Online First: 20140708]
236. Chepurny OG, Hussain MA, Holz GG. Exendin-4 as a Stimulator of Rat Insulin I Gene Promoter Activity via bZIP/CRE Interactions Sensitive to Serine/Threonine Protein Kinase Inhibitor Ro 31-8220. *Endocrinology* 2002;143(6):2303-13. doi: 10.1210/endo.143.6.8870
237. Drucker DJ, Buse JB, Taylor K, et al. Exenatide once weekly versus twice daily for the treatment of type 2 diabetes: a randomised, open-label, non-inferiority study. *The Lancet* 2008;372(9645):1240-50.
238. Buse JB, Drucker DJ, Taylor KL, et al. DURATION-1: exenatide once weekly produces sustained glycemic control and weight loss over 52 weeks. *Diabetes care* 2010;33(6):1255-61.
239. Heppner KM, Kirigiti M, Secher A, et al. Expression and Distribution of Glucagon-Like Peptide-1 Receptor mRNA, Protein and Binding in the Male Nonhuman Primate (Macaca mulatta) Brain. *Endocrinology* 2015;156(1):255-67. doi: 10.1210/en.2014-1675
240. Turton MD, O'Shea D, Gunn I, et al. A role for glucagon-like peptide-1 in the central regulation of feeding. *Nature* 1996;379(6560):69-72. doi: 10.1038/379069a0
241. Flint A, Raben A, Astrup A, et al. Glucagon-like peptide 1 promotes satiety and suppresses energy intake in humans. *J Clin Invest* 1998;101(3):515-20. doi: 10.1172/jci990 [published Online First: 1998/03/21]
242. Carraro-Lacroix LR, Malnic G, Girardi AC. Regulation of Na+/H+ exchanger NHE3 by glucagon-like peptide 1 receptor agonist exendin-4 in renal proximal

tubule cells. *Am J Physiol Renal Physiol* 2009;297(6):F1647-55. doi: 10.1152/ajprenal.00082.2009 [published Online First: 2009/09/25]
243. Gao L, Huang H, Zhang L, et al. Comparison of beinaglutide versus metformin for weight loss in overweight and obese non-diabetic patients. *Exp Clin Endocrinol Diabetes* 2022;130(06):358-67.
244. Rubino DM, Greenway FL, Khalid U, et al. Effect of Weekly Subcutaneous Semaglutide vs Daily Liraglutide on Body Weight in Adults With Overweight or Obesity Without Diabetes: The STEP 8 Randomized Clinical Trial. *JAMA* 2022;327(2):138-50. doi: 10.1001/jama.2021.23619
245. Scotton WJ, Botfield HF, Westgate CS, et al. Topiramate is more effective than acetazolamide at lowering intracranial pressure. *Cephalalgia* 2018;55:033310241877645-10. doi: 10.1177/0333102418776455
246. Mitchell JL, Lyons HS, Walker JK, et al. The effect of GLP-1RA exenatide on idiopathic intracranial hypertension: a randomized clinical trial. *Brain* 2023:awad003. doi: 10.1093/brain/awad003
247. Arenkiel BR, Peca J, Davison IG, et al. In vivo light-induced activation of neural circuitry in transgenic mice expressing channelrhodopsin-2. *Neuron* 2007;54(2):205-18. doi: 10.1016/j.neuron.2007.03.005 [published Online First: 2007/04/20]
248. Nagel G, Szellas T, Huhn W, et al. Channelrhodopsin-2, a directly light-gated cation-selective membrane channel. *Proc Natl Acad Sci* 2003;100(24):13940. doi: 10.1073/pnas.1936192100 [published Online First: 2003/11/15]
249. Jiang L, Ma D, Grubb BD, et al. ROS/TRPA1/CGRP signaling mediates cortical spreading depression. *J Headache Pain* 2019;20(1):25. doi: 10.1186/s10194-019-0978-z [published Online First: 2019/03/08]
250. Dreier JP, Major S, Pannek H-W, et al. Spreading convulsions, spreading depolarization and epileptogenesis in human cerebral cortex. *Brain* 2011;135(1):259-75. doi: 10.1093/brain/awr303 [published Online First: 2011/11/29]
251. Schindelin J, Arganda-Carreras I, Frise E, et al. Fiji: an open-source platform for biological-image analysis. *Nat Methods* 2012;9(7):676-82. doi: 10.1038/nmeth.2019
252. Desousa BR, Kim KK, Jones AE, et al. Calculation of ATP production rates using the Seahorse XF Analyzer. *EMBO reports* 2023;24(10):e56380. doi: 10.15252/embr.202256380
253. Moye LS, Pradhan AAA. Animal Model of Chronic Migraine-Associated Pain. *Curr Protoc Neurosci* 2017;80:9.60.1-9.60.9. doi: 10.1002/cpns.33 [published Online First: 2017/07/06]
254. Harriott AM, Strother LC, Vila-Pueyo M, et al. Animal models of migraine and experimental techniques used to examine trigeminal sensory processing. *J Headache Pain* 2019;20(1):91. doi: 10.1186/s10194-019-1043-7 [published Online First: 2019/08/30]
255. Burstein R, Jakubowski M, Garcia-Nicas E, et al. Thalamic sensitization transforms localized pain into widespread allodynia. *Ann Neurol* 2010;68(1):81-91. doi: 10.1002/ana.21994 [published Online First: 2010/06/29]
256. Dixon WJ. The Up-and-Down Method for Small Samples. *J Am Stat Assoc* 1965;60(312):967-78. doi: 10.1080/01621459.1965.10480843

257. Chaplan SR, Bach FW, Pogrel JW, et al. Quantitative assessment of tactile allodynia in the rat paw. *J Neurosci Methods* 1994;53(1):55-63. doi: 10.1016/0165-0270(94)90144-9 [published Online First: 1994/07/01]
258. Saengjaroentham C, Strother LC, Dripps I, et al. Differential medication overuse risk of novel anti-migraine therapeutics. *Brain* 2020;143(9):2681-88. doi: 10.1093/brain/awaa211
259. Holland PR, Akerman S, Andreou AP, et al. Acid-sensing ion channel 1: a novel therapeutic target for migraine with aura. *Ann Neurol* 2012;72(4):559-63. doi: 10.1002/ana.23653
260. Terrin A, Bello L, Valentino ML, et al. The relevance of migraine in the clinical spectrum of mitochondrial disorders. *Sci Rep* 2022;12(1):4222-22. doi: 10.1038/s41598-022-08206-z
261. Guldiken B, Guldiken S, Taskiran B, et al. Migraine in metabolic syndrome. *Neurologist* 2009;15(2):55-8. doi: 10.1097/NRL.0b013e31817781b6 [published Online First: 2009/03/12]
262. Sinclair AJ, Matharu M. Migraine, cerebrovascular disease and the metabolic syndrome. *Ann Indian Acad Neurol* 2012;15(Suppl 1):S72-7. doi: 10.4103/0972-2327.100015 [published Online First: 2012/10/02]
263. Kelman L. The Triggers or Precipitants of the Acute Migraine Attack. *Cephalalgia* 2007;27(5):394-402. doi: 10.1111/j.1468-2982.2007.01303.x
264. Nadelson C. Sport and exercise-induced migraines. *Curr Sports Med Rep* 2006;5(1):29-33.
265. Yuzawa I, Sakadžić S, Srinivasan VJ, et al. Cortical spreading depression impairs oxygen delivery and metabolism in mice. *J Cereb Blood Flow Metab* 2012;32(2):376-86. doi: 10.1038/jcbfm.2011.148 [published Online First: 2011/10/20]
266. Arzua T, Yan Y, Jiang C, et al. Modeling alcohol-induced neurotoxicity using human induced pluripotent stem cell-derived three-dimensional cerebral organoids. *Transl Psychiatry* 2020;10 doi: 10.1038/s41398-020-01029-4
267. Marek GJ, Aghajanian GK. 5-HT2A receptor or α1-adrenoceptor activation induces excitatory postsynaptic currents in layer V pyramidal cells of the medial prefrontal cortex. *Eur J Pharmacol* 1999;367(2):197-206. doi: 10.1016/S0014-2999(98)00945-5
268. Buskila Y, Breen PP, Tapson J, et al. Extending the viability of acute brain slices. *Sci Rep* 2014;4:5309-09. doi: 10.1038/srep05309 [published Online First: 2014/06/17]
269. Fried NT, Moffat C, Seifert EL, et al. Functional mitochondrial analysis in acute brain sections from adult rats reveals mitochondrial dysfunction in a rat model of migraine. *Am J Physiol Cell Physiol* 2014;307(11):C1017-C30. doi: 10.1152/ajpcell.00332.2013 [published Online First: 2014/09/24]
270. Sawant-Pokam PM, Suryavanshi P, Mendez JM, et al. Mechanisms of Neuronal Silencing After Cortical Spreading Depression. *Cerebral Cortex* 2017;27(2):1311-25. doi: 10.1093/cercor/bhv328 [published Online First: 2016/01/07]
271. Stoppini L, Buchs PA, Muller D. A simple method for organotypic cultures of nervous tissue. *J Neurosci Methods* 1991;37(2):173-82. doi: 10.1016/0165-0270(91)90128-m [published Online First: 1991/04/01]
272. Dyhrfjeld-Johnsen J, Berdichevsky Y, Swiercz W, et al. Interictal spikes precede ictal discharges in an organotypic hippocampal slice culture model of

epileptogenesis. *J Clin Neurophysiol* 2010;27(6):418-24. doi: 10.1097/WNP.0b013e3181fe0709
273. Makrecka-Kuka M, Krumschnabel G, Gnaiger E. High-Resolution Respirometry for Simultaneous Measurement of Oxygen and Hydrogen Peroxide Fluxes in Permeabilized Cells, Tissue Homogenate and Isolated Mitochondria. *Biomolecules* 2015;5(3):1319-38. doi: 10.3390/biom5031319 [published Online First: 2015/07/02]
274. Burtscher J, Zangrandi L, Schwarzer C, et al. Differences in mitochondrial function in homogenated samples from healthy and epileptic specific brain tissues revealed by high-resolution respirometry. *Mitochondrion* 2015;25:104-12. doi: 10.1016/j.mito.2015.10.007 [published Online First: 2015/10/31]
275. Dias C, Lourenco CF, Barbosa RM, et al. Analysis of respiratory capacity in brain tissue preparations: high-resolution respirometry for intact hippocampal slices. *Anal Biochem* 2018;551:43-50. doi: 10.1016/j.ab.2018.05.010 [published Online First: 2018/05/14]
276. Viggiano A, Viggiano E, Valentino I, et al. Cortical spreading depression affects reactive oxygen species production. *Brain Research* 2011;1368:11-18. doi: 10.1016/j.brainres.2010.10.062
277. Shatillo A, Koroleva K, Giniatullina R, et al. Cortical spreading depression induces oxidative stress in the trigeminal nociceptive system. *Neuroscience* 2013;253:341-9. doi: 10.1016/j.neuroscience.2013.09.002 [published Online First: 2013/09/17]
278. Olesen J. The role of nitric oxide (NO) in migraine, tension-type headache and cluster headache. *Pharmacol Ther* 2008;120(2):157-71. doi: 10.1016/j.pharmthera.2008.08.003
279. Herst PM, Tan AS, Scarlett D-JG, et al. Cell surface oxygen consumption by mitochondrial gene knockout cells. *Biochim Biophys Acta* 2004;1656(2):79-87. doi: 10.1016/j.bbabio.2004.01.008
280. Gniel HM, Martin RL. Changes in Membrane Potential and the Intracellular Calcium Concentration During CSD and OGD in Layer V and Layer II/III Mouse Cortical Neurons. *J Neurophysiol* 2010;104(6):3203-12. doi: 10.1152/jn.00922.2009
281. Basarsky TA, Duffy SN, Andrew RD, et al. Imaging spreading depression and associated intracellular calcium waves in brain slices. *J Neurosci* 1998;18(18):7189-99. doi: 10.1523/jneurosci.18-18-07189.1998 [published Online First: 1998/09/16]
282. Enger R, Tang W, Vindedal GF, et al. Dynamics of Ionic Shifts in Cortical Spreading Depression. *Cerebral Cortex* 2015;25(11):4469-76. doi: 10.1093/cercor/bhv054
283. Amrutkar DV, Ploug KB, Olesen J, et al. Role for voltage gated calcium channels in calcitonin gene-related peptide release in the rat trigeminovascular system. *Neuroscience* 2011;172:510-17. doi: 10.1016/j.neuroscience.2010.10.032
284. Bickler PE, Fahlman CS. Moderate increases in intracellular calcium activate neuroprotective signals in hippocampal neurons. *Neuroscience* 2004;127(3):673-83. doi: 10.1016/j.neuroscience.2004.05.035 [published Online First: 2004/07/31]
285. Almeida A, Delgado-Esteban M, Bolaños JP, et al. Oxygen and glucose deprivation induces mitochondrial dysfunction and oxidative stress in

neurones but not in astrocytes in primary culture. *J Neurochem* 2002;81(2):207-17. doi: 10.1046/j.1471-4159.2002.00827.x
286. Kourti M, Liaropoulou D, Paschou M, et al. Enhanced Ca(2+) Entry Sustains the Activation of Akt in Glucose Deprived SH-SY5Y Cells. *Int J Mol Sci* 2022;23(3) doi: 10.3390/ijms23031386 [published Online First: 2022/02/16]
287. Dietz RM, Weiss JH, Shuttleworth CW. Zn2+ influx is critical for some forms of spreading depression in brain slices. *J Neurosci* 2008;28(32):8014-24.
288. Li J, Ye X, Zhou Y, et al. Energy Metabolic Disorder of Astrocytes May Be an Inducer of Migraine Attack. *Brain Sci* 2022;12(7) doi: 10.3390/brainsci12070844 [published Online First: 2022/07/28]
289. Li H-T, Feng L, Jiang W-D, et al. Oxidative stress parameters and anti-apoptotic response to hydroxyl radicals in fish erythrocytes: Protective effects of glutamine, alanine, citrulline and proline. *Aquatic Toxicology* 2013;126:169-79. doi: 10.1016/j.aquatox.2012.11.005
290. Grosser N, Oberle S, Berndt G, et al. Antioxidant action of l-alanine: heme oxygenase-1 and ferritin as possible mediators. *Biochem Biophys Res Commun* 2004;314(2):351-55. doi: 10.1016/j.bbrc.2003.12.089
291. Lourenço CF, Ledo A, Gerhardt GA, et al. Neurometabolic and electrophysiological changes during cortical spreading depolarization: multimodal approach based on a lactate-glucose dual microbiosensor arrays. *Sci Rep* 2017;7(1):6764. doi: 10.1038/s41598-017-07119-6
292. Rogers ML, Leong CL, Gowers SA, et al. Simultaneous monitoring of potassium, glucose and lactate during spreading depolarization in the injured human brain - Proof of principle of a novel real-time neurochemical analysis system, continuous online microdialysis. *J Cereb Blood Flow Metab* 2017;37(5):1883-95. doi: 10.1177/0271678x16674486 [published Online First: 2016/11/01]
293. Circu ML, Maloney RE, Aw TY. Low glucose stress decreases cellular NADH and mitochondrial ATP in colonic epithelial cancer cells: Influence of mitochondrial substrates. *Chem Biol Interact* 2017;264:16-24. doi: 10.1016/j.cbi.2017.01.001 [published Online First: 20170110]
294. Divakaruni AS, Wallace M, Buren C, et al. Inhibition of the mitochondrial pyruvate carrier protects from excitotoxic neuronal death. *J Cell Biol* 2017;216(4):1091-105. doi: 10.1083/jcb.201612067 [published Online First: 20170302]
295. Kohlhauer M, Dawkins S, Costa AS, et al. Metabolomic profiling in acute ST-segment–elevation myocardial infarction identifies succinate as an early marker of human ischemia–reperfusion injury. *J Am Heart Assoc* 2018;7(8):e007546.
296. Huang LY, Ma JY, Song JX, et al. Ischemic accumulation of succinate induces Cdc42 succinylation and inhibits neural stem cell proliferation after cerebral ischemia/reperfusion. *Neural Regen Res* 2023;18(5):1040-45. doi: 10.4103/1673-5374.355821
297. Chouchani ET, Pell VR, Gaude E, et al. Ischaemic accumulation of succinate controls reperfusion injury through mitochondrial ROS. *Nature* 2014;515(7527):431-35. doi: 10.1038/nature13909
298. Kudo C, Harriott AM, Moskowitz MA, et al. Estrogen modulation of cortical spreading depression. *J Headache Pain* 2023;24(1):62. doi: 10.1186/s10194-023-01598-x

299. Brennan KC, Romero Reyes M, López Valdés HE, et al. Reduced threshold for cortical spreading depression in female mice. *Ann Neurol* 2007;61(6):603-6. doi: 10.1002/ana.21138
300. Grech O, Mollan SP, Wakerley BR, et al. Emerging themes in idiopathic intracranial hypertension. *J Neurol* 2020;267(12):3776-84. doi: 10.1007/s00415-020-10090-4 [published Online First: 2020/07/24]
301. Pomschar A, Koerte I, Lee S, et al. MRI evidence for altered venous drainage and intracranial compliance in mild traumatic brain injury. *PLoS One* 2013;8(2):e55447.
302. Ropper AH. Brain edema after stroke: clinical syndrome and intracranial pressure. *Archives of neurology* 1984;41(1):26-29.
303. Bristol RE. Hydrocephalus. In: Aminoff MJ, Daroff RB, eds. Encyclopedia of the Neurological Sciences (Second Edition). Oxford: Academic Press 2014:636-39.
304. Kalyvas A, Neromyliotis E, Koutsarnakis C, et al. A systematic review of surgical treatments of idiopathic intracranial hypertension (IIH). *Neurosurg Rev* 2020 doi: 10.1007/s10143-020-01288-1 [published Online First: 2020/04/27]
305. Ball AK, Howman A, Wheatley K, et al. A randomised controlled trial of treatment for idiopathic intracranial hypertension. *J Neurol* 2011;258(5):874-81. doi: 10.1007/s00415-010-5861-4 [published Online First: 2010/12/17]
306. Hagen SM, Eftekhari S, Hamann S, et al. Intracranial pressure and optic disc changes in a rat model of obstructive hydrocephalus. *BMC Neurosci* 2022;23(1):29. doi: 10.1186/s12868-022-00716-w [published Online First: 2022/05/24]
307. Di Curzio DL, Turner-Brannen E, Del Bigio MR. Oral antioxidant therapy for juvenile rats with kaolin-induced hydrocephalus. *Fluids and Barriers of the CNS* 2014;11(1):23. doi: 10.1186/2045-8118-11-23
308. Jugé L, Pong AC, Bongers A, et al. Changes in Rat Brain Tissue Microstructure and Stiffness during the Development of Experimental Obstructive Hydrocephalus. *PLoS One* 2016;11(2):e0148652. doi: 10.1371/journal.pone.0148652 [published Online First: 20160205]
309. Li J, McAllister JP, Shen Y, et al. Communicating hydrocephalus in adult rats with kaolin obstruction of the basal cisterns or the cortical subarachnoid space. *Experimental Neurology* 2008;211(2):351-61. doi: 10.1016/j.expneurol.2007.12.030
310. Nagra G, Li J, McAllister JP, et al. Impaired lymphatic cerebrospinal fluid absorption in a rat model of kaolin-induced communicating hydrocephalus. *Am J Physiol Regul Integr Comp Physiol* 2008;294(5):R1752-R59. doi: 10.1152/ajpregu.00748.2007
311. Skjolding AD, Rowland IJ, Søgaard LV, et al. Hydrocephalus induces dynamic spatiotemporal regulation of aquaporin-4 expression in the rat brain. *Cerebrospinal Fluid Research* 2010;7(1):20. doi: 10.1186/1743-8454-7-20
312. Silverberg GD, Miller MC, Machan JT, et al. Amyloid and Tau accumulate in the brains of aged hydrocephalic rats. *Brain Research* 2010;1317:286-96. doi: 10.1016/j.brainres.2009.12.065
313. Olopade FE, Shokunbi MT, Sirén A-L. The relationship between ventricular dilatation, neuropathological and neurobehavioural changes in hydrocephalic rats. *Fluids and Barriers of the CNS* 2012;9(1):19. doi: 10.1186/2045-8118-9-19

314. Guild S-J, McBryde FD, Malpas SC. Recording of intracranial pressure in conscious rats via telemetry. *J Appl Physiol* 2015;119(5):576-81.
315. Williamson M, John R, Colbourne F. Measurement of Intracranial Pressure in Freely Moving Rats2018:17-25.
316. Rogatsky GG, Sonn J, Kamenir Y, et al. Relationship between intracranial pressure and cortical spreading depression following fluid percussion brain injury in rats. *J Neurotrauma* 2003;20(12):1315-25. doi: 10.1089/089771503322686111
317. Eide PK, Hasan-Olive MM, Hansson HA, et al. Increased occurrence of pathological mitochondria in astrocytic perivascular endfoot processes and neurons of idiopathic intracranial hypertension. *J Neurosci Res* 2021;99(2):467-80. doi: 10.1002/jnr.24743 [published Online First: 2020/10/27]
318. Eide PK, Pripp AH, Ringstad G, et al. Impaired glymphatic function in idiopathic intracranial hypertension. *Brain Commun* 2021;3(2) doi: 10.1093/braincomms/fcab043
319. Zhang ZG, Chopp M, Maynard KI, et al. Cerebral blood flow changes during cortical spreading depression are not altered by inhibition of nitric oxide synthesis. *J Cereb Blood Flow Metab* 1994;14(6):939-43. doi: 10.1038/jcbfm.1994.125 [published Online First: 1994/11/01]
320. Owler BK, Pena A, Momjian S, et al. Changes in cerebral blood flow during cerebrospinal fluid pressure manipulation in patients with normal pressure hydrocephalus: a methodological study. *J Cereb Blood Flow Metab* 2004;24(5):579-87. doi: 10.1097/00004647-200405000-00012 [published Online First: 2004/05/07]
321. Zheng S, Mu S, Li J, et al. Cerebral venous hemodynamic responses in a mouse model of traumatic brain injury. *Brain Research* 2022;1792:148014. doi: 10.1016/j.brainres.2022.148014 [published Online First: 2022/07/16]
322. Acharya D, Ruesch A, Schmitt S, et al. Changes in neurovascular coupling with cerebral perfusion pressure indicate a link to cerebral autoregulation. *J Cereb Blood Flow Metab* 2022;42(7):1247-58. doi: 10.1177/0271678x221076566
323. Tong LS, Guo ZN, Ou YB, et al. Cerebral venous collaterals: A new fort for fighting ischemic stroke? *Prog Neurobiol* 2018;163-164:172-93. doi: 10.1016/j.pneurobio.2017.11.001 [published Online First: 2017/12/05]
324. Lipton RB, Bigal ME, Ashina S, et al. Cutaneous allodynia in the migraine population. *Ann Neurol* 2008;63(2):148-58. doi: 10.1002/ana.21211 [published Online First: 2007/12/07]
325. Oseguera-Zavala BS, Munguía-Rodríguez AG, Carranza-Rentería O, et al. Prevalence of elevated intracranial pressure in patients with classical trigeminal neuralgia with overweight and obesity. *Archivos de Neurociencias* 2020;25(3):6-13.
326. Rivera M, Aguilar E, Perez A, et al. Trigeminal Neuralgia as An Atypical Manifestation of Intracranial Hypertension. Case Report and Literature Review. *SOVA Neurology* 2023;5(1)
327. Iftikhar PM, Maham Munawar M, Pour MA, et al. A Typical Presentation of Trigeminal Neuralgia Induced by Intracranial Hypertension Mimicking Sinusitis. *Arch Clin Med Case Rep* 2020;4(2):285-91.
328. Elliott MB, Oshinsky ML, Amenta PS, et al. Nociceptive neuropeptide increases and periorbital allodynia in a model of traumatic brain injury. *Headache*

2012;52(6):966-84. doi: 10.1111/j.1526-4610.2012.02160.x [published Online First: 2012/05/10]
329. Macolino CM, Daiutolo BV, Albertson BK, et al. Mechanical allodynia induced by traumatic brain injury is independent of restraint stress. *J Neurosci Methods* 2014;226:139-46. doi: 10.1016/j.jneumeth.2014.01.008 [published Online First: 2014/02/04]
330. Al-Hassany L, Haas J, Piccininni M, et al. Giving Researchers a Headache - Sex and Gender Differences in Migraine. *Front Neurol* 2020;11:549038. doi: 10.3389/fneur.2020.549038 [published Online First: 2020/11/17]
331. Piper RJ, Kalyvas AV, Young AM, et al. Interventions for idiopathic intracranial hypertension. *Cochrane Database Syst Rev* 2015(8):Cd003434. doi: 10.1002/14651858.CD003434.pub3 [published Online First: 2015/08/08]
332. IIH Pressure Med: A randomised, sequential, trial of the effect on intracranial pressure of five drugs commonly used in Idiopathic Intracranial Hypertension. J Headache Pain; 2021.
333. Grech OM, James; Yiangou, Andreas; Alimaistorovic, Zerin; Brock, Kristain; Mollan, Susan; Sinclair, Alex. Evaluation of cognitive performance with medicines for raised intracranial pressure: implications for spaceflight associated neuro-ocular syndrome [abstract]. *Aerospace Medicine And Human Performance* 2022;93(3)
334. Grech O, Clouter A, Mitchell JL, et al. Cognitive performance in idiopathic intracranial hypertension and relevance of intracranial pressure. *Brain Commun* 2021;3(3):fcab202. doi: 10.1093/braincomms/fcab202 [published Online First: 2021/10/28]
335. Vahedi K, Taupin P, Djomby R, et al. Efficacy and tolerability of acetazolamide in migraine prophylaxis: A randomised placebo-controlled trial. *J Neurol* 2002;249(2):206-11. doi: 10.1007/PL00007866
336. Painter NA, Morello CM, Singh RF, et al. An evidence-based and practical approach to using Bydureon™ in patients with type 2 diabetes. *J Am Board Fam Med* 2013;26(2):203-10.
337. Rubino D, Abrahamsson N, Davies M, et al. Effect of continued weekly subcutaneous semaglutide vs placebo on weight loss maintenance in adults with overweight or obesity: the STEP 4 randomized clinical trial. *JAMA* 2021;325(14):1414-25.
338. Jensterle M, Rizzo M, Haluzík M, et al. Efficacy of GLP-1 RA Approved for Weight Management in Patients With or Without Diabetes: A Narrative Review. *Adv Ther* 2022;39(6):2452-67. doi: 10.1007/s12325-022-02153-x [published Online First: 2022/05/04]
339. Singh I, Wang L, Xia B, et al. Activation of arcuate nucleus glucagon-like peptide-1 receptor-expressing neurons suppresses food intake. *Cell & Bioscience* 2022;12(1):178. doi: 10.1186/s13578-022-00914-3
340. Li Y, Perry T, Kindy MS, et al. GLP-1 receptor stimulation preserves primary cortical and dopaminergic neurons in cellular and rodent models of stroke and Parkinsonism. *Proc Natl Acad Sci* 2009;106(4):1285-90.
341. Nizari S, Basalay M, Chapman P, et al. Glucagon-like peptide-1 (GLP-1) receptor activation dilates cerebral arterioles, increases cerebral blood flow, and mediates remote (pre)conditioning neuroprotection against ischaemic stroke. *Basic Res Cardiol* 2021;116(1):32. doi: 10.1007/s00395-021-00873-9 [published Online First: 2021/05/05]

342. Tu X-k, Chen Q, Chen S, et al. GLP-1R Agonist Liraglutide Attenuates Inflammatory Reaction and Neuronal Apoptosis and Reduces Early Brain Injury After Subarachnoid Hemorrhage in Rats. *Inflammation* 2021;44(1):397-406. doi: 10.1007/s10753-020-01344-4
343. Daou BJ, Sweid A, Weinberg JH, et al. Effect of Shunting on Visual Outcomes and Headache in Patients with Idiopathic Intracranial Hypertension. *World Neurosurg* 2020;142:e73-e80. doi: 10.1016/j.wneu.2020.05.186 [published Online First: 2020/06/01]
344. Krajnc N, Itariu B, Macher S, et al. Treatment with GLP-1 receptor agonists is associated with significant weight loss and favorable headache outcomes in idiopathic intracranial hypertension. *J Headache Pain* 2023;24(1):89. doi: 10.1186/s10194-023-01631-z
345. Farkas E, Szilvásy-Szabó A, Ruska Y, et al. Distribution and ultrastructural localization of the glucagon-like peptide-1 receptor (GLP-1R) in the rat brain. *Brain Structure and Function* 2021;226(1):225-45. doi: 10.1007/s00429-020-02189-1
346. Jing F, Zou Q, Wang Y, et al. Activation of microglial GLP-1R in the trigeminal nucleus caudalis suppresses central sensitization of chronic migraine after recurrent nitroglycerin stimulation. *J Headache Pain* 2021;22(1):86. doi: 10.1186/s10194-021-01302-x
347. Jing F, Zou Q, Pu Y. GLP-1R agonist liraglutide attenuates pain hypersensitivity by stimulating IL-10 release in a nitroglycerin-induced chronic migraine mouse model. *Neurosci Lett* 2023;812:137397. doi: 10.1016/j.neulet.2023.137397
348. Katsurada K, Nandi SS, Sharma NM, et al. Does glucagon-like peptide-1 induce diuresis and natriuresis by modulating afferent renal nerve activity? *Am J Physiol Renal Physiol* 2019;317(4):F1010-F21. doi: 10.1152/ajprenal.00028.2019
349. Wettergren A, Schjoldager B, Mortensen PE, et al. Truncated GLP-1 (proglucagon 78–107-amide) inhibits gastric and pancreatic functions in man. *Dig Dis Sci* 1993;38(4):665-73. doi: 10.1007/BF01316798
350. Walker CS, Li X, Whiting L, et al. Mice Lacking the Neuropeptide α-Calcitonin Gene-Related Peptide Are Protected Against Diet-Induced Obesity. *Endocrinology* 2010;151(9):4257-69. doi: 10.1210/en.2010-0284
351. Tough IR, Moodaley R, Cox HM. Mucosal glucagon-like peptide 1 (GLP-1) responses are mediated by calcitonin gene-related peptide (CGRP) in the mouse colon and both peptide responses are area-specific. *Neurogastroenterol Motil* 2018;30(1) doi: 10.1111/nmo.13149 [published Online First: 20170711]
352. Tang C, Unekawa M, Kitagawa S, et al. Cortical spreading depolarisation-induced facial hyperalgesia, photophobia and hypomotility are ameliorated by sumatriptan and olcegepant. *Sci Rep* 2020;10(1):11408. doi: 10.1038/s41598-020-67948-w
353. Edvinsson L, Ho TW. CGRP receptor antagonism and migraine. *Neurotherapeutics* 2010;7(2):164-75. doi: 10.1016/j.nurt.2010.02.004 [published Online First: 2010/05/01]
354. Banks WA, During MJ, Niehoff ML. Brain uptake of the glucagon-like peptide-1 antagonist exendin (9-39) after intranasal administration. *J Pharmacol Exp Ther* 2004;309(2):469-75.

355. Kastin AJ, Akerstrom V. Entry of exendin-4 into brain is rapid but may be limited at high doses. *Int J Obes* 2003;27(3):313-18. doi: 10.1038/sj.ijo.0802206
356. Melo-Carrillo A, Schain AJ, Stratton J, et al. Fremanezumab and its isotype slow propagation rate and shorten cortical recovery period but do not prevent occurrence of cortical spreading depression in rats with compromised blood brain barrier. *Pain* 2020;161(5):1037.
357. Tvedskov JF, Tfelt-Hansen P, Petersen KA, et al. CGRP receptor antagonist olcegepant (BIBN4096BS) does not prevent glyceryl trinitrate-induced migraine. *Cephalalgia* 2010;30(11):1346-53. doi: 10.1177/0333102410363491
358. Petersen KA, Birk S, Doods H, et al. Inhibitory effect of BIBN4096BS on cephalic vasodilatation induced by CGRP or transcranial electrical stimulation in the rat. *Br J Pharmacol* 2004;143(6):697-704. doi: 10.1038/sj.bjp.0705966 [published Online First: 20041025]
359. Mulder IA, Li M, de Vries T, et al. Anti-migraine Calcitonin Gene-Related Peptide Receptor Antagonists Worsen Cerebral Ischemic Outcome in Mice. *Ann Neurol* 2020;88(4):771-84. doi: 10.1002/ana.25831 [published Online First: 2020/06/26]
360. De Logu F, Landini L, Janal MN, et al. Migraine-provoking substances evoke periorbital allodynia in mice. *J Headache Pain* 2019;20(1):18. doi: 10.1186/s10194-019-0968-1
361. Wu S, Ren X, Zhu C, et al. A c-Fos activation map in nitroglycerin/levcromakalim-induced models of migraine. *J Headache Pain* 2022;23(1):128. doi: 10.1186/s10194-022-01496-8
362. Munro G, Petersen S, Jansen-Olesen I, et al. A unique inbred rat strain with sustained cephalic hypersensitivity as a model of chronic migraine-like pain. *Sci Rep* 2018;8(1):1836. doi: 10.1038/s41598-018-19901-1 [published Online First: 2018/02/01]
363. Covasala O, Stirn SL, Albrecht S, et al. Calcitonin gene-related peptide receptors in rat trigeminal ganglion do not control spinal trigeminal activity. *J Neurophysiol* 2012;108(2):431-40. doi: 10.1152/jn.00167.2011
364. Sixt M-L, Messlinger K, Fischer MJM. Calcitonin gene-related peptide receptor antagonist olcegepant acts in the spinal trigeminal nucleus. *Brain* 2009;132(11):3134-41. doi: 10.1093/brain/awp168
365. Liu Y, Song XD, Liu W, et al. Glucose deprivation induces mitochondrial dysfunction and oxidative stress in PC12 cell line. *J Cell Mol Med* 2003;7(1):49-56. doi: 10.1111/j.1582-4934.2003.tb00202.x
366. Mies G, Paschen W. Regional changes of blood flow, glucose, and ATP content determined on brain sections during a single passage of spreading depression in rat brain cortex. *Experimental Neurology* 1984;84(2):249-58. doi: 10.1016/0014-4886(84)90222-X
367. Ghaemi A, Alizadeh L, Babaei S, et al. Astrocyte-mediated inflammation in cortical spreading depression. *Cephalalgia* 2018;38(4):626-38. doi: 10.1177/0333102417702132 [published Online First: 20170403]
368. Agersø H, Jensen L, Elbrønd B, et al. The pharmacokinetics, pharmacodynamics, safety and tolerability of NN2211, a new long-acting GLP-1 derivative, in healthy men. *Diabetologia* 2002;45:195-202.
369. Karsan N, Goadsby PJ. Biological insights from the premonitory symptoms of migraine. *Nat Rev Neurol* 2018;14(12):699-710. doi: 10.1038/s41582-018-0098-4

370. Schürks M, Rist PM, Bigal ME, et al. Migraine and cardiovascular disease: systematic review and meta-analysis. *Bmj* 2009;339
371. Bernstein C, Burstein R. Sensitization of the trigeminovascular pathway: perspective and implications to migraine pathophysiology. *J Clin Neurol* 2012;8(2):89-99. doi: 10.3988/jcn.2012.8.2.89 [published Online First: 2012/06/29]
372. Dixon WJ. Efficient analysis of experimental observations. *Ann Rev Pharmacol Toxicol* 1980;20:441-62. doi: 10.1146/annurev.pa.20.040180.002301